Defining glycoprotein determinants associated with cross-species transmission of Old World Arenaviruses

School of Life Sciences, Virus Research Group, Queen's Medical Centre, University of Nottingham, UK.

Supervisors

Professor Jonathan Ball
Dr Patrick McClure
Dr Richard Urbanowicz

PhD candidate

Arwa Bagasi

Table of Contents

Abstract 7

Acknowledgement 8

Chapter. 1: General background and introduction 9

1.1 Arenaviridae 9

1.2 Morphology and structure 14
1.2.1 Genome 14
1.2.2 L protein 16
1.2.3 Nucleoprotein 16
1.2.4 Z protein 17
1.2.5 Glycoprotein Complex 18

1.3 Immunogenicity and antigenicity 25

1.4 Genetic diversity of OWAs 27

1.5 Pathogenicity and epidemiology 29

1.6 Treatment 35

1.7 Life cycle 37
1.7.1 Entry 38
1.7.2 Gene expression and replication 40
1.7.3 Maturation, assembly, and budding 41

1.8 Lymphocytic Choriomeningitis Virus 42
1.8.1 α-DG as the primary receptor for LCMV 43
1.8.2 Alternative receptors 47

1.9 Emergence, zoonosis and host switch 48
1.9.1 Predicting viral emergence 49
1.9.2 Host and viral genetic factors contributing to emergence 51

1.10 Pseudotyping system as a tool to study the early steps of the viral life cycle 53
1.10.1 Pseudotyping history and applications 53
1.10.2 Frequently used packaging systems and their modifications 56
1.10.3 Reporter genes 59
1.10.4 Pseudotype producer cells 59
1.10.5 Optimizing production and infectivity 60
1.10.6 Reliability and consistency of pseudotyping systems 62

1.11 A preface of the study 63
1.11.1 Description of the outbreak 63
1.11.2 General aims 66

Chapter. 2: Methods and materials 67

2.1 Samples 67

2.2 Primers 68

2.3 PCR 74

2.4 Sequencing analysis 75

2.5 Plasmids 76
2.6 Digestion enzymes 77
2.7 InFusion cloning 77
2.8 Mutagenesis 78
2.9 Plasmid extraction 78
2.10 Gel Electrophoresis 79
2.11 Spectrophotometry 79
2.12 Cells 79
2.13 Pseudotype production 81
2.14 Infection assays 82
2.15 Antibodies 82
2.16 Western blot experiments 83
2.16.1 Western blot samples preparation 83
2.16.2 Western blot 83
2.16.3 Western blot signal analysis 84
2.17 Dot blot analysis of virus-α-DG binding 85
2.18 Transduction and flow cytometry experiments of HAP1 cells 85
2.18.1 Transduction of DAG1 in HAP1 KO cells 85
2.18.2 Cell sorting and flowcytometry 86
2.19 α-DG-Fc designing, expression, purification, staining, and quantification 86
2.19.1 α-DG-Fc constructs 86
2.19.2 α-DG-Fc expression 87
2.19.3 α-DG-Fc purification and concertation 88
2.19.4 Quantification of α-DG-Fc 89
2.19.5 Coomassie staining 89
2.19.6 Silver staining 89
2.20 Inhibition assays using soluble α-DG 90
2.21 Overexpression of LARGE1 90
2.22 Statistical analysis and graphs 91
2.23 DAG1 transcript variants and protein conservation analysis 92
2.24 Mapping key residues in crystal structures 92
Chapter. 3: The phylogeny and sequence analysis of the LCMV GPC isolates 93
3.1 Introduction 93
3.2 Results 93
3.2.1 The isolated GPC sequences belong to LCMV lineage I 93
3.2.2 The study isolates segregated according to species 94
3.2.3 The sequence alignment revealed multiple positions showing species specificity 99
3.3 Discussion 102
Chapter. 4: LCMV pseudotype production and optimization 104

4.1 Introduction 104
4.2 Results 104
4.2.1 The envelope plasmid type and amount affected the infectivity of the LCMV pseudotypes 104
4.2.2. The incorporation of GPC into pseudoparticles was similar across the study clones. 106
4.3 Discussion 109
Chapter. 5: The infectivity of the pseudotypes in murine and NHP cell lines 112
5.1 Introduction 112
5.2 Results 112
5.2.1 NHP-derived pseudotypes displayed higher infectivity in L929 cells compared to the mouse-derived pseudotypes 112
5.2.2 The infectivity of the mutants indicated complex amino acid interactions 115
5.3 Discussion 119
Chapter. 6: The receptor usage of the study isolates 123
6.1 Introduction 123
6.2 Results 124
6.2.1 The infectivity of the study clones correlated with the levels of α-DG expressed in KO cells 124
6.2.2 The infectivity in the KO cells increased when the NHP-defining mutations were introduced to the non-infectious mouse clone 129
6.2.3 KM155-DAG-KO cells were permissive to an NHP clone 130
6.2.4 Alternative splicing of DAG1 could not explain the residual infectivity in the KO cell lines. 132
6.2.5 Murine soluble α-DG caused a dose-dependent inhibition of the NHP clones and M10 but not M1 or M8 in L929 cells 133
6.2.6 The NHP-defining mutations altered the inhibitory effect of α-DG in L929 135
6.2.7 The NHP and the mouse clones showed comparable inhibition by NHP soluble α-DG 138
6.2.8 The mutations in Gp1 are located within the same region of residues previously found to affect α-DG affinity. 145
6.3 Discussion 147
Chapter. 7: Discussion 152
7.1 Overview 152
7.2 The study's relevance to the current arenavirus status 153
7.3 The limitations and areas of improvements 154
7.4 Technical challenges 156
7.4.1 Standardizing pseudotypes input using p30 signal 156
7.4.2 Assessing α-DG level in cell lysates 157
7.4.3 Overexpressing LARGE1 in HEK293T 157
7.4.4 Purification of α-DG-Fc recombinant protein using AKTA 158
7.4.5 Dot blot to measure virus-α-DG binding 158
7.5 Future perspectives 160
7.6 Summary 163

Chapter. 8: Appendices _____ **165**

8.1 The NHP samples serology and PCR results: _____ **165**

8.2 The mouse samples serology and PCR results: _____ **167**

8.3 Pathology records as provided by Twycross zoo for LCMV-confirmed cases: 169

8.4 Pathology records as provided by Twycross zoo for LCMV-suspected cases 172

8.5 LCMV strains used to design the outer set of the nested PCR primers for GPC amplification: _____ **177**

8.6 iRis digital cell images of EGFP expression in HAP1 transduced and KO cells 178

8.7 α-DG-Fc constructs _____ **179**

Chapter. 9: References _____ **182**

List of figures:

Figure 1-1: Illustration of the common features of Old World arenaviruses. 14
Figure 1-2: Genome organization of arenaviruses.....15
Figure 1-3: OWA GPC structure. 21
Figure 1-4: Putative N-linked glycan sites of LASV GPC. 25
Figure 1-5: Global map of arenavirus outbreaks 35
Figure 1-6: The life cycle of OWAs. 38
Figure 1-7: Component of the lentiviral- and gammaretroviral-based pseudotyping systems.....58
Figure 3-1: The phylogenetic relationship between worldwide LCMV GPC isolates and the study isolates. 97
Figure 3-2: The phylogenetic relationship between the GPCs of the study isolates. 98
Figure 3-3: Heat map of pairwise genetic distances of the mouse and the NHP sequences.....99
Figure 3-4: Alignment of the mouse and the NHP amino acid sequences and identifying NHP/Mouse changes. 101
Figure 4-1: Optimization of the envelope plasmid concentration.....106
Figure 4-2: Detection of LCMV glycoprotein in cell lysates and pseudotype pellets. 108
Figure 5-1: Optimization of target cell density. 113
Figure 5-2: Infectivity of the NHP and the mouse clones in Vero and L929. 115
Figure 5-3: The effect of introducing six NHP-defining residues to the two mouse clones M1 and M8.....116
Figure 5-4: Introducing the NHP-defining mutations to the mouse clone M10. 118
Figure 5-5: Introducing the mouse residue at 211 to NHP1. 118
Figure 6-1: Selecting and sorting HAP1 $\boldsymbol{DAG1}+$ cells based on EGFP expression. 125
Figure 6-2: DAG1 expression in HAP1 $\mathbf{DAG1}+$ cells.....127
Figure 6-3: The infectivity of the wild-type clones in HAP1 KO and $\mathbf{DAG1}+$ cells.128
Figure 6-4: The infectivity of the mutants in HAP1 KO cells. 129
Figure 6-5: The ability of soluble α-DG to inhibit the entry of NHP3 to HAP1 KO cells. 131
Figure 6-6: The infectivity in KM155 WT and α-DG-KO cells. 131
Figure 6-7: Mapping HAP1 KO, KM155 KO, and the virus-binding sites in α-DG transcript variants. 133
Figure 6-8: Western blot, coomassie blue, and silver staining of murine α-DG-Fc. 134
Figure 6-9: Inhibition of entry of LCMV pseudotypes by murine α-DG-Fc. 138
Figure 6-10: NHP and mouse DAG1 protein alignment of the regions involved in the virus binding. 142
Figure 6-11: Inhibition of pseudotypes entry to Vero cells by NHP α DG. 144
Figure 6-12: Mapping the study mutations together with the mutations previously identified to affect the receptor binding in LCMV and LASV crystal structures. 146
Figure 8-1: EGFP expression in HAP1 KO/KI cells.....178

List of tables:

Table 1-1: Mammarenaviruses distribution, reservoirs, and pathogenicity in humans. 11
Table 1-2: NHP samples included in the current study that tested positive for LCMV either by serology or PCR during the 2005/2006 outbreak. 65
Table 1-3: Mouse samples included in the current study that tested positive for LCMV by PCR following the 2005/2006 outbreak. 65
Table 2-1: The study Samples. 68
Table 2-2: In-house primer sets used for InFusion cloning, screening and sequencing, or mutagenesis. 70
Table 6-1: α-DG protein sequence identity of NHP species versus *M.musculus*..... 140

Abstract

Viruses often acquire adaptive changes to be successfully established in a new host. The early steps of the viral life cycle including the receptor binding and the subsequent entry process constitute the first barrier towards a productive viral infection. Thus, adaptations in the viral genes involved in these steps were frequently implicated in the emergence of many important human viruses. Lymphocytic choriomeningitis virus is an Old World arenavirus that occasionally infects primates including humans via isolated spillover events from the natural host (mice) while primate-to-primate transmission is rarely observed. In this study, a naturally occurring LCMV outbreak in non-human primates (NHP) was investigated. At least 24 confirmed cases and six deaths were reported. Given the scale of this outbreak, adaptive changes particularly in the viral glycoproteins may have existed. To test this hypothesis, LCMV GPCs isolated from the infected NHPs were compared to those isolated from mice found on the premises of the outbreak both genotypically and phenotypically. Seven NHP-defining changes were identified and were associated with a distinct phenotype in pseudotype-based infectivity assays. The NHP clones showed increased infectivity over the mouse clones in most of the cell lines tested. Introducing the identified mutations on a mouse background reproduced the NHP-associated phenotype. Additionally, assays including knockout/knock-in and entry inhibition assays were performed to elucidate the role of the receptor affinity in the observed phenotype. The data obtained from these assays indicated the involvement of the cellular receptor and different virus-receptor interactions between the NHP and the mouse clones.

Acknowledgement

I would like to express my deepest gratitude to my supervisors Professor Jonathan Ball, Dr Patrick McClure, and Dr Richard Urbanowicz whose guidance, advice, and support throughout the course of my study were invaluable. I am immensely grateful for the tutoring and the support that I received from Professor Jonathan Ball each and every step of the way. Many thanks to Dr Patrick McClure and Dr Richard Urbanowicz for guiding me through the molecular and the tissue culture techniques and for sharing their expertise in these areas. I would also like to extend my thanks to all the staff, colleagues, and friends in the Virology Research Group for their help and kindness. Special thanks to Fernando Ruiz and Joshua Duncan for always finding the time to walk me through new assays and experiments.

I would like to thank everyone who provided essential materials and data which constituted the basis of this study including Dr Rachael Tarlinton and Dr Okechukwu Onianwa. I would also like to thank the people who kindly shared important materials and reagents: Professor Kevin Campbell for sharing the Ad5-hLARGE1-EGFP plasmid, Dr Daniel Pinschewer for sharing the KL25 antibody, Dr Melinda Brindley for sharing HAP1-WT/αDG-KO cells, and Dr Steve Winder for sharing KM155-WT/αDG-KO cells.

I am deeply indebted to my mother for her unconditional support and continuous encouragement. Her words were my only solace during hard times and her smile was my only joy during good times. To her I will always be indebted. I am also very thankful to my brothers for always being there for me.

Chapter. 1: General background and introduction

1.1 Arenaviridae

Arenaviridae is a family of *Bunyavirales,* an order that encompasses viral families with segmented single-stranded negative- or ambi-sense RNA genomes (Abudurexiti *et al.*, 2019). The inclusion criteria of the family are: i) enveloped virions with spherical or pleomorphic shape; ii) two segments of single-stranded RNA without 3'-end polyadenylation; iii) complementarity of sequences at the 5'- and 3'-ends; iv) hairpin structure at the intergenic region; v) capped mRNA but not polyadenylated; and vi) induction of asymptomatic chronic infection in natural hosts with viremia and/or viruria (Radoshitzky *et al.*, 2015). Four *Arenaviridae* genera (*Mammarenavirus* in mammals, *Hartmanivirus* and *Reptarenavirus* in reptiles, and *Antennavirus* in fish) and more than 40 species have been identified; the majority of them are mammarenaviruses (Abudurexiti *et al.*, 2019, Radoshitzky *et al.*, 2019). *Mammarenavirus* is further subdivided into Old (OWA) and New World Arenavirus (NWA) based on genetic and antigenic properties and geographical distribution (Bowen *et al.*, 1996b, Rowe *et al.*, 1970). Their geographical distribution reflects that of their natural hosts (rodents), as each mammarenavirus is associated with one or several rodent species (Bowen *et al.*, 1997). Members of the NWA are found in the Americas but mainly in South America. OWAs, on the other hand, are mostly endemic to Africa, in addition to a few Southeast Asian strains **(Table 1-1).** While the majority of mammarenaviruses are non-pathogenic or of unknown pathogenicity to humans, they are considered the genus with the largest number of haemorrhagic fever-causing viruses (Moolla and Weyer, 2020). Viral haemorrhagic fever is characterized by febrile illness and varying degrees of vascular abnormality and is usually associated with high mortality rates (Paessler and Walker, 2013). The NWAs Junín virus, Machupo virus,

Guanarito virus, and Sabia virus cause Argentine, Bolivian, Venezuelan, and Brazilian haemorrhagic fevers, respectively, with high case fatality rates in South American countries. The most significant human pathogen of mammarenavirus, however, is the OWA Lassa virus (LASV) the aetiologic agent of Lassa fever (LF), with estimated annual infections of 100,000 to 300,000 cases and 5000 deaths (CDC, 2022). Cases are mainly reported from West African countries such as Guinea, Liberia, Nigeria, and Sierra Leone. Despite the high human cost, treatment and prophylactic interventions for most arenaviruses are limited.

Table 1-1: Mammarenaviruses distribution, reservoirs, and pathogenicity in humans.

Virus classification and new species in addition to the recent nomenclature of rodent species were adapted from (Abudurexiti *et al.*, 2019) and (Moolla and Weyer, 2020).
*Type species LCMV.

Species	Group	Geographical distribution	Rodent host	Pathogenicity in human	Reference
Allpahuayo virus	NWA	Peru	*Oecomys bicolor and Oecomys paricola*	Unknown	(Moncayo et al., 2001)
Amaparí virus	NWA	Brazil	*Neocomys guianae*	Unknown	(Cajimat et al., 2007)
Chapare virus	NWA	Bolivia	Uncertain	Haemorrhagic fever	(Escalera-Antezana et al.,
Cupixi virus	NWA	Brazil	*Oryzomys megacephalus*	Unknown	(Charrel et al., 2002)
*Dandenong virus**	OWA	Australia	Uncertain	Febrile illness	(Palacios et al., 2008)
Flexal virus	NWA	Brazil	*Nephelomys albigularis,*	Laboratory acquired infection	(Carlton et al., 2012)
Gairo virus	OWA	Tanzania	*Mastomys natalensis*	Unknown	(Gryseels et al., 2015)
Guanarito virus	NWA	Venezuela	*Zygodontomys brevicauda and*	Venezuelan haemorrhagic fever	(Weaver et al., 2000)
Ippy virus	OWA	Central Africa Republic	*Arvicanthis spp*	Unknown	(Swanepoel et al., 1985)
Lassa virus	OWA	West Africa (Guinea, Liberia, Nigeria, and	*Mastomys natalensis*	Lassa fever	(Monath et al., 1974, Mylne et

Latino virus	NWA	Bolivia	*Calomys callosus*	Unknown	(Fernandes et al., 2018)
Loei River virus	OWA	Thailand	*Bandicota savilei*	Unknown	(Blasdell et al., 2016)
Lujo virus	OWA	Zambia, South Africa	Unknown	Haemorrhagic fever (a single outbreak)	(Briese et al., 2009)
Luna virus	OWA	Zambia	*Mastomys natalensis*	Unknown	(Ishii et al., 2012)
Lunk virus	OWA	Zambia	*Mus minutoides*	Unknown	(Ishii et al., 2012)
Lymphocytic choriomeningitis	OWA	Worldwide	*Mus musculus*	Meningitis and systemic infection, congenital	(Armstrong et al., 1940)
Machupo virus	NWA	Bolivia	*Calomys spp.*	Bolivian haemorrhagic fever	(Aguilar et al., 2009)
Mariental virus	OWA	Namibia	*Micaelamys namaquencis*	Unknown	(Witkowski et al., 2015)
Merino Walk virus	OWA	South Africa	*Myotomys unisulcatus*	Unknown	(Palacios et al., 2010)
Mobala virus	OWA	Central African Republic	*Praomys spp.*	Unknown	(Gonzalez et al., 1984)
Mopeia virus	OWA	South and East Africa	*Myotomys unisulcatus,*	Unknown	(Günther et al., 2009)
Okahandja virus	OWA	Namibia	*Micaelamys namaquencis*	Unknown	(Witkowski et al., 2015)
Oliveros virus	NWA	Argentina, Brazil	*Necromys benefactus,*	Unknown	(Mills et al., 2007)
Paraná virus	NWA	Paraguay	*Sooretamys angouya*	Unknown	(Webb et al., 1970)

Pichindé virus	NWA	Colombia	*Nephelomys albigularis*	Unknown	(Trapido and Sanmartín, 1971)
Pirital virus	NWA	Venezuela	*Sigmodon alstoni*	Unknown	(Fulhorst et al., 1997)
Ryukyu virus	OWA	China	*Mus caroli*	Unknown	(Jin et al., 2017)
Sabiá virus	NWA	Brazil	Unknown	Haemorrhagic fever (a single outbreak)	(Ellwanger and Chies, 2017)
Solwezi virus	OWA	Zambia	*Grammomys spp.*	Unknown	(Moolla and Weyer, 2020)
Souris virus	OWA	Cameroon	Unknown	Unknown	(Maes et al., 2018)
Tacaribe virus	NWA	Trinidad, United States	Uncertain	Laboratory-acquired infection	(Cogswell-Hawkinson et al.,
Tamiami virus	NWA	United States	*Sigmodon hispidus, Neotoma spp*	Unknown	(Kosoy et al., 1996)
Wēnzhōu virus	OWA	China, Cambodia	*Rattus spp.*	Unknown	(Blasdell et al., 2016)
Whitewater Arroyo virus	NWA	United States	*Neotoma albigula, Neotoma mexicana*	Non-specific febrile illness	(Cajimat et al., 2008)

1.2 Morphology and structure

Arenaviruses share a common structure and genomic organization (Compans, 1993). They are pleomorphic enveloped viruses with a diameter ranging from 50 to 300 nm and mostly possess bi-segmented genomes **(Figure 1-1).** The envelope shows external projections and internal granules corresponding to the viral glycoprotein complex (GPC) and host cell-derived ribosomes, respectively. This general granular appearance gave the family the prefix Arena- which is derived from the Greek word arenosa (sandy).

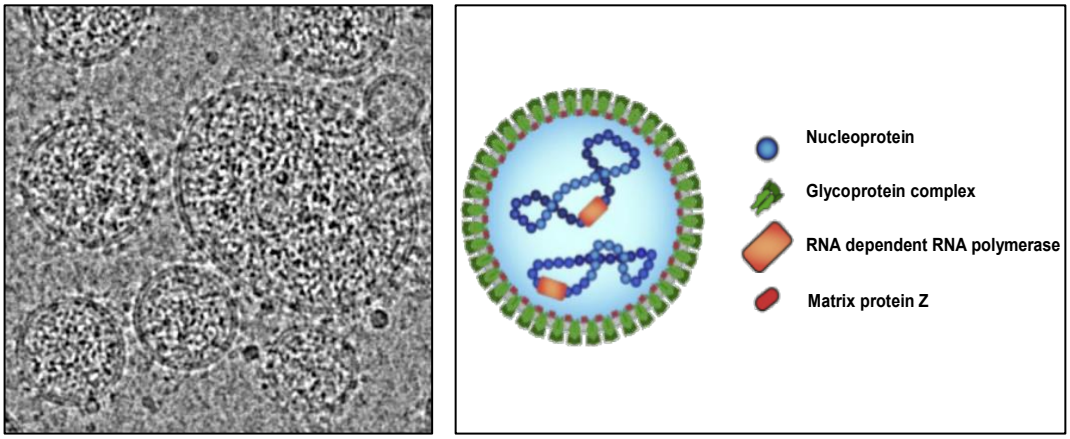


Figure 1-1: Illustration of the common features of Old World arenaviruses.

OWAs share common features which include a bi-segmented genome encapsulated by the nucleoprotein, attached RdRp molecules, and a glycoprotein complex protruding from the matrix. Electron cryomicroscopy image (left) of LCMV virions was adapted from (Neuman *et al.*, 2005). The cartoon (right) was adapted from (Fedeli *et al.*, 2018a).

1.2.1 Genome

Most arenaviruses, except *Antennavirus* which possesses a tri-segmented genome, have bi-segmented single-stranded RNA genomes (Shi *et al.*, 2018, Pontremoli *et al.*, 2019, Vezza *et al.*, 1978). Each segment consists of two

non-overlapping open reading frames arranged in opposite orientations so the 3’ end half is in an anti-sense orientation and the 5’ end is in a sense orientation **(Figure 1-2).** This genomic arrangement is known as ambisense. The short segment (S) is 3.4 kb in size and encodes the GPC (sense) and the nucleoprotein (NP) (anti-sense) (Auperin *et al.*, 1984). The large segment L is 7.2 kb and encodes the RNA-depending RNA polymerase (RdRp) (anti-sense) and the matrix protein Z (sense) (Singh *et al.*, 1987, Salvato *et al.*, 1992). The genes in both segments are separated by non-coding intergenic regions (IGR) that were found to form stable secondary structures that serve as transcription termination signals (López and Franze-Fernández, 2007). The two IGRs are assumed to have distinct functions as the replacement of the IGR of the L segment with that of the S segment resulted in the attenuation of a recombinant LCMV *in vivo* (Iwasaki *et al.*, 2015). The untranslated regions (UTR) in 3' and 5' ends were also found important for the transcription and replication processes. Particularly, the 19 complementary nucleotides at both ends were found to possess promotor activities (López and Franze-Fernández, 2007).

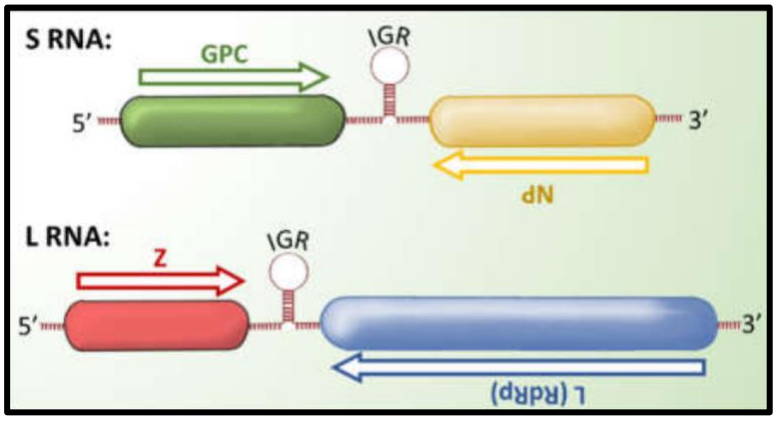


Figure 1-2: Genome organization of arenaviruses.

The S and L segments are depicted showing two non-overlapping open reading frames/each separated by Intergenic regions (IGR). The S segment encodes the GPC (sense) and the NP (anti-sense) genes. The L segment encodes the Z (sense) and the RbRp (anti-sense) genes. Illustration was adapted from (Stott *et al.*, 2020b)

1.2.2 L protein

The L protein (200 kDa) of arenavirus shows RdRp sequence identity (Singh *et al.*, 1987). Specifically, six motifs constitute the core of many negative-strand-RNA virus polymerases including polymerases of rhabdoviruses, orthomyxoviruses, bunyaviruses and paramyxoviruses were identified (Poch *et al.*, 1990, Lukashevich *et al.*, 1997). The structural analysis revealed a high similarity to influenza virus and *Bunyavirus* polymerases (Peng *et al.*, 2020). The protein forms homodimers where each monomer is composed of three functional domains: an N terminal domain, a central catalytic domain, and a C terminal domain. The dimeric form appears to be important for the enzyme as the disruption of the dimeric face interactions resulted in a significant reduction in its activity. The structure analysis of the N terminal domain revealed motifs typical of type II endonucleases (Morin *et al.*, 2010a). It is believed to initiate viral mRNA synthesis by a cap-snatching mechanism which is preceded by the binding of the C terminal domain to host mRNA caps. The central domain is responsible for the replicase/transcriptase activity of L protein and the UTR in the 5' terminus was found to play a role in this switch (Peng *et al.*, 2020). It contains the typical catalytical motifs of viral RdRps in addition to segmented negative-sense RNA virus polymerase-specific motifs. The L protein also displays arenavirus-specific features including an insertion that was found to be important for transcription and replication regulation. It was also found that, unlike some viral polymerases, it is inherently active and does not require binding to viral RNA for activation (Peng *et al.*, 2020).

1.2.3 Nucleoprotein

Arenavirus NP is the most abundant protein in infected cells and viral particles (Strecker *et al.*, 2003). It is 63 kDa in size and oligomerizes to encapsidate the viral genome. NP is essential for transcription and replication as viral RNA encapsidation is a prerequisite for L polymerase activity (Pinschewer *et al.*,

2003a). Two NP functional domains were identified: an N terminal domain involved in the oligomerization and mRNA cap-binding and a C terminal domain that interacts with the Z protein and displays an exonuclease activity (Qi *et al.*, 2010). Its interaction with Z protein was found to play an important role in vRNP packaging in nascent virions (Levingston Macleod *et al.*, 2011). NP was also implicated in arenavirus pathogenicity by inhibiting interferon (IFN) production. This is achieved by its exonuclease activity through the degradation of dsRNAs, a hallmark of viral infection, preventing them from interacting with cellular factors that activate the interferon production pathway.

1.2.4 Z protein

The Z matrix protein belongs to the RING finger protein family with a zinc-finger domain (Salvato *et al.*, 1992). It is the smallest protein encoded by the arenavirus genome with a molecular mass of 11 kDa. Nonetheless, it is essential at multiple points of the virus life cycle (Shao *et al.*, 2018). Similar to other viral matrix proteins, it plays a major role in nascent viral particles assembly and budding through oligomerization (Strecker *et al.*, 2003). It is composed of three domains: a RING domain, an N-terminal domain, and a C-terminal domain responsible for recruiting to, attachment to, and budding from the plasma membrane, respectively (Urata and Yasuda, 2012). The RING domain was also involved in the remodelling of viral gene expression and repressing vRNA synthesis by locking the polymerase-promoter complex in an inactive form (Kranzusch and Whelan, 2011). This in turn is believed to result in the polymerase packaging in virions. Beyond virus morphogenesis, it was found to be involved in host immune response as Z proteins of pathogenic but not non-pathogenic arenaviruses inhibited type I IFN responses (Xing *et al.*, 2015).

1.2.5 Glycoprotein Complex

The glycoprotein complex is the sole antigen on arenavirus surface showing a tripod shape under the electron microscope (Li *et al.*, 2016). It is expressed as a polyprotein precursor that is processed and cleaved by cellular proteases to give three subunits: a stable signal peptide (SSP, amino acids 1-58), a receptor-binding subunit (Gp1, amino acids 59-266), and a transmembrane fusion subunit (Gp2, amino acids 267-498) (Burri *et al.*, 2012, Agnihothram *et al.*, 2007). The three subunits are non-covalently bonded to form monomers of heterotrimers. In mature virions, heterotrimers are further assembled into trimers each consisting of three monomers (Hastie *et al.*, 2017). Some studies, however, suggested that a dimer form of arenavirus GPC might play an important role at some point during the viral life cycle (Hastie *et al.*, 2016).

Stable signal peptide

The structure of the 6 KDa SSP consists of an N terminal conserved myristylation site, two hydrophobic regions separated by a loop, and a C terminal cleavage region (Saunders *et al.*, 2007). It is retained in mature virions and has important functions (Saunders *et al.*, 2007). Cell surface localization of GPC shows that both N and C termini of SSP are located in the cytosol with the internal loop connecting the hydrophobic transmembrane domains interacting with Gp2 ectodomain, hence spanning the membrane twice (Agnihothram *et al.*, 2007). Like other viral signal peptides, SSP of arenaviruses directs the GPC precursor to the endoplasmic reticulum (ER) promoting post-translational modification and trafficking of the complex. Also, it was found to be necessary for the cleavage of Gp1 and Gp2 into two separate subunits. Besides its role in viral morphogenesis, the myristoylated site and the interaction with Gp2 at K33 of SSP were found essential for pH-sensing and fusion.

Glycoprotein 1 subunit

Gp1 is the receptor-binding subunit (44 kDa). Due to its critical role in the early steps of the viral life cycle, the crystal structures of the subunit have been determined for several arenaviruses including the NWAs Machupo virus and Junín virus, in addition to the OWAs LASV and lymphocytic choriomeningitis virus (LCMV) to map the functional domains and identify the structure-function relationship (Hastie *et al.*, 2016, Hastie *et al.*, 2017, Mahmutovic *et al.*, 2015, Bowden *et al.*, 2009). The core structure of the Gp1 prefusion form was found to be conserved between all compared arenaviruses despite a sequence identity of only 20% at the amino acid level in some cases, while the main differences resided in the connecting loops. The structure can be divided into three regions: an N terminal β-strand, an upper β-sheet, and a lower α-helix region **(Figure 1-3. A).** The β-sheet is composed of six antiparallel strands connected by flexible loops. It contains residues important for transferrin receptor 1 (TfR1) binding (the cellular receptor for NWAs) and the lysosomal-associated membrane protein 1 (LAMP1) binding (the endosomal receptor required for LASV membrane fusion). LAMP1 is not required for LCMV entry, but another endosomal receptor (CD164) was found to facilitate membrane fusion of LCMV at acidic pH (Bakkers *et al.*, 2022). The β-sheet face of both viruses (LCMV and LSAV) shows high structural similarity. The pronounced structural differences in this part of Gp1 at neutral pH compared to low pH indicated that conformational changes in this region were required for the membrane fusion in the acidic environment of the late endosome. The lower region is composed of five α-helices and three extended loops. Residues important for the alpha-dystroglycan (α-DG) binding (the cellular receptor of OWAs) are located in this region. Those residues are believed to either directly interact with α-DG or maintain the quaternary structure required for the receptor binding. The residues include leucine or isoleucine at position 260, serine at position 153, tyrosine at position 155, histidine at position 136, and arginine at position 190 of LCMV Gp1 (Hastie *et al.*, 2016).

Although Gp1 is the receptor binding unit and was found in some NWAs to be sufficient for receptor binding, the Gp1 of OWAs alone was insufficient to engage the receptor and the quaternary structure and the presence of Gp2 were necessary for such engagement (Hastie *et al.*, 2016, Abraham *et al.*, 2010). Interestingly, residues important for α-DG binding were all mapped to the trimeric interface of the viral glycoprotein **(Figure 1-3. B)** (Hastie *et al.*, 2017). Additionally, the majority of neutralizing epitopes involve both subunits, emphasizing the critical role of this topology in viral entry (Robinson *et al.*, 2016b). In the monomeric prefusion form, the two subunits interact at several points: the N terminal β-strand of Gp1 interacts with two β-strands in Gp2 forming a β-sheet of three antiparallel strands, the Gp1 interacts with Gp2 heptad repeats at two different points, and the fusion peptide contacts an α-helix in the lower face of Gp1 (Hastie *et al.*, 2016). In the trimeric context, the structure is held together by interactions between helices 1, 2, and 3 of Gp1, the C terminal tail of Gp1, and HR1 of Gp2 of different monomers (Hastie *et al.*, 2017).

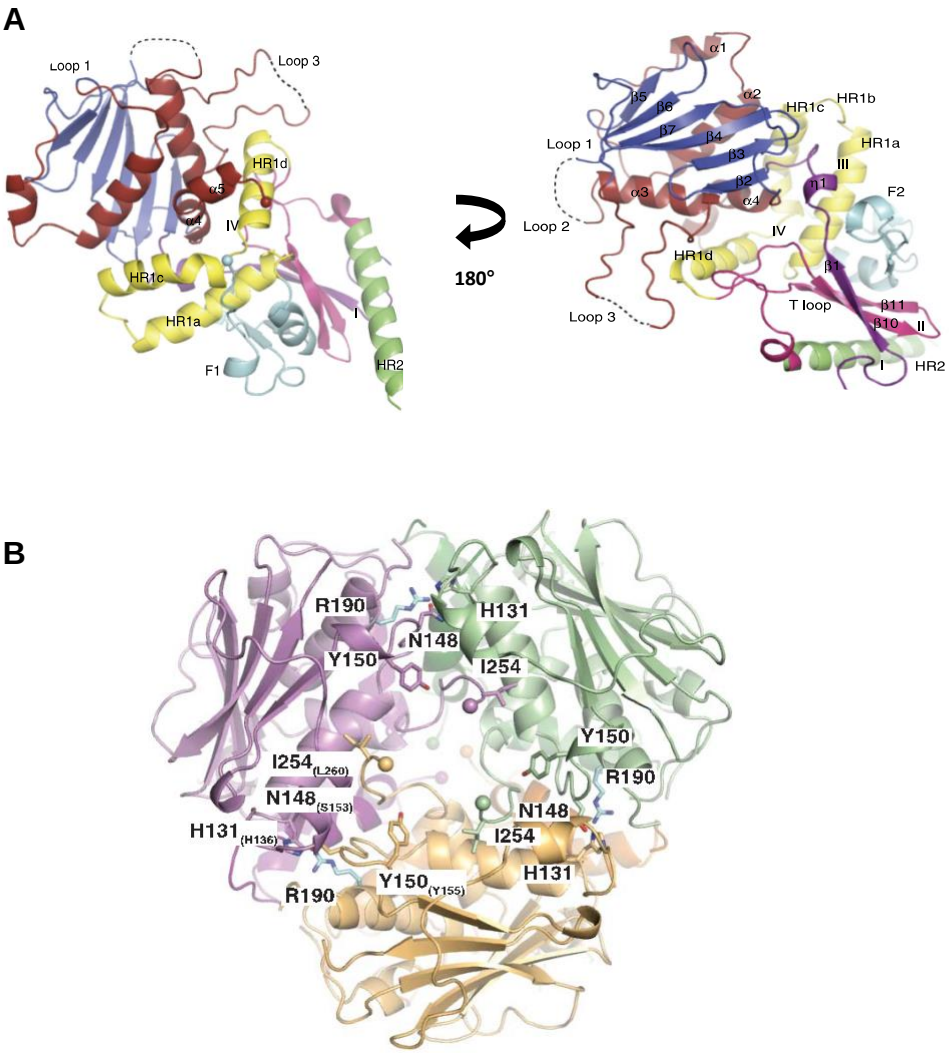


Figure 1-3: OWA GPC structure.

A) LCMV Gp1-Gp2 protomer showing the main structural domains. The Gp1 domains consist of an N-terminal β-strand (purple), an upper β-sheet (blue), and a lower helix-loop surface (red). The Gp2 domains consist of heptad repeat 1 (HR1 in yellow) and heptad repeat 2 (HR2 in green) separated by T loop (pink). The fusion peptide and loop (F1 and F2) are coloured in cyan. **B)** LASV GPC trimer showing the positions of the residues important for α-DG binding. The equivalent residues in LCMV are noted as a subscript. **A** and **B** were adapted from (Hastie *et al.*, 2016) and (Hastie *et al.*, 2017), respectively.

Glycoprotein 2 subunit

The transmembrane fusion protein Gp2 (35 kDa) is highly conserved among mammarenaviruses with 75% amino acid sequence identity (Hastie *et al.*, 2016). The prefusion form of the Gp2 subunit is composed of a fusion region and heptad repeats (HR1 and HR2) (Hastie *et al.*, 2016). Just like most class I fusion proteins, Gp2 of arenaviruses has an N-terminal fusion peptide (F1). Additionally, it contains an internal fusion loop (F2), a feature shared with class II fusion proteins. Another feature in which arenavirus Gp2 deviates from typical class I fusion protein is the lack of a central three-helix core in the prefusion trimeric form (Hastie *et al.*, 2017). The post-fusion structure of Gp2 is substantially different from that at a neutral pH (Igonet *et al.*, 2011). While the prefusion form is a mixture of β-strands and helices, the post-fusion form is strictly helical showing a typical class I type. In this post-fusion form, each protomer adapts a hairpin conformation stabilized by interactions between the N and the C termini and a trimeric structure of three protomers is formed with a central six-helix bundle. The interaction between the N- and C- termini in each protomer ensures that the two membranes (the viral and the target membranes which are associated with the C- and N- termini, respectively) are brought together to initiate the fusion process.

The transmembrane (TM) and cytoplasmic domains (CD) of LCMV Gp2 were found to be essential for GPC biosynthesis and function. The role of the two domains in the processing, trafficking, and incorporation of envelope glycoproteins is well documented for many viruses (Cifuentes-Munoz *et al.*, 2017, Rose and Bergmann, 1983, Dubay *et al.*, 1992, Scolari *et al.*, 2016). Several putative endocytosis and trafficking motifs in the envelope cytoplasmic domain have been identified and were associated with maturation and incorporation into nascent virions (Cifuentes-Munoz *et al.*, 2017, Bhakta *et al.*, 2011). However, for some viruses the CD alone was not sufficient to promote those functions and direct or indirect interactions with the TM were required (Cifuentes-Munoz *et al.*, 2017). Similarly, both domains (TM and CD) were found to be important for the biosynthesis and incorporation of LCMV and

LASV GPC, however, co-dependence was not observed (Sommerstein *et al.*, 2014, Kunz *et al.*, 2003, Willard *et al.*, 2018). Additionally, cleavage of LCMV GPC, which is largely dependent on intact TM and CD, was found to be a prerequisite for incorporation as only cleaved GPC were observed in viral particles. In particular, residues 462 to 498 of LCMV CD were found necessary for cleavage and hence incorporation and production of infectious particles (Kunz *et al.*, 2003).

Besides their role in the biosynthesis and maturation of GPC, there is evidence that the TM and CD are integral to LCMV and LASV Gp2 functions. In a comprehensive mutational study to map key residues in LASV Gp2, residues important for fusion resided mainly in the fusion peptide and loop or the heptad repeats (Willard *et al.*, 2018). However, a couple of mutations one in the TM (465 LASV numbering) and the other in CD (448 LASV numbering) were not associated with defective production, cleavability, or trafficking, yet pseudotypes carrying these mutations were non-infectious. Another study found that the F446L mutation located in the TM of LASV GPC was associated with a reduction in the pH threshold at which the fusion occurred (Guo *et al.*, 2020). It was also proposed that the CD of LCMV Gp2 had a role in its pathogenicity. An *in vivo* study found that an increase in persistence and viral load were associated with elements in the LCMV Gp2 cytoplasmic tail (Sommerstein *et al.*, 2014).

Residues in Gp2 were also tested for their effect on α-DG binding. LCMV Gp1 alone was found to be unable to bind α-DG and the presence of Gp2 was necessary for this binding (Hastie *et al.*, 2016). Thus, it was proposed that residues in Gp2 might be critical for α-DG binding. However, in a panel of 39 constructs carrying mutations spanning the LASV Gp2 subunit including the TM and CD, the infectivity was unaffected by α-DG as the KO and WT cells showed comparable infectivity (Willard *et al.*, 2018). Also, a LASV mutant that showed an increased fusion, was inhibited by blocking α-DG in a similar way to the WT indicating that the mutation had no effect on α-DG binding (Guo *et*

al., 2020). Altogether, the findings of these studies suggest that residues of Gp2, at least for LASV, are unlikely to affect α-DG binding and the requirement for Gp2 could be sequence-independent.

N-linked glycans of GPC

The glycoproteins of arenaviruses are shielded by an intensive network of N-linked glycans **(Figure 1-4)** (Watanabe *et al.*, 2018, Sommerstein *et al.*, 2015). This was seen as a reduction of the native molecular masses of Gp1 and Gp2 by around 30% following PNgase F treatment. There are 11 glycosylated sites in LASV GPC (nine in LCMV GPC), seven in Gp1 (six in LCMV Gp1) and four in Gp2. The analysis of the composition of the glycans in LASV GPC showed a high percentage of oligomannose-type glycans, but also hybrid and highly processed complex glycans were observed. Functions including cleavage of GPC, virus interaction with cell surface attachment factors, and even virus viability have been documented for arenavirus glycans (Goncalves *et al.*, 2013, Bonhomme *et al.*, 2011, Bonhomme *et al.*, 2013). Importantly, glycans of arenavirus GPC play a key role in immune escape and neutralizing antibody evasion. The next section sheds more light on the role of GPC glycans in immune evasion and in shaping the antigenicity of OWAs.

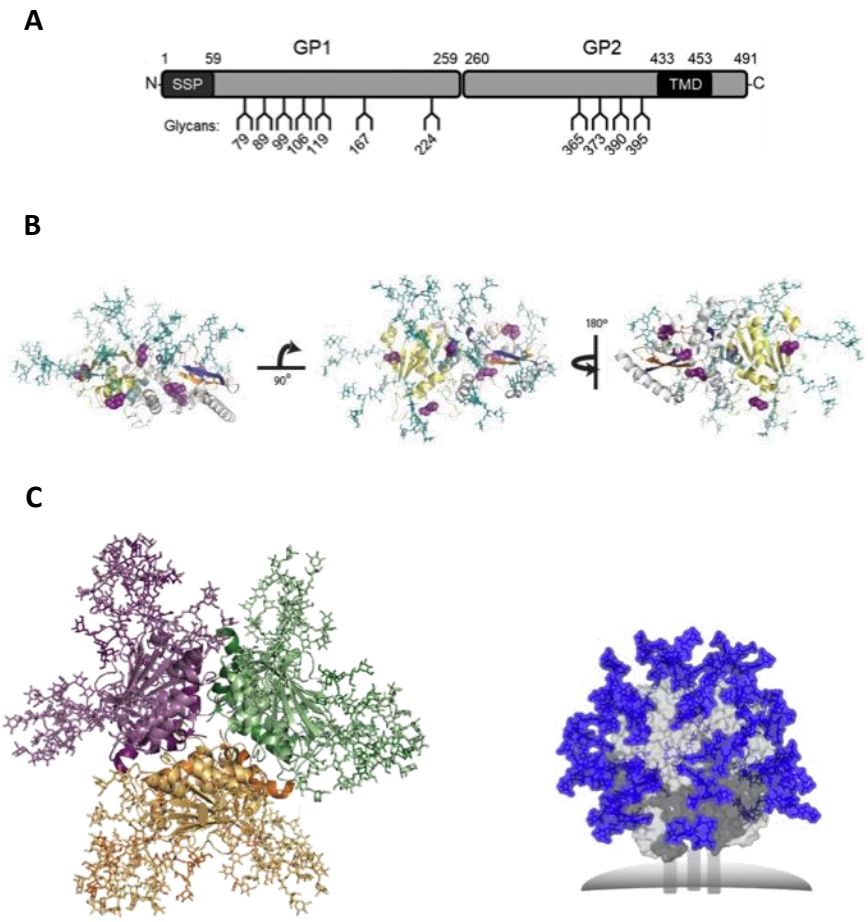


Figure 1-4: Putative N-linked glycan sites of LASV GPC.

A) Linear depiction of GPC showing the positions of the N-linked glycans and their distribution in Gp1 and Gp2 subunits. **B)** View of the glycan shield (sticks) in the monomeric form of LASV GPC. **(C)** The area covered by the glycans and the area left exposed in the context of LASV GPC trimer, upper view (left) and side view (right). Structures were adapted from (Watanabe *et al.*, 2019) and (Hastie *et al.*, 2017).

1.3 Immunogenicity and antigenicity

OWAs infections were found to be mostly controlled by CTL while humoral responses were found inefficient. The weak Ab responses were attributed to both poor induction and maturation (Eschli *et al.*, 2007). The former is believed to be a result of early control of viremia by CTL responses and the latter is due to the CTL-mediated destruction of lymphoid tissue. However, other studies

showed sufficient antibody induction later during infection but of poor affinity and neutralizing ability (Sommerstein *et al.*, 2015). It was also found that induction correlated with the number of GPC glycans as the OWAs with fewer glycans and the removal of some glycans from the highly glycosylated LASV GPC induced better responses compared to the WT LASV GPC. Additionally, the addition of the missing LASV glycans to LCMV resulted in a reduction of these responses. Furthermore, the antibody response induced by the fully glycosylated GPC predominantly neutralized non-glycosylated GPC (Sommerstein *et al.*, 2015). Taken together, the poor humoral responses seen in OWAs infections are not just due to generalized immunosuppression but also due to glycan-mediated immune evasion. It was indeed found that the major antigenic sites targeted by neutralizing and non-neutralizing Abs fall in gaps in the glycan shield (Robinson *et al.*, 2016b, Watanabe *et al.*, 2018). Immune-escape mutations were associated with these antigenic sites and together with other predicted B cell epitopes are enriched with non-synonymous mutations (Watanabe *et al.*, 2018, Andersen *et al.*, 2015).

Four and three antigenic sites were found in Gp1 and Gp2 of LCMV, respectively. A subset of them was strain-specific (Parekh and Buchmeier, 1986). The fourth site, for example, was found exclusively in LCMV Arm strain and Abs targeted this site did not cross-react with other strains. The monoclonal Abs from LF survivors were also tested and their epitopes were mapped (Robinson *et al.*, 2016b). Most mAbs especially the neutralizing mAbs (7 out of 11) also cross-reacted with LCMV confirming the antigenic similarity between LASV and LCMV. Neutralizing mAbs targeted four epitopes one in Gp1 (named GP1-A) and three required both Gp1 and Gp2 (named GPC-A, GPC-B and GPC-C). Gp1-A (amino acids 115 to 122 LCMV numbering) was also found to be a major antigenic site for neutralizing mouse mAbs (Seiler *et al.*, 1999, Sommerstein *et al.*, 2015). Specifically, the mouse KL25 Ab targets this epitope and an immune-escape mutation was associated with abolished reactivity (Seiler *et al.*, 1999). Additionally, an N-linked glycan at position 124 altered KL25 affinity as the removal of this glycan significantly reduced the

half-maximal inhibitory concertation (IC50) emphasizing the role of glycans in immune evasion (Sommerstein *et al.*, 2015).

1.4 Genetic diversity of OWAs

Although re-assortments are a major source of diversity in some viruses with segmented genomes such as influenza viruses, re-assortment was rarely observed in natural infections of arenavirus (Andersen *et al.*, 2015). Recombination events are believed to also be rare as evidence of such events was only seen in two NWAs (Archer and Rico-Hesse, 2002, Charrel *et al.*, 2001). Hence arenavirus diversity seems to be mainly driven by the high mutation rate due to the error-prone RdRp. The estimated substitution rates are $3.3X10^{-4}$ and $3.7X10^{-4}$ substitution/site/year for the S and the L segments of LCMV, respectively, which are comparable with other RNA viruses (Albariño *et al.*, 2010, Bird *et al.*, 2008). The rate for LASV which was derived from a partial region of the NP gene was estimated to be 7-$11X10^{-4}$ sub/site/year (Fichet-Calvet *et al.*, 2016). The intra-host evolution was also assessed for LASV and showed a substitution rate of $2.1X10^{-3}$ sub/site/year from full genome analysis of samples from human LF cases (Andersen *et al.*, 2015). Nevertheless, arenavirus was found to evolve mainly under purifying selection (e.g. ~0.2 dNs/dS ratio in LASV), except for the L segment in which evidence of positive selection was detected at multiple sites (Forni *et al.*, 2018, Pontremoli *et al.*, 2017, Andersen *et al.*, 2015). Indeed, the nucleotide divergence of the L segment was found to be higher than that of the S segment for both LASV (32% and 25%, respectively) and LCMV strains (25% and 18%, respectively). At the level of individual genes, the diversity of the GPC was frequently analysed (Amanat *et al.*, 2018, Andersen *et al.*, 2015, Watanabe *et al.*, 2018). The analysis revealed the accumulation of non-synonymous mutations significantly higher than expected at antibody-accessible sites and B-cell epitopes (Watanabe *et al.*, 2018, Andersen *et al.*, 2015). It also showed that the Gp1 subunit is more diverse than Gp2 which

showed %75 conservation across very diverse arenaviruses (Amanat *et al.*, 2018, Hastie *et al.*, 2016).

The phylogeny of mammarenavirus has been frequently analyzed. Based on both the L and S segments, LCMV was assigned to four lineages (I to IV) with most strains belonging to lineage I including all lab strains (Albariño *et al.*, 2010). Strains of lineage I are widely distributed with a poor genetic-geographic association (isolates from the same geographic areas do not cluster together). Lineages II and IV are confined to Europe, while lineage III is composed of one member that was isolated in the United States. LASV strains also fall into four established lineages that originated from Nigeria and spread throughout West Africa. Lineages I, II, and III were isolated in Nigeria, while strains of lineage IV were isolated from Guinea, Liberia, and Ivory Coast, but mostly in Sierra Leone (Andersen *et al.*, 2015). Additional three LASV lineages (V, VI, and VII) were proposed and were isolated from Mali and Ivory Coast, Nigeria, and Togo, respectively (Olayemi *et al.*, 2016, Whitmer *et al.*, 2018, Manning *et al.*, 2015, Ibukun, 2020). Unlike LCMV, a clear geographic correlation has been established for LASV. This correlation is evident in the position of the Nigerian strains basal to the out-of-Nigeria strains and with larger root-to-tip distances of the latter. NWAs have also been classified into four clades A, B, C, and D (or A recombinant) mostly found in South America but also North America (Forni *et al.*, 2018, Sarute and Ross, 2017, Bowen *et al.*, 1996b). The estimated within-group genetic distances are higher in NWA compared to OWA (Charrel *et al.*, 2008, Bowen *et al.*, 1997). Nonetheless, the OWA LASV showed uniquely high between-strains diversity with ~30% and ~25% nucleotide variation in L and S segments, respectively (Andersen *et al.*, 2015). This is much higher than what has been reported for other RNA viruses such as EBOV which showed more than 97% conservation between different strains (Andersen *et al.*, 2015).

Despite the high diversity that was found between some strains isolated from the same rodent species (e.g. LASV strains), the diversity of arenavirus has been in part attributed to its host specificity. *Murinae* and *Sigmodontiae*

subfamilies of the order *Rodentia* are the hosts of OWAs and NWAs, respectively, with each virus associated with a certain or few species (Bowen *et al.*, 1997, Forni *et al.*, 2018). It has been postulated that this host specificity is a result of rodent-virus coevolution based on several observations where the arenaviruses' phylogeny mirrored that of their rodent hosts (Bowen *et al.*, 1996a, Bowen *et al.*, 1997). For example, the NWAs Latino virus and Oliveros virus are monophylogenetic as well as their rodent hosts *Calomys* and *Bolomys*, respectively. Flexal virus, Paraná virus, and Pichindé virus, also NWAs, are monophyletic and all are exclusively found in *Oryzomys* species. Additionally, the distance between LCMV and NWAs is reflected in the distance between their hosts (*Mus musculus* and *Sigmonitdea*, respectively). However, different arenaviruses were detected in the same rodent species, and vice versa. LASV for instance, which is mostly associated with *M. natalysis,* was also detected in several *Mystomus* species and other rodent genera (Olayemi *et al.*, 2016, Fichet-Calvet *et al.*, 2014b). On the other hand, *M. natalysis* was found to be the host for relatively distant arenaviruses (Gryseels *et al.*, 2015, Gryseels *et al.*, 2017). Furthermore, the time of the most recent common ancestor (tMRCA) of mammarenavirus was estimated to be ~ 16,000 years ago which is inconsistent with their rodent hosts' tMRCA (~20 million years ago) (Forni *et al.*, 2018). While the tMRCA of RNA viruses is often underestimated, given the other observations, it is likely that co-evolution is not the sole explanation of the host specificity and a combination of co-evolution and host switch with subsequent adaptation may have occurred.

1.5 Pathogenicity and epidemiology

Arenaviruses mostly cause persistent asymptomatic infections in their natural host with life-long shedding of the virus (Traub, 1939). The dynamics of natural arenavirus infections in wild rodents, however, have not been well studied. Most of the current knowledge regarding arenavirus pathogenicity in the natural host was derived from lab-induced infections of inbred lab rodents. In

those animal model experiments, different arenaviruses showed similar outcomes in their corresponding hosts mediated mainly by cytotoxic T lymphocyte response of $CD8^{+}$T (Oldstone, 2002, Webb *et al.*, 1975, Flatz *et al.*, 2010, Borrow *et al.*, 1991, Walker *et al.*, 1975). The animals either mounted good immune responses and cleared the virus (acute), acquired life-long infections and shedding of the virus with immunosuppression (chronic), or developed immunopathology and died.

Many variables were found to affect the outcome including viral and host factors. Different viral strains can lead to completely different outcomes. Cl13 and Arm strains of LCMV, for instance, which are only two amino acids different cause chronic and acute infections, respectively (Borrow *et al.*, 1991, Sevilla *et al.*, 2000b). The same strain can also lead to different outcomes depending on host genetic factors as mice with certain genetic backgrounds develop high immune responses and death even when infected with Cl13 (Oldstone *et al.*, 2018). Interestingly, an individualized immune response was reported despite similar virus strain and host genetics (Kräutler *et al.*, 2020). This observation was independent of age which is usually a key player in determining the outcome of arenavirus infections. Mice infected neonatally tend to develop persistence and chronic infections, while acute infections are usually associated with adulthood (Gilden *et al.*, 1972). Infections are believed to be mainly acquired neonatally in nature as a significant inverse correlation was found between age and vRNA detection in wild mice (Fichet-Calvet *et al.*, 2014a, Benny Borremans, 2011). Other factors including dose and route of inoculation also affected the course of infection. High dosage was associated with chronicity, while low dosage resulted in clearance (Cornberg *et al.*, 2013). Different routes of inoculation also resulted in different disease manifestations ranging from asymptomatic to weight loss, reduced fertility, organ enlargement, respiratory failure, and brain inhernation (Hotchin and Benson, 1963, Matullo *et al.*, 2010, Seamer, 1965, Armstrong *et al.*, 1940). For example, subcutaneous inoculation was mostly associated with asymptomatic infections while other routes including intracerebral, intraperitoneal,

intravenous, and footpad inoculations were associated with one or more symptoms.

Human and non-human primate (NHP) arenavirus infections are believed to be acquired through multiple independent rodent-to-human/NHP transmissions by coming in contact with rodent excreta, while human-to-human transmission was found to be uncommon (Andersen *et al.*, 2015, Montali *et al.*, 1993). Human-to-human transmission mostly occurred nosocomially and the majority of index cases reported rodent exposure. Rodent-to-primate transmission as the main cause of arenavirus emergence was also inferred from phylogenetic analysis of LASV sequences derived from LF cases and rodents of the same geographical area (Andersen *et al.*, 2015). Human-to-human transmission is expected to result in human-specific lineages and separate clustering of human and rodent sequences. Instead, the analysis showed intermingling of human and rodent sequences. Additionally, a correlation between the date of sample collection and root-to-tip distance is expected in human-to-human transmission but the analysis showed an absence of such correlation.

The first arenavirus infection in primates and the first arenavirus ever identified was documented in 1933 as a result of a monkey-to-monkey passage of material from a fatal human Saint Louis encephalitis case (Armstrong and Lillie, 1934). Infections in those monkeys were characterized by fever and loss of appetite and weight. The virus isolated was found to be distinct from the virus used for the initial inoculation and subsequently named LCMV. It is unclear whether the source of the virus was the SLE subject or the NHPs themselves. Since the 1980s, several fatal LCMV outbreaks in NHPs took place in zoos mainly in the United States but also in Europe (Montali *et al.*, 1993, Montali *et al.*, 1995, Asper *et al.*, 2001). Those natural outbreaks mainly occurred in the new world monkeys of the *Callitrichidae* family and prior exposure to mice was frequently reported. The infections were characterized mainly by intensive liver damage (Callitrichid Hepatitis) but also renal failure,

enlargement of lymph nodes, pulmonary oedema, and encephalitis. Clinical signs included: fever, general weakness, ataxia, anorexia, and seizures.

In humans, LCMV is mostly asymptomatic or causes mild flu-like symptoms (Biggar *et al.*, 1975, Baum *et al.*, 1966). LCMV infections were detected worldwide and exposure to rodents has been frequently documented **(Figure 1-5. B)** (Biggar *et al.*, 1975, Vilibic-Cavlek *et al.*, 2021). In a minority of cases, the virus can cause serious illnesses such as meningitis (Biggar *et al.*, 1975, Barton and Hyndman, 2000). Symptoms included fever, headache, vomiting, photophobia, and confusion. The virus can also be transmitted prenatally causing life-threatening defects and high mortality rates (30%) (Barton *et al.*, 2002, Wright *et al.*, 1997). The most frequent symptoms in infected newborns are macrocephaly and ocular abnormality. Surviving infants usually develop impaired vision, hearing loss, mental retardation, and/or cardiopathology. More recently, LCMV was suggested as the main aetiology of Sudden Infant Death Syndrome (SIDS) (Goldwater, 2022). Moreover, deadly LCMV infections were reported in solid organ transplant patients (Fischer *et al.*, 2006, Macneil *et al.*, 2012). Recipients of organs including kidneys, lungs, and liver from common donors experienced fever, diarrhoea, respiratory failure, abdominal pain, central nervous system symptoms, and eventually death.

Arenaviruses in humans, however, are mostly known for their haemorrhagic fever (HF) outbreaks **(Figure 1-5. A)**. The first of such outbreaks to be reported was in 1958 in Argentina caused by the NWA Junín virus (Enria and Oro, 2002, Enria *et al.*, 2008, Greenway *et al.*, 1959). Before the introduction of Candid #1 vaccine in the 1990s to high-risk groups, the virus had been responsible for outbreaks ranging from 300 to 1000 cases annually with a 15-30% case fatality rate (CFR) (Enria *et al.*, 2008). Separate HF outbreaks followed and continue to occur in Bolivia, Venezuela, and Brazil with Machupo and Chapare, Guanarito, and Sabia NWAs as aetiologic agents, respectively, and CFRs as high as 60% (Escalera-Antezana *et al.*, 2020, Aguilar *et al.*, 2009, Salas *et al.*, 1991, Sarute and Ross, 2017, Ellwanger and Chies, 2017). An outbreak in

North America between 1999 and 2000 was also suspected to be caused by the NWA Whitewater Arroyo virus (Enserink, 2000). All pathogenic NWAs belong to clade B and share common clinical manifestations. The most frequent manifestations include fever, headache, myalgia, dehydration, tremors, diarrhoea, vomiting, and mucosal membrane haemorrhage, especially in the upper digestive tract (Escalera-Antezana *et al.*, 2020, Aguilar *et al.*, 2009, Salas *et al.*, 1991, Sarute and Ross, 2017, Ellwanger and Chies, 2017).

Although fewer members of OWA cause HF, they are associated with the highest CFR (LUJV) and the highest incidence (LASV). LUJV was first recognized in 2008 in a nosocomial outbreak in Johannesburg, South Africa (Sewlall *et al.*, 2014). The index case had acquired the infection in Zambia where she resided and was subsequently evacuated to Johannesburg. She presented with a severe illness that spread to four other medical staff. Of the five cases, only one survived making LUJV the arenavirus with the highest CFR (80%). Perhaps the most significant arenavirus to human health, however, is LASV due to its endemicity and high incidence with no effective therapy or licensed vaccine. Unlike the sporadic nature of most arenaviruses, LASV has been yearly and at constant rates causing outbreaks in countries of West Africa. The first LASV case was described in 1969 in Lassa village in northern Nigeria (Pinneo and Pinneo, 1971). In the early 1970s, LF outbreaks spread to other West African countries such as Guinea, Liberia and Sierra Leone (Monath *et al.*, 1973, Monath, 2019, Fraser *et al.*, 1974, Mylne *et al.*, 2015). The outbreaks continue to happen annually, particularly in Nigeria and SL with a peak in reported cases in the dry season (December to March) (Okokhere *et al.*, 2018, Asogun *et al.*, 2012, Shehu *et al.*, 2018, Shaffer *et al.*, 2014). From 3 to 30 January 2022, 211 confirmed cases were reported from Nigeria with 19% CFR (WHO, 2022a). This was higher than what was reported in 2021 (54 confirmed cases) and lower than in 2020 (472 confirmed cases) for the same time period with ~20% and 15% CFR, respectively (WHO, 2020, WHO, 2022a). The total number of annual LASV cases from all West African

countries, however, is believed to be much higher than the official numbers due to underreporting of cases with mild symptoms. Indeed, some reports estimated annual cases to be between 100,000 and 300,000 with 1 out of 5 cases showing symptoms (WHO, 2022b, McCormick *et al.*, 1987b). This was also indicated in studies of LASV seroprevalence in some rural areas in Nigeria and Mali where up to 58% of tested people were seropositive (Sogoba *et al.*, 2016, Tobin *et al.*, 2015). Like other arenavirus HF, severe illness manifests as haemorrhage from mucosal membranes due to platelets dysfunction and multiorgan failure (Macher and Wolfe, 2006, McCormick *et al.*, 1987a, Fisher-Hoch *et al.*, 1988). Additionally, long-term LF is associated with 20% deafness in recovered patients (Cummins *et al.*, 1990).

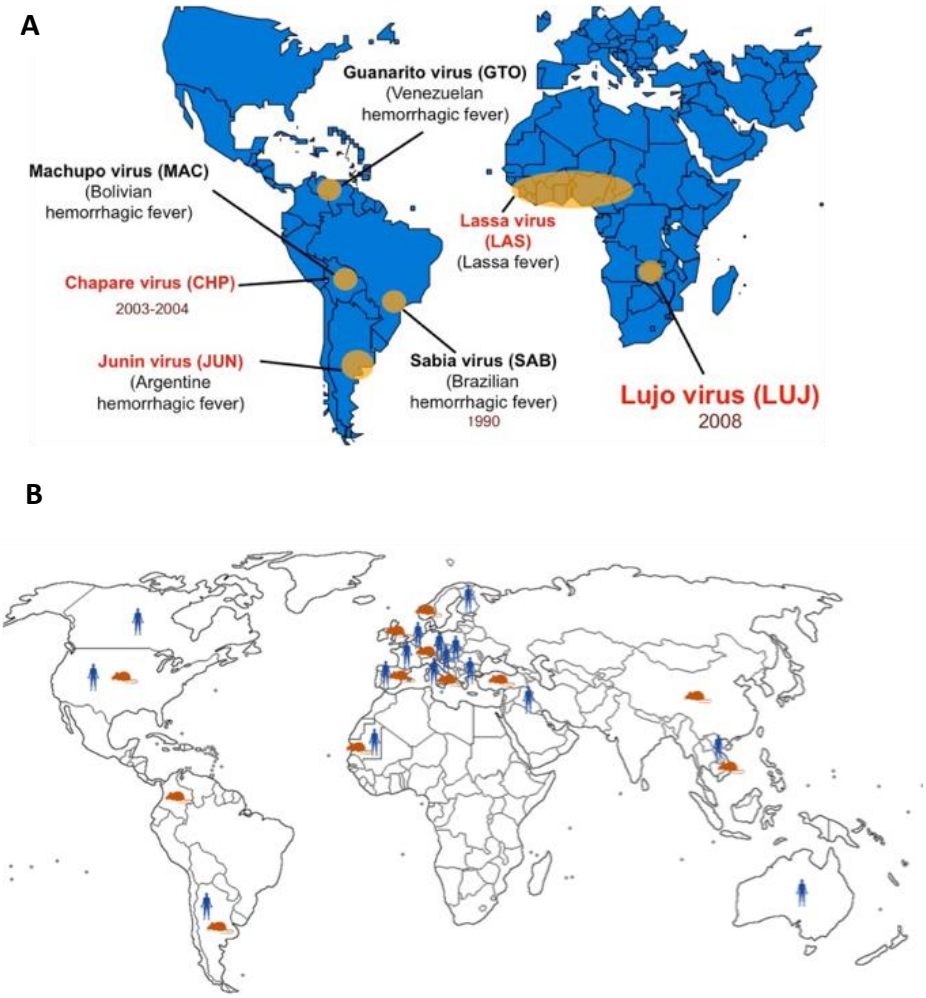


Figure 1-5: Global map of arenavirus outbreaks

A) Arenavirus haemorrhagic fever outbreaks. The locations of haemorrhagic fever outbreaks caused by members of NWA and OWA are shown. Image was adapted from (Tani, 2014). **B)** The worldwide distribution of LCMV infections in humans is shown together with the reservoir host (house mouse) distribution. Image was adapted from (Vilibic-Cavlek *et al.*, 2021).

1.6 Treatment

Despite the human health burden of arenaviruses, current treatment and prophylactic options are limited. Arenavirus HF cases are usually treated with the nucleoside analogue ribavirin which in the case of LF is only effective when administered early during the course of the infection (Alli *et al.*, 2021, Salam *et al.*, 2021, McCormick *et al.*, 1986). A CFR of 26-47% was observed among patients treated with ribavirin after the sixth day of the onset of fever compared

to 5-9% on the sixth day or before. Similarly, CFR decreased from 33.3% to 12.5% in ribavirin-treated AHF (Enria and Maiztegui, 1994). In addition to the time-dependent outcome of ribavirin, adverse effects such as anaemia may occur in treated patients (McCormick *et al.*, 1986, Enria *et al.*, 1987). A recent re-evaluation of the studies supporting the use of ribavirin for LF, however, argued against its efficacy and raised a concern about the method used in those studies. It was also concluded that the drug can increase mortality in some cases (Salam *et al.*, 2021).

Convalescent sera were also found to be effective in treating AHF with a ~15 % reduction in CFR (Maiztegui *et al.*, 1979). It was, however, found to be ineffective in treating LF patients a finding that was attributed to the poor humoral response induced by LASV as opposed to JUNV (McCormick *et al.*, 1986, Jahrling and Peters, 1984). The role of the humoral response in the success of plasma treatment in AHF was also indicated in the correlation between the antibody titres in the plasma and the survival rates (Enria *et al.*, 1984). Nonetheless, ~10% of recovered patients developed late neurological symptoms after plasma treatment (Maiztegui *et al.*, 1979).

The adverse effects of the available treatments in addition to their low efficacy in some cases rendered the development of arenavirus vaccines a high priority by the WHO particularly for LASV. Unlike JUNV, a highly virulent NWA with high incidence, for which a licensed vaccine has been developed to immunize high-risk groups, no licensed LASV vaccine is available at the moment (Maiztegui *et al.*, 1998). 34 LASV vaccine candidates are currently under trial and only four progressed to clinical trials (Salami *et al.*, 2019, Isaac *et al.*, 2022). Two of them are particularly promising: rVSV∆G/LASVGPC and MV-LASV. The rVSV∆G/LASVGPC is a recombinant replication-competent VSV/LASV virus produced by the replacement of VSV G with LASV GPC (Cross *et al.*, 2022). The MV-LASV is an attenuated measles virus expressing LASV GPC and NP (Mateo *et al.*, 2021). However, all candidates were associated with one or more caveats including induction of non-sterilizing

immunity, the requirement of multiple doses, strain specificity, pre-existing immunity, and high technology requirement (e.g. electroporation) (Salami *et al.*, 2019, Murphy and Ly, 2022).

1.7 Life cycle

Targeting virus-specific processes with antiviral therapies is an attractive strategy to minimize adverse effects and toxicity. A treatment regimen for HIV, for example, usually consists of a combination of antivirals targeting specific steps in the virus life cycle including reverse transcription, integration, and viral maturation (Lv *et al.*, 2015, Zhuang *et al.*, 2019, Cihlar and Ray, 2010). For this purpose, a thorough understanding of the virus life cycle is instrumental. The development of vaccines also relays on the understanding of the early steps of the virus life cycle. Failure of some vaccine trials, for example, has been attributed in the past to poor understanding of viral entry and receptor-binding sites (Cui *et al.*, 2008, Hsu *et al.*, 2001).

The life cycle of arenaviruses is confined to the cytosol. Following attachment to a cellular receptor, they undergo an unusual endocytotic pathway to deliver their genome to the cytoplasm where expression/replication occurs. Replication of the viral genome is preceded by an early transcription to express necessary replication elements. Other structural components are produced in a late transcription step followed by maturation, assembly, and egress. Multiple cellular factors were found to contribute to different steps of the arenavirus life cycle and in a virus- and cell-type-depending manner (**Figure 1-6** summarizes the arenavirus life cycle).

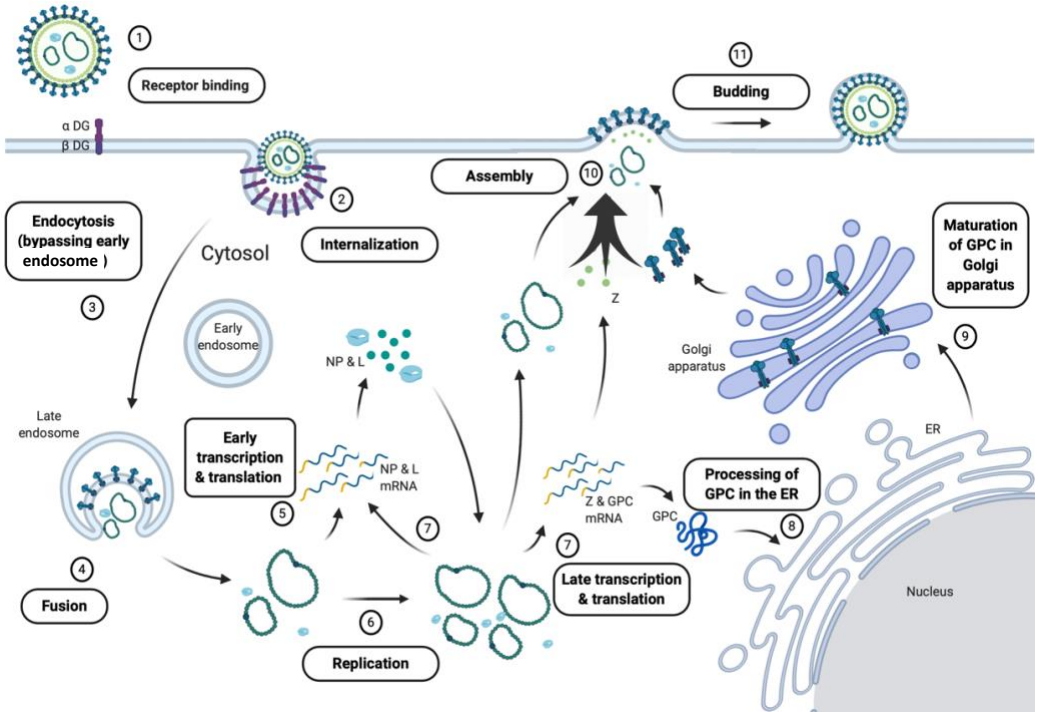


Figure 1-6: The life cycle of OWAs.

The image illustrates the steps in the OWAs life cycle from receptor binding to budding. Following receptor binding, the virus is internalized via an endocytotic pathway where fusion takes place at the late endosome. Early transcription/translation produces the components necessary for replication. Late transcription/translation produces structural components. GPC maturation then takes place in the ER and Golgi. All components are then transported to the plasma membrane for assembly and budding. Image created with **BioRender.com**.

1.7.1 Entry

Virus entry to target cells is initiated by binding to cell surface receptor/attachment factors. OWAs and NWAs enter cells via distinct receptors. While LASV and LCMV strains, in addition to clade C of NWA, use α-DG as a primary receptor, pathogenic NWAs use TFN1 (Cao *et al.*, 1998b, Radoshitzky *et al.*, 2007). The receptor usage within each group can also vary as LUJV, an OWA, enters cells in α-DG-independent manner using neuropilin 2 (NRP2) and CD63 as host factors (Raaben *et al.*, 2017). Even for each virus, cellular factors can differ depending on the cell type indicating redundancy in arenavirus tropism. LASV, for example, efficiently infects epithelial cells,

macrophages, dendritic cells (DC), liver cells, and endothelial cells (Fedeli *et al.*, 2018b, Goncalves *et al.*, 2013, Schlie *et al.*, 2010, Dylla *et al.*, 2008, Flatz *et al.*, 2010). Similarly, LCMV can infect a wide variety of human cell lines. LASV/LCMV engage the mitraglycan polysaccharide on the surface of α-DG and the length of this glycan determines the virus binding affinity (Hara *et al.*, 2011, Kunz *et al.*, 2005). In cells where α-DG is underglycosylated such as in liver and endothelial cells, LASV is believed to use alternative receptors for entry (Fedeli *et al.*, 2018b, Brouillette *et al.*, 2018).

α-DG recognition by LASV/LCMV was found to highly resemble that of its natural ligands (the extra-cellular matrix laminins), however, the following uptake process is believed to be distinct (Rojek *et al.*, 2007). Upon binding, the cytosolic subunit of the receptor (β-DG) is triggered releasing its attachment to the adaptor protein utrophin which anchors the receptor to the cytoskeleton (Moraz *et al.*, 2013). This in turn leads to the internalization of the virus-receptor complex which is believed to deviate from the normal internalization of the receptor and that the virus manipulates the process to its requirements. The endocytosis of LASV/LCMV takes an unusual pathway which is clathrin-, caveolar-, and dynamin-independent (Oppliger *et al.*, 2016, Rojek *et al.*, 2008, Kunz, 2009). It also does not require Rab5 or Rab7, factors involved in trafficking to and from early endosomes, respectively. This finding, together with the remarkably low pH requirement for fusion, indicates the bypassing of the early endosome and fusion at late endosome compartments. Delivery to late endosomes was also found to be independent of actin but requires microtubular transport to Multi-Vesicular Bodies (MVB) with multiple Endosomal Sorting Complex Required for Transport (ESCRT) proteins involvement (Pasqual *et al.*, 2011, Rojek *et al.*, 2008). The pathway is sensitive to cholesterol depletion and may involve macropinocytosis (Vela *et al.*, 2007, Oppliger *et al.*, 2016). Apoptotic mimicry was also suggested as AxI, which was identified as an alternative receptor for LASV, is involved in apoptosis (Fedeli *et al.*, 2018b).

Like other enveloped viruses, delivery of the arenavirus genome to the cytosol is achieved via membrane fusion. The membrane fusion is mediated by the Gp2 subunit and is triggered by the low pH in the late endosome that disassociates the glycoprotein freeing Gp2 from the complex. pH-induced conformational changes in Gp1 were found to be necessary for this disassociation which involved a histidine triad conserved among OWAs (Hastie *et al.*, 2017). LASV then undergoes receptor switching and binds Lamp1 and the histidine triad is critical for this binding. Although dispensable for LASV infection, Lamp1 promotes membrane fusion at a significantly lower pH (Cohen-Dvashi *et al.*, 2015, Hulseberg *et al.*, 2018). On the other hand, the entry of other OWAs including LCMV is not affected by Lamp1 (Israeli *et al.*, 2017, Hulseberg *et al.*, 2018). Another endosomal receptor (CD146) was proposed for LCMV to facilitate membrane fusion (Bakkers *et al.*, 2022).

1.7.2 Gene expression and replication

Viruses with ambisense genomes follow a negative sense transcription strategy despite the existence of both sense and antisense strands in genome segments (Nguyen and Haenni, 2003). That is, the replication-intermediate antigenomic RNA has to be synthesized first to serve as a template for mRNA production for the genes in the sense orientation. On the other hand, transcripts are directly made from the antisense half of the segments. This strategy is believed to provide a temporal regulation of gene expression in this class of viruses. For arenavirus transcription/replication to occur, NP and L must be provided as minimal trans-acting factors and 3' and 5' UTRs and IGR as cis-acting signals (Pinschewer *et al.*, 2003b, Lee *et al.*, 2000). On the other hand, Z protein was associated with dose-dependent inhibition of both processes (Cornu and de la Torre, 2001).

mRNAs are shortly detected following acute infection (Fuller-Pace and Southern, 1988). They are non-polyadenylated at the 3’ end and their 5’ end is characterized by non-templated nucleotide stretches ranging from 1 to 7 and

a cap structure (Meyer and Southern, 1993). The non-templated nucleotides are believed to be of a host-mRNA origin excised by the endonuclease activity of L protein in what is known as a cap-snatching mechanism (Morin *et al.*, 2010b, Lelke *et al.*, 2010). A transcription complex is then formed to produce nascent mRNAs. NP in infected cells was suggested to control the transcriptase to replicase switching of L protein by binding secondary structures in the IGRs preventing RNA synthesis termination (Pinschewer *et al.*, 2003b).

Arenavirus replication involves interactions with several cellular factors. RNA helicases, particularly DDX3, were found to be important for replication through RNA unwinding (Loureiro *et al.*, 2018). This interaction was also found to antagonize the cellular innate response by suppressing type I IFN production. Colocalization of cellular factors with viral components was also used to map the replication site. LCMV vRNAs, for example, aggregated and colocalized with the early endosome marker Rab5c late during infection near the perinuclear MicroTubule Organizing Centre (MTOC) (King *et al.*, 2017). Other components such as NP and GPC were also detected in the same compartment indicating early endosomes as a replication/pre-assembly site for LCMV.

1.7.3 Maturation, assembly, and budding

The modification and processing of arenavirus GPC take place in the ER and Golgi apparatus. Upon delivery to ER which is mediated by the N-terminal SSP of GPC, the complex undergoes extensive N-linked glycosylation by the oligosaccharyltransferase (OST) complex (see section **1.2.5**) (Zhu *et al.*, 2019). Subsequently, GPC is cleaved into three subunits by the cellular subtilase SKI-1/S1P. The spatiotemporal dynamics of this cleavage, however, can be virus-specific (Burri *et al.*, 2012, Eichler *et al.*, 2006). While LASV GPC cleavage occurs at ER/Cis-Golgi apparatus before the conversion of the mannose-rich N-linked glycans to complex type, it occurs at the late Golgi

apparatus following the transition to complex carbohydrates for LCMV GPC. Although both processes (glycosylation and cleavage) were found to be prerequisites for incorporation in mature virions, they did not affect trafficking to the plasma membrane (Beyer *et al.*, 2003, Eichler *et al.*, 2006).

Recruitment of viral components to the plasma membrane and budding are orchestrated by arenavirus Z matrix protein. The middle RING domain interacts with NP and L in the vRNP recruiting the complex to the site of budding (Shtanko *et al.*, 2011, Loureiro *et al.*, 2011). Then, myristylation at G2 in the N-terminus of Z anchors the protein to the plasma membrane inducing Z protein multimerization (Loureiro *et al.*, 2011). Interaction with GPC was also mapped to the N terminus (Urata and Yasuda, 2012). Lastly, the L motifs of the C-terminal domain of Z interact with the ESCRT complex promoting the budding of progeny (Bieniasz, 2006, Strecker *et al.*, 2003).

1.8 Lymphocytic Choriomeningitis Virus

Following its discovery in the 1930s, LCMV has been intensively studied in animal models. The distinct phenotype it induced in mice compared to other animal models such as NHPs and Guinea pigs further supported the notion that mice are the natural LCMV reservoir (Traub 1936, Armstrong *et al.*, 1940, Zapata *et al.*, 2011, Walker *et al.*, 1975). The virus has been used since as a powerful tool to understand immune responses due to its ability to cause both acute and chronic infections in mice. The findings obtained from these early studies shaped our current understanding not just of immune responses to chronic viral infections, but also of general immune phenomena associated with other conditions such as tumour formation and control. The ability of T cells to recognize self-antigen and the immunopathology associated with the failure of this recognition were first identified in the context of LCMV infection (Raju, 2000). Subsequently, $CD8^+$ T cell exhaustion and the underlying mechanism of this process have been identified (Kahan and Zajac, 2019).

Studies on LCMV also demonstrated that some viral variants are selected to promote chronicity. A mutation at position 1079 of L protein was found to increase viral replication and viremia which in turn correlated with T cell exhaustion (Bergthaler *et al.*, 2010). Another variant harbouring a mutation at position 260 of GPC was associated with a higher receptor-binding affinity (Sullivan *et al.*, 2011). This variant also displayed altered tropism infecting immune cells including DCs and macrophages and causing persistence. Besides cell-mediated immune response, albeit to a lesser extent, LCMV was also used to assess and characterize humoral immune response during chronic viral infection. (Greczmiel *et al.*, 2017, Fallet *et al.*, 2020).

In addition to its contribution to immunology, LCMV has been used as a surrogate model for other OWAs specifically to investigate the entry of the highly pathogenic LASV. Both use α-DG as a cellular receptor and neutralizing antibodies against GPC from sera of LF survivors cross-react with LCMV (Robinson *et al.*, 2016b). Thus, LCMV GPC has been intensively studied to identify key residues for α-DG binding and for mapping antigenic determinants (Parekh and Buchmeier, 1986, Weber and Buchmeier, 1988, Hastie *et al.*, 2016). Several residues important for α-DG binding were, indeed, identified based on LCMV GPC and interestingly all resided in the trimeric interface of LASV GPC (Hastie *et al.*, 2017). The integrity of this configuration was found to be essential for LASV binding to α-DG.

1.8.1 α-DG as the primary receptor for LCMV

α-DG was first identified as the cellular receptor for LCMV using a Virus Overlay Protein Blot Assay (VOPBA) which showed the viral binding to a high molecular weight glycoprotein (Cao *et al.*, 1998b). The glycoprotein was isolated from LCMV permissive cells and the purified peptides showed complete homology with the dystroglycan (DG) protein. The α-DG-dependent entry of LCMV was further confirmed by the loss of infectivity in α-DG-null ES

cell line compared to the highly susceptible wild type. Furthermore, the infectivity in those cells was restored after the reconstitution of α-DG. The entry of other OWAs including LASV and the NWA clade C was also found to be α-DG-dependent (Cao *et al.*, 1998b).

α-DG is the extracellular subunit of the integral protein DG which is, in turn, a part of a complex expressed ubiquitously in cells adjacent to basement membranes in many tissues (Barresi and Campbell, 2006). It maintains the integrity of tissues by connecting the extracellular matrix proteins with the intracellular cytoskeleton. It is generated from a single gene *(DAG1)* located on chromosomes 3 and 9 in human and mouse, respectively (C.Górecki *et al.*, 1994, Ibraghimov-Beskrovnaya *et al.*, 1993). The polyprotein is then cleaved at Ser654 into two subunits: β and α. The α- subunit is believed to be further processed by convertase at 312/313 (Kanagawa *et al.*, 2004). While it typically shows a molecular weight of ~120-150 kDa, full chemical deglycosylation indicated a contribution of the post-translational modification to the bulk of the subunit mass (Yoshida-Moriguchi *et al.*, 2010, Barresi and Campbell, 2006). It was found that α-DG indeed contains a highly *O*-glycosylated mucin-like domain (MLD) separating the two globular N- and C-termini and three potential *N*-glycosylation sites. The β subunit contains a transmembrane domain and a cytosolic tail with one potential *N*-glycosylation site. The two subunits remain non-covalently linked following cleavage which was found essential for the receptor function.

The amino acid sequence of DG is highly conserved among vertebrates (Barresi and Campbell, 2006). Outside the coding sequence, high conservation was also observed at the intron-exon boundaries and the regulatory elements of the 3' UTR between mammalian species (Brancaccio and Adams, 2017). Within the same species, core DG is expressed at comparable levels across different tissues (Kunz *et al.*, 2005, Ibraghimov-Beskrovnaya *et al.*, 1993). There is evidence that even between different mammalian species, comparable levels were observed from preparations of

the same tissue (skeletal muscle) (Ibraghimov-Beskrovnaya *et al.*, 1993). Nonetheless, the glycosylation of α-DG showed considerable tissue specificity. For example, in healthy mouse tissues, the liver and heart have comparable levels of core DG but only the heart showed detectable levels of glycosylated DG (Kunz *et al.*, 2005, Durbeej *et al.*, 1998). Similarly, high variation in glycosylation levels is believed to exist between human tissues (Peyrard *et al.*, 1999). Importantly, glycosylation was found to be crucial for DG binding to the laminin-G domains of its ligands which include laminin-1, laminin-2, agrin, and perlecan (Kanagawa *et al.*, 2004).

In a group of congenital muscular dystrophies known as dystroglycanopathies including Fukuyama congenital muscular dystrophy, congenital muscular dystrophy, muscle-eye-brain disease, Walker-Warburg syndrome, and congenital muscular dystrophy 1D, no defect was found in the core DG protein. Instead, aberrant glycosylation of α-DG was observed that was attributed to mutations in one or more of α-DG known or putative glycosyltransferases involved in the *O*-mannosylation of the MLD (Muntoni *et al.*, 2007). α-DG from defective tissues of patients with these disorders showed markedly impaired binding to laminin (Yoshida-Moriguchi *et al.*, 2010). Interestingly, when the glycosyltransferase LARGE1 was co-expressed in those tissues, α-DG restored its function and the affinity correlated with the degree of glycosylation (Barresi *et al.*, 2004).

Several studies compared the virus binding to α-DG with that of laminin (Kunz *et al.*, 2001, Kunz *et al.*, 2005, Yoshida-Moriguchi *et al.*, 2010). The two binding sites were found to overlap as laminin blocked the virus entry in a dose-dependent manner. In line with this finding is the requirement of LARGE1 glycosylation for viral entry. Producing deletion mutants expressing different domains of soluble α-DG, domains important for LCMV/laminin-binding were mapped (Kunz *et al.*, 2001, Kanagawa *et al.*, 2004). It was found that the MLD and the N-terminus of α-DG (amino acids 30 to 408) are essential and sufficient for this binding. Further investigation, however, revealed that only

amino acids from 313 to 408 contain the elements essential for the binding while amino acids from 30 to 312 were found essential for LARGE1 recognition and glycosylation but dispensable for LCMV/laminin binding.

In addition, viral factors can be detrimental to α-DG affinity as it was shown to be strain-specific (Smelt *et al.*, 2001b). While LCMV Cl13 and WE54, were associated with high affinity that was affected by the level of α-DG glycosylation, LCMV WE2.2 and Armstrong were associated with low-affinity binding regardless of the glycosylation pattern. This, in turn, was reflected in distinct *in vivo* tropism and disease pathogenesis of the two groups, with the high-affinity group infecting DG^{+} dendritic cells of the marginal white bulb of the spleen causing downregulation of the antigen-presenting molecules, generalized immunosuppression and chronicity. The low-affinity group, on the other hand, replicates mainly in the spleen red bulb and induced a potent CTL response leading to clearance of the virus. The existence of yet unidentified alternative receptors was proposed for the low-affinity LCMV strains which could explain their distinct phenotype both *in vitro* and *in vivo* (Smelt *et al.*, 2001b, Salvato *et al.*, 1991).

A variety of *in vitro* assays characterizing virus-receptor binding have been described in the literature to assess the receptor affinity of different viral strains, tissue tropism, and/or host range. For LCMV, VOPBA was intensively applied to characterize α-DG-LCMV GPC interactions (Kunz *et al.*, 2005, Kunz *et al.*, 2001, Hastie *et al.*, 2016). The experiments involved transferring SDS-PAGE-separated α-DG to an appropriate membrane and probing with the virus. The complex can then be detected by anti-LCMV GPC. Other assays included comparing the ability of soluble α-DG to block cell entry of different LCMV strains (Cao *et al.*, 1998a). The use of entry-blocking molecules that are known to specifically interfere with α-DG-LCMV GPC binding, such as Laminin-1 (biological ligand of α-DG) and anti-α-DG mAbs, has also been described (Kunz *et al.*, 2005, Kunz *et al.*, 2001). Other infectivity-based assays that were used to assess LCMV receptor usage are knockout/knock-in assays

coupled with a viral infectivity quantification method. Immunofluorescence staining, for example, has been frequently used for this purpose in LCMV studies (Kunz *et al.*, 2005, Kunz *et al.*, 2001, Cao *et al.*, 1998a). More recently, receptor transduction has been combined with more advanced fluorescence or chemiluminescence assays where the correlation between the level of receptor expression and viral infectivity can be measured (Herrador *et al.*, 2019, Shi *et al.*, 2020).

1.8.2 Alternative receptors

Alternative receptor use has been proposed for some LCMV strains that have low affinity to α-DG and/or efficient entry into α-DG-knock out cells (Kunz *et al.*, 2004, Smelt *et al.*, 2001b, Kunz *et al.*, 2005). Although putative alternative receptors for LCMV are yet unknown, alternative receptors for LASV have been identified and intensively studied. While some factors such as Lamp1 (an endosomal receptor) and C-type lectin receptors (DG-SIGN and LSEctin) have been implicated in LASV entry, these do not facilitate entry that is independent of α-DG. Lamp1 is required for LASV entry a feature not shared by other OWAs including LCMV (Hulseberg *et al.*, 2018, Israeli *et al.*, 2017). This molecule plays a role in fusion and endosomal escape, and whilst knocking it out significantly reduces infectivity, it does not eliminate it (Hulseberg *et al.*, 2018). Inhibition of C-type lectins, which bind mannose-rich glycans also had a modest effect, but these are considered attachment factors rather than receptors (Goncalves *et al.*, 2013).

However, there is evidence that some phosphatidylserine (PtdSer)-binding receptors can solely promote entry of LASV. Specifically, TIM-1 of the T cell immunoglobulin and mucin receptor (TIM) family and Axl a tyrosine kinase of the Tyro3/Axl/Mer (TAM) family were found by some studies to act as primary receptors for LASV (Brouillette *et al.*, 2018, Fedeli *et al.*, 2020). Both families are involved in the regulation of innate immunity and apoptosis (Monney *et al.*, 2002, Lemke and Rothlin, 2008). They interact with PtdSer either directly (TIM)

or indirectly (TAM) on the surface of apoptotic bodies (Naeini *et al.*, 2020). Many enveloped viruses were found to enter cells via these receptors by incorporating PtdSer in their envelopes in a mechanism known as apoptotic mimicry (Jemielity *et al.*, 2013). This was found to be independent of viral glycoproteins in some cases. For example, EBOV matrix particles bearing no GPC and expressing GFP were still able to use TIM-1 for entry (Jemielity *et al.*, 2013). For LASV, on the other hand, this effect seems to be GPC specific as it was evident only when using pseudotypes bearing LASV GPC but not the GPC of a control virus (Shimojima *et al.*, 2012, Fedeli *et al.*, 2018b). Additionally, the effect of Axl and TIM-1 on LASV entry was only observed when α-DG was absent or reduced. In HT-1080 cells which express core α-DG but undetectable levels of surface α-DG, LASV could be inhibited by the Axl inhibitor R428 (Fedeli *et al.*, 2020). In line with this finding, is the overexpression of TIM-1 in 293T where there was a significant increase in entry only when α-DG was knocked out but not in the WT (Brouillette *et al.*, 2018). Furthermore, when TIM-1 was knocked out in Vero E6 cells which showed no surface expression of glycosylated α-DG, entry was abolished (Brouillette *et al.*, 2018).

An Axl enhancement of α-DG-mediated entry for LASV was also proposed in some cell lines, as infection-inhibition by dual blocking of α-DG and AxI was increased, compared to α-DG alone, whereas blocking AxI alone did not have an effect (Shimojima *et al.*, 2012). However, colocalization of Axl and α-DG was not observed post-infection and indirect interactions may exist (Fedeli *et al.*, 2020).

1.9 Emergence, zoonosis and host switch

Emerging/re-emerging viral infections can be defined as the introduction of a virus to a new host population or the significant increase of incidence in an already existing host after a significant decline (Woolhouse, 2002). An

example of emerging viruses is the initial appearance of HIV-1 in the human population in the last century. Viruses causing periodic epidemics, such as EBOV in humans, are considered re-emerging viruses. Many important human pathogens in the past are believed to be introduced to humans upon the advent of agriculture and the domestication of animals which in turn bridged humans and wild animals (Wolfe *et al.*, 2007). Indeed, the vast majority of emerging viruses in humans are zoonotic (Woolhouse and Gaunt, 2007). Thus, cross-species transmission and host switching of viruses have been intensively studied and discussed in the literature which reveals the complexity and multifactorial nature of these processes.

1.9.1 Predicting viral emergence

Predicting viral emergence is difficult due to the complexity of the process and the vast number of animal viruses in nature. However, attempts have been made to develop models and identify criteria for viruses that pose epidemic threats. One of the simplest criteria is the binary system based on the basic reproductive value (R0: the average number of secondary cases arising from a single primary case) (Woolhouse *et al.*, 2005, Antia *et al.*, 2003). Viral infections where most human cases are acquired from the animal reservoir are associated with R0 values of <1 and are less likely to cause an epidemic. An R0 value of >1, suggests efficient human-to-human transmission and a potential epidemic threat. R0, however, requires an initial pool of cases for accurate measures to be made.

A more thorough classification proposed five stages for a pathogen to transition towards human endemicity (Wolfe *et al.*, 2007). Stage one includes pathogens that are confided to animals and have not naturally been detected in humans. Animal pathogens causing primary but not secondary infections in humans fall into stage two while those causing limited secondary transmission fall into stage three. An animal pathogen that causes extended cycles of onward transmission in humans after the initial spillover event belongs to stage

four. Pathogens found exclusively in humans such as smallpox and HIV-1 are included in stage five. The transition from one stage to the next is believed to be rare as many factors are involved and multiple barriers must be overcome by the pathogen (Parrish *et al.*, 2008, Wolfe *et al.*, 2007). The transition from early stages is likely to be affected the most by ecological factors including the density of the reservoir population, the probability of an encounter, and/or the behaviour of both the reservoir and humans. On the other hand, the transition to later stages of viruses causing dead-end or short-chain infections in humans is likely to be restricted by factors such as host genetics and viral adaptive ability.

Another model that was proposed was based on the biological traits of viruses infecting humans (Geoghegan *et al.*, 2016). The traits included: mortality, chronicity, genome type (DNA or RNA) and length, segmentation, recombination rate, route of transmission (vector- or non-vector borne), and structure (enveloped or non-enveloped). It was found that some of these traits were more associated with viruses causing efficient human-to-human transmission compared to viruses with limited transmissibility in humans. For example, they found viruses that are non-segmented, non-enveloped, and cause chronicity with low host mortality have an increased probability of human-to-human transmission. This model has the advantage of being more generalizable than models incorporating ecological and host factors as these can be viral-specific. However, a limitation of this model is that most of these traits are interrelated and can confound each other. For example, segmentation and genome type.

1.9.2 Host and viral genetic factors contributing to emergence

Host genetics

One of the most important barriers for a virus to emerge is the genetics of the new host population. It is widely accepted that host switch is likely to occur between closely related hosts due to the minimum number of changes the virus needs to acquire. A study on rabies virus in North American bat species, for example, showed that emergence correlated with species genetic relatedness (Streicker *et al.*, 2010). This was also seen in humans, as NHPs were found to contribute the most to pathogen emergence while contribution diminished going from mammals, vertebrates, to non-vertebrates species (Wolfe *et al.*, 2007). Nonetheless, there are instances where viruses were able to make the jump even to distantly related hosts. This might be facilitated by high evolution rates, conserved cellular targets, or/and the involvement of intermediate hosts (Parrish *et al.*, 2015, Li *et al.*, 2014, Woolhouse *et al.*, 2012). For example, in a study where factors contributing to viral emergence were analyzed, a significant correlation was found between host range and receptor conservation (Smith *et al.*, 2009).

Viral genetics

Sustained transmission of a virus in a new host is usually associated with the acquisition of adaptive changes (Dortmans *et al.*, 2013, Li *et al.*, 2020, Taubenberger and Kash, 2010, Wolfe *et al.*, 2007). Rapidly evolving viruses are more capable of adapting to environmental challenges and establishing infections in new hosts. Adaptation arises from three evolutionary mechanisms: recombination, re-assortment, and substitution (Moya *et al.*, 2004). RNA viruses have the highest mutation rates in nature that typically range between $1X10^{-3}$ and $1X10^{-4}$ sub/site/year (Jenkins *et al.*, 2002). Together with their high replication rates and large population sizes, they represent one of the most diverse and rapidly adapting biological entities making them a major public health concern (Moya *et al.*, 2004). Indeed, the last century witnessed multiple pandemics caused by RNA viruses including

the influenza pandemics and the HIV pandemic (Taubenberger and Kash, 2010, Weiss, 2003). The high mutation rate, however, is not the only driver of the adaptive changes in this class of viruses. Re-assortment in influenza A viruses, for example, is one of the most important mechanisms by which they acquire new combinations of HA and NA antigens enabling them to emerge in a previously unexposed population (Holmes *et al.*, 2005). Additionally, HIV-1 was found to recombine resulting in the emergence of immune-escape variants and antiretroviral resistance (Song *et al.*, 2018, Kellam and Larder, 1995). Different bat sarbecoronaviruses are also believed to have undergone multiple recombination events giving rise to SARS-CoV-2 (Temmam *et al.*, 2022).

Adaptive changes can occur anywhere in a viral genome to overcome challenges at different steps of the life cycle of the virus. More often, a virus must acquire polygenic changes to successfully establish itself in a new host. This provides an additional obstacle for host switching as those changes are believed to occur independently and under different selective pressures. Adaptation of avian IAVs to humans, for instance, involves a switch in HA-biding specificity from α2,3-SA (the predominant sialic acid in avian upper respiratory tract) to α2,6- SA(the predominant sialic acid in human upper respiratory tract) (Glaser *et al.*, 2005). However, additional mutations, especially in the PB2 subunit of the polymerase gene, were also found to contribute to virulence and efficient replication in mammals (Taft *et al.*, 2015, Taubenberger *et al.*, 2005, de Wit *et al.*, 2010, Zhang *et al.*, 2012).

Among the most well-studied adaptations are those affecting genes involved in receptor binding (Baranowski *et al.*, 2001). Binding to a cellular receptor is the first event for a virus to establish a productive infection in a novel host. Those genes are also subjected to host immune pressure. Subsequently, viral glycoprotein spikes show a substantial level of variation and plasticity. Their role in host switching has been the focus of many studies investigating the emergence of viral infections of high impact in humans. Human pandemics caused by IAVs, for example, were associated with adaptation in HA as

discussed above. The 2002-2003 SARS coronavirus pandemic was characterized by high transmissibility, which was attributed to mutations in the receptor-binding domain of the viral spike (Holmes, 2005). Two mutations at positions 479 and 487 conferred a higher affinity to human ACE2 (the cellular receptor of SARS) by forming a loop that is missing in the less transmissible strains of SARS. The mutations that arose during the 2013-2016 epidemic in the RBD of EBOV Gp were also associated with increased infectivity in human cells (Urbanowicz *et al.*, 2016b). In the current SARS-CoV-2 pandemic, some of the spike mutations characterizing the variants of concern were associated with increased affinity to the cellular receptor ACE2 and contributed to the spread and increased infectivity of the variants (Liu *et al.*, 2022).

1.10 Pseudotyping system as a tool to study the early steps of the viral life cycle

As early steps in viral infections play a major role in emergence, understanding these steps has been the focus of many studies, especially for viruses of high human impact. Pseudotyping is a powerful tool that is frequently employed for this purpose. It enables the uncoupling of the entry from the subsequent steps in the virus life cycle. This lack of replication also allows the investigation of highly pathogenic viruses in low-containment facilities. This section describes the different pseudotyping systems and components and ways to optimize production, incorporation, and infectivity.

1.10.1 Pseudotyping history and applications

A viral pseudotype can be defined as a viral pseudo-particle (PP) in which the outer coat protein is derived from a virus that is antigenically distinct from that of which the genome is derived (Li *et al.*, 2018). They are generated using plasmid systems to provide the required elements *in trans*. This ability of

viruses to carry foreign surface glycoproteins allowed them to be widely used as vehicles for gene transfer including *in vivo* transfer of human genes involved in some genetic disorders and cancers. By expressing the glycoproteins of viruses with specific tropism, genes can be delivered to target cells where they are transiently or stably expressed. Replacing the transferred gene with a reporter gene and expressing a viral glycoprotein of interest enabled the study of early steps in the life cycle of enveloped viruses especially viruses requiring high containment levels. Ever since, pseudotyping has been a powerful tool in studying steps mediated by the viral glycoproteins including receptor usage, endocytosis and fusion (Bartosch *et al.*, 2003, Liu *et al.*, 2009, Evans *et al.*, 2007, Hsu *et al.*, 2016). Neutralization assays for measuring antibodies in sera and screening entry inhibitors are also important applications of this platform (Carnell *et al.*, 2015).

The pseudotyping platform was widely exploited to investigate the entry and early steps of important human viruses. For example, determining the receptor requirement for hepatitis C virus was only achieved following the advent of pseudotyping, as it was previously impeded by the inability of the virus to propagate in cell culture (Bartosch *et al.*, 2003). Several studies employing murine leukaemia virus (MLV)- or human immunodeficiency virus (HIV)-based vectors to produce HCV-Gp pseudotypes were able to identify cellular factors required for the entry and their sequential roles (Bartosch *et al.*, 2003, Liu *et al.*, 2009, Evans *et al.*, 2007). It was also found that not all these factors were required for every genotype as comparing major HCV genotypes revealed genotype-specific requirements for entry (Lavillette *et al.*, 2005). This in turn provided a valuable basis for the development and testing of entry inhibitors targeting common entry factors to achieve broader neutralization.

Viral emergence and reemergence studies have also employed pseudotyping to characterize viral entry and virus-receptor interactions. Furthermore, cellular tropism and humoral responses can also be determined for many emerging viruses. For example, this system has provided a safe platform for highly

pathogenic or transmissible viruses that have emerged or re-emerged over the last two decades, such as MERS and SARS coronaviruses, EBOV, and influenza A (Qian *et al.*, 2013, Garcia *et al.*, 2010, Giroglou *et al.*, 2004, Kaletsky *et al.*, 2007, Nie *et al.*, 2004). Manipulating viral glycoproteins and introducing mutations are also easier in pseudotyping systems. This allows the study of the impacts of viral glycoprotein evolution and variability on receptor affinity for glycoproteins of ancestral/animal origin, as well as representatives of extant/human origin. For example, EBOV pseudotypes derived from sequences of the 2013-2016 outbreak were found to be more infectious than those derived from bat sequences due to several adaptive amino acid changes (Urbanowicz *et al.*, 2016b). Additionally, pseudotyping can be used as a rapid assay of licensed entry inhibitors for therapeutic potential against highly pathogenic emerging viruses. Several inhibitors have indeed been identified using comparatively high-throughput screening pseudotype inhibition assays. Targets included highly pathogenic influenza virus H5N1, Marburg virus, LASV, and EBOV (Wang *et al.*, 2014, Basu *et al.*, 2011).

Pseudotype antibody-neutralization assays are also widely used (Carnell *et al.*, 2015). They have been intensively employed to assess the efficacy of seasonal influenza vaccines. A comparison of this system with traditional serological assays such as hemagglutinin inhibition, single radial hemolysis, or microneutralization assays revealed a significant correlation (Alberini *et al.*, 2009). More recently, efforts have been made to produce a universal influenza vaccine. Using traditional assays for this purpose has been hampered previously as they usually measure subtype-specific antibodies targeting the HA globular head involved in the sialic acid binding. Pseudotypes, on the other hand, are capable of measuring antibodies that target conserved epitopes in the HA stem involved in membrane fusion (Mallajosyula *et al.*, 2014, Carnell *et al.*, 2015). This ability of pseudotypes has been attributed to less incorporation of HA molecules compared to authentic viruses which in turn exposes the complete HA stalk.

1.10.2 Frequently used packaging systems and their modifications

Several packaging systems are in use for reporter gene assays, but lentiviral- and gammaretroviral-based systems are the most widely used and reported in the literature (Blesch, 2004, Li *et al.*, 2018, Walther and Stein, 2000, King *et al.*, 2016, Gutierrez-Guerrero *et al.*, 2020). Gammretroviral-based systems such as the MLV-based reporter system can only integrate into dividing cells which can limit their use in non-dividing cells such as neurons or muscle cells. Conversely, lentiviral-based systems such as HIV-1-based systems can be used with both dividing and non-dividing cells. Lentiviral vectors underwent several modifications and genetic manipulations to ensure safety and optimize expression including splitting cis-acting and trans-acting sequences in separate plasmids and deletion of accessory and regulatory genes involved in replication and virulence, producing replication-incompetent particles. Regulatory sequences were also modified, for example, the U3 region of 3'LTR was deleted which resulted in the inactivation of LTR after reverse transcription. This is important to avoid the activation of the surrounding cellular genes by the inserted LTR. A heterologous promoter is also usually included in the 5'LTR to enhance expression.

The first generation of this system consisted of three plasmids while the latest version consisted of four plasmids to further reduce the chance of recombination and production of replication-competent particles **(Figure 1-7).** lentiviral-based systems where the packaging and the reporter sequences are combined in one plasmid are also widely used **(Figure 1-7).** HIV-1-NL4-3 vectors and derivatives are an example of such systems (Zeng *et al.*, 2020). The four-plasmid system includes two packaging plasmids: one expressing the Gag/Pol gene and the other expressing the *rev* gene, which is necessary for Gag/pol expression. The envelope plasmid expresses the viral glycoprotein of interest. The three plasmids (the envelope and the two packaging plasmids) lack the packaging signal psi (ψ) and the 3'LTR and 5'LTR are replaced by a polyadenylation signal and a heterologous promoter, respectively. The

transfer plasmid encodes the reporter gene with an upstream ψ packaging signal. An internal promoter is also encoded to enhance the reporter gene expression as the LTRs are inactivated following reverse transcription. Similar modifications have been made to MLV-based vectors, however, MLV lacks the accessory and regulatory genes of lentiviruses.

VSV-based vectors have also been frequently used in pseudotyping, although this is a more complex procedure compared to the gammaretroviral and lentiviral systems (Whitt, 2010). Multiple genes must be provided in trans in separate plasmids, in addition to a VSVΔG-Luc transfer plasmid and an exogenous T7 polymerase promotor to produce VSV-G pseudotypes. This in turn is used to infect a second batch of packaging cells expressing the viral glycoprotein of interest to produce the final desired pseudotypes. A disadvantage of this system is that the presence of residual VSV-G pseudotypes in the final prep requires additional steps to eliminate or may otherwise interfere with subsequent assays (Yahalom-Ronen *et al.*, 2020, Whitt, 2010).

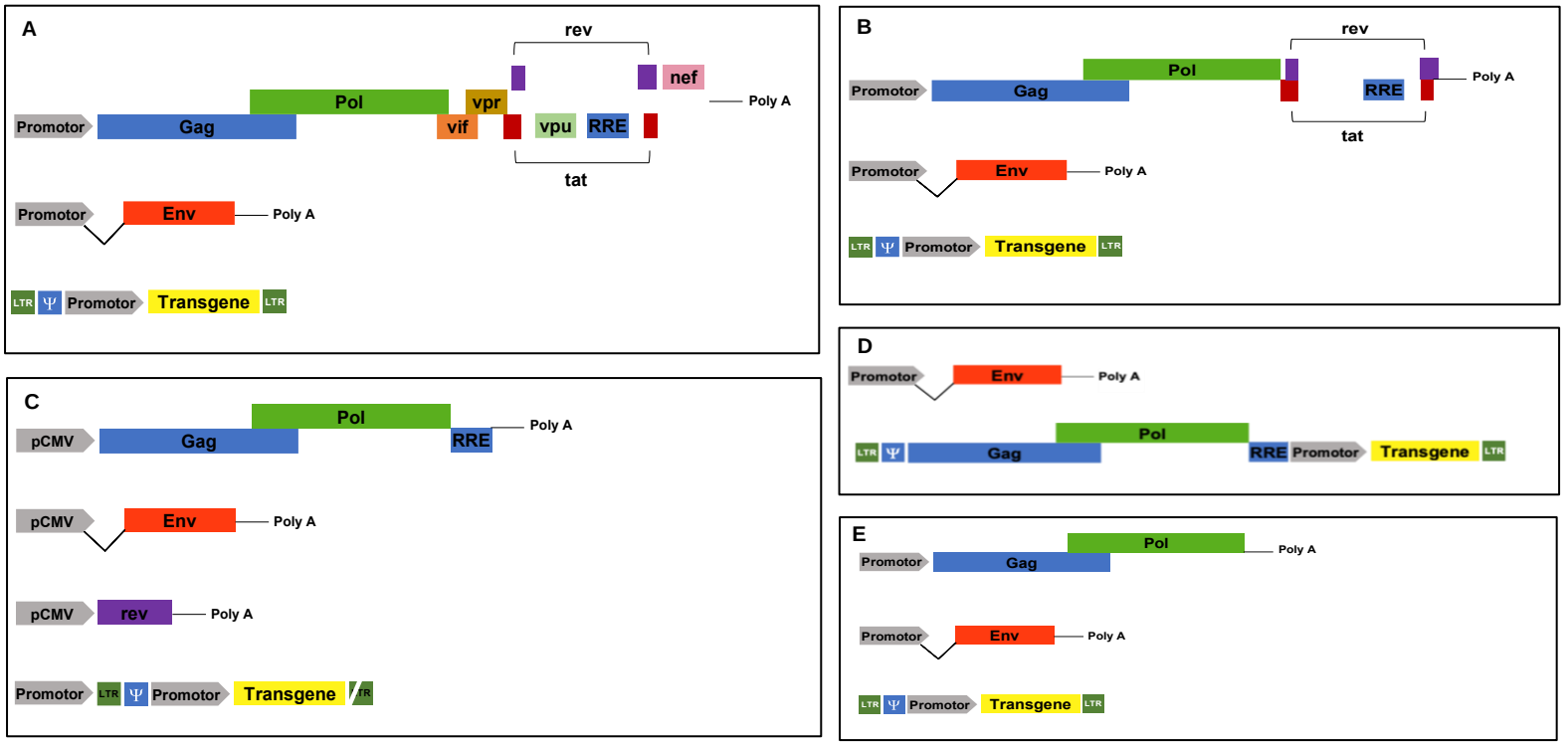


Figure 1-7: Component of the lentiviral- and gammaretroviral-based pseudotyping systems.

The three generations of the lentiviral-based system **(A, B &C)** are illustrated. The system was enhanced to increase expression efficiency and reduce risk. The first generation **(A)** included all regulatory and accessory genes while the third generation **(C)** included one regulatory gene (rev) provided in trans but lacked all accessory genes. **(D)** Lentiviral-based two-plasmid system. **(E)** Gammaretroviral-based system. When producing pseudotypes to study virus entry, the transgene encodes for a reporter gene.
*LTR = Long Terminal Repeat, Ψ Packaging signal (psi).

1.10.3 Reporter genes

The firefly luciferase derived from the *Luc* gene of *Photinus pyralis* is one of the most used reporter genes in pseudotyping (Schenborn and Groskreutz, 1999). It has the advantage of a wide linear range between its concentration and activity. In general, chemiluminescence assays are more sensitive and have lower background than fluorescence proteins such as the green fluorescent protein (GFP). However, an enhanced GFP derivative (EGFP) generated by mutating and codon-optimising GFP greatly increased the sensitivity of the assay and has been used in many pseudotyping systems (Zhang *et al.*, 1996). β-Galactosidase is another reporter gene widely used, especially in MLV-and HIV-based systems (Li *et al.*, 2018).

1.10.4 Pseudotype producer cells

A variety of cell lines have been used for pseudotype production. Producing cells can either be stably or transiently expressing structural genes necessary for production. One of the most commonly used cell lines for pseudotyping is the human 293 cells and its derivative 293T (Lin *et al.*, 2014). Originally, these cells are believed to be derived from human embryonic kidney cells, hence the prefix HEK. Karyotyping, genetic, and transcriptomic analysis revealed that the cells are pseudo-triploid and of adrenal tissue origin. They exhibit neuronal progenitor properties and hence are believed to be of neuronal lineage (Shaw *et al.*, 2002). They were transformed using adenovirus 5 DNA, which interferes with the cell cycle resulting in an infinite division. Additionally, the 293T cell line expresses SV40 T antigen which supports the replication of plasmids containing the SV40 origin sequence (SV40 Ori).

1.10.5 Optimizing production and infectivity

Many factors can influence pseudotype titres and many solutions are provided in the literature for optimisation. One important factor that should be considered is the promotor/enhancer driving the expression of genes. Comparing the activity of the constitutive promoters simian virus 40 early promoter (SV40), human Ubiquitin C promoter (UBC), cytomegalovirus immediate-early promoter (CMV), human elongation factor 1α promoter (EF1A), mouse phosphoglycerate kinase 1 promoter (PGK), chicken β-Actin promoter coupled with CMV early enhancer (CAGG), and RSV promotor in mammalian cells revealed a cell-type-specific variation for some promotors (Qin *et al.*, 2010, Zarrin *et al.*, 1999). For example, CMV, which is usually associated with high levels of expression, showed low activity in rat mesenchymal stem cells and the human fibroblasts MRC5. Other non-coding-sequence modifications such as the inclusion of introns in the 5'-LTR can also increase the expression of particular genes (Huang and Gorman, 1990).

Genetic modifications of the glycoprotein genes to enhance their expression and incorporation were also found to increase titres. Glycoprotein codon optimisation, for example, resulted in the production of highly infectious pseudoparticles of MERS- and SARS-coronaviruses (Grehan *et al.*, 2015, Nie *et al.*, 2004). Other modifications such as deleting the cytoplasmic domain of the glycoproteins or replacing it with that of another virus can also increase titres, which was attributed to enhanced glycoprotein incorporation. For instance, the truncation of Nipah virus cytoplasmic domain, or production of chimeric glycoproteins consisting of the extracellular domains of the gibbon ape leukaemia virus or the feline endogenous virus RD114 and the cytoplasmic domain of MLV, both resulted in a significant increase in titres (Sandrin *et al.*, 2002, Palomares *et al.*, 2013). Additionally, the glycoproteins for some viruses require cellular proteases for processing and maturation. For example, proper processing of HA of Influenza virus with specific proteases is usually needed to produce the fusogenic-active form. This can be provided in

trans by co-transfecting producing cells with plasmids encoding proteases such as HAT and TMPRSS2 (Ferrara *et al.*, 2013). For other viruses, treatment of pseudotypes with exogenous proteases might be required (Letko *et al.*, 2020).

Some modifications or treatments of the glycoproteins might be required to enhance infectivity in target cells. Deletion of the highly glycosylated mucin-like domain (MLD) of EBOV Gp, for example, was found to increase the infectivity of pseudotypes by exposing the receptor-binding domain which is shielded by the MLD in the native conformation (Kaletsky *et al.*, 2007). Moreover, the treatment of pseudotypes with cationic polymers such as polybrene neutralizes the negative charge on the pseudotypes surface reducing repulsive electrostatic interactions between the glycoproteins and the attachment factors of the host cell (Davis *et al.*, 2004).

Importantly, the type of expression vectors and ratios were found to greatly impact the titres of pseudotypes yield. The same glycoproteins when pseudotyped with different packaging systems resulted in significant variation in yields. For example, pseudotyping LASV with MLV or VSV backbones was superior to pseudotypes with an HIV backbone (Cosset *et al.*, 2009, Li *et al.*, 2018). Additionally, glycoproteins of different strains of the same virus can be pseudotyped better using one packaging system compared to another. This was observed in different HCV genotypes and EBOV strains emphasizing the importance of considering the packaging systems in experiment design (Urbanowicz *et al.*, 2016a). Specific ratios of each expression plasmid to obtain optimum titres and infectivity were also found to be glycoprotein-specific (Urbanowicz *et al.*, 2016a). Interestingly, glycoproteins of some strains of the same virus were found to tolerate a wide range of variation in this ratio while others displayed less flexibility.

Psuedotype titres can also be increased by concentrating or/and purifying supernatants. Several techniques have been used for this purpose including

ultracentrifugation, low-speed centrifugation, chemical precipitation, anion exchange or affinity resins (Merten *et al.*, 2014).

1.10.6 Reliability and consistency of pseudotyping systems

The use of pseudotyping as a surrogate to make inferences about authentic viruses necessitate the evaluation of the reliability of this system. This is particularly important when the inferences and conclusions derived from a pseudotype-based study are to have clinical implications. For this purpose, many studies comparing pseudotypes with replication-competent viruses have been conducted. In many vaccine trials, the ability of pseudotypes to be neutralized was compared with the neutralization of viruses. In those trials, high correlations were observed between the two systems. The neutralization of rabies pseudotypes, for example, by antibodies induced using a vaccine candidate correlated well with the results of the fluorescent antibody virus neutralization test approved by WHO with a correlation coefficient of 0.89 (Wright *et al.*, 2008). Similarly, neutralization assays of the avian H5N1 influenza virus pseudotypes showed a high correlation with conventional serological assays such as the hemagglutination inhibition (HI) and the viral micro-neutralization (MN) assays (Alberini *et al.*, 2009). It is important, however, to mention that some inconsistencies were also observed (Owsianka *et al.*, 2008, Alberini *et al.*, 2009, Heyndrickx *et al.*, 2012). This was seen in some cases as increased sensitivity or resistance of pseudotypes to neutralization compared to wild-type viruses. Factors such as size difference, lack of essential viral proteins in pseudotypes, or different glycosylation patterns were suggested as explanations for these inconsistencies.

Additionally, pseudotyping-based systems were compared to *in vivo* studies which also showed a high correlation. For example, similar dissemination of enterovirus A71 pseudotypes and the wild type *in vivo* was reported (Zhou *et al.*, 2016). Another example is the cellular tropism and host range of SARS-CoV pseudotypes that mirrored that of the wild type (Giroglou *et al.*, 2004).

Additionally, entry host factors required for EBOV entry were also found to be required for EBOV pseudotypes entry (Shimojima *et al.*, 2006). In some cases where specific cell lines showed reduced susceptibility to pseudotypes compared to the wild type, restriction on the pseudotype packaging system used was identified (Wright *et al.*, 2008). An increase in the susceptibility of pseudotypes in some cell lines was also observed and was attributed to restriction on native viral replication in that specific cell line (Shimojima *et al.*, 2006).

1.11 A preface of the study

1.11.1 Description of the outbreak

This study investigated an LCMV outbreak in captive NHPs that took place in a zoo in the United Kingdom between 2005 and 2006 and resulted in several deaths of different NHPs species. Similar outbreaks have been reported since the 1980s in the United States and Europe including an outbreak in the United Kingdom that resulted in the death of 12 marmosets (Scanga *et al.*, 1993, Asper *et al.*, 2001, Lucke and Bennett, 1982). In these outbreaks, LCMV was identified as the causative agent which was believed to be acquired from mice fed to the animals or through exposure to mice excreta. The prevalence of LCMV is estimated to be ~ 4% in wild rodents in the UK with a high prevalence in *M.musclus* species (Blasdell *et al.*, 2008).

This more recent outbreak was investigated first by the UK Health Security Agency (UKHSA) and subsequently by the University of Nottingham (Onianwa, 2017). The exact number of deaths due to LCMV is unknown as many deaths before the time of the outbreak were not tested for the virus and were reported as deaths of unknown aetiology. Earlier cases that go back as far as 2003 were also reported and included unexplained abortions and deaths. Notably, 20 undiagnosed deaths among marmosets and tamarins,

species known to be highly susceptible to Callitrichid Hepatitis caused by LCMV (Montali *et al.*, 1995, Montali *et al.*, 1993, Asper *et al.*, 2001), occurred since 2003. The symptoms reported for some of those cases were highly consistent with cases that were confirmed later. The two species were confirmed by the zoo to be in the same enclosure during an event "World of small monkeys" in early 2006.

When the number of deaths noticeably increased in 2005/2006, testing was carried out which included serology, PCR, necroscopy, and histology. At least six confirmed LCMV-related deaths were reported among different NHP species. Those included three marmosets, one black and white colobus, one purple-faced langur, and one concolor gibbon. The reported symptoms were mainly dehydration, loss of weight, weakness, and in some cases neurological symptoms. Histology and post-mortem examination revealed multi-organ involvement with liver necrosis, kidney fibrosis, pneumonia, splenomegaly, abdominal oedema, subcutaneous haemorrhage, and encephalitis frequently reported. 124 NHP were tested for LCMV antigen/antibodies and 18 were positive. Those included ten chimpanzees, two Linne's two-toed sloth, two marmosets, one black & white colobus, one Allen's swamp monkey, one spider monkey, and one gorilla. Of the 121 samples that were PCR tested either by UKHSA or our lab seven were positive (Onianwa, 2017). In total, 24 NHP samples were positive by either serology and/or PCR (overall prevalence ~ 19%). **Table 1-2** summarizes the results of serology and PCR of positive NHP samples used in the current study (see appendix **8.1** for all NHP samples tested by either UKHSA or the lab prior to this study).

Subsequently, 47 rodents from the premises were tested by PCR and 23 samples were positive and all the positives were *M.musculus* samples**. Table 1-3** shows the mouse samples included in this study (see appendix **8.2** for all mouse samples tested by either UKHSA or the lab prior to this study).

Table 1-2: NHP samples included in the current study that tested positive for LCMV either by serology or PCR during the 2005/2006 outbreak.

UKHSA ID, study ID, date of collection, date of receiving, species, and results are shown.

UKHSA ID	Study ID	Species	Date collected	Date received	UKHSA result		Lab result
					Serology	PCR	
H06 336 0621 01	NHP1	Geoffroy's marmoset	-	23/08/2006	NT	Positive	Positive
H06 336 0625 01	NHP2	Black & white colobus	06/07/2005	23/08/2006	NT	Positive	Positive
H06 094 0753 01	NHP3	Geoffroy's marmoset	27/01/2006	-	NT	Positive	Positive
H06 336 0613 01	NHP4	Concolor gibbon	-	23/08/2006	Negative	Negative	Positive

Table 1-3: Mouse samples included in the current study that tested positive for LCMV by PCR following the 2005/2006 outbreak.

UKHSA ID, study ID, date of collection, and results are shown.

UKHSA ID	Study ID	Date collected	UKHSA PCR	Lab PCR Results
H07 196 0643 01	M1	08/08/2006	NT	Positive
H07 196 0645 01	M2	08/08/2006	NT	Positive
H07 196 0647 01	M3	08/08/2006	NT	Positive
H07 196 0650 01	M4	20/07/2006	NT	Positive
H07 196 0656 01	M5	19/07/2006	NT	Positive
H07 196 0638 01	M6	18/08/2006	Positive	Positive
H07 196 0649 01	M7/M8	20/07/2006	Positive	Positive
H07 196 0658 01	M9	17/07/2006	Positive	Positive
H07 196 0665 01	M10	24/07/2006	Positive	Positive
H07 196 0674 01	M11	01/10/2006	Positive	Positive

1.11.2 General aims

OWA infections are mainly characterized by rodent-to-primate transmission while primate-to-primate transmission is rarely observed. Surges in LF infections, for example, were frequently attributed to changes in the surrounding rodent population rather than viral factors leading to sustained human-to-human transmission (Siddle *et al.*, 2018). Similarly, LCMV infections are often sporadic due to isolated spillover events from mice. The scale of the outbreak investigated by the current study, however, warrants a further examination of potential viral adaptations.

As the first step of the viral life cycle, entry is considered one of the most important barriers for a virus to be established in a new host. Mutations in the virus glycoproteins altering virus-receptor interactions have been frequently associated with emergence and zoonosis (see previous section). LCMV GPC is the sole surface antigen which promotes viral entry from attachment to endosomal escape. Thus, this study aims to analyze the LCMV GPCs isolated from the NHP samples taken during the outbreak and compare them to those isolated from the natural host both genotypically and phenotypically. The proposed hypothesis is that the virus acquired adaptive changes in the GPC that increased the infectivity and contributed to the cross-species transmission. To test the hypothesis, GPC sequences from the outbreak samples were generated and analyzed. Using an MLV-based pseudotyping system, pseudotypes carrying the NHP- and mice-derived LCMV GPCs were produced. The infectivity of the pseudotypes was tested in several cell lines including NHP, murine, and αDG-KO cells. The infectivity of a panel of mutants was also tested.

Chapter. 2: Methods and materials

2.1 Samples

Samples used in this study were screened by a previous doctoral student to investigate the prevalence and diversity of arenaviruses in rodents and non-human primates in the United Kingdom (Onianwa, 2017). Initially, tissues were collected and processed by Public Health of England during an outbreak in a zoo in the United Kingdom between 2005 and 2006 (more information including postmortem reports is provided in the appendices **8.3** and **8.4**). RNA extraction was carried out in our lab using the GenEluteTM Mammalian Total RNA Miniprep Kit (Sigma-Aldrich). Out of the tested samples in our lab, 24 were positive for LCMV by PCR of those 19 were mouse samples. 15 of these samples (four from NHPs and 12 from mice) were used in this study to generate full-length GPC clones. The list of samples and their corresponding animal species from which they were isolated is shown in **Table 2-1.** Randomly-primed cDNAs were made using the RNA to cDNA EcoDry Premix kit from Takara Bio. The manufacturer's protocol was followed, using between 5ng-5μg of total extracted RNA as a template. Additionally, the GPC gene of LCMV WE54 was added to the panel as a positive control (Eurofins Genomics). WE54 glycoprotein sequence was derived from a sequence deposited in GenBank by Beyer et al (Beyer *et al.*, 2001) (WEHPI; accession number AJ318512). Originally this strain was isolated from a meningoencephalitis patient in 1935 and the passage history is not well documented (Rivers and McNair Scott, 1935, Albariño *et al.*, 2010). WEHPI sequence contains a mutation that was found by Beyer *et al* to be required for a detectable level of cell surface expression (P110L). The sequence was further edited to contain two mutations (H155Y and A211T) found in other α-DG high-affinity strains (WE54 and Cl13) (Hastie *et al.*, 2016).

Table 2-1: The study Samples.

The list of samples from which full-length sequences of LCMV GPC could be obtained and their corresponding animal species.

Sample	Clone/s isolated from the sample	Source	Species
1	NHP1	NHP	*C. geoffroyi*
2	NHP2	NHP	*C. guereza occidentalis*
3	NHP3	NHP	*C. geoffroyi*
4	NHP4	NHP	*N. leucogenys*
5	M1	Murine	*M. musculus*
6	M2	Murine	*M. musculus*
7	M3	Murine	*M. musculus*
8	M4	Murine	*M. musculus*
9	M5	Murine	*M. musculus*
10	M6	Murine	*M. musculus*
11	M7/M8	Murine	*M. musculus*
12	M9	Murine	*M. musculus*
13	M10	Murine	*M. musculus*
14	M11	Murine	*M. musculus*
15	M12	Murine	*M. musculus*

2.2 Primers

Table 2-2 shows the sets of in-house primers used for LCMV GPC nested amplification, InFusion cloning, mutagenesis, and sequencing and screening primers. In-house primers were designed using the Primer3web or NEBaseChanger online tools and synthesized by Eurofins Genomics.

Sequencing primers provided by Source Bioscience were also used including pCMVF and EGFP-Nrev for insert/multiple cloning site (MCS) and internal ribosome entry site (IRES) sequencing, respectively. The primers used for LCMV GPC amplification (outer set) were initially designed based on an alignment of full-length LCMV S sequences retrieved from GenBank database (see appendix **8.5**). The inner set (InFusion primers) to amplify LCMV GPC was designed based on sequences generated by Okechukwu Onianwa (Onianwa, 2017).

The primers used for *DAG1* gene and α-DG fragment amplification were designed based on *M.musculus* or human/non-human primate *DAG1* gene sequences retrieved from GenBank (accession numbers shown in **Table 6-1**).

InFusion cloning primers were designed with In-fusion tags so that the 3' end sequence is insert-specific and the 5' end sequence is vector-specific. The forward primers also included a Kozak sequence to enable subsequent expression in mammalian cells. Digestion enzyme sequons were also included in some InFusion cloning forward primers.

Table 2-2: In-house primer sets used for InFusion cloning, screening and sequencing, or mutagenesis.

For the InFusion cloning primers: grey-highlighted sequences are vector-specific, sequences in bold are restriction enzyme sites (EcoR1/BamH1), underlined sequences are Kozak sequences, and non-highlighted sequences are insert-specific.

Primer set	Sequence (5' to 3')	Use
A. **InFusion cloning primers:**		
LCMV_gp_INFf (forward)	CAGTGTGGTG**GAATTC**CACCATGGGCCAGATTGTGACGATGTTTGAG	Inner set of nested PCR for GPC amplification (InFusion primers).
LCMV_gp_INFr (reverse)	GATATCTGCA**GAATTC**TCAGCGTCTCTTCCAGACAGTCCTTAC	
LCMV_gp_OF (forward)	GCCAGACTCTGTTGTGCAAG	Outer set of nested PCR for GPC amplification.
LCMV_gp_OR (reverse)	AGAGGCCCAAATGTTGTGAC	

DAG1-pHIV-F **DAG1-pHIV-R**	ACCCGGGCTA**GGATC**CACCATGTCTGTGGACAACTGGCT GGAGAGGGGC**GGATC**TTAAGGGGGAACATACGGAGG	InFusion primers for amplifying *DAG1* gene from L929 cDNA and cloning into pHIV-EGFP.
α-DG-Fc-F (primate/mouse) **α-DG-Fc-R (primate)** **α-DG-Fc-R (mouse)**	TCCAGGTTCCACTGGtCACTGGCCCAGTGAACCC CATGTGTGAGTTTTGTCACTGGTGGTGGTGCGAATAC CATGTGTGAGTTTTGTCACTGGTGGTAGTACGGATTCC	Cloning α-DG fragment into pcDNA3.1-Fc plasmid
B. **Sequencing and screening primers:**		
LCMV_5'_ter **LCMV_3'_ter**	AGACACTGCCTTATAGTTGGAGT GCGAAGACTGGGGAGACTAG	Sequencing of GPC termini
LCMV_211Scr_F **LCMV_211Scr_R**	ACTCCAACTATAAGGCAGTGTCT CATATGTGCAATGGTTCTCCC	For screening the 250 pb spanning aa 211

pI.18-F **pI.18-R**	TCCATGGGTCTTTTCTGCAG CAGGCGTGACACGTTTATTG	Screening and sequencing of inserts cloned into pI.18.
BGHr **T7f**	TAGAAGGCACAGTCGAGG TAATACGACTCACTATAGGG	Screening and sequencing of inserts cloned into pcDNA 3.1
pHIV-Scr-F **pHIV-Scr-R**	TGGAATTTGCCCTTTTTGAG TCGTGAAGGAAGCAGTTCCT	Screening and sequencing of inserts cloned into pHIV-EGFP.
DAG-F **DAG-R**	TCTCCAKCYATTGCWCCTCC CATCGTTGGRCGAATCTGGC	DAG1 internal sequencing primers
C. **Mutagenesis primers:**		
LCMV_F106S_F **LCMV_F106S_R**	ATGGGAACTTcTGGCTTGGAA ACTGATGTAATGGTGTGAGTTG	Mutagenesis
LCMV_K211T_F **LCMV_K211T_R**	TGGGGTTGGAcAAGTTCAGATG ACCACTTCTCATGTATTTTC	Mutagenesis

LCMV_I260L_F	GACAAAATTTcTCACTAGAAGACTTG	Mutagenesis
LCMV_I260L_R	TTTTCCTGGGCAAAAAGG	
LCMV_V451I_F	TTTAATCAGCaTATTTTTACATCTCATAAAG	Mutagenesis
LCMV_V451I_R	TATGCCGATGTGGAGAAC	
LCMV_L468S_F	AAAGGTGGTTcATGCCCAAAG	Mutagenesis
LCMV_L468S_R	TATATGTCTATGTGTTGGTATC	
LCMV_S119H_F	TTCCATCATTcaTCACAACCATTGCAAC	Mutagenesis
LCMV_S119H_R	TCATTGGTGAAGGTTAATTC	
LCMV-I247M-F	CTTTCGGAATGTCTAGAATTCTTTTTGC	Mutagenesis
LCMV-I247M-R	GGCCTGCATATGTGCAAT	
LCMV-T211K-F	TGGGGTTGGAAAAGTTCAGATG	Mutagenesis
LCMV-T211K-R	ACCACTTCTCATGTATTTTCC	
FLAG-F	AGGACGACGACGACAAGTGAGAATTCTGCAGATATCCTC	Addition of FLAG tag to
FLAG-R	GTAGTCGCTGCCGCCGCCGCGTCTCTTCCAGACAGT	GPC C terminal
FLAG-R	GTAGTCGCTGCCGCCGCCGCGTCTCCTCCAGACAGT	

2.3 PCR

Full-length LCMV GPC was amplified in two rounds of nested PCR. A reaction of 15 μl was prepared for the first round containing 7.5 μl of the proofreading enzyme CloneAmp, 0.3 μl of the forward/reverse primers, 5.9 μl of DECP-treated water, and 1 μl of template. A 25 μl was prepared for the second round (12.5 μl of CloneAmp premix, 0.5 μl of forward/reverse primers, 10.5 μl of DECP-treated water, and 1 μl of 1 in 100 diluted PCR products from the first round). The cycling conditions for both rounds of PCR were adjusted to 35 cycles of a 10-second denaturation step at 98 °C, a 15-second annealing step at 55 ºC, and a two-minute extension step at 72 ºC.

For full-length *DAG1* and α-DG fragment amplification, a reaction of 15 μl was prepared to contain 7.5 μl of the proof-reading enzyme CloneAmp, 0.3 μl of the forward/reverse primers, 5.9 μl DECP-treated water, and 1 μl of template. The template was prepared from cDNA of total RNA extracts from either L929 or Vero E6 cells as described in the **Samples** section. The PCR thermocycle included 30-40 rounds of a 10-second denaturation step at 98 ºC, a 15-second annealing step at 55 or 58 ºC, and a 3 or 1.5-minute extension step at 72 ºC for *DAG1* or α-DG, respectively.

For colony screening, a 15 μl reaction was prepared (1.5 μl of x10 PCR buffer, 0.3 of the forward/reverse vector-specific primers, 0.6μl of dNTPs, 0.075 of Hot Start Taq Polymerase enzyme, and 12.225 μl of DECP-treated water). Each screening mix was spiked with a single colony before thermocycling. An initiating step of 15 minutes for enzyme activation at 95 ºC was followed by 35 cycles of PCR (20 seconds at 95 ºC for the denaturation step, 20 seconds at 55 ºC for the annealing step, and 2 minutes at 72 ºC for the extension step).

2.4 Sequencing analysis

PCR samples were sent to Source BioScience for sequencing. Sequencing data were visualized in 4Peaks (v 1.8) and sequences were analysed in MEGAX (version 0.1). Reads of consensus sequences were then assembled to generate full-length sequences. The alignment of the generated sequences was achieved using MUltiple Sequence Comparison by Log-Expectation (MUSCLE) tool. After cloning into the desired vectors, sequences were further scrutinized and only inserts with 100% identity to PCR consensus sequences were included in the following experiments.

To choose the best-fitted model to infer phylogeny, a model selection test was run based on nucleotide substitution. To infer the GPC gene phylogeny of LCMV strains isolated worldwide (GeneBank accession numbers shown in **Figure 3-1**) and their relationship to the study isolates, the Maximum Likelihood method and Kimura 2-parameter model (K2) with 1000 bootstraps were applied. To model evolutionary rate differences among sites, a discrete gamma distribution was used (K2+G). The data set was selected from the GenBank database by applying a sequence length filter to only include full-length sequences (nucleotides 1 to 1497) of the LCMV S segment. The list which included 60 sequences was further manually filtered to exclude 10 irrelevant sequences. For the analysis of partial GPC sequences (nucleotides 1 to 225), the UK sequences were selected by searching using the country qualifier (/country=United Kingdom). 97 partial UK sequences were found. All the obtained sequences (147) were then aligned and trimmed for the subsequent phylogenetic analysis.

To infer the full-length GPC phylogeny of the study isolates, the Maximum Likelihood method and Tamura 3-parameter model (T92) with 1000 bootstraps were applied. To model evolutionary rate differences among sites, a discrete gamma distribution was used (T92+G). The analysed 16 GPC sequences were derived from 11 mouse samples and four NHP samples. An outgroup

(accession number AJ318512.1) was added to the full-length analysis to infer the evolutionary direction of the unrooted tree.

2.5 Plasmids

Two vectors were used for mammalian cell expression of LCMV glycoproteins, pcDNA 3.1$^+$ and pI.18. Both vectors are high-copy-number plasmids. pcDNA 3.1$^+$ contains human CMV promoter, multiple cloning sites, bovine growth hormone (BGH)/SV40 polyadenylation termination signal, and ampicillin-resistant gene (pcDNA3.1/V5-His-TOPO, Life Technologies). pI.18 is derived from plasmid pI17 which is believed to be pCU-based. It contains a full promotor, a full intron A gene, and a terminator from human CMV. It also contains an ampicillin-resistant gene, and a truncated enhancer region (Cox *et al.*, 2002). Additionally, it has been modified in-house by the addition of the pcDNA 3.1-specific tags of the cloning primers.

The MLV-based packaging system used consisted of two plasmids: the phCMV5349 plasmid encoding the Gag/Pol gene and the pTG126 plasmid encoding the luciferase gene. phCMV5349 contains a human CMV promotor, ampicillin and HPH resistance genes, and an SV40 early promotor (patent WO1997035996A1). The pTG126 luciferase gene possesses an upstream Ψ packaging signal and flanking MLV long terminal repeats.

Plasmids used to produce the transduction units for *DAG1* expression in HAP1 KO cells included pHIV-EGFP (addgene #21373), pMD2.G (addgene #12259), and pCMV delta R8.74. pHIV-EGFP (transfer plasmid) was derived from pSICO by removing the U6-TATAlox-CMVie-EGFP-TATAlox- WPRE and adding the EF1-alpha promoter, an MCS, an IRES and EGFP for bicistronic expression (Welm *et al.*, 2008). pMD2.G is a lentivirus-based plasmid expressing Vesicular Stomatitis Virus glycoprotein (VSV-G). pCMV delta R8.74 (packaging plasmid) is a derivative of pCMV delta R8.2 (addgene #12263) lacking the four accessory genes *vif, nef, vpr,* and *vpu*. pCMV delta

R8.2 is an HIV1-based packaging plasmid with truncated *Env* gene but expressing *Gag/Pol, Tat, Rev*, and all accessory genes.

2.6 Digestion enzymes

High-Fidelity (HF) restriction enzymes from New England Biolabs (NEB) were used for all plasmid digestion reactions. 20-50 μl reactions contained 5-10 μg of plasmid and 1:1 enzyme to X10 rCutSmart buffer. The mix was then incubated overnight at 37 ºC.
BamHI-HF, EcoRI-HF, and BmtI-FH enzymes were used to digest pHIV-EGFP, pI.18/pcDNA3.1, and pcDNA-Fc construct, respectively.

2.7 InFusion cloning

PCR products were first treated with cloning enhancer (NEB) or DpnI-FD (Thermo Fisher). Then PCR products and digested vectors were purified using the Monarch PCR & DNA Cleanup Kit (NEB). A reaction of 2.5 μl, containing 0.5 μl of Infusion premix, 1 μl (50-100 ng) of linearized vector, and 1 μl (50-100 ng) of treated/purified PCR product, was prepared. The mixtures were incubated for 15 minutes at 50 ºC. The reactions were then placed immediately on ice after incubation. The mixtures were next added to 30 μl of stellar competent cells (Takarabio) or NEB Stable Competent *E. coli* (C3040H) and incubated for 30 minutes on ice followed by a heat shock step at 42 ºC for 45 seconds. The mixtures then were incubated with recovery media for an hour, plated in an appropriate selection agar, and incubated overnight at 37 ºC (Stellar cells) or 30 ºC (NEB stable cells).

2.8 Mutagenesis

To introduce point mutations, site-directed mutagenesis (SDM) kit from BioLabs was used. The NEBaseChanger (v1.2.9) online tool was used to design mutagenesis primers with the forward primers harbouring the substitution or insertion **(Table 2-2).** 0.5-12.5 ng of template was used in SDM reactions, which contained 6.25 μl Q5 Hot Start High-Fidelity 2X master mix, 0.625 μl forward/reverse primers, 4 μl of nuclease-free water, and 1 μl of diluted template. Reactions were performed using the following cycling conditions: an initial step for 30 seconds at 98 ºC followed by 30 cycles of denaturation (98 ºC for 10 seconds), annealing (60 ºC for 20 seconds), and extension (72 ºC for 30 sec/1kb) steps. For product phosphorylation and ligation and template removal, KLD enzyme mix (kinase, ligase, and DpnI) and buffer were used. Each reaction contained 5 μl of 2X KLD buffer, 1 μl of 10X KLD enzyme mix, and 1 μl of SDM product with 3 μl of nuclease-free water to make a total volume of 10 μl. The reaction was incubated for 5 minutes at 22 ºC then immediately followed by transformation into competent cells.

2.9 Plasmid extraction

For plasmid extraction, two GenElute HF kits from Sigma Aldrich were used: the Miniprep and the Midiprep kits. Spin-column and vacuum methods were used to recover up to 15 μg and 350 μg of plasmid from 5 ml (Miniprep) and 50 ml (Midiprep) of E.coli culture, respectively. The steps included a single colony inoculation of LB broth containing 0.1% penicillin then incubation at 30 or 37 ºC for ~18 hours with continuous shaking. Cultures were then spun for 5-10 minutes at > 11000 X g. Pelleted bacterial cells were lysed, filtered, or spun, and cleared lysates were passed through binding columns. Bound DNA was eluted in 60-600 μl of elution buffer (10 mM Tris-HCl, 1 mM EDTA, pH 8.0).

2.10 Gel Electrophoresis

All PCR products were visualized under UV light after running 2%(w/v)-agarose-gel electrophoresis with ethidium bromide. It was performed using a voltage of 90V for 36-42 minutes depending on product size.

2.11 Spectrophotometry

To measure the yield and purity of PCR products and plasmids, NanoDrop model 1000 from ThermoFisher was used. Nucleic acid concentrations were read at a wavelength of 260 nm and reported in ng/μl. Purity was reported as a 260/280 ratio.

2.12 Cells

HEK 293T cells were used for transient expression to produce pseudotypes. The parental line was initially transformed using fragments of adenovirus 5 DNA (Lin *et al.*, 2014). Its variant HEK 293T contains SV40 large T antigen which in the presence of a plasmid harbouring the SV40 origin of replication results in a high expression level of the encoded protein (DuBridge *et al.*, 1987).

Two lines of cells were used in infection assays, Vero E6 and L929 cells. Vero cells are a fibroblast-like cell line derived originally from a kidney of an African green monkey (Ammerman *et al.*, 2008). L929 cells are fibroblasts derived from a male mouse C3H/An connective tissue (Sanford *et al.*, 1948). Cells were passaged every 72-96 hours in 30 ml of Dulbecco's Modified Eagle Medium (DMEM, Gibco 11965-084) supplemented with 10% fetal bovine serum and 0.1mM non-essential amino acids. Cells were seeded at a density

of 1.5 to 2 $x10^6$ cells per 175 cm^2 flask and maintained in a 37 ºC 5% CO_2 incubator.

For α-DG-Fc production, Free-style 293 cells (Thermo Fisher Scientific R79007) were used. This line of cells is a variant of HEK 293 that was adapted to suspension growth in serum-free media allowing high-density large-scale cultivation (Malm *et al.*, 2020). The cells were grown and maintained in Gibco Expi293 Expression Medium (Thermo Fisher Scientific A1435101). Upon passaging, 10-12X10^6 cells were transferred to fresh media in a total volume of 40 ml (3X10^5 cell/ml). The cells were passaged every ~ 72-96 hour and maintained at 37 ℃ and 5% CO2 with continuous agitation.

Two DAG1 KO cell lines and their respective WT were used HAP1 and KM155. HAP1 WT/KO cells were a kind gift from Dr Melinda Brindley from the University of Georgia, USA. HAP1 is a human near-haploid cell line that has a single copy of almost every human chromosome. They were derived from the chronic myelogenous leukaemia (CML) cell line KBM-7which, in turn, was derived from a male patient and lack a Y chromosome (Kotecki *et al.*, 1999). The cells were originally obtained from Horizon Discovery (HZGHC000120c016) which produced the KO cells by introducing a single base pair deletion at the end of the first coding exon of DAG1 gene using CRISPR-Cas9 gene-editing technology resulting in an N terminal fragment of 79 amino acids. The cells were maintained in Gibco IMDM media (Iscove's Modified Dulbecco's Medium, ThermoFisher 12440053) supplemented with 10% FBS. The cells were passaged every 72-96 hours and confluency of <70% was maintained at all times.

KM155 WT/KO cells were a kind gift from Dr Steve Winder at the University of Sheffield. They are immortalized human skeletal myoblasts that were edited using CRISPR-Cas9 to knockout *DAG1* gene using two gRNAs flanking the ATG region in the first coding exon resulting in deletions at both sites or excision of the entire flanked region. The KO was confirmed according to the provider based on the lack of the β-DG subunit in western blotting and

immunofluorescence analysis. The parental cell line was described by Mamchaoui et al. (Mamchaoui *et al.*, 2011). They were maintained in skeletal muscle cell growth media (PromoCell, C-23160) supplemented with fetal calf serum, fetuin, epidermal growth factor, basic fibroblast growth factor, insulin, and dexamethasone (final supplement concentrations 0.05 ml/ml, 50 μg/ml, 10 ng/ml, 1 ng/ml, 10 μg/ml, and 0.4 μg/ml, respectively). The cells were passaged every 72-96 hours with maximum confluency of 60% at all times.

2.13 Pseudotype production

A three-plasmid expression system was used for the production of pseudotypes; a packaging plasmid (MLV Gag/Pol), a transfer plasmid (Luciferase), and an envelope plasmid (pI.18/pcDNA3.1^{+}). The plasmids pcDNA 3.1^{+} or pI.18 encoded the study GPC sequence from eleven of the 15 samples from which a full-length GPC could be obtained (seven mouse and four NHP samples). The protocol followed was as described previously (Urbanowicz *et al.*, 2016a). Briefly, HEK293T cells were seeded in pramaria-coated dishes at a density of 1.5x10^{6} cells per dish in 10 ml of DMEM supplemented with 10% fetal bovine serum and 0.1 mM non-essential amino acids. After overnight incubation at 37 ºC and 5% CO_2, the cells (confluency of ~50%) were transfected with 2 μg of each plasmid together with a transfection reagent (polyethylenimine) topped with Opti-Mem (reduced serum media, Gibco 31985-070) to give a total volume of 600 μl and incubated in 7ml of Opti-Mem for six hours. The Opti-Mem was then replaced with 10 ml supplemented DMEM and incubated. After 72 hours, pseudotypes were harvested by passing the supernatant through a 0.45 μM filter. If not immediately used, pseudotypes were stored at 4 ºC for a maximum of 2-3 weeks.

2.14 Infection assays

Infection assays were carried out in solid-bottom 96-well corning plates seeded with $1x10^4$ Vero cells or $2x10^4$ L929 cells per well and incubated overnight. HAP1 cells including WT, KO, and transduced cells were seeded at $1X10^4$ cell/well in a 96-well plate 18-24 hours prior to infection. KM155 (WT/KO) were seeded at $5X10^3$ cell/well in a 96-well plate 18-24 hours prior to infection. Cells were infected with 100 μl/well of pseudotypes and incubated for 72 hours. Following incubation, 50 μl of 1:5 diluted lysis buffer (Cell Culture Lysis Reagent, Promega Cat.# E1531) was added to each of the wells, the plates then were placed for 15 minutes on a shaker at a speed of 20 rpm. To read plates, FLUOstar Omega microplate reader from BMG LABTECH was used. The machine injects 50 μl of luciferase substrate (Promega Cat.# E152A) into each well then reads the luminescence emitted within one second. Lens was set as the emission filter at a PMT gain of 3600 to measure infectivity in all cells except KM155, a gain of 2800 was instead used. In all infection assays samples were run in triplicates.

2.15 Antibodies

Primary antibodies: IIH6C4 is a mouse IgM monoclonal antibody recognizing a glycosylated epitope in α-DG (Merck Millipore 05-593). The species reactivity includes rabbit, human, and mouse. The α-DG polyclonal antibody (Thermo Fisher PA5-193223) is a goat IgG antibody against a short synthetic peptide (HVGKHEYFMHATDK) corresponding to an internal sequence of α-DG. The species reactivity includes rat, human, and mouse. The 22.5D antibody (Zalgen Ab00225D) is an anti-LASV Gp2 human monoclonal antibody targeting a conserved epitope across OWAs (amino acids 300 - 315 LASV GPC, Josiah strain). KL25 was a kind gift from Dr Daniel Pinschewer, University of Basel, Switzerland. It is a monoclonal Ab raised in mouse against LCMV Gp1. Anti-MLV p30 antibody (Abcam 4B2 ab130757) is a mouse

monoclonal IgG antibody recognizing the MLV capsid protein. Anti-β-actin clone AC-74 is a mouse IgG monoclonal antibody (Sigma-Aldrich A2228) with broad species reactivity. Anti-GAPDH goat polyclonal antibody (R&D Systems, AF5718) was used. Both anti- β-actin and anti-GAPDH were used to normalise total protein input in western blots.

Secondary antibodies: II/41 is a monoclonal antibody that reacts with mouse IgM heavy chain and is PE-Cyanine 7 conjugate used in FACS analysis (Thermo Fisher 25-5790-82). For western blots, three HRP conjugated antibodies were used a rabbit anti-mouse antibody (Dako P0260), a rabbit anti-goat antibody (Sigma Aldrich A8919), and a goat anti-human IgG Fc antibody (Merck Millipore AP113P).

2.16 Western blot experiments

2.16.1 Western blot samples preparation

Cell pellets were lysed in 1 ml of lysis buffer containing 50 mM Tris (7.4 pH), 150 mM NaCl, 1 mM EDTA, 1% TritonX100, and 10% protease inhibitor cocktail. After centrifugation for 10 minutes at maximum speed, supernatants were collected and stored at -20 ºC if not used immediately. Pseudotypes were concentrated by ultra-centrifugation (Beckman XL-90) using a 20% sucrose solution as a sedimentation matrix. A fixed-angle rotor (Beckman type 70.1 Ti) was used to pellet samples at a speed of 40,000 X rpm for 150 minutes. The supernatant was then discarded, and the pellets were resuspended overnight in 30 μl of PBS.

2.16.2 Western blot

Total proteins from cell lysates were quantified using the ThermoFisher Scientific Pierce BCA Protein Assay kit following the manufacturer's manual. 5X reducing buffer containing 25% β-Mercaptoethanol was added to samples

in a 1:4 buffer-to-sample ratio and incubated at 95 ºC for 5 minutes. Volumes then were calculated to yield 10 μg of total protein for each sample.

10% Mini Protean TGX gels (BioRad) were used for all samples and were run in a buffer containing 25 mM Tris base, 192 mM glycine, and 0.1% SDS for 60-90 minutes at a constant voltage of 90v. Separated proteins were transferred to a polyvinylidene difluoride membrane (Amersham Hybond P Western blotting membranes, PVDF pore size 0.45 μm) at a constant amp of 100 mAm for one hour. The membrane was then incubated for one hour in a blocking solution containing 0.1% TWEEN, 10% PBS, and 10% reduced milk. Primary antibodies were diluted (anti-GAPDH 1:5000, anti-KL25 1:200, anti-α-DG 1:1700, and anti- β-actin 1:2000) in a 0.1% TWEEN, 10% PBS, and 5% reduced milk and incubated overnight with membranes at 4 ºC. Membranes then were washed in a 0.1% TWEEN and 10% PBS solution 3-5 times for 5 minutes each. After the membranes were incubated with the secondary antibodies (anti-goat 1:1000-10000, and anti-mouse 1:1000-2000) for one hour, the washing step was repeated. Horseradish peroxidase substrate (Azure Biosystems) was then added for the detection of immunocomplexes in SYNGENE GBOX imaging system.

For purified α-DG-Fc, ~45 μl of sample/loading buffer mix was loaded in a 50 μl 10% gel and 1:1000 dilution of anti-human Fc-HRP antibody was used. To blot pseudotype pellets, 10 μl of sample/loading buffer mix was loaded in a 15 μl 10% gel. A dilution of 1:1000 or 4 μg/ml of anti-MLV p30 or 22.5D were used, respectively. Western blot was performed under reducing conditions following the same steps described above.

2.16.3 Western blot signal analysis

Densitometry analysis of western blots was carried out in ImageJ software (v 1.53). Among other functions, this software enables the conversion of signals and pixel values to numeric values.

2.17 Dot blot analysis of virus-α-DG binding

Dot blot analysis was conducted in Bio-Dot microfiltration apparatus by Bio-Rad. The process involved applying the sample to a nitrocellulose membrane (Amersham Protran, pore size 0.45 μm) under the vacuum of a pump connected to the apparatus. The membrane was then blocked in filtered 5% milk PBS and incubated with dilutions of soluble α-DG. The complex was detected using anti-Fc antibody. ΔE and VSV were included as negative controls. Anti-LCMV Gp2 was also used to confirm the immobilization of the virus antigen.

2.18 Transduction and flow cytometry experiments of HAP1 cells

2.18.1 Transduction of DAG1 in HAP1 KO cells

Full-length *DAG1* was amplified from cDNA of L929 cells' total RNA extract (primers shown in **Table 2-2)**. It was then cloned into pHIV-EGFP using InFusion cloning. To produce the transduction unit, HEK293t were seeded at a density of $1.5X10^6$ cell/dish for a total of three dishes 18-24 hours pre-transfection. 2 μg/dish of each plasmid (PMD-VSV-2G, PMCV-R87.4, & pHIV-DAG1-EGFP/pHIV-EGFP) were used to prepare the transfection mix (for more detailed transfection protocol see section **2.13)**. 66-72 hours post-transfection supernatants were collected and ultracentrifuged at 40,000X rpm for 150 minutes. Pellets were resuspended in 150 μl of PBS overnight. Three pellets were combined (450 μl) and topped up with media to a final volume of 1 ml. 24-18 hours before transduction, HAP1-KO cells were seeded in a 24-well plate at a density of $3x10^4$ cell/well. 500 μl/well of resuspended pellets were used to transduce the KO cells then topped up with 1 ml/well of media 4 hours post-transduction. EGFP expression was examined after 66-72 hours using iRiS Digital Cell Imaging System (Logos Biosystems) under similar parameters (light, gain and exposure (ms)) across cell populations. The contents of two

wells were then transferred to a t25 flask and passaged as mentioned in section **2.12.**

2.18.2 Cell sorting and flowcytometry

After two passages, transduced HAP1 cells were sorted in Beckman Coulter Astrios EQ based on EGFP expression into low- (MFI 125.33), medium- (MFI 636.68), and high- (MFI 2358.03) EGFP expressing populations using non-transduced cells as a baseline (MFI 25.81). Sorting required cells to be first washed three times in PBS then resuspended in sorting buffer containing 1mM EDTA, 25 mM HEPES pH7.0, and 1% bovine serum albumin (final concentration 5-10X10^6 cell/ml). A million cells were sorted for each of the populations, transferred into a t25 flask, and passaged in the presence of penicillin/streptomycin at 1% (v/v).

The level of α-DG expression in the three populations was measured using a Beckman Coulter Astrios EQ. The cells were first washed three times in PBS then resuspended in sorting buffer to a final concentration of 1X10^6 cell/ml. Cells were stained with primary antibody (IIH6C4) at 1:10 dilution for 30 minutes then washed with buffer three times. The secondary antibody (PE-Cyanine7) was applied at a dilution of 1:300 for 30 minutes. After three washes, cells were resuspended in 1 ml sorting buffer. All centrifugation steps were carried out at X300 g for 5 minutes. All flow cytometry data were analyzed in Kaluza 2.1.2 software by Beckman Coulter.

2.19 α-DG-Fc designing, expression, purification, staining, and quantification

2.19.1 α-DG-Fc constructs

To produce soluble α-DG-Fc fusion protein, a human-IgG- Fc fusion cassette was first generated. Based on pFuse InVivoGen vectors, the Fc sequences

include the hinge region plus CH2 and CH3 and either the pFuse IL-2 signal sequence or kappa signal sequence used in the pMam-IgKL. Thus, a kappa signal sequence was included upstream to the Fc region separated by a BmtI restriction site. The final cassette was codon-optimized and synthesized (Thermo Fisher). The cassette was then inserted into pI.18 or pcDNA3.1 plasmids after digestion with EcoRI. The constructs were subsequently digested with BmtI to insert the α-DG. The α-DG fragment (amino acids 30 to 485) was amplified from either L929 or Vero E6 cDNA using InFusion primers with Fc/kappa signal tags. To ensure the reinstatement of the kappa signal peptide sequence, a 'T' nucleotide at the 5' end of the insert-specific region and the 3' end of the kappa signal sequence homology arm in the sense primer was added. Additionally, a TC dinucleotide at the 5' end of the insert-specific region and 3' of the Fc-homology arm-specific region of the reverse primer was added to reinstate the Fc sequence reading frame. The product was then cloned into the pI.18/pcDNA3.1-Fc digests for mammalian cell expression.

2.19.2 α-DG-Fc expression

α-DG-Fc was expressed in Free-Style HEK 293 cells using TransIT-Lenti transfection reagent from Mirus Bio. Briefly, 35 μg of plasmid was first mixed with 90 μl of the transfection reagent and topped up with Opti-Mem to make a total volume of 3 ml. The mixture was incubated for 15 minutes then added to the cell culture. The density of the cell culture at the time of transfection was $2x10^6$ cell/ml in a total volume of 30 ml. 72 hours post-transfection, the culture was split equally into three flasks and topped up with 20 ml of fresh media each. After an additional 72 hours, the cultures were centrifuged at 3000 Xg for 10 minutes. The supernatants were collected and filtered through a 0.45 μm filter.

2.19.3 α-DG-Fc purification and concertation

Purification of α-DG-Fc recombinant protein using AKTA

After expressing the α-DG-Fc construct, the supernatants were collected and passed through HiTrap protein G high-performance purification column installed in a Fast Protein Liquid Chromatography instrument (AKTA Amersham Biosciences). Briefly, the collected supernatant was mixed with the binding buffer (0.02 M sodium phosphate, pH 7.0) and passed through the column. After washing the unbound material, the elution buffer was applied (0.1 M glycine-HCl, pH 2.7). The elutes were then neutralized in 1 M Tris-HCl, pH 9.0. The absorption of UV light at 280 nm was monitored in real-time which would allow the collection of the fractions that most likely contained the protein.

Protein G purification column

50 ml of supernatant was concentrated to 8.5 ml using Amicon Ultra-centrifugal filter tubes from Merck Millipore (50 kDa molecular weight cut-off). The concentrate was then passed through a protein G purification column following the manufacturer's protocol with minor changes (Thermo Scientific NAb Protein G Spin Kit). Briefly, after the storage solution was discarded, the column was equilibrated by adding 2 ml of binding buffer (100 mM phosphate, 150 mM sodium chloride; pH 7.2 in 500 ml of ultrapure water). After discarding the flow-through, 2 ml of the sample was applied and incubated at room temperature with end-over-end mixing for 20 minutes then the flow-through was discarded. The last step was repeated three more times, then the column was washed three times in the binding buffer. The protein was then eluted in 100 μl of neutralization buffer (1M Tris•HCl, pH 8.5) by adding 1 ml of elution buffer (pH 2.8) to the column. A total of six elutions were made, protein concentration was measured for each of the elutions via spectrophotometry, and the elutions with a concentration of 0.1 mg/ml or more were pooled. The pooled elutions were further concentrated by Amicon tubes to 1 ml. If not used immediately, the concentrate was aliquoted and stored at -20 ºC.

2.19.4 Quantification of α-DG-Fc

Protein G column purified α-DG-Fc was quantified by NanoDrop (model 1000 ThermoFisher) and Pierce BCA Protein Assay (23227 Thermo Fisher). The absorbance in the nanodrop was measured at 280 nm using the generic default extinction coefficient (1 Abs =1 mg/ml) and a baseline normalization at 340 nm.

The BCA assay was performed to construct a standard curve using albumin standards with a working range of 20-2000 μg/ml. The colourimetric reaction results in a linear absorbance at 562 nm with increasing concentrations of protein. The BCA standards and reagents were prepared as per the manual.

2.19.5 Coomassie staining

0.125 % (W/V) Coomassie blue stain (50 % methanol and 10 % glacial acetic acid) was incubated with resolved proteins in polyacrylamide gels for 2 hours with continuous shaking. Gels were then placed in distilled water for ~ 48 hours to allow for de-staining.

2.19.6 Silver staining

Purified αDG-Fc was stained using a Dodeca Silver Stain Kit from Bio-rad following the manufacturer's instructions. Briefly, after running SDS-PAGE gel, the gel was fixed in a solution containing 40% ethanol and 10% Glacial acetic acid, for 30 minutes. Next, the gel was incubated with sensitizing solution (1:10 sensitizing concentrate, 1:100 background reducing concentrate, 30% ethanol) for 30 minutes. The gel was then washed with distilled water three times for five minutes each. The staining solution (1:50 silver staining

concentrate) was incubated with the gel for 20 minutes then washed in distilled water for 10 minutes. The developing solution (1:10 development buffer concentrate, 1:5000 image developer concentrate, 1:20000 background reducing concentrate) was applied for 25 minutes before washing with a stopping solution (5% Glacial acetic acid). The stained gel was then imaged in SYNGENE GBOX imaging system.

2.20 Inhibition assays using soluble α-DG

18-24 hours pre-infection, L929 or Vero cells were seeded in a 384-well plate at a density of $5X10^3$ or $2.5X10^3$ cell/well, respectively. Purified murine or NHP α-DG-Fc was serially diluted (X2 folds) in PBS with a starting concentration of 60 and an ending concentration of 0 μg/ml. 3 μl of each dilution were mixed with 27 μl of pseudotypes (1:10 dilution) and incubated at 37 ºC for 1 hour. Media was then removed from the plates and 25 μl of α-DG-Fc/pseudotypes mixes were transferred to each well matching the α-DG-Fc species with that of the target cells. Four hours post-infection, the inocula were removed and replaced with 75 μl of media. Results were read ~ 72 hours following infection.

2.21 Overexpression of LARGE1

Production of LARGE1 transduction units

The Ad5/hLARGE1-EGFP construct was a kind gift from Professor Kevin Campbell, University of Iowa. Upon receiving, LARGE1 was sub-cloned into pHIV-blasticidin (pHIV-BSD) expression vector. 18-24 hours pre-transfection, HEK293t cells were seeded at a density of $1.5X10^6$ cell/dish for a total of 3 dishes. 2 μg/dish of each plasmid (PMD-VSV-2G, PMCV-R87.4, & pHIV-LARGE1-BSD) were used to prepare the transfection mix (for more detailed transfection protocol see section **2.13**). 66-72 hours post-transfection supernatants were collected.

LARGE1 transduction

In a 12-well plate, HEK293T cells were seeded at a density of $8X10^4$ cell/well. After 18-24 hours, wells seeded on the first day were infected with 800 μl/well of transduction unit (supernatant) then topped up with supplemented DMEM to a total volume of 2 ml/well. The media was changed with media containing 10, 4, 2, or 0 μg/ml blasticidin every day for the next two days. On the fifth day, HEK293T-LARGE$^+$ cells from the 10 μg/ml well were transferred into a 6-well plate alongside WT HEK293T, in media containing either 10 or 12.5 μg/ml blasticidin. After ~ 72 hours, the HEK LARGE$^+$ cells at 12.5 μg/ml were transferred to t75 and t25 flasks (1.7 and 0.6 $X10^6$ cells, respectively) and passaged as per WT HEK293T cells.

2.22 Statistical analysis and graphs

GraphPad Prism software version 7 was used to perform the statistical tests and to generate the graphs. The data in all graphs represent RLU values after subtracting the baseline (average RLU of ΔE). Before conducting the statistical tests, normality tests were performed when possible to determine the type of distribution the data follow. These included: D'Agostino- Pearson omnibus or Shapiro–Wilk normality tests. Accordingly, parametric or non-parametric tests were applied. To compare two groups, t-test or Mann-Whitney tests were used to determine the statistical significance. To compare more than two groups, one-way ANOVA with Tukey's multiple comparisons test or Kruskal Wallis test were used.

For L929 inhibition assay, a nonlinear regression analysis was carried out to compare the inhibition curves and determine significance. The best-fit model was determined based on a model comparison test and the R^2 values. Accordingly, a sigmoidal dose-response (variable slope) model was adapted

for all data. The Top (maximum inhibition) values of different clones were compared. For all tests, a P-value of <0.05 was considered significant.

2.23 DAG1 transcript variants and protein conservation analysis

DAG1 human transcript variants list was generated in RefSeq database (gene ID 1605) to include naturally occurring variants in normal human tissues. The transcripts RefSeq ID are shown in **Figure 6-7**. For protein conservation analysis, full-length *M.musculus* DAG1 protein was searched in Blastp database. The sequence coverage was set at 95% to 100% to only include full-length sequences. Repeated species were filtered out to include only one sequence per species. The reference numbers for the sequences included are shown in **Table 6-1.** The alignment of NHP DAG1 amino acid sequences and *M.musculus* was generated in Constraint-based Multiple Alignment Tool (COBALT NCBI).

2.24 Mapping key residues in crystal structures

The crystal structures of LCMV Gp1-Gp2 (5FINE) and LASV Gp1-Gp2 (LASV GPCysR4) in their pre-fusion forms were visualized and analysed in UCSF Chimera (1.12.0). The PDB files were deposited in Research Collaboratory for Structural Bioinformatics PDB by Hastie, K.M. and Saphire, E.O.(Hastie *et al.*, 2016, Hastie *et al.*, 2017). The structures were based on the LCMV WE HPI strain (amino acids 63 to 427) and LASV Josiah strain (amino acids 60 to 424) delineating the Gp1-Gp2 ectodomains. The residues of interest were mapped based on the alignments provided within each file.

Chapter. 3: The phylogeny and sequence analysis of the LCMV GPC isolates

3.1 Introduction

16 Full-length LCMV GPCs were isolated from 15 samples taken from the animals during the outbreak. Those included 12 mouse (M1 to M12) and four NHP (NHP1 to NHP4) clones. Clones M7 and M8 were isolated from the same sample. Before analyzing the generated GPC sequences in-depth to map changes between NHP and mouse clones that may exist, a phylogenetic analysis of the study isolates and LCMV GPCs isolated worldwide was carried out. Additionally, local analysis to elucidate phylogeny within the study isolates was performed.

3.2 Results

3.2.1 The isolated GPC sequences belong to LCMV lineage I

A phylogeny was generated to see how the study isolates were related to other LCMV strains. To this end, 46 full-length LCMV GPC sequences, obtained from both wild mice and clinical isolates, were retrieved from GenBank (accession numbers are shown in **Figure 3-1. A**). The sequences were then aligned with the study sequences and a phylogenetic tree was constructed using the Maximum Likelihood Method and Kimura 2-parameter model with 1000 bootstraps. The obtained phylogeny showed that the study sequences were more related to sequences belonging to lineage I. The study isolates, however, form a distinct cluster with a relatively long branch length probably due to the lack of genetic intermediates and sequences from the same geographical area (UK sequences). To expand the analysis to include sequences from the UK, a country identifier was applied to retrieve LCMV sequences from GenBank that were specifically isolated from the UK. 97 partial LCMV GPC sequences isolated from wild mice trapped in the UK were

found. The partial sequences were aligned with the corresponding region of the full-length sequences and the unaligned regions were trimmed. A phylogenetic tree was constructed using the Maximum Likelihood Method and Kimura 2-parameter model with 1000 bootstraps **(Figure 3-1. B)**. The obtained phylogeny showed clustering of the study sequences with other UK sequences with more than 90% support. Similar, to the previous analysis, both the study and the UK sequences were most related to sequences belonging to lineage I.

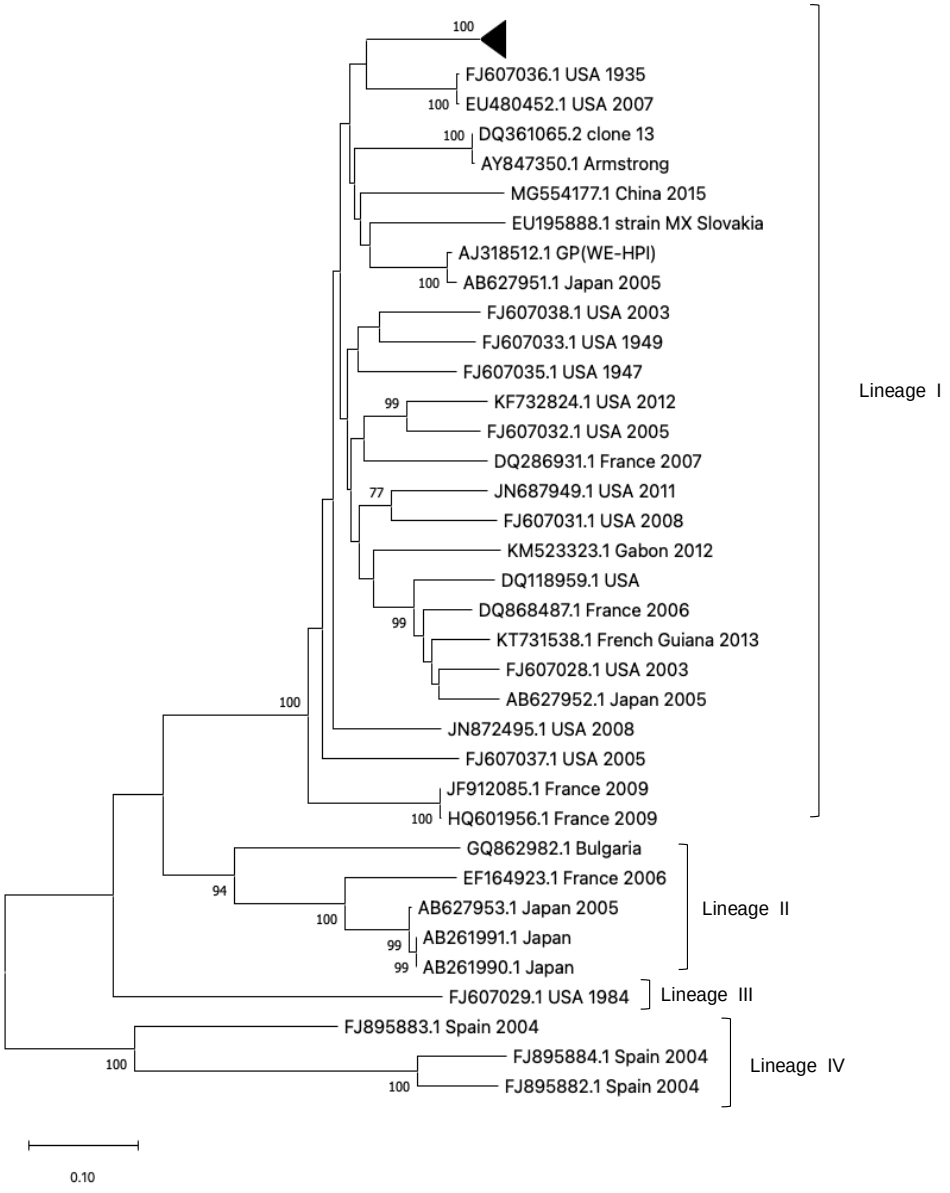
3.2.2 The study isolates segregated according to species

To elucidate the evolutionary relationship between the study clones, phylogenetic trees based on nucleotide and amino acid sequences were constructed using the Maximum Likelihood method and Tamura 3-parameter model with 1000 bootstraps. The LCMV WE sequence (Genbank Accession Number: AJ318512) was used as an outgroup to infer the evolutionary direction of the tree **(Figure 3-2).** The nucleotide-based phylogeny showed that the mouse- and NHP-derived sequences clustered separately. The mouse-derived sequences consisted of a main cluster of highly related sequences in addition to a single sequence (M10) that was genetically distinct and basal to the main cluster. Similar to the nucleotide-based tree, the amino acid-based tree showed that the sequences clustered mainly based on species. Three of the NHP sequences (NHP1, NHP3, and NHP4) showed 100% amino acid identity with each other. Of the mouse sequences, M6 and M9 were also identical. To further explore the genetic diversity within and between clusters, pairwise distances were calculated based on the nucleotide and the amino acid sequences **(Figure 3-3).** Within the main mouse cluster, the mean pairwise distances were 0.005 and 0.007 at the nucleotide and amino acid levels, respectively. Within the NHP cluster, mean pairwise distances of 0.007 and 0.003 at the nucleotide and the amino acid levels, respectively, were observed. The distance between the main mouse cluster and M10 (0.018 at the level of nucleotide/amino acid) was comparable to the

distance between the main mouse cluster and the NHP cluster (0.022 and 0.018 at the nucleotide and the amino acid levels, respectively).

A correlation between the root-to-tip distance and the collection date can be used to infer the dynamics of viral transmission. Within-species transmission is expected to produce a positive correlation between the root-to-tip distance and the collection date. Comparing the root-to-tip distances of the NHP clones for which the collection dates were known (NHP2 and NHP3) showed a correlation with the collection dates. This correlation was absent within the mouse cluster for some clones. For example, M11 has the latest collection date yet it has a root-to-tip distance that is shorter than most mouse sequences.

A


100
FJ607036.1 USA 1935
100
EU480452.1 USA 2007
100
DQ361065.2 clone 13
AY847350.1 Armstrong
MG554177.1 China 2015
EU195888.1 strain MX Slovakia
AJ318512.1 GP(WE-HPI)
100
AB627951.1 Japan 2005
FJ607038.1 USA 2003
FJ607033.1 USA 1949
FJ607035.1 USA 1947
99
KF732824.1 USA 2012
FJ607032.1 USA 2005
DQ286931.1 France 2007
77
JN687949.1 USA 2011
FJ607031.1 USA 2008
KM523323.1 Gabon 2012
DQ118959.1 USA
99
DQ868487.1 France 2006
KT731538.1 French Guiana 2013
FJ607028.1 USA 2003
AB627952.1 Japan 2005
100
JN872495.1 USA 2008
FJ607037.1 USA 2005
JF912085.1 France 2009
100
HQ601956.1 France 2009
Lineage I
GQ862982.1 Bulgaria
EF164923.1 France 2006
94
100
AB627953.1 Japan 2005
99
AB261991.1 Japan
99
AB261990.1 Japan
Lineage II
FJ607029.1 USA 1984
Lineage III
FJ895883.1 Spain 2004
100
FJ895884.1 Spain 2004
100
FJ895882.1 Spain 2004
Lineage IV
0.10

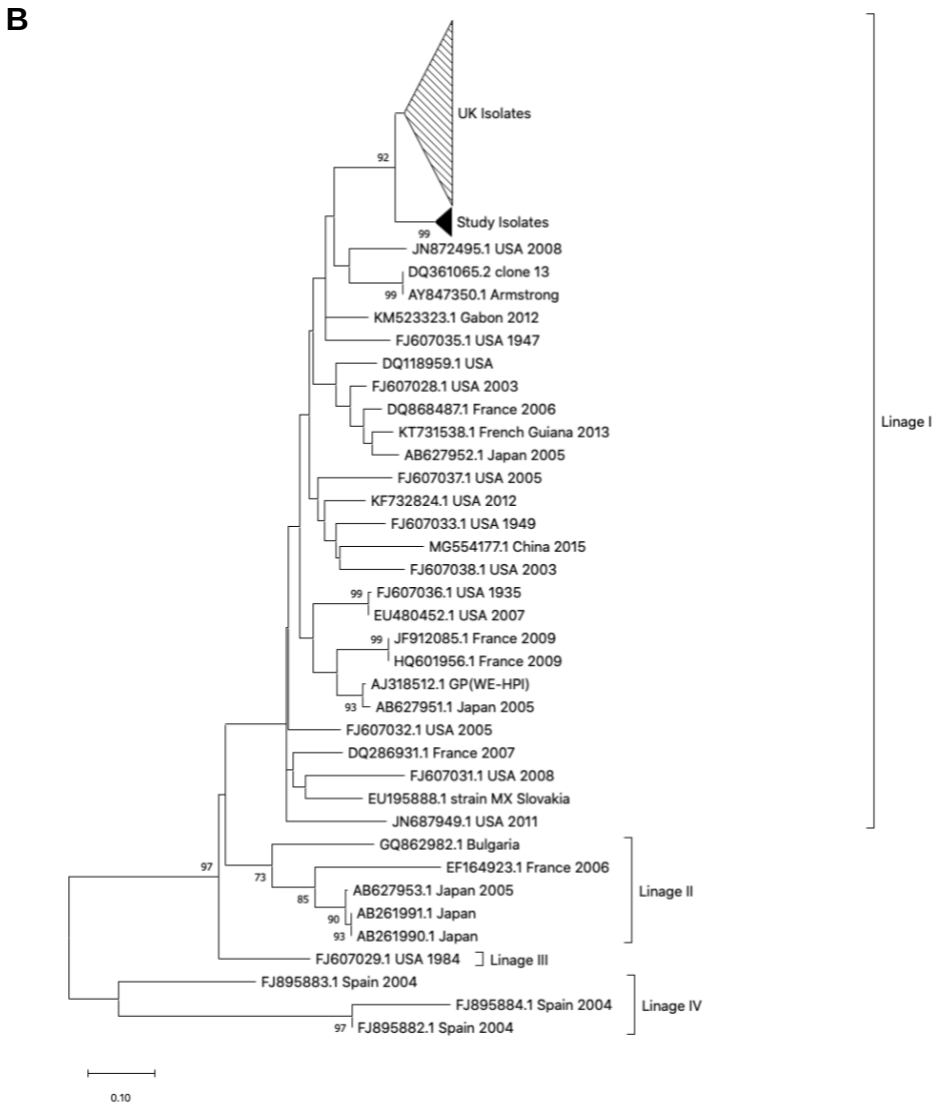


Figure 3-1: The phylogenetic relationship between worldwide LCMV GPC isolates and the study isolates.

After running a model selection test, the phylogeny was constructed using the Maximum Likelihood method and Kimura 2-parameter model as this model showed the lowest Bayesian Information Criterion (BIC) score (lower score indicates a better substitution model). To model evolutionary rate differences among sites, a discrete gamma distribution was used. **A)** The analysis included 46 full-length GPC sequences isolated worldwide, in addition to the study isolates (filled triangle). **B)** The analysis included 147 partial GPC sequences (nucleotides 1 to 225) isolated from both human and mouse samples. The patterned triangle represents the United Kingdom isolates (accession numbers DQ275200.1 to DQ275294.1) and the filled triangle represents the study isolates (15 sequences). Lineages are assigned in accordance with Albarino *et al* classification(Albariño *et al.*, 2010). The trees were drawn to scale, with branch lengths measured in the number of substitutions per site. Numbers on the nodes represent bootstrapping support of 70% or more. For both trees, 1000 bootstraps were applied.

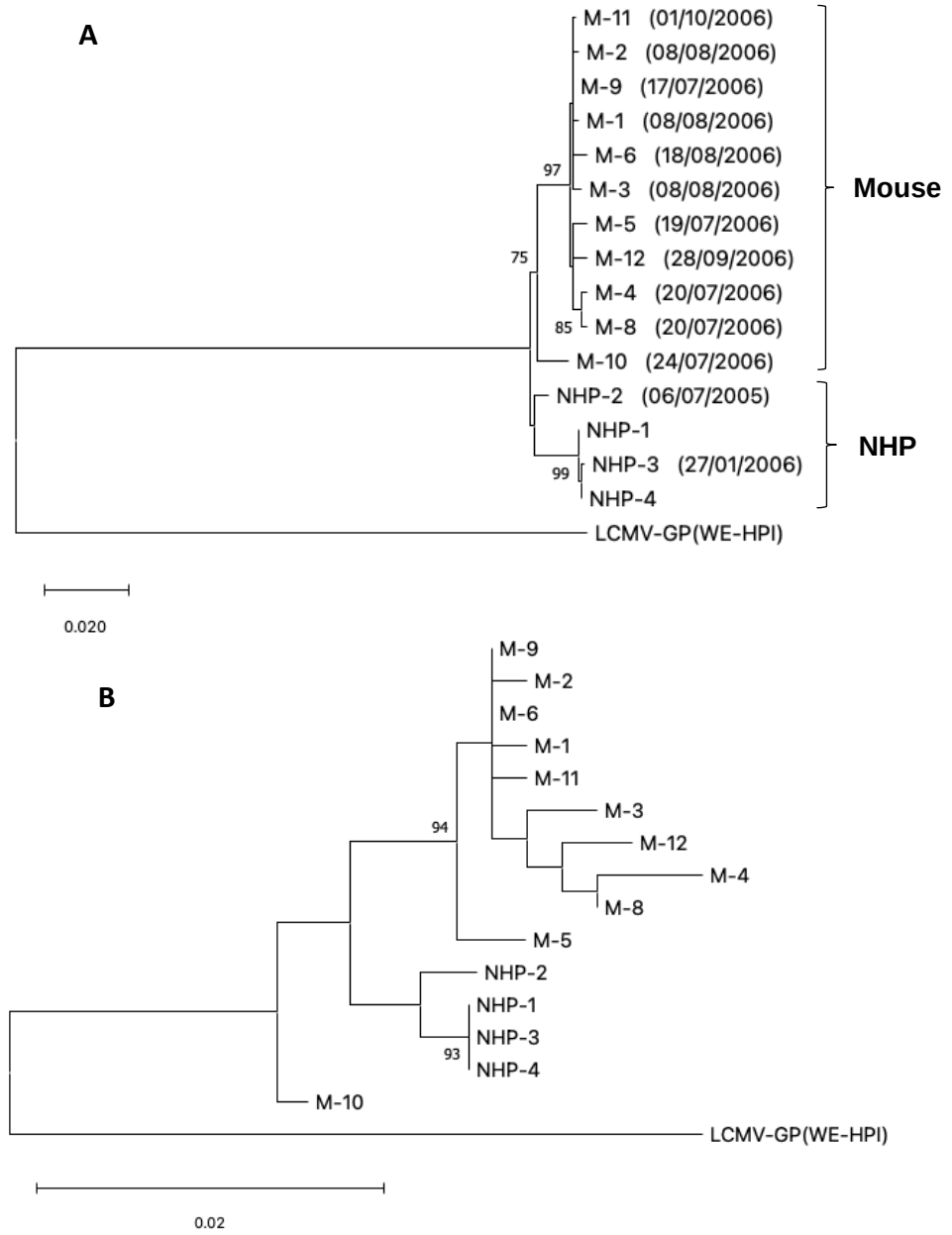


Figure 3-2: The phylogenetic relationship between the GPCs of the study isolates.

After running a model selection test, the phylogeny was constructed using the Maximum Likelihood method and Tamura 3-parameter model as this model showed the lowest Bayesian Information Criterion (BIC) score (lower score indicates a better substitution model). To model evolutionary rate differences among sites, a discrete gamma distribution was used. The analysis included 15 full-length (nucleotides 1 to 1497) wild-type GPC sequences and an outgroup (full-length LCMV WE-HPI GPC). **A)** Phylogenetic tree based on the nucleotide sequences. Collection dates are shown next to each sample. **B)** Phylogenetic tree based on the amino acid sequences. The trees were drawn to scale, with branch lengths measured in the number of substitutions per site. Numbers on the nodes represent bootstrapping support of 70% or more. For both trees, 1000 bootstraps were applied.

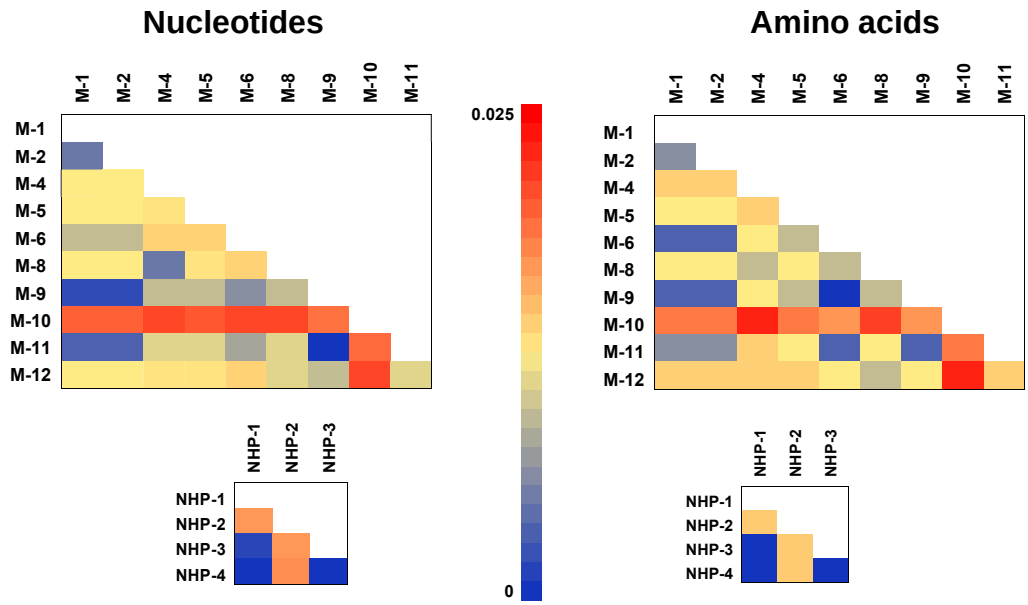


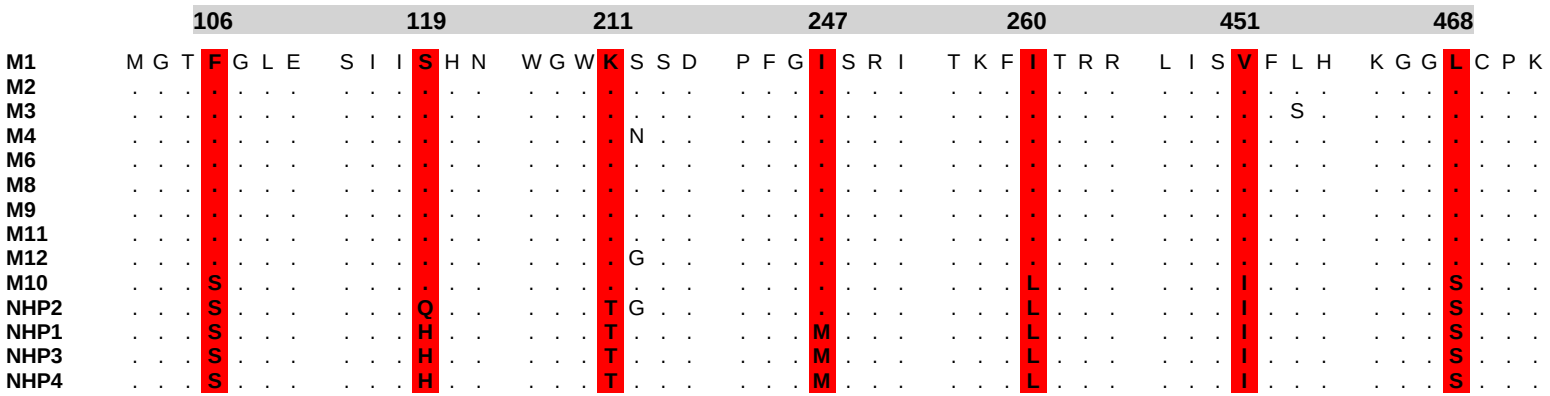
Figure 3-3: Heat map of pairwise genetic distances of the mouse and the NHP sequences.

Pairwise genetic distance analysis was conducted using Maximum Composite Likelihood model (nucleotide) or Poisson correction model (amino acid) with a gamma distribution to model variation among sites. A bootstrap of 1000 replicates was applied. The number of substitutions per site was colour coded as depicted.

3.2.3 The sequence alignment revealed multiple positions showing species specificity

To identify changes that may exist in the NHP clones relative to the mouse clones, the amino acid sequences of the study isolates were aligned and analyzed. The sequence analysis showed mouse/NHP split at multiple sites. The mouse clones (all except M10) had in common four amino acid changes compared to the NHP clones: a serine-to-phenylalanine change at position 106, a leucine-to-isoleucine change at position 260, an isoleucine-to-valine change at position 451, and a serine-to-leucine change at position 468. In addition, they all had a threonine-to-lysine change at position 211 compared to the NHP clones. The M10 sequence was also compared to the NHP clones which further pinpointed two positions, 119 and 247. M10 had a histidine-to-serine change at 119 and methionine-to-isoleucine change at 274, which were also present in the main cluster of the mouse clones, compared to the majority

of the NHP clones (all except NHP2). This places M10 and NHP2 genetically intermediate relative to the main clusters. **Figure 3-4** summarizes the mutations identified.


106 119 211 247 260 451 468
M1 M G T F G L E S I I S H N W G W K S S D P F G I S R I T K F I T R R L I S V F L H K G G L C P K
M2 . . .

3.3 Discussion

LCMV lineage I has a wide distribution and most LCMV isolates belong to this lineage (Albariño *et al.*, 2010). Lineages II and IV together with I were all previously detected in wild rodents in Europe. LCMV GPC sequences isolated from rodents across Europe are readily available in databases and frequently analyzed (Palacios *et al.*, 2008, Albariño *et al.*, 2010, Asper *et al.*, 2001). In contrast, sequences derived from the UK are scarce despite previous studies showing a high prevalence of the virus in mice. Indeed, the only UK sequences available in GenBank were partial and ~200 nucleotides in length. In this study, full-length LCMV GPC sequences were generated from the NHP and the mouse samples taken during the outbreak that occurred in Leicestershire, UK. Comparing the study isolates with LCMV GPC sequences isolated worldwide showed clustering of the study isolates with sequences belonging to lineage I. When the sequences were trimmed to include in the analysis the partial UK sequences generated prior to this study, the study isolates clustered with the other UK sequences with high statistical support (92% bootstrap replicate trees). This indicates a genetic homogeneity and endemicity of LCMV in the mouse population within the UK. This is in line with the high seroprevalence of LCMV in mice (~21%) in the UK found by some studies (Kaplan *et al.*, 1980, Greenwood and Sanchez, 2002). However, the extremely short sequences available from the UK, which were all provided by a single study, may underestimate the real diversity of LCMV in the country.

The transmission dynamics of viral infections can also be inferred from phylogenies. Previous work has suggested that multiple rodent-to-primate transmission events account for most primate cases of LASV. This was based on several observations inferred from the phylogenetic trees including the intermixing of primate and rodent sequences and the lack of a clock-like accumulation of mutations over short time scales, as has been observed in other acute virus outbreaks where primate-to-primate transmission is frequent (Andersen *et al.*, 2015). The phylogeny of GPC sequences in the current study

showed that the NHP and the mouse sequences clustered separately which might be suggestive of primate-to-primate transmission especially since there is an indication that different species were housed together. However, sampling bias may have contributed to this observation and the limited number of samples included in the analysis cannot conclusively determine the transmission pattern. The limited number of NHP samples also made the correlation between the root-to-tip distance and the collection date, a correlation usually seen in within-species transmission, difficult to establish. Even in the mouse cluster which contains a larger number of sequences, the correlation was absent probably due to the lack of statistical support of the branches within the cluster. The chronic nature of LCMV infections in mice may also explain the absence of the correlation.

The variability between sequences was analyzed by calculating the pairwise distances at the level of nucleotides and amino acids. The analysis revealed low variation especially within the NHP cluster indicating a strong spatiotemporal association. However, amino acid variation between the main NHP and mouse clusters was observed at multiple sites. Some of these sites (119, 211, and 260) were described in previous studies (discussed in detail in the following chapters).

Chapter. 4: LCMV pseudotype production and optimization

4.1 Introduction

In the previous section, the phylogenetic analysis revealed a split between the NHP- and the mouse-derived GPC sequences. The sequence analysis highlighted seven sites that showed species-specific signature. To test whether the variants isolated from either NHP or murine samples were also phenotypically distinct, an MLV-based pseudotyping system was employed to generate pseudotypes carrying either NHP- or mouse-derived GPC. This system was repeatedly proven superior to other packaging systems in producing high LASV/LCMV pseudotype titers and recapitulating the entry dynamics of replication-competent LASV system (Cosset *et al.*, 2009, Rojek *et al.*, 2008, Li *et al.*, 2018). Besides the effect of different packaging systems on pseudotype titers, the envelope plasmid backbone and concentration were also found to have a significant impact (Urbanowicz *et al.*, 2016a). Thus, upon pseudotypes production in this study, the type and amount of the envelope plasmid were adjusted to obtain maximum infectivity. The infectivity was optimized in two cell lines, an NHP line (Vero E6) and a murine line (L929), that would be later used in the infectivity assays.

4.2 Results

4.2.1 The envelope plasmid type and amount affected the infectivity of the LCMV pseudotypes

As the type of plasmid used can have a significant impact on GPC production and hence pseudotypes yield, we compared the ability of two plasmid backbones (pI.18 and pcDNA3.1^{+}) to produce infectious pseudotypes. Using the Gag/pol:Luc:pI.18/pcDNA ratio (1:1:1) routinely used in our lab, we

transfected 293T cells to produce pseudotypes bearing LCMV WE54 GPC (a widely used LCMV strain). The infectivity of the two groups of pseudotypes was then assessed in Vero E6 cells. While the pseudotypes produced using pI.18 were infectious and showed an average RLU value of 24579 compared to a value of 7.33 obtained from the negative control ΔE, the pseudotypes produced using pcDNA3.1^{+} showed an infectivity that was comparable to that of ΔE. Thus, for pseudotype production, pcDNA3.1^{+} was excluded and all the GPC were cloned into pI.18.

We next tested whether the plasmid ratio of 1:1:1 Gag/pol:Luc:envelope frequently used in pseudotyping assays was also optimum for LCMV pseudotypes production. To this end, the infectivity of pseudotypes produced using varying amounts of envelope plasmid encoding LCMV WE54 GPC while keeping the amount of the MLV plasmids constant (2 μg each) was measured. One of the study clones (NHP3) was also included. The infectivity was measured in Vero and L929 cells **(Figure 4-1).** For WE54, the infectivity continued to increase in both cell lines with increasing amount of transfected envelope plasmid. For NHP3, however, the infectivity significantly (p-value of 0.002 and < 0.001 in Vero and L929, respectively) declined when more than 2 μg were transfected. Thus, 2 μg of envelope plasmid was adapted throughout the study.

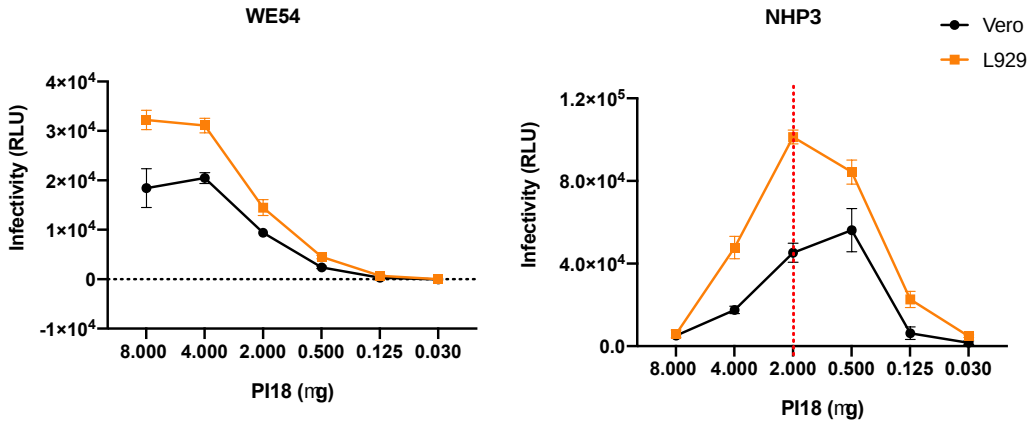


Figure 4-1: Optimization of the envelope plasmid concentration.

Six WE54/NHP3 pseudotype preparations were produced using 2 µg of Gag/Pol and Luc plasmids each. Two-fold dilutions of pI.18 encoding either WE54 or NHP3 GPC starting from 8 µg were performed. $1x10^4$ and $2x10^4$ cells/well of Vero and L929 cells, respectively, were seeded and infectivity of different preps expressed in relative light unit (RLU) was assessed 72 hours post-infection. Each point represents the mean of three replicas ± SD.

4.2.2. The incorporation of GPC into pseudoparticles was similar across the study clones.

The incorporation of GPC into the pseudoparticles was next assessed across the clones to avoid biases that may result from different GPC production/incorporation. Western blot analysis to assess the matrix-to-GPC ratio can be used for this purpose. The only commercially available anti-LCMV GPC was KL25, which targets a slightly variable epitope in Gp1 that may impact its ability to detect GPC from different LCMV strains. Thus, we first tested the ability of this antibody to detect WE54 in addition to clone NHP3.

The antibody reacted with clone WE54 in the cell lysate and showed two bands at ~ 70 kDa and 44 kDa corresponding to GPC and Gp1 monomer, respectively **(Figure 4-2. A).** No signal was detected from the cell lysate of NHP3 confirming the variability of the epitope. To eliminate the effect of epitope variability, we next added a c-terminal tag (FLAG sequence) to NHP3 GPC. The tagged clone, nonetheless, showed a log reduction in infectivity compared to the wild type (data not shown). Hence, the experiment was not pursued further. Finally, we used an anti-LASV Gp2 antibody (22.5D) targeting a highly conserved epitope across OWAs. Using this antibody we compared the incorporation of five of the study clones. Applying densitometric analysis, p30 and Gp2 signals were measured and compared across the clones. The comparison revealed a high correlation between the two signals with matrix-to-GPC ratios ranging between 0.3 and 0.5 for the study clones **(Figure 4-2. B).**

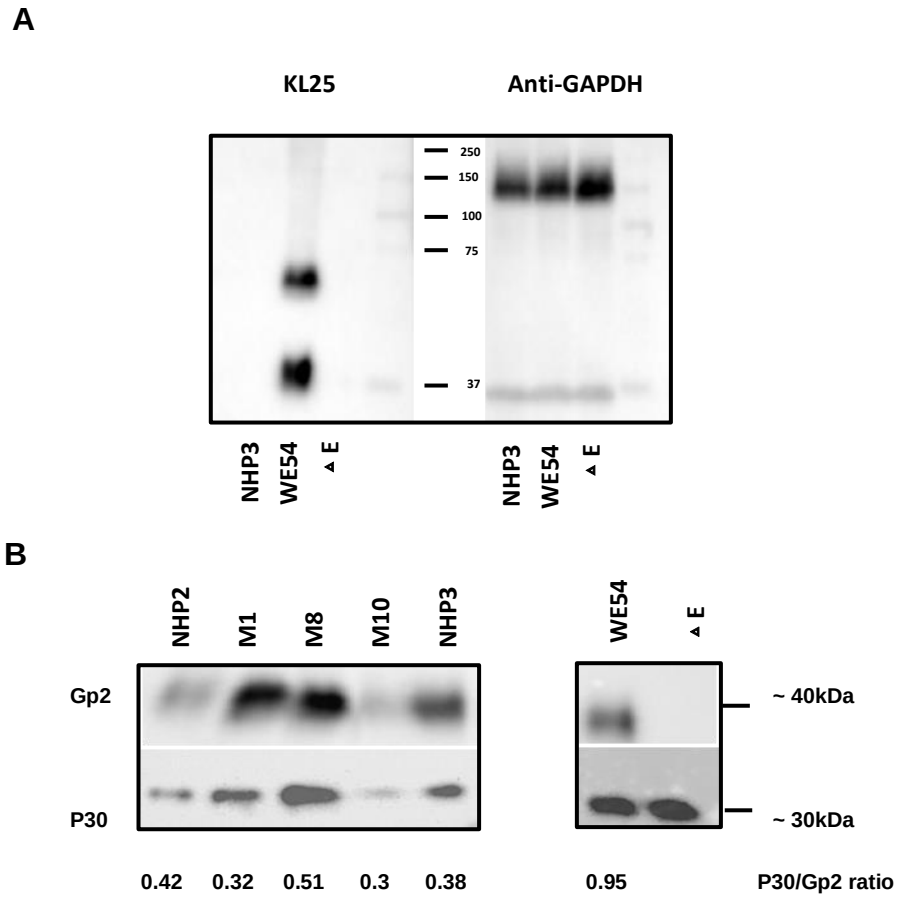


Figure 4-2: Detection of LCMV glycoprotein in cell lysates and pseudotype pellets.

A) Lysates from NHP3, WE54 (positive control), and ∆ E (negative control) were subjected to SDS-PAGE. KL25 recognizes an epitope in Gp1 sensitive to disulfide reduction, hence WB was performed under non-reducing conditions. It reacted with WE54, but not with NHP3 or ∆E, showing two bands of ~ 70kDa and ~44kDa which corresponded to GPC and Gp1, respectively. GAPDH was used as a loading control which showed bands for all samples with similar intensities at ~144 kDa and ~36 kDa corresponded to tetramers and monomers, respectively. **B)** Samples included a subset of the study clones and controls (WE54 and ∆E) were pelleted and resuspended in 30 µl of PBS. 10 µl/well of sample/loading buffer were loaded and run under reducing conditions. Glycoproteins and capsids were detected using anti-Gp2 (22.5D) and anti-MLV p30, respectively. Signals at ~40 kDa (Gp2) and ~ 30 kDa (p30) were detected. P30/Gp2 ratio was calculated by obtaining a density score for each band using ImageJ densitometric analysis software.

4.3 Discussion

The type and amount of the envelope plasmid were found in previous studies to have a significant impact on the production of glycoproteins and pseudotype yields (Urbanowicz *et al.*, 2016a). This effect was found to be glycoprotein-specific and a universal protocol could not be adapted even for glycoproteins of different strains of the same virus. Thus, upon pseudotype production in this study, two factors were considered: the type and the ratio of the envelope plasmid. On the MLV backbone, we tested the infectivity of pseudotypes carrying GPC expressed by either pI.18 or pcDNA 3.1^+ envelope plasmids. While pseudotypes produced by pI.18 were highly infectious, pcDNA3.1^+-produced pseudotypes showed infectivity that was comparable to the baseline. Both plasmids are high-copy number and utilize an hCMV promotor. The pI.18 plasmid, however, also contains the intron A sequence of the hCMV intermediate-early gene (IE1) which may explain the observed difference in the assay. It has been previously demonstrated that the inclusion of intron A in expression plasmids resulted in a significant increase in the levels of glycoproteins expressed under the control of hCMV promotor in some cases up to 100-fold (Chapman *et al.*, 1991). Introns included in the 5' UTR were proposed to enhance expression by several mechanisms. Transcription factor-binding sites and regulatory elements involved in transcription activation were identified in some introns including intron A (Lin *et al.*, 1991, Yutzey *et al.*, 1989, Chapman *et al.*, 1991). Introns were also suggested to enhance expression by increasing the processing, stability, or nuclear transport of transcripts (Huang and Gorman, 1990). Another difference between pI.18 and pcDNA3.1^+ is the presence of SV40 origin of replication in pcDNA3.1^+ but not pI.18 which in a cell line expressing the large T antigen (e.g. HEK 293T), results in high levels of expression. This may have resulted in overly expressed glycoproteins that caused cytotoxicity or overwhelmed the cellular machinery making it unavailable for other viral components.

After determining the envelope plasmid backbone, the optimal concentration of the plasmid was determined. Increasing the concentration of the envelope plasmid was found in some cases to increase glycoprotein production. However, for some glycoproteins, the production was only optimum within a specific range beyond which the pseudotypes infectivity inversely correlated with the amount of plasmid (Urbanowicz *et al.*, 2016a). To determine the optimum concentration for the envelope plasmid, six pseudotype preparations for WE54 and NHP3 each were produced using an increasing concentration of pI.18 while keeping the amount of the MLV plasmids constant (2 μg). The infectivity of WE54 continued to increase with increasing concentrations of pI.18. The infectivity of NHP3, however, significantly dropped when more than 2 μg of the plasmid was added. An explanation of the different effects of plasmid concentration on the infectivity of the two clones could be that WE54 is a highly-passaged culture-adapted lab strain that causes minimum toxicity to cells. Thus, cells are more tolerant to larger amounts of WE54 GPC than a wild-type clone.

After the study clones were produced using the conditions indicated above, the GPC incorporation was assessed. The mouse antibody KL25 that targets the Gp1 subunit could not be used for this purpose due to epitope variability. This antibody was previously shown to select for an escape mutation at position 119 and exclusively required an asparagine at this position for binding (Seiler *et al.*, 1999). The study clones have either histidine or serine at this position and showed no reactivity with KL25 in western blot analysis. On the other hand, WE54 which has asparagine at 119 showed a strong signal. We then attempted to assess incorporation using a c-terminal tag to avoid the effect of epitope variability on binding. Although the FLAG-tagged LCMV GPC was shown previously to have similar cell surface trafficking and pseudotypes infectivity to that of the WT (Capul *et al.*, 2007), we observed a log reduction in the infectivity for the clone we tested. Thus, the experiment was not pursued further. The Gp2 subunit is highly conserved among OWAs and anti-LASV Gp2 antibodies are commercially available. We were able to compare the

incorporation across five of the study clones using anti-LASV Gp2 and anti-MLV p30 in western blot analysis. The clones showed a high correlation between the Gp2 and p30 signal indicating comparable incorporation.

Chapter. 5: The infectivity of the pseudotypes in murine and NHP cell lines

5.1 Introduction

In the previous section, the pseudotype production was optimized to obtain maximum infectivity in the target cell lines by adjusting the type and amount of the envelope plasmid. The GPC incorporation of the pseudotypes produced under the optimized conditions was found to be comparable between the NHP- and the mouse-derived pseudotypes.

In this section, the infectivity of a set of pseudotypes expressing either NHP- or mouse-derived GPCs was tested and compared in L929 and Vero-E6 cell lines. The set was selected to include clones from within and outside the main clusters. The effect of the mutations separating the NHP and the mouse sequences on the infectivity of pseudotypes was also tested by introducing them either individually or in different combinations on different GPC backgrounds.

5.2 Results

5.2.1 NHP-derived pseudotypes displayed higher infectivity in L929 cells compared to the mouse-derived pseudotypes

After optimizing the pseudotype production and ensuring comparable GPC incorporation across the clones, we tested if the NHP and the mouse clones would display a distinct infectivity pattern. The cell density needed to obtain maximum infectivity in both L929 and Vero cells was first determined to ensure that any differences that may or may not exist between clones were genuine and not due to sub-optimal cell density. The cells were seeded at densities

ranging from $5x10^3$ to $3x10^4$ cell/well and infected with equal amounts of WE54 pseudotypes. For Vero cells, the infectivity decreased as the number of cells increased but the difference was only significant when the count was $2x10^4$ or more (p-value 0.034). On the other hand, the infectivity in L929 continued to increase with increasing density but the difference was only significant when the count was $1x10^4$ or less (p-value 0.049) **(Figure 5-1).** Accordingly, cell densities of $1x10^4$ cell/well and $2x10^4$ cell/well for Vero and L929 cells, respectively, were adapted for the subsequent experiments as these seeding densities gave equivalent levels of infectivity.

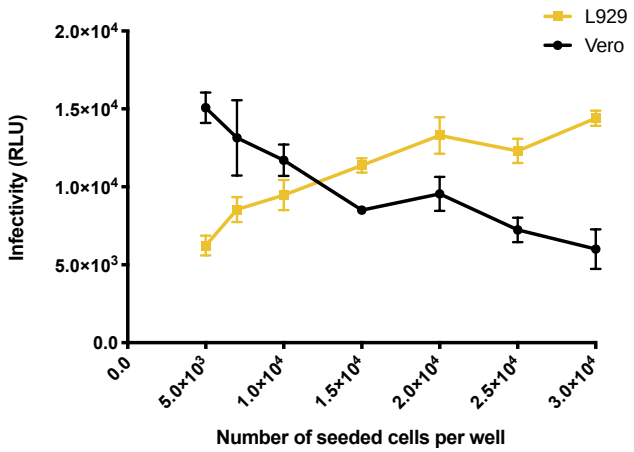


Figure 5-1: Optimization of target cell density.

Vero/L929 cells were seeded at varying densities that ranged from $5x10^3$ to $3x10^4$ cell/well. After 18-24 hours cells were infected with equal volumes of WE54 pseudotypes and results were read 72 hours post-infection. Results are reported in relative light unit (RLU). Each point represents the mean of three replicas ± SD.

After optimal target cell densities were determined, the infectivity of pseudotypes carrying either mouse-derived GPC (clones M1, M3, M4, M7, M8 and M12 from the main cluster and clone M10) or NHP-derived GPC (clones NHP1, NHP2, NHP3, and NHP4) was measured in the two cell lines. Two clones (M3 and M7) were not infectious and hence were excluded from subsequent experiments. The sequences of the two clones were analyzed to

identify mutations that may have contributed to their phenotype. Two mutations were recognized. M7 had a single amino acid change (threonine-to-methionine) at position six compared to M-8 that was isolated from the same sample and was highly infectious. M3 had an asparagine-to-serine change at position 95 (N95S) compared to all other clones. These changes were not explored further.

All other tested clones were highly infectious and displayed a species-specific pattern. Clones NHP1, NHP3, and NHP4 are identical at the amino acids level. Thus, only one of them was included in any given experiment to avoid resampling. To achieve an equal sample size between the NHP and the mouse groups, only clones M1 and M8 from the main mouse cluster were included while M4 and M12 were excluded as these have similar genetic distances to M1 as M8 (p-distance 0.006). The difference between M1 and M8 lies at four positions (T133A, D163N, N164S, and K496 found in M8 compared to M1). Clone M10 was also included in the analysis. Three independent experiments were performed which reproducibly showed that the infectivity of the NHP and the mouse clones was comparable in Vero cells but the NHP clones were significantly more infectious in L929 cells (p-value 0.007) **(Figure 5-2).** The infectivity of M10 was also significantly higher in L929 than the other mouse clones (p-value 0.035). The difference in the infectivity between M10 and the NHP clones in both L929 and Vero cells was insignificant.

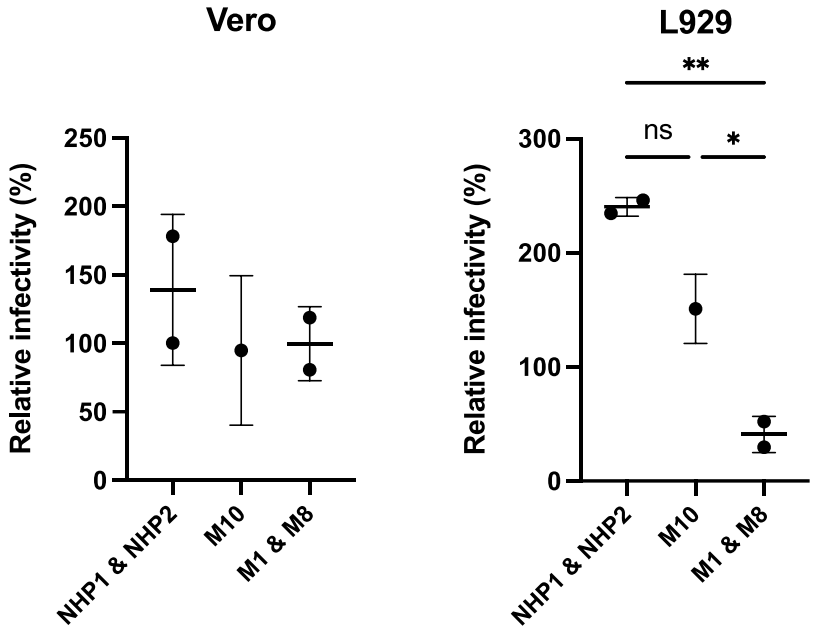


Figure 5-2: Infectivity of the NHP and the mouse clones in Vero and L929.

Results from three independent experiments were pooled. RLU values were converted to percentages. 0% is equivalent to the ∆ E RLU mean and 100% is equivalent to the WE54 RLU mean. The mean percentages of two NHP clones (NHP1 and NHP2), M10, and two mouse clones (M1 and M8) were compared. Each point represents the average percentage of individual clones and horizontal lines represent mean ± SD. The range of the Y-axis varied depending on the data. To determine significance, one-way ANOVA was used with Tukey's multiple comparisons test to compare every mean with every other mean in the data set. (*) indicates significance (p-value of <0.05 is considered significant).

5.2.2 The infectivity of the mutants indicated complex amino acid interactions

To see to which extent the NHP-defining mutations contributed to the observed phenotype in L929, they were introduced either solely or collectively. The first panel of mutants involved the introduction of S106F, K211T, I260L, V451I, L468S, and S119H to M1 and M8. When the mutations were introduced individually, one mutation (I260L) resulted in a significant increase in the infectivity of M8 in L929 (p-value 0.002) **(Figure 5-3).** Also, mutants harbouring the six mutations together for both clones (referred to as M1+6 & M8+6)

showed a significant increase in infectivity compared to the wild types (p-value of 0.01 and <0.0001, respectively).

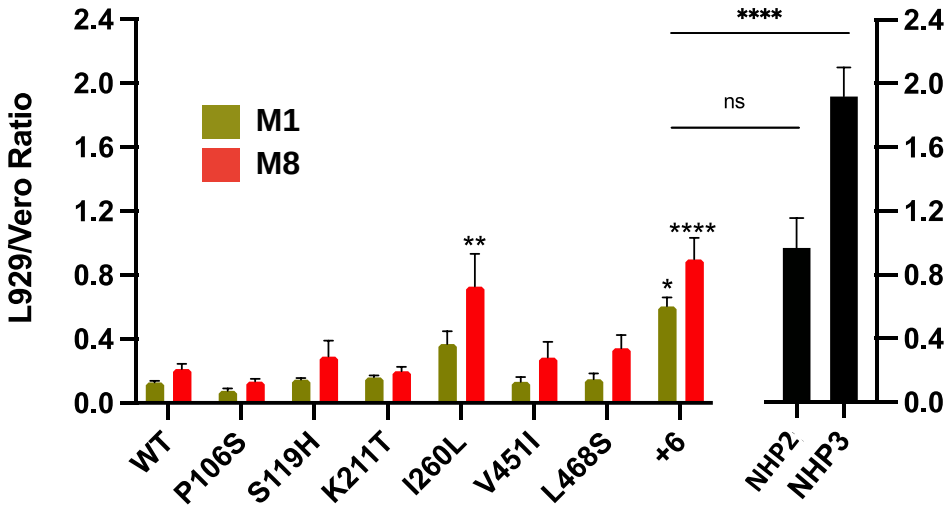


Figure 5-3: The effect of introducing six NHP-defining residues to the two mouse clones M1 and M8.

Six mutations were introduced individually and combined into two mouse clones (M1 and M8). The infectivity of the mutants in L929 was normalized using the L929/Vero ratio. The mutants were compared with their respective WT (M1 & M8). The mutants M1+6 and M8+6 were also compared with the NHP clones NHP2 and NHP3. The bars represent the mean of three replicates ±SD. To determine significance, a normality test was first performed. Accordingly, One-way ANOVA was used with Tukey's multiple comparisons test to compare every mean with every other mean in the data set. (*) indicates significant change compared to the respective wild type unless otherwise indicated (p-value of <0.05 is considered significant).

However, even when the six mutations were introduced together the infectivity did not reach that displayed by NHP3 and the difference was still significant (p-value <0.0001) **(Figure 5-3).** The infectivity of the mutants M1+6 and M8+6, however, was comparable to NHP2. Out of the seven identified mutations, NHP2 lacks two (Q119H and I247M) compared to NHP3. M10 also lacks these mutations in addition to K211T.

To further explore the effect of these positions, a second panel of mutants in which S119H, K211T, and I247M were introduced in different combinations to M10 was generated **(Figure 5-4).** When the mutations were introduced individually, S119H or I247M significantly increased the infectivity (p-values of <0.0001 and 0.007, respectively). K211T reduced the infectivity compared to the WT but the difference was not significant. Additionally, S119H or I247M on a K211T background had no significant effect. When combined so that the resultant mutant completely matched the sequence of NHP3 at all seven positions, the infectivity was comparable to NHP3. Interestingly, the highest impact was achieved when S119H and I247 were introduced together without changing position 211. The infectivity of this mutant was significantly higher than all other clones including NHP3 (p-value <0.0001).

Since position 211 is strictly species-specific and the K211T mutation seemed to negatively affect the infectivity in L929 when introduced to M10, the effect of the reverse mutation on an NHP background was next tested. The mutant (NHP1 T211K) had a ratio that was significantly higher than the WT (p-value <0.033) **(Figure 5-5).**

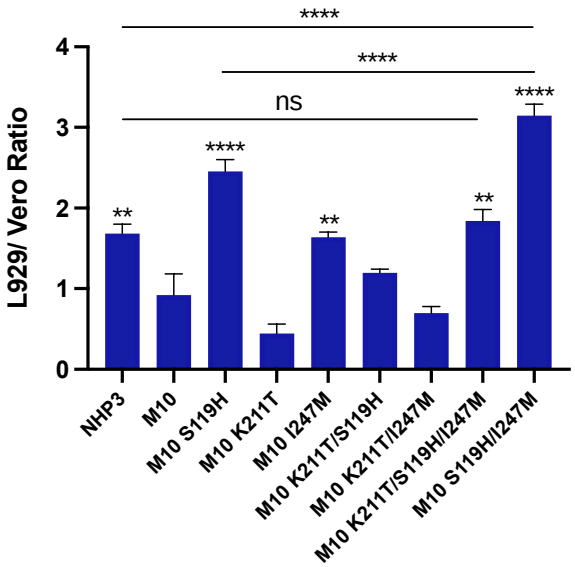


Figure 5-4: Introducing the NHP-defining mutations to the mouse clone M10.

A panel of M10 mutants with different combinations of S119H, I247M, and K211T was generated. The infectivity in L929 was measured and normalized by using the L929/Vero ratio. Results were pooled from two infection assays. The infectivity of the mutants was compared to the wild-type clone (M10) and clone NHP3. Bars represent mean ± SD. To determine significance, a normality test was first performed. Accordingly, One-way ANOVA was used with Tukey's multiple comparisons test to compare every mean with every other mean in the data set. (*) indicates significance compared to M10 unless otherwise indicated (p-value of <0.05 is considered significant).

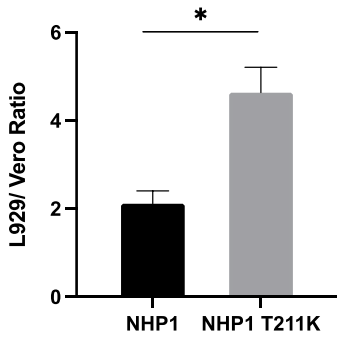


Figure 5-5: Introducing the mouse residue at 211 to NHP1.

The mouse residue (lysine) was introduced at position 211 to NHP1. The infectivity in L929 was measured and normalized by using the L929/Vero ratio. The infectivity of the mutant was compared to the wild-type clone. The bars represent mean ± SD. To determine significance, a normality test was first performed. Accordingly, Unpaired t-test was used for comparison and (*) indicates significance (p-value of <0.05 is considered significant).

5.3 Discussion

Psuedotyping systems are highly tractable and readily genetically manipulated. This made them a valuable tool in studying the effect of mutations in the viral glycoproteins on entry. The uncoupling of mutations of a certain haplotype offered by these systems allows testing the effect of individual mutations. Pseudotypes carrying different combinations of mutations can also be produced to investigate epistasis or additive effects of mutations. In this chapter, the infectivity of a panel of pseudotypes carrying LCMV GPCs derived either from the NHP or the mouse samples in addition to a panel of mutants was described. First, the infectivity of the WT clones was tested and compared in a murine line (L929) and an NHP line (Vero E6). The two mouse clones M3 and M7 were non-infectious and two mutations that might have contributed to their phenotype were identified (N95S and T6M, respectively) but not further explored. Position 95 of the GPC was previously identified as a highly conserved N-linked glycan site among OWAs (Watanabe *et al.*, 2018). The oligomannose-type glycan at this position was found to be necessary for the GPC cleavage which may explain the abolished infectivity of M3 (Eichler *et al.*, 2006). The T6M mutation was the only difference between M7 and M8 the latter was highly infectious. The mutation is located in the SSP region involved in the processing and maturation of the GPC. Yet, a T6A mutation was reported previously to have no effect on LCMV-GPC expression and processing nor the infectivity of viral-like particles (Saunders *et al.*, 2007). Further investigation is required to identify the step in pseudotypes formation or entry that this mutation is affecting.

All other tested clones were highly infectious in both lines. However, in L929 a significant difference was observed between the clones of the main mouse cluster and the other tested clones. Namely, NHP1, NPH2, and M10 were more infectious in L929 with at least a 3-fold increase over M1 and M8. The reason this difference was observed in L929 but not Vero is unclear. Many factors might have contributed to this difference, including the species the cell

lines were derived from, and the level of receptor expression in each cell line. It could also be due to different glycosylation of α-DG between the two cell lines. It has previously been reported that α-DG glycosylation in Vero cells is aberrant and α-DG derived from WT Vero showed weak virus/laminin-1 binding compared to α-DG that was produced in Vero cells overexpressing the enzyme involved in α-DG glycosylation (LARGE1) (Kunz *et al.*, 2005, Brouillette *et al.*, 2018). Additionally, an antibody (IIH6C4) recognizing the fully-glycosylated functional α-DG could not recognize the Vero E6 α-DG (Kunz *et al.*, 2005, Brouillette *et al.*, 2018). This may indicate that the increased infectivity of the NHP clones could be due to increased affinity to a properly glycosylated and functional α-DG.

The panel of mutants in which the seven identified mutations were introduced individually or in different combinations on different backgrounds was next tested. Introducing the mutations S106F, S119H, K211T, V451I, and L468S individually to the mouse clones M1 and M8 which showed low infectivity in L929 did not have a significant effect on the infectivity. The mutation I260L alone, however, significantly increased the infectivity of M8 compared to the WT clone. Position 260 was previously found to be associated with high α-DG affinity (Sevilla *et al.*, 2000a, Salvato *et al.*, 1991). However, in these studies both isoleucine and leucine at 260 were found to confer high affinity. Our data, on the other hand, suggest that leucine and isoleucine have different effects and the two residues were not interchangeable despite the conservative nature of this change.

Combined, the mutations S106F, S119H, K211T, I260L, V451I, and L468S significantly increased the infectivity of M1 and M8 compared to the WT clones. Nonetheless, M1+6 and M8+6 were still significantly less infectious than the main cluster of the NHP clones but as infectious as clones NHP2 and M10. When the three NHP-defining mutations (S119H, K211T, and I247M) missing in clone M10 were combined the M10 mutant showed an infectivity that was comparable to a clone of the NHP main cluster (NHP3). Mutations S119H and I247M also resulted in a significant increase when introduced individually to M10. Interestingly, the M10 containing both mutations without K211T was associated with an infectivity that was significantly higher than this displayed by all the clones in the panel including NHP3. A lysine at 211 was also associated with higher infectivity in an NHP background (NHP1 T211K) than a threonine (NHP1 WT). A threonine at 211 was associated in previous studies with α-DG-high affinity clones, however, when A211T was introduced to a low-affinity clone it had no effect on the receptor binding (Hastie *et al.*, 2016). This is in line with the finding in this study which indicated that a threonine at 211 did not enhance the infectivity and rather reduced it. Mutations at position 119 were also described in previous studies and found to promote immune evasion in mice (discussed in **4.3**). The S119H mutation tested here, had a variable effect when introduced alone depending on the background. When introduced to M1 and M8, no change was observed in the infectivity. However, the mutant M10 S119H showed a significant increase in infectivity compared to the WT. This is suggestive of epistatic interactions between the histidine at 119 and other residues in M10 which are absent in M1 and M8.

The two mutations located in the Gp2 (V451I and L468S) were not found to affect the infectivity when introduced separately. However, their ability to exert an effect when introduced in combination with other mutations and allosterically alter the quaternary structure of the protein including the receptor-binding domain cannot be excluded. V451I is located in the transmembrane domain (TM) and L468S is located in the cytoplasmic domain

(CD). Both domains (TM and CD) are known to be important for the biosynthesis, cleavage, and incorporation of LCMV and LASV GPC (Sommerstein *et al.*, 2014, Kunz *et al.*, 2003, Willard *et al.*, 2018). In addition, there is evidence they are integral for fusion and Gp2 function (see introduction section **1.2.5**). The V451I and L468S mutations are located within close proximity to residues in LASV Gp2 (448 and 465 correspond to positions 454 and 471 in LCMV GPC, respectively) that were previously found to affect infectivity without affecting the production or processing of GPC (Willard *et al.*, 2018). It was hence proposed that they affected either incorporation or fusion (Willard *et al.*, 2018). The data obtained here, on the other hand, suggest that V451I and L468S do not affect GPC incorporation. The western blot analysis also showed single bands at ~ 40 kDa corresponding to Gp2 in purified pseudotypes confirming that V451I and L468S are cleavage efficient.

Chapter. 6: The receptor usage of the study isolates

6.1 Introduction

The data in previous sections demonstrated that the NHP clones were more infectious in L929 compared to the mouse clones. The key residues associated with this increase were also identified and their effect by introducing them individually and combined was empirically tested. It was found that the high infectivity displayed by the main cluster of NHP clones could be reproduced in a mouse background when the mutations were combined. It was next hypothesized that the increased infectivity of the NHP clones caused by the identified mutations was due to an increase in the affinity to the receptor. To test this hypothesis, assays were performed to assess the receptor requirement of the study clones. These included: knockout/knock-in (KO/KI) assays and inhibition assays. For the KO/KI assay, the infectivity of the study clones was tested in HAP1-αDG-KO cells in addition to HAP1-αDG-KO cells where α-DG was reintroduced at increasing levels. The inhibition assays involved the preincubation of the pseudotypes with soluble NHP/murine α-DG prior to infection. The infectivity of the α-DG-bound pseudotypes was then assessed in Vero and L929 cells.

The previously determined crystal structures of LCMV and LASV GPC were also exploited and used to map the mutations identified here together with residues that were found in previous studies to affect α-DG binding.

6.2 Results

6.2.1 The infectivity of the study clones correlated with the levels of α-DG expressed in KO cells

To elucidate the role of α-DG in the infectivity of the study clones, HAP1 cells were used in which *DAG1* gene was edited using CRISPR/Cas9 technology by deleting a single nucleotide in the first coding exon, resulting in a frameshift premature stop-codon and production of a nonfunctional α-DG polypeptide corresponding to the first 79 amino acids. The *DAG1* gene (murine) was reintroduced by transducing the cells with VSV-G -pseudotyped HIV-based particles carrying pHIV-*DAG1*-EGFP as the transfer plasmid. This plasmid allows a stable bi-cistronic expression and quantification of the trans-gene based on EGFP signal. After two passages, EGFP-expressing cells were sorted into three populations low-, medium-, and high-EGFP-expressing cells using Fluorescence-Activated Cell Sorting (FACS). The gating process involved selecting viable, singlet, then EGFP-expressing cells **(Figure 6-1).**

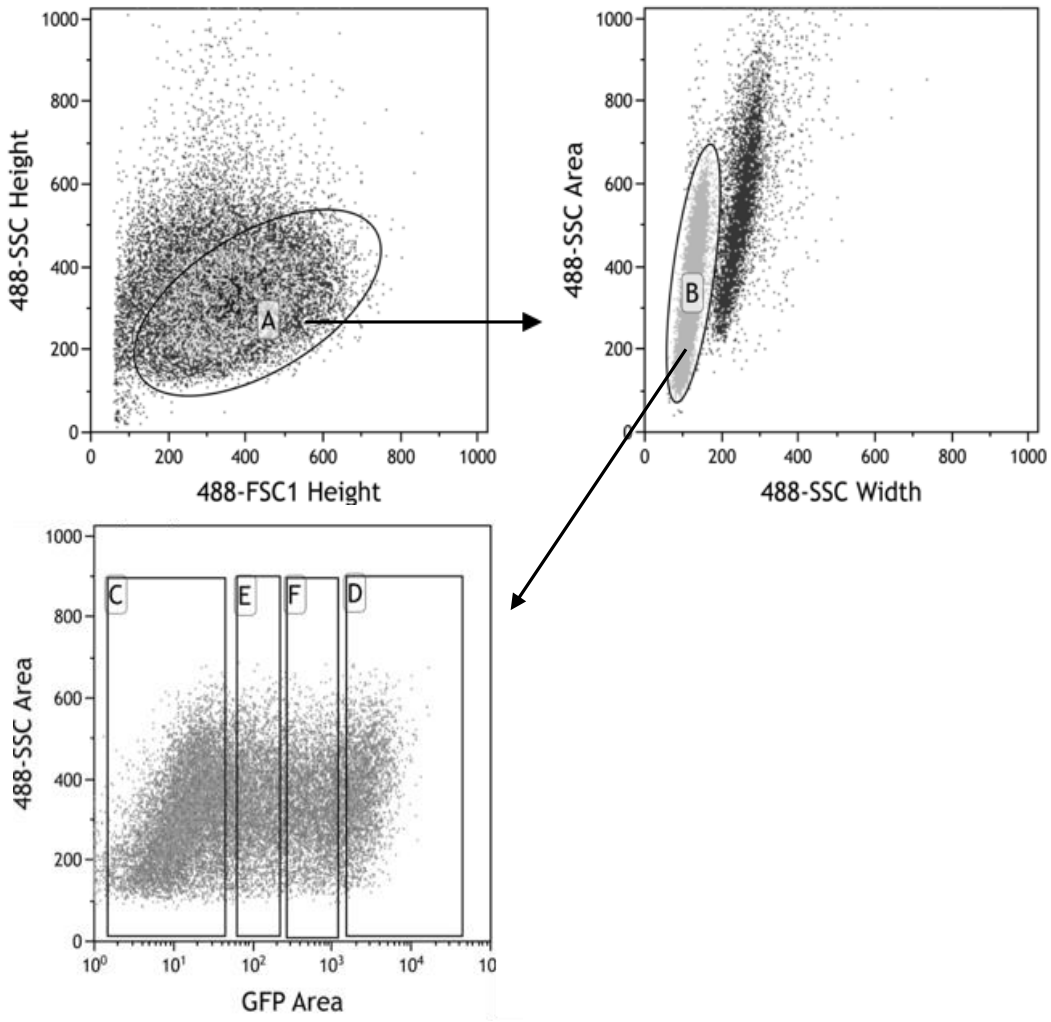


Figure 6-1: Selecting and sorting HAP1 $DAG1^{+}$ cells based on EGFP expression.

The flow cytometry dot plots show the gates for selecting viable **(A)** then singlet **(B)** cells of DAG1-transduced HAP1 KO cells. The singlet population was gated to select EGFP^{-} **(C)** and EGFP^{+}**(D)** cells based on the non-transduced HAP1-α-DG-KO cells. The population in between was arbitrarily divided into low- **(E)** and medium- **(F)** EGFP-expressing cells. Subsequently, cells were sorted into three populations low-, medium-, and high-EGFP-expressing cells. Y access shows the side scatter at a wavelength of 488 nm. The x-axis shows the forward scatter (first plot), the side scatter (second plot), or the EGFP expression (third plot) at 488 nm.

Growth and EGFP expression were regularly monitored before and after sorting and the distinct signal intensities observed within each sorted population remained stable **(8.6).** No difference in growth was observed between the four populations (low, medium, high, or KO). The cells were allowed to recover for 3 to 4 passages before they were used in infectivity

experiments as some cell death was observed following FACS analysis. Upon infection, the levels of surface α-DG (PE-Cy7) in addition to EGFP in the cell populations were analyzed and found that the two correlated but higher EGFP expression was observed **(Figure 6-2).** Some heterogeneity in both EGFP and α-DG expression within each population at the time of the infection was also noticed, which was possibly caused by the elimination of the transduced gene in a subpopulation of cells.

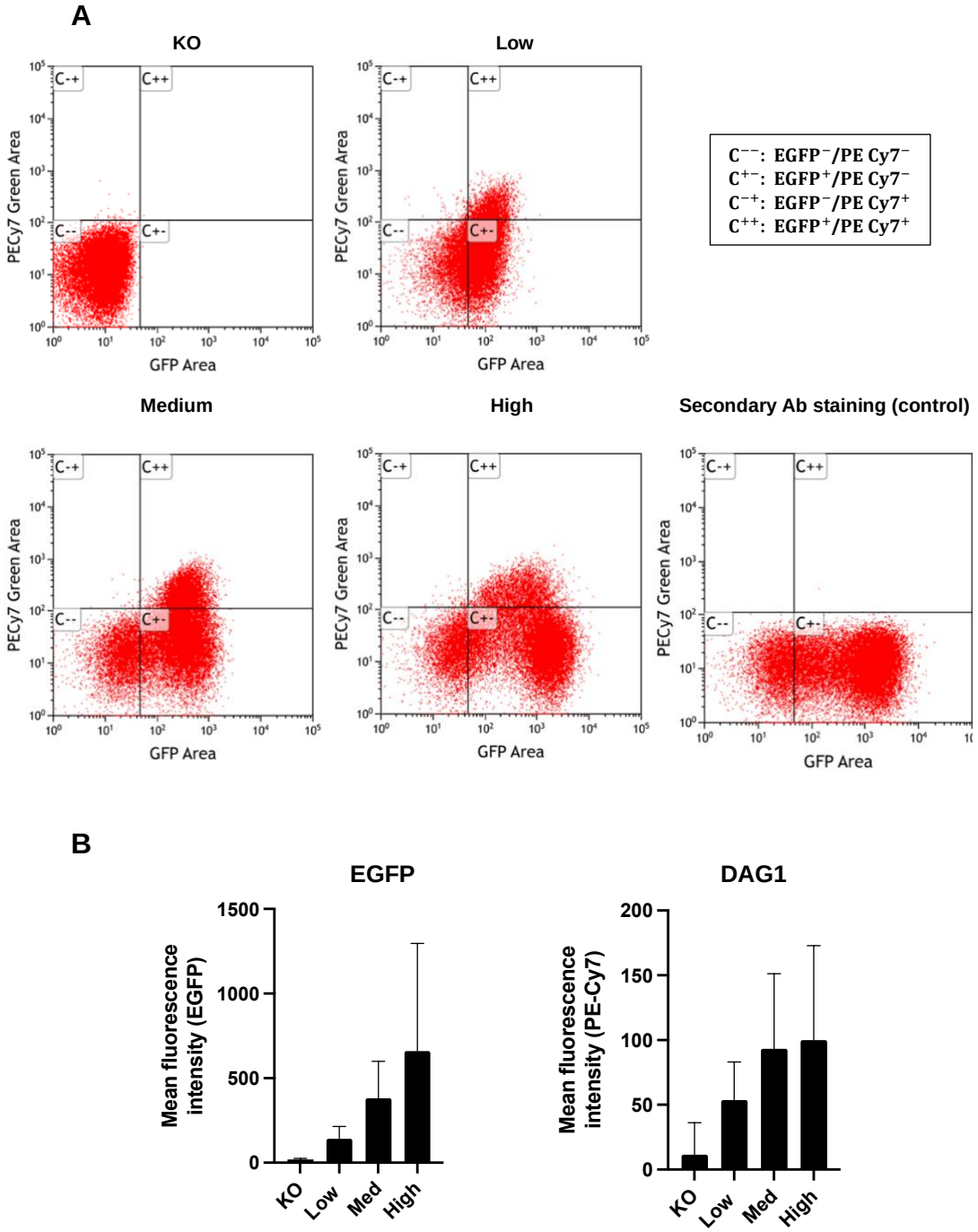


Figure 6-2: DAG1 expression in HAP1 $DAG1^{+}$ cells.

A) Low, Medium, High, and KO populations were assessed for EGFP and DAG1 (PE-Cy7) expression via FACS analysis. For surface DAG1 detection, all cell populations were stained with anti-DAG1 (IIH6C4) then with PE-Cy7 secondary antibody without permeabilization or fixing. Staining High-EGFP-expressing cells with the secondary antibody alone was used to define the baseline. **B)** Mean fluorescence intensity of EGFP (C^{+-}) and DAG1 (C^{++} for Low, Med, and High and C^{-+} for KO) expressing cells. Bars represent mean ± SD.

The infectivity of the study clones in each of the populations together with WE54 (an αDG-high affinity strain) and VSV was next assessed. The study clones and WE54 but not VSV showed increasing infectivity that correlated with α-DG levels **(Figure 6-3. A).** We also observed efficient infectivity of the NHP clones and M10 but not the mouse clones M1 or M8 in the non-transduced KO cells. This was expressed as a percentage of the infectivity in the KO cells relative to the cells expressing high levels of α-DG. This showed a ~13-20% increase in the infectivity of the NHP clones and M10 over M1 and M8 **(Figure 6-3. B).**

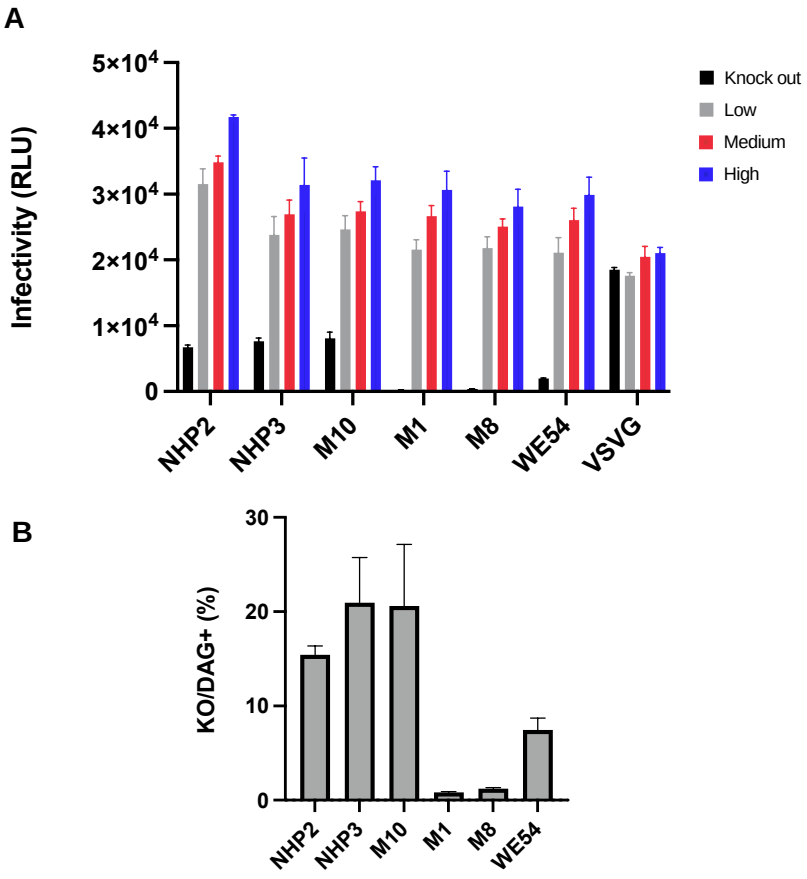


Figure 6-3: The infectivity of the wild-type clones in HAP1 KO and $DAG1^+$ cells.

A) Infectivity of the NHP clones NHP3 and NHP2 and the mouse clones M1, M8, and M10 in Low, Medium, High, and KO cell lines is shown in relative light unit. LCMV WE54, VSV-G, and ▵E were included as controls. Bars represent mean ± SD. **B)** The ability of the WT clones to infect KO cells relative to cells expressing high levels of DAG (shown as KO to $DAG1^+$ infectivity percentage). Bars represent the mean ± SD of two independent experiments.

6.2.2 The infectivity in the KO cells increased when the NHP-defining mutations were introduced to the non-infectious mouse clone

As the introduction of S106F, S119H, K211T, I260L, V451I, and L468S into the mouse clone M1 significantly increased its infectivity in L929, we next assessed if these mutations were also able to affect the infectivity in the KO cells in a similar way. K211T alone did not affect the infectivity significantly while I260L increased it to ~ 10% (p-value 0.0096). However, the highest increase was achieved with the mutant harbouring the six mutations together and that increase was significantly higher than that of the mutant with I260L alone (p-value 0.0031) **(Figure 6-4).** For M10, introducing K211T alone significantly reduced the infectivity (p-value 0.036) but on an S119H/I247M background did not have an effect and the infectivity was comparable to the WT **(Figure 6-4).** Similar to its effect in L929, Introducing T211K to clone NHP1 significantly increased the infectivity in the KO cells (p-value <0.0001) **(Figure 6-4).**

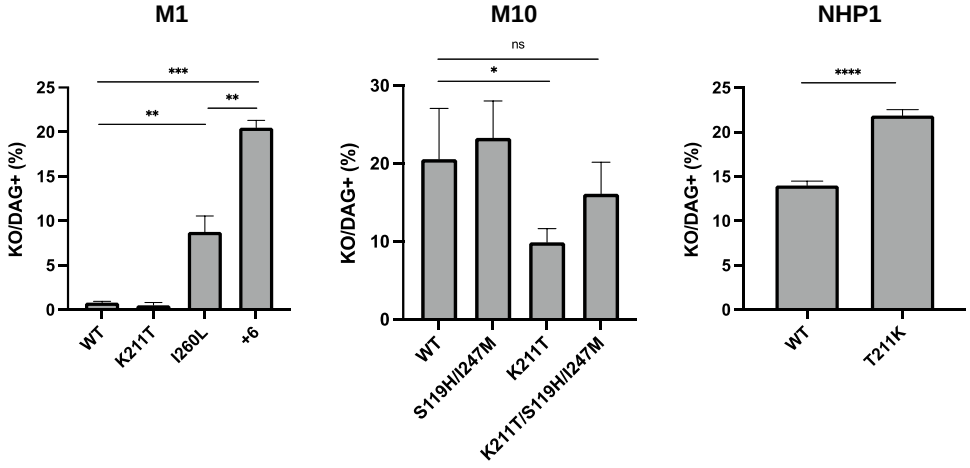


Figure 6-4: The infectivity of the mutants in HAP1 KO cells.

The ability of a panel of mutants for clones M1, M10, and NHP1 to infect KO cells relative to cells expressing high levels of DAG (shown as KO to $DAG1^{+}$ infectivity percentage). A total of two independent experiments were performed for each clone (except clone NHP1). Bars represent mean ± SD. The scale of the Y-axis may change depending on the data. To determine significance, a normality test was first performed. Accordingly, repeated measures one-way ANOVA with Tukey's multiple comparisons test to compare every mean with every other mean in the data set (M1 & M10) or unpaired t-test were used (NHP1). (*) signifies the level of significance (p-value of <0.05 is considered significant).

6.2.3 KM155-DAG-KO cells were permissive to an NHP clone

The efficient infectivity of some clones in HAP1 KO cells suggested that these clones were able to enter the cells independently of α-DG as the FACS analysis showed no surface expression of α-DG in HAP1 KO cells **(Figure 6-2).** To confirm this finding, surface expression was further assessed via other means. Blocking the entry in HAP1 KO by soluble α-DG was used as an indicator for the presence of residual surface α-DG. The infectivity of clone NHP3 was reduced by the soluble protein up to ~80 % in a dose-dependent manner indicating that surface α-DG might exist **(Figure 6-5).**

As the presence of residual α-DG in HAP1 KO cells could not be ruled out, the infectivity of clone NHP3 in another α-DG KO cell line (KM155-αDG-KO) was tested and compared to the infectivity in WT cells. KM155 cells are human skeletal muscle cells permissive to LCMV infection in their undifferentiated myoblast form but become refractory at high density as they differentiate into myotubes (Iwasaki *et al.*, 2014). Hence, the cell density was first optimized for the WT cells which showed that the infectivity decreased with increasing seeding density **(Figure 6-6. A).** After determining the optimum cell density, we compared the infectivity of NHP3 and VSV in the WT and KO cell lines. While VSV was similarly infectious in the two cell lines, a ~ 70% reduction in NHP3 infectivity was observed in the KO cells compared to the WT **(Figure 6-6. B).** Nonetheless, KO cells were not refractory and NHP3 was still highly infectious.

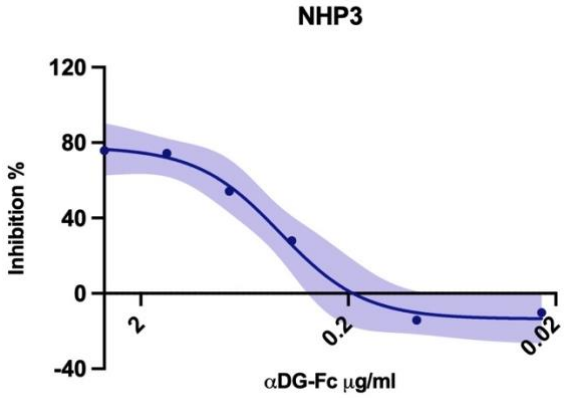


Figure 6-5: The ability of soluble α-DG to inhibit the entry of NHP3 to HAP1 KO cells.

NHP3 pseudotypes were preincubated with an increasing concentration (0-3 μg/ml) of soluble α-DG-Fc before infection. A 100% inhibition was defined as the level of infectivity equivalent to ▵E average infectivity and 0% inhibition was defined as the infectivity at α-DG-Fc concentration of 0 μg/ml. The curve was generated using a nonlinear-regression analysis. The shaded area around the curve represents the 95% CI. The X-axis is shown on a log scale.

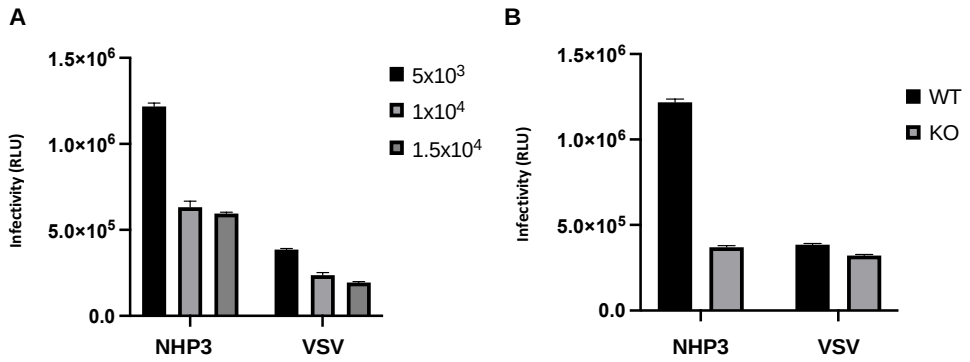


Figure 6-6: The infectivity in KM155 WT and α-DG-KO cells.

A) Optimization of seeding density of KM155. WT KM155 cells were seeded at $5X10^3$, $1X10^4$, or $1.5X10^4$ cell/well and infected with equal volumes of NHP3 and VSV after 18-24 hours. Infectivity is expressed in relative light units, bars represent mean ± SD. **B)** Comparing the infectivity in the WT and the KO cells. WT/KO cells were seeded at $5X10^3$ cell/well and infected with equal volumes of NHP3 and VSV (control) after 18-24 hours. Infectivity is expressed in relative light units, bars represent mean ± SD.

6.2.4 Alternative splicing of DAG1 could not explain the residual infectivity in the KO cell lines.

13 naturally occurring DAG1 transcript variants from normal human tissues were reported in RefSeq database (gene ID 1605). Since alternative splicing was found to be one of the mechanisms by which cells can overcome CRISPR/Cas9 editing, the DAG KO sites in HAP1 and KM155 together with the virus binding site were mapped in all the reported transcripts **(Figure 6-7)**. The KO sites for both cell lines (HAP1 KO and KM155 KO) were mapped to the first coding exon, while the virus binding site was located in the second exon. Mapping these sites in each variant showed that all possessed both exons and encoded for the same 895 amino acid protein. Thus, regenerating the virus binding site via alternative splicing is unlikely to be the explanation for the observed residual infectivity in the KO cell lines and α-DG-independent entry route for the NHP clones may exist.

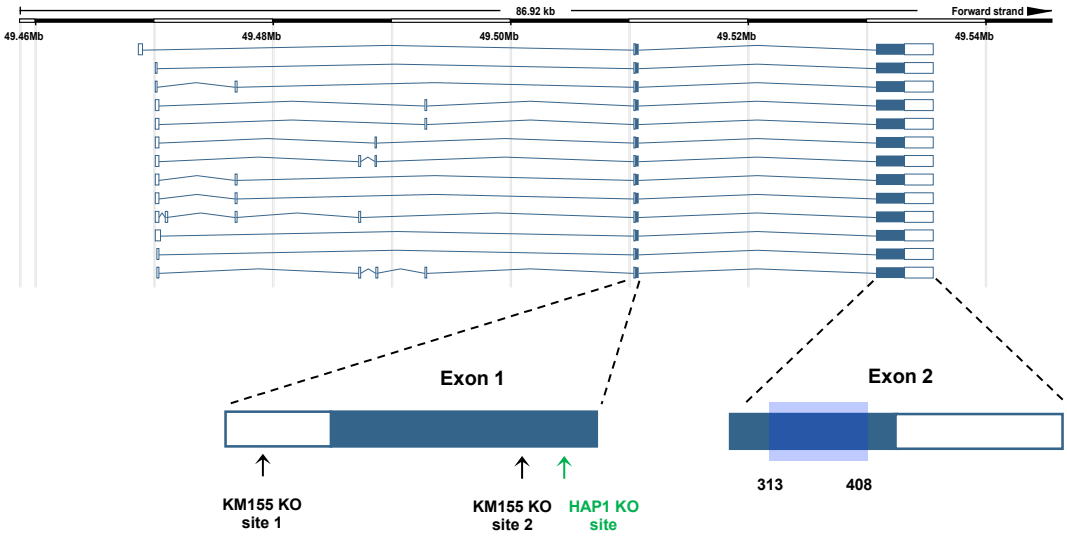


Figure 6-7: Mapping HAP1 KO, KM155 KO, and the virus-binding sites in α-DG transcript variants.

The region in human chromosome 3 (49,468,703- 49535618) corresponding to *DAG1* gene is depicted. 13 naturally occurring transcript variants from normal human tissues were reported in RefSeq database (NM-001177634.2 to NM-001177644.2, NM-1165928.4, and NM-004393.6). The two coding exons are further enlarged to show the KO sites for HAP1 KO and KM155 KO cells as described by the providers. For KM155, the KO resulted in deletions of 1-5 pb at each site or excision of the entire flanked region. For HAP1, the KO resulted in a single pb deletion. Filled and empty rectangles represent coding and UnTranslated Regions (UTR) of the exons, respectively. The virus binding site in exon 2 (amino acids 312 to 408) is highlighted. The diagram was adapted from Ensembl (ENSG00000173402) RefSeq gene ID 1605.

6.2.5 Murine soluble α-DG caused a dose-dependent inhibition of the NHP clones and M10 but not M1 or M8 in L929 cells

The ability to inhibit LCMV infection using soluble α-DG was previously used as an indicator of the affinity to the receptor (Hastie *et al.*, 2016). To this end, a fragment of α-DG containing the necessary sequence for the virus binding (amino acids 30 to 485) fused with the human IgG Fc sequence at the c-terminus was produced. The α-DG sequence included in the construct was

derived from the *M.musculus DAG1* gene. The construct was expressed in two cell lines HEK 293T and 293F. The supernatant containing the soluble protein was collected and passed through a G-protein affinity-purification column. Western blot analysis of the purified protein showed a molecular weight (~100 kDa) consistent with that previously reported for this construct **(Figure 6-8)** (Kunz *et al.*, 2005). The purity was then assessed by spectrophotometry, coomassie blue, and silver staining. There was a high level of contaminating proteins in the purified supernatant from 293T cells unlike that from 293F which displayed a high purity **(Figure 6-8).** Thus, the purified protein expressed in 293F was quantified by spectrophotometry and BCA assay and used in all subsequent assays.

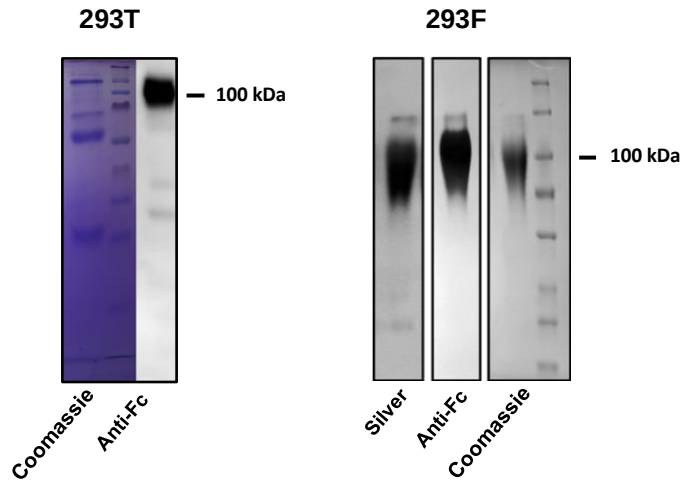


Figure 6-8: Western blot, coomassie blue, and silver staining of murine α-DG-Fc.

pcDNA 3.1 α-DG-Fc construct was either expressed in HEK 293T or 293F**.** After the supernatants were collected and purified, the purified proteins were analyzed by western blot, coomassie blue, and/or silver staining to assess purity. Western blot was performed under reducing conditions and anti-human Fc was used to detect the recombinant protein at ~100 kDa.

For the inhibition assays, pseudotypes were preincubated with the murine αDG-Fc (0-6 µg/ml) for one hour at 37 C° before infecting L929 cells. A 100% inhibition was defined as the level of the infectivity equivalent to the average of △E infectivity, and 0% as the average of the infectivity at α-DG-Fc

concentration of 0 μg/ml. The NHP clones in addition to the mouse clone M10 were inhibited in a dose-dependent manner and showed maximum inhibition of ~ 60%. On the other hand, the mouse clones M1 and M8 were not inhibited and showed a reproducible enhancement at high α-DG-Fc concentrations **(Figure 6-9. A).**

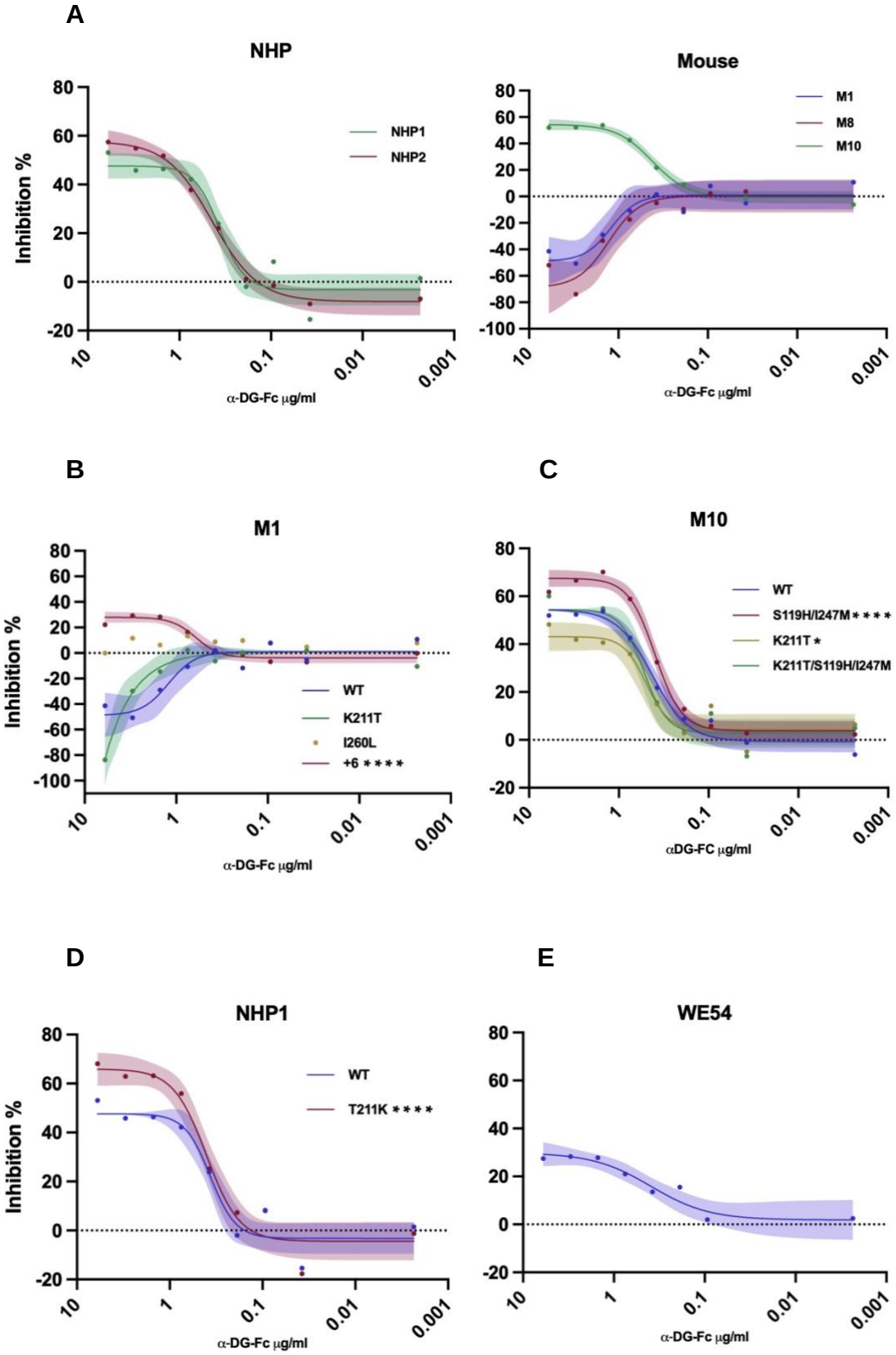
6.2.6 The NHP-defining mutations altered the inhibitory effect of α-DG in L929

The ability of the soluble murine α-DG to inhibit the mutants was tested next. A nonlinear regression analysis was carried out to compare the inhibition curves. The best-fit model was determined based on a model comparison test and the R^2 values. Accordingly, a sigmoidal dose-response (variable slope) model was adapted and the maximum percentage inhibition was compared across clones.

The M1 mutant M1+6 showed a maximum percentage inhibition that was significantly higher than that of the WT (p-value <0.0001) **(Figure 6-9. B).** The M1 mutant with the single mutation K211T showed a reduced inhibition compared to the WT but the difference was not significant. No comparison was made for M1 I260L as no curve could be interpolated from the data.

For M10, the mutant M10 S119H/I247M showed a significantly higher maximum inhibition than the WT (p-value <0.0001) while the mutant M10 K211T showed a significantly lower inhibition than the WT (p-value 0.04) **(Figure 6-9. C).** M10 K211T/S119H/I247M showed a maximum inhibition that was comparable to the WT. The mutation T211K on an NHP background (clone NHP1) increased the inhibition compared to the WT (p-value <0.0001) **(Figure 6-9. D).** It was also observed that the high-affinity strain WE54 showed a dose-dependent inhibition, however, was less than the inhibition observed for the NHP clones and M10 **(Figure 6-9. E).** The inhibitory effect on VSV-G clone was tested at 6 and 3 μg/ml as these concentrations achieved the

highest inhibition of the LCMV clones. As expected, the infectivity of the VSV-G clone was not affected by α-DG at either concentration **(Figure 6-9. F).**


A
NHP
Inhibition %
NHP1
NHP2
α-DG-Fc μg/ml
Mouse
M1
M8
M10
α-DG-Fc μg/ml
B
M1
Inhibition %
WT
K211T
I260L
+6 ****
α-DG-Fc μg/ml
C
M10
WT
S119H/I247M****
K211T*
K211T/S119H/I247M
αDG-FC μg/ml
D
NHP1
Inhibition %
WT
T211K****
α-DG-Fc μg/ml
E
WE54
α-DG-Fc μg/ml

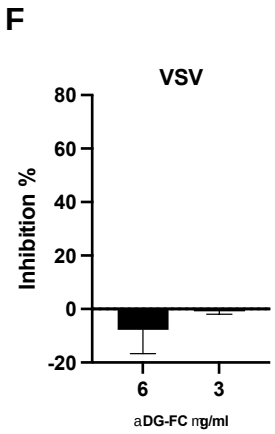


Figure 6-9: Inhibition of entry of LCMV pseudotypes by murine α-DG-Fc.

Pseudotypes were preincubated with increasing concentrations of soluble murine α-DG-Fc before infecting L929. A 100% inhibition was defined as the level of infectivity equivalent to ▵ E average infectivity and 0% inhibition for each clone was defined as the infectivity at α-DG-Fc concentration of 0 µg/ml. The curves were generated using a nonlinear-regression analysis. The goodness of fit was determined by comparing the R^2 values of different models and running a comparison test. Accordingly, a sigmoidal dose-response (variable slope) model was applied for all data sets. The Top (maximum percentage inhibition) values were compared across clones to determine significance. The shaded area around the curves represents the 95% CI. The X-axis is shown on a log scale. The range of the Y-axis may vary depending on the data. (*) indicates significance compared to the respective WT (p-value of <0.05 is considered significant). **(A)** Inhibition curves of WT clones. **(B & C)** The effect of introducing the NHP-defining residues to the two mouse clones M1 and M10 on inhibition. **(D)** The effect of introducing the mouse residue at 211 to the NHP clone NHP1 on inhibition. **(E)** Inhibition of WE54 (control) by murine α-DG. **(F)** Inhibition of VSV by murine α-DG at concentrations of 6 and 3 µg/ml (%). Bars represent mean ± SD. For all data sets, results were pooled from two independent experiments.

6.2.7 The NHP and the mouse clones showed comparable inhibition by NHP soluble α-DG

To determine if the host species receptor could impact differently on entry, the inhibitory effect of soluble NHP α-DG on pseudotypes entry was tested. Alignment of NHP and mouse full-length DAG1 amino acid sequences **(Table 6-1)** showed at least 92% conservation between NHPs and mice. Also, amino acid sequences corresponding to the NHP species from which the study

clones were isolated were aligned with the mouse sequence and the conservation of the regions involved in LCMV/Laminin binding was analyzed. The amino acids 312-408 were previously found to be necessary and sufficient for LCMV/Laminin binding but the region 30-311 was required for the modifications of α-DG (see introduction section **1.8.1**). The alignment showed that the 312-408 region is highly conserved between mouse and NHP with a single mouse/NHP split at position 405. The 30-311 region, on the other hand, showed multiple positions that differed between mouse and NHP α-DG **(Figure 6-10).**

Table 6-1: α-DG protein sequence identity of NHP species versus *M.musculus*.

Blastp database was used to compare the α-DG amino acid sequences of all NHP species reported in the database to that of the murine α-DG (NP_001263411.1). Query coverage was set at 95% to 100% to show only full-length protein sequences.

Scientific Name	Common Name	Per. identity	Length	Accession
Lemur catta	Ring-tailed lemur	94.49	893	XP_045386187.1
Propithecus coquereli	Coquerel's sifaka	93.88	893	XP_012493414.1
Pongo abelii	Sumatran orangutan	93.88	895	XP_003776294.3
Pan troglodytes	chimpanzee	93.88	895	XP_001164638.1
Pan paniscus	pygmy chimpanzee	93.76	895	XP_003818904.2
Homo sapiens	human	93.67	895	NP_001159400.3
Nomascus leucogenys	northern white-cheeked gibbon	93.65	895	XP_003257112.1
Hylobates moloch	silvery gibbon	93.65	895	XP_032017411.1
Colobus angolensis palliates	NA	93.65	894	XP_011794469.1
Aotus nancymaae	Ma's night monkey	93.54	895	XP_012323154.1
Gorilla gorilla gorilla	western lowland gorilla	93.54	894	XP_004034193.3
Carlito syrichta	Philippine tarsier	93.54	893	XP_008061357.1
Sapajus apella	tufted capuchin	93.53	895	XP_032145726.1
Cercocebus atys	sooty mangabey	93.42	894	XP_011889102.1
Piliocolobus tephrosceles	Ugandan red Colobus	93.31	894	XP_023087278.1
Rhinopithecus roxellana	golden snub-nosed monkey	93.31	894	XP_010367983.1
Macaca mulatta	Rhesus monkey	93.20	892	EHH16363.1

Mandrillus leucophaeus	drill	93.20	894	XP_011836288.1
Chlorocebus sabaeus	green monkey	93.20	894	XP_007982428.2
Rhinopithecus bieti	black snub-nosed monkey	93.20	894	XP_017723565.1
Cebus imitator	Panamanian white-faced capuchin	93.19	895	XP_017359996.1
Saimiri boliviensis boliviensis	Bolivian squirrel monkey	93.08	895	XP_003936708.1
Trachypithecus francoisi	Francois's langur	93.08	894	XP_033063288.1
Callithrix jacchus	white-tufted-ear marmoset	92.97	895	XP_035131401.1
Macaca fascicularis	crab-eating macaque	92.57	900	XP_005547176.1
Microcebus murinus	gray mouse lemur	92.52	892	XP_012626738.1
Otolemur garnettii	small-eared galago	91.95	895	XP_012667384.1

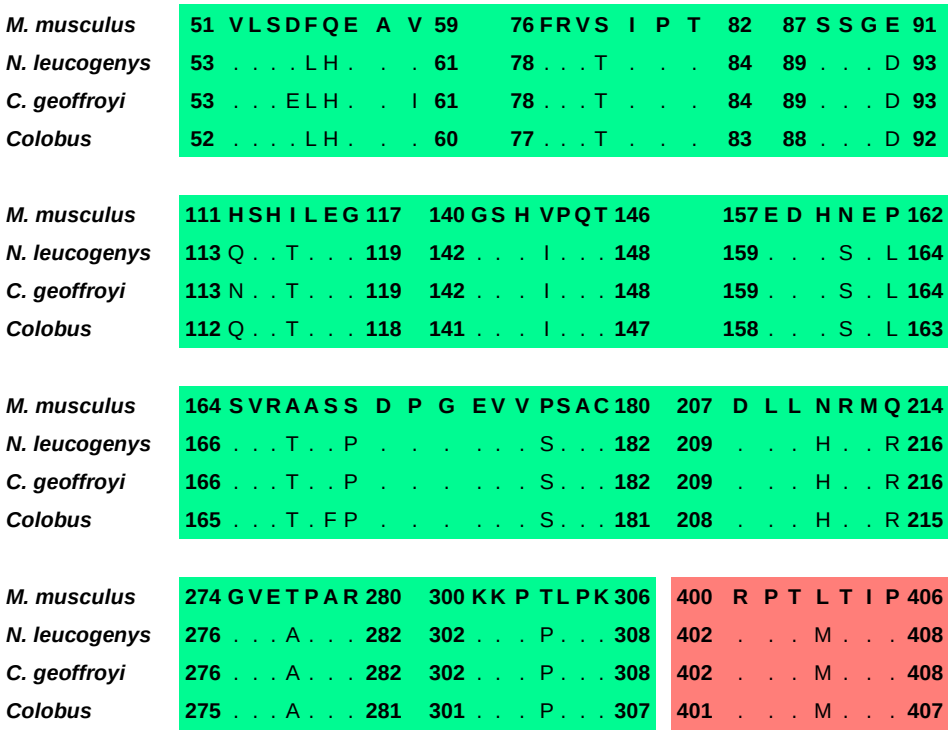


Figure 6-10: NHP and mouse DAG1 protein alignment of the regions involved in the virus binding.

DAG1 amino acid sequence (893 amino acids) of *M. musculus* (NP_001263411.1) was aligned with that of the three NHP species from which the study clones were isolated (*N. leucogens* XP_003257112.1, *C. geoffroyi* XP_035131401.1, and *Colobus* XP_011794469.1). The alignment was trimmed to show the regions of interest. The region important for proper glycosylation of the mucin-like domain (MLD) is highlighted in green. The region of the MLD important for LCMV/laminin-1 binding is highlighted in red. *M. musculus* DAG1 protein sequence was set as the reference sequence. Dots indicate complete match with the reference sequence.

The ability of NHP soluble α-DG to inhibit entry to Vero cells was then measured. NHP soluble α-DG was expressed, purified, and quantified as described for murine α-DG in the previous section. It was found that all WT study clones were similarly affected by the NHP α-DG and, unlike the murine α-DG assay, no clear species-specific pattern was observed**.** Additionally, the dose-response correlation was poor and no model provided an adequate fit for the data (data not shown). Thus, the clones were compared at a single α-DG concentration (6 µg/ml) **(Figure 6-11).**

For the M1 mutants, clone M1+6 showed a significantly higher inhibition (p-value 0.016) while M1 K211T showed a significantly lower inhibition (p-value 0.0003) than the WT **(Figure 6-11. B)**. The NHP1 mutant with T211K mutation showed a significantly higher inhibition compared to the WT (p-value 0.046) **(Figure 6-11. D)**. No significant difference was observed between the M10 mutants and WT M10 **(Figure 6-11. C)**.

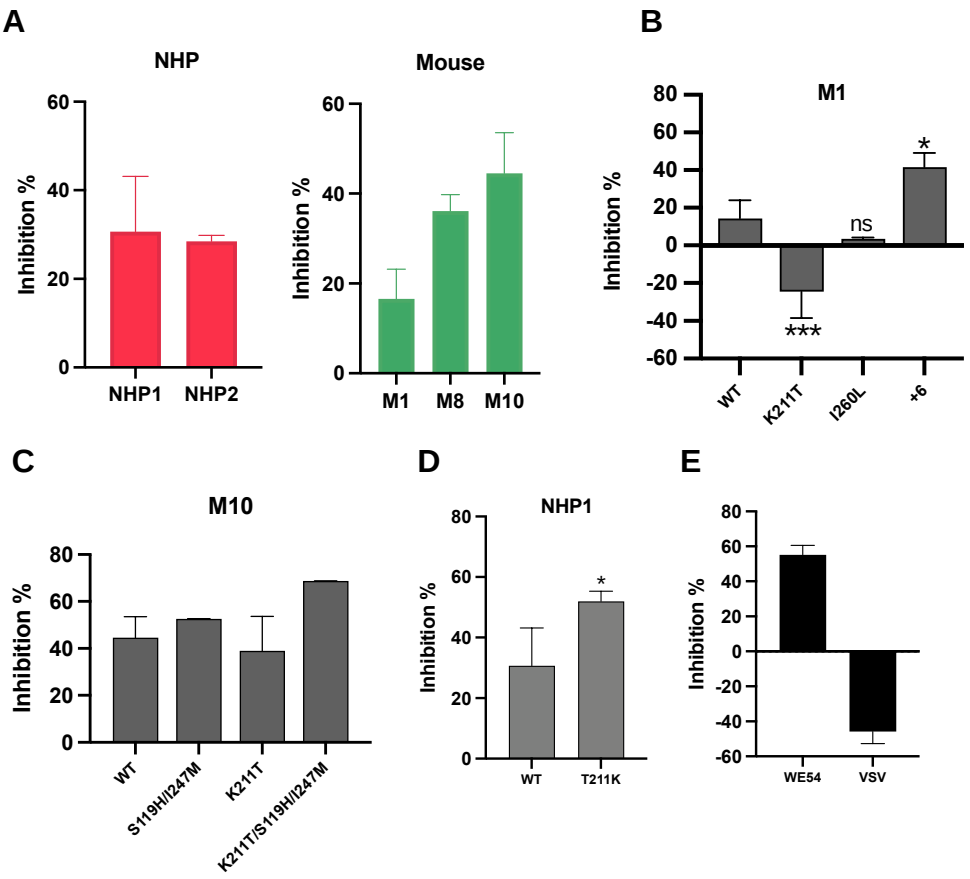


Figure 6-11: Inhibition of pseudotypes entry to Vero cells by NHP α DG.

Pseudotypes were preincubated with soluble NHP α DG-Fc (6 µg/ml) before infecting Vero. A 100% inhibition was defined as the level of infectivity equivalent to ▵E average infectivity and 0% inhibition for each clone was defined as the infectivity at α DG-Fc concentration of 0 µg/ml. **(A)** Inhibition of WT clones by α DG-Fc at a concentration of 6 µg/ml. **(B, C, & D)** The inhibition of M1, M10, and NHP1 mutants by NHP α-DG at a concentration of 6 µg/ml. **(E)** The Inhibition of the positive (WE54) and the negative (VSV) controls by NHP α-DG at a concentration of 6 µg/ml. The range of the Y-axis may vary depending on the data. For **A, B, D,** and **E**, The bars represent mean ± SD. For **C**, the bars represent median ± 95% CI. To determine significance, normality tests were first run and accordingly either One-way ANOVA test **(B),** Kruskal Wallis test **(C),** or t-test **(D)** were applied. (*) indicates significance compared to the respective WT (p-value of <0.05 is considered significant).

6.2.8 The mutations in Gp1 are located within the same region of residues previously found to affect α-DG affinity.

The inhibition data in L929 suggested that the NHP and the mouse clones had a distinct affinity to α-DG and that the identified mutations affected α-DG binding. The region of LCMV Gp1 involved in α-DG binding and residues in this region important for the receptor affinity were previously described (Hastie *et al.*, 2016). Using the previously determined crystal structures of LCMV and LASV, the Gp1 mutations identified in this study were located together with those identified by previous studies. The residues were first mapped in a crystal structure of LCMV Gp1-Gp2 monomer in its prefusion form that was determined at 3.5 A°. Five of the mutations identified here are located in Gp1. Based on the aforementioned study, Gp1 was divided into an N-terminal β-strand, an upper β-sheet, and a lower helix-loop face. Mapping the residues at 106, 119, 211, 247, and 260 with those of previous studies (136, 153, 155, 190, and 260), showed that all, except 106, were located in the lower helix-loop face **(Figure 6-12. A).**

In a previous study (Hastie *et al.*, 2017), a trimeric conformation was found to be necessary for LASV-α-DG interactions. To locate the mutations in the context of a trimer, LASV crystal structures were used. Both monomeric and trimeric prefusion forms of LASV GPC were previously determined at 3.2 A and the core structure of the monomer was found to greatly align with that of the LCMV monomer with a root-mean-square deviation of 1 A°. Thus, we next located the positions in LASV Gp1 that corresponded to the LCMV Gp1 residues and visualised them in the trimeric structure **(Figure 6-12. B).** While the previously identified residues were located in the trimeric interface, three of the residues identified here were located away from the centre of the trimer (106, 119, and 247). The mutations at 211 (208 LASV numbering) and 260 (254 LASV numbering), however, resided at the trimeric interface and in close proximity to the residues from previous studies.

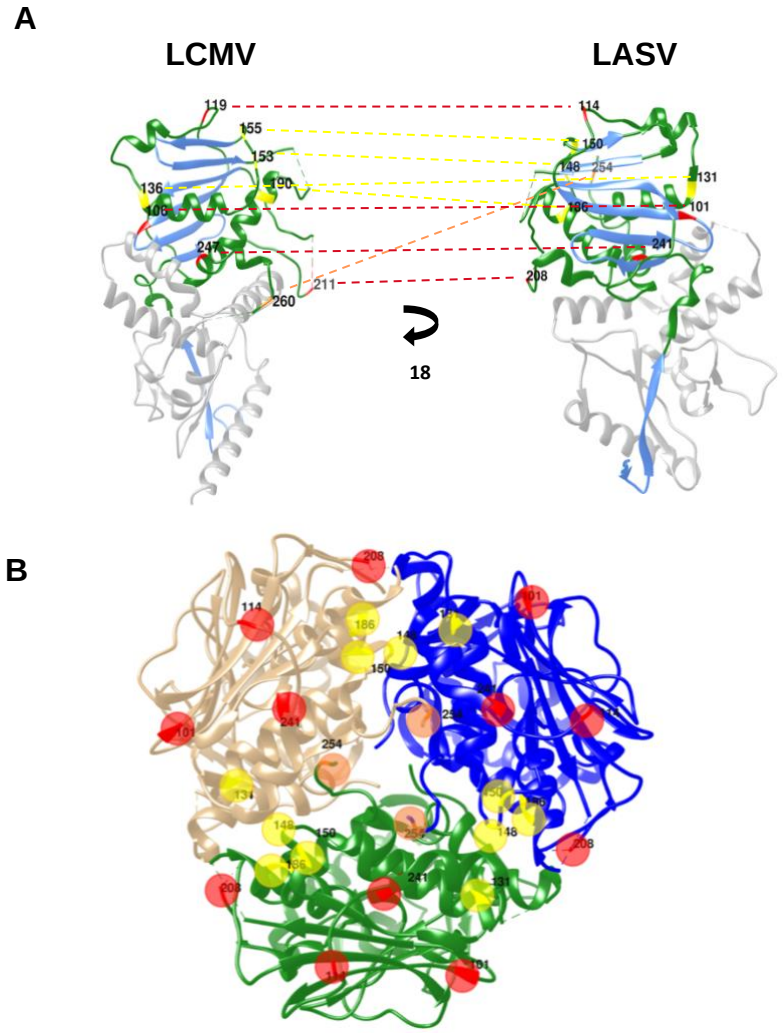


Figure 6-12: Mapping the study mutations together with the mutations previously identified to affect the receptor binding in LCMV and LASV crystal structures.

A) A side view of LCMV and LASV monomers. Different regions of the Gp1 subunit are shown including the N terminal and the upper face β strands (light blue) and the helix-loop face (green). Gp2 is shown in grey. **B)** A top view of LASV trimer. Blue, green, and nude chains represent three monomers arranged in a tripod-like shape resembling the arrangement found in authentic LASV virions.
The residues identified in this study (Red) and previous studies (yellow) or both (orange) are shown in **A** & **B**. The LCMV and LASV structures were adapted from (Hastie *et al.*, 2016) and (Hastie *et al.*, 2017), respectively. The LCMV structure was based on the LCMV WE HPI strain (amino acids 63 to 427). After crystallisation, the structure was determined by heavy atom phasing with a resolution of 3.5 A° (PDB 5INE). The LASV structure was based on Josiah strain (amino acids 60 to 424). Both monomeric and trimeric crystals were obtained and phases were determined by molecular replacement with the LCMV structure 5INE with a resolution of 3.2 A° (LASV GPCysR4).

6.3 Discussion

Altered affinity to cellular receptors was frequently reported in host-switching events of many viruses. Thus, it was next hypothesized that the identified mutations here affected the virus-receptor interactions. To assess the receptor usage of the study isolates, two α-DG-KO cell lines were used: HAP1-α-DG-KO and KM155-α-DG-KO. HAP1 cells are known to be permissive to LCMV and LASV (Jae *et al.*, 2014). Additionally, cellular factors known to be required for LASV infection both *in vitro* and *in vivo* were also identified using HAP1 KO cell lines (Jae *et al.*, 2014, Jae *et al.*, 2013). In the HAP1-α-DG KO cells used here, the NHP clones and M10 were infectious but the infectivity was much lower than in HAP1 KO cells transduced with α-DG. The mouse clones, on the other hand, were only infectious in the transduced cells. The infectivity in the transduced cells highly correlated with the levels of α-DG (expressed at low, medium, and high levels) for both the NHP and the mouse clones with no observed species-specific difference indicating high α-DG dependence of both groups.

While the infectivity of the mouse clones M1 and M8 was abolished in HAP1 KO cells, the mouse mutant harbouring six of the NHP-defining mutations (M1+6) displayed a phenotype similar to the NHP clones. M1+6 was also more infectious than M1 with the mutation I260L alone. Similar to its effect in L929, the K211T mutation reduced the infectivity of M10 in HAP1 KO cells. On S119H/I247M background, the effect of K211T was mitigated as the mutant M10 S119H/K211T/I247M showed comparable infectivity as the WT M10. Also, the reverse mutation (T211K) increased the infectivity of NHP1 in the KO cells.

The second KO cell line KM155-αDG-KO was also permissive to an NHP clone (NHP3), albeit less than the WT KM155. The fact that the NHP clones were infectious in two different KO cell lines and the mutations increased the infectivity in HAP1-KO cells, indicated that the NHP clones could enter cells

independently of α-DG and that the mutations increased the affinity to an alternative receptor.

Alternative receptors have been proposed for LASV and some LCMV strains (see introduction section **1.8.2**). The KI/KO data obtained here also suggest that the existence of an alternative receptor for the NHP clones is plausible. The KO of α-DG was genotypically confirmed in those cells by the providers. Our FACS analysis also indicated the absence of surface α-DG in the HAP1-αDG-KO cells. Although a dose-dependent inhibition by soluble α-DG was observed in the KO cells and may indicate the existence of residual surface α-DG, it could also be a result of blocking the GPC causing steric hindrance and rendering it inaccessible to other receptors. Additionally, the naturally occurring splice variants of α-DG in humans were analyzed. The analysis showed that the KO sites and the virus-binding site are located in two different coding exons and all the splice variants reported from normal human tissues possessed both exons. This indicated that the regeneration of the virus receptor via alternative splicing was unlikely unless the alternative splicing profile of cultured cell lines deviates from that occurring naturally. It is also possible that the KO itself induced distinct splicing events not observed in the WT. Indeed, the CRISPR/Cas9 technology used to produce the two cell lines was previously found to induce such events in HAP1 (Smits *et al.*, 2019).

The CRISPR/Cas9 system for genome engineering has been widely applied to explore host factors of different viruses (Han *et al.*, 2018, Gebre *et al.*, 2018). This technology exploits the endonuclease activity of Cas9 enzyme isolated from the bacterial strain *Streptococcus pyogenes*. The mechanism involves the use of a guide RNA (gRNA) that measures 20 nucleotides and specifically directs the nuclease machinery to the genomic target site through sequence homology. The choice of the target site is only limited to those which are adjacent to a PAM motif (NGG) (Le Rhun *et al.*, 2019). The enzyme then introduces a double-strand break at the target site. In eukaryotic cells, the repair of the break is error-prone unless a template with sequence homology is provided. In the absence of a template, the ORF is thrown off resulting in

the KO of the target gene. While the specificity of CRISPR/Cas9 has improved to minimize off-target effects by altering the gRNA design and protein engineering, some mechanisms by which cells can overcome CRISPR/Cas9 editing exist (Doench *et al.*, 2016, Kleinstiver *et al.*, 2016). Namely, alternative splicing leading to exon skipping and/or re-initiation of translation via in-frame downstream ATG were frequently reported (Zhang *et al.*, 2020, Smits *et al.*, 2019, Tuladhar *et al.*, 2019, Mou *et al.*, 2017). Truncated proteins were produced as a result which were found to retain partial functionality of the native proteins. In a study where 136 genes in HAP1 cells were knocked out, one-third of the set displayed residual protein expression (Smits *et al.*, 2019). In-depth analysis showed that alternative splicing resulting in transcript variants not seen in the WT line was induced in the KO lines. In other KO lines, no difference in alternative splicing was observed, however, it was found that re-initiation of translation occurred at a downstream ATG. Protein expression analysis using a highly-sensitive mass spectrometry assay detected residual proteins in a third of the HAP1-KO lines albeit with reduced levels. Assessing the functionality of those proteins revealed partial retention. For example, the cell line where the DNMT1 gene involved in DNA methylation was knocked out showed a near WT methylation level while complete inhibition of DNMT1 abolished methylation. Another protein involved in the de-glycosylation of N-linked glycans (NGLY1) showed residual de-glycosylation following the KO that was further reduced by NGLY1 inhibitor. Interestingly, protein analysis using mass spectrometry of this protein showed no expression indicating that protein levels falling below the detection threshold can still impart a measurable phenotype.

Our data highly suggest the existence of an alternative receptor for the NHP clones and M10. However, as overcoming the CRISPR/Cas9 editing was reported in HAP1-KO lines with high rates, the absence of α-DG could not be established with high certainty, especially since the antibody used in the FACS analysis (IIH6C4) is glycosylation sensitive and may not recognize all forms of α-DG. For example, IIH6C4 did not recognize surface α-DG on Vero cells

although both LCMV and laminin could bind α-DG purified from WT Vero cells. But when LARGE1 was overexpressed the antibody showed high reactivity (Kunz *et al.*, 2005, Brouillette *et al.*, 2018). If residual α-DG did exist, this could mean that the NHP clones have a higher affinity to primate α-DG than the mouse clones. The comparable affinity between the two groups in the KO cells transduced with murine α-DG, further suggested that the species of α-DG impart distinct phenotypes.

To further elucidate the receptor usage of the study clones, the ability of soluble α-DG-Fc to inhibit the infectivity was assessed. This construct (αDGFc4) was previously described and was found to inhibit α-DG-high affinity clones in a dose-dependent manner while the low-affinity clones were unaffected by it (Hastie *et al.*, 2016).

Two inhibition assays were performed: either murine soluble α-DG was used to inhibit the infectivity in murine cells (L929) or NHP soluble α-DG was used to inhibit the infectivity in NHP cells (VeroE6). In L929, a distinct inhibitory effect of α-DG-Fc was observed between the NHP and the mouse clones. While the NHP clones (in addition to M10) were inhibited in a dose-dependent manner, the mouse clones were not inhibited. Thus, in addition to acquiring affinity to an alternative receptor as suggested by the transduction data, the NHP clones may also have a higher affinity to α-DG compared to the mouse clones. It was also noticed that a 100% inhibition was not achievable, another indicator of the existence of an alternative receptor. However, an enhancement was seen in the infectivity of the mouse clones and VSV at high αDG-Fc concentrations. This could indicate that a 100% inhibition of the NHP clones is unachievable under the assay conditions.

Interestingly, in Vero cells, no species-specific pattern was observed and all LCMV clones showed comparable inhibition. This is in line with the transduction assay which indicated, in case residual α-DG existed in the KO cells, that NHP and murine α-DG impart distinct phenotypes. The sequence

analysis, however, revealed a high degree of conservation between the NHP and the murine α-DG, particularly in the virus-binding site. It is possible that the different inhibitory effect of the NHP and the murine α-DG was cell-line specific. It was frequently reported that α-DG glycosylation level in Vero cells was reduced (see section **5.3**). Consequently, this could have caused both the NHP and the mouse clones to bind the soluble α-DG with a higher affinity than binding the surface under-glycosylated Vero α-DG regardless of the soluble α-DG species.

Despite the different inhibitory effects observed between the NHP and the murine α-DG on the WT clones, the mutants generally showed a similar pattern of inhibition in the two assays.

Chapter. 7: Discussion

7.1 Overview

Factors contributing to the emergence of viruses are usually complex and interrelated. Nonetheless, viral factors especially those involving the early steps of the viral life cycle usually play a major role in emergence. Adaptive changes in the surface glycoproteins of viruses whether to increase the affinity to a cellular receptor or to promote more efficient entry by evading immunity or entry restriction factors have been associated with the emergence of many viruses (Glaser *et al.*, 2005, Holmes, 2005, Urbanowicz *et al.*, 2016b, Ozono *et al.*, 2021, Cao *et al.*, 2022). Thus, investigating the viral glycoproteins can provide a better understanding of cell entry and transmissibility which in turn can be pivotal in developing preventive and therapeutic measures. Arenavirus is a family that was frequently associated with rodent-to-human outbreaks. LASV is considered the arenavirus with the highest human impact. Indeed, it comes fourth in the blueprint list of the priority diseases issued by WHO (WHO, 2022b). It is estimated to cause between 100,000 and 300,000 infections annually with around 1% CFR (CDC, 2022). LCMV is another OWA closely related to LASV. They display similar receptor usage and antigenicity. α-DG is the primary receptor for most LASV and LCMV strains. Additionally, major antigenic determinants are shared by the two viruses evident in the high cross-reactivity of antibodies induced by either virus especially neutralizing antibodies (Robinson *et al.*, 2016a). Hence, LCMV was frequently exploited as a model for LASV. However, most studies were based on culture-adapted lab strains that may not reflect the properties of the authentic virus.

In this study, *ex vivo* sequences isolated from naturally LCMV-infected NHPs and mice were used. The outbreak that took place in a zoo in the United Kingdom involved different species of NHP. The initial testing carried out by UKHSA showed an overall ~ 19 % positivity in NHPs either by serology or

PCR with at least six LCMV-related deaths. 16 full-length LCMV GPC were obtained from 11 mouse samples and four NHP samples to investigate the existence of glycoprotein determinants that might have contributed to the NHP outbreak. We generated nine LCMV GPC clones, four NHP- and five mouse-derived, then tested the infectivity of the pseudotypes supplemented with these clones in several cell lines including murine, primate, and αDG-KI/KO cells. The clones reproducibly displayed a species-specific pattern of infectivity that seemed to be related to the receptor affinity. The sequence analysis denoted multiple sites with a species-specific signature. Mutagenesis assays indicated that the phenotype could indeed be explained by the identified changes or a subset of them.

7.2 The study's relevance to the current arenavirus status

This study identified adaptive changes in LCMV GPC which could be implicated in an outbreak of LCMV in NHPs. While adaptive changes, including some of the changes identified here, were previously reported and were found to contribute to the receptor affinity, pathogenicity, and prognosis of the disease, these findings were based on lab-induced infections using culture-adapted LCMV strains. To our knowledge, this is the first time adaptive changes in LCMV GPC were identified from naturally occurring infections. There is a wealth of information in the literature implicating adaptations affecting the early steps in the virus life cycle in the emergence of many viruses. The results of this study indicate that arenavirus is no exception and whilst outbreaks of arenaviruses are usually attributed to changes in the ecology or behaviour of the host population, adaptations can also emerge. Arenavirus, specially LASV, is considered by many scientific bodies to be an urgent epidemic threat. The habitat of its natural host heavily overlaps with the human habitat which increases the chances of spillover. Additionally, the majority of infections are asymptomatic allowing the virus to circulate undetected for a longer period of time compared to viruses associated with severe illness. This could in turn allow sufficient time for adaptations to emerge

and less time to respond and contain the spread. Thus, this study and similar studies can contribute to the ongoing surveillance in areas where arenaviruses are endemic. Knowing the sites and regions in the GPC where adaptations are more likely to occur would allow guided screening of the circulating strains and more timely response to public health concerns.

Additionally, such knowledge should be implemented in vaccine and therapy designs. For example, a promising monoclonal antibody cocktail was recently developed for LASV and is soon to advance to clinical trials (Li *et al.*, 2022). An important group of antibodies included in the cocktail targets the α-DG binding site in LASV GPC. Thus, it is of the utmost relevance to consider mutations that could arise in this region and reduce the effectiveness of the regimen before clinical approval.

7.3 The limitations and areas of improvements

Some limitations existed at different stages of this study due to time and resource restraints or shortage of information. One important question that this study tried to answer was if the virus had adapted to cause sustained primate-to-primate transmission. The phylogenetic analysis was not very informative in this regard due to two reasons: the limited number of NHP samples and the gap in the collection dates between the NHP and the mouse samples. Although the NHP and the mouse sequences clustered separately which is suggestive of a primate-to-primate transmission, the small number of NHP sequences could not unequivocally indicate transmission. Additionally, the collection of the mouse samples at least six months after the NHP samples made species specificity difficult to establish. This gap in collection dates could have resulted in the separate clustering of sequences due to temporal association rather than species specificity. Some information about the circumstances surrounding the outbreak was also lacking. Different NHP species were involved in the outbreak. If the outbreak was mainly caused by primate-to-primate transmission, this would mean that different species were

in close proximity to each other. While there is an indication that different species were housed together during exhibits and events predated the outbreak, this was never confirmed by the zoo.

The data obtained in this study was solely based on infectivity assays. Thus, the choice of the *in vitro* models was of high relevance. Both murine and primate cell lines were included in the study. However, as the mouse is the natural host of LCMV, the infectivity of the pseudotypes should have been tested in more than one murine cell line. Some phenotypes can be cell line specific and discrepancies in the phenotypes seen in different cell lines were frequently reported for some viruses. For example, an infectivity advantage of some SARS-CoV-2 variants was detected in cell lines expressing low levels of ACE2 (the primary receptor) but not in cells where ACE2 is expressed in abundance (Niemeyer *et al.*, 2022). Additionally, sensitivity to neutralization may vary across cell lines. For example, sera collected from individuals vaccinated against certain viruses (e.g. SARS-CoV-2 and CMV) failed to neutralize these viruses in specific cell lines (Cui *et al.*, 2008, Criscuolo *et al.*, 2022). This was attributed to distinct entry mechanisms utilised by the virus in different cell lines. These examples and others emphasize the importance of using multiple cell lines to fully capture the range of phenotypes imparted by a virus.

The receptor usage is central to the hypothesis of this study. Yet, the absence of α-DG in the KO cells could not be confirmed. Although the FACS analysis showed no surface expression of the receptor, the antibody used targets the α subunit and is known to be glycosylation sensitive. Thus, the experiment could have benefited from using multiple antibodies, preferably antibodies that target β-DG, or applying qPCR spanning the exon-exon junctions to confirm the KO. Additionally, the role of the α-DG species in the observed increased affinity of the NHP clones was unclear. The KO/KI assay indicated that, in case of residual α-DG existed in the KO cells, the NHP clones had an increased

affinity to primate α-DG over the mouse clones. In contrast, the inhibition assay indicated an increased affinity of the NHP clones to murine α-DG. Both assays are indirect measures of the virus-receptor binding and could not conclusively determine the role of α-DG species in the observed phenotypes. Another drawback of the inhibition assay is the possibility of interference from the Fc tag. Similar α-DG-Fc constructs were frequently used by many studies with no reported interference from the Fc tag (Kunz *et al.*, 2005, Kanagawa *et al.*, 2004, Hastie *et al.*, 2016). However, the inclusion of additional controls, for example, a non-specific Fc-tagged recombinant protein, would have further confirmed that the observed phenotype is exclusively α-DG specific.

7.4 Technical challenges

The course of progress of this study was faced with some difficulties and technical challenges. These included but were not limited to pseudotype standardization, α-DG expression and purification, and quantification of virus-receptor interactions. More details are provided in the following sections.

7.4.1 Standardizing pseudotypes input using p30 signal

The input of pseudotypes produced using an MLV-based system can be standardized by detecting the principal component of the MLV backbone, p30. To this end, the pseudotypes of the study clones were concentrated and subjected to western blot analysis as described in the Methods and Materials section. Densitometric analysis was then applied to quantify the signals and transform them into a fold difference. The RLU values of the infectivity assays could then be normalized accordingly. The process, however, was compromised by the loss of a different subset of the pellets in every attempt probably during the discard of the supernatants following the ultracentrifugation. This was seen as undetectable signals in the western blot of highly infectious samples. Thus, normalizing the entire set was not possible

using this method. Standardizing the samples that produced detectable signals, however, resulted in a pattern similar to that produced when the data were normalized by taking ratio/percentage. Hence, to compare the infectivity across all the clones, ratios/percentages were used throughout the study.

7.4.2 Assessing α-DG level in cell lysates

Western blot was applied to analyze α-DG expression in the lysates of target cells used in the infectivity assays. The analyzed cell lines included: Vero E6, L929, HAP1-α-DG KO/KI and KM155 WT/α-DG KO cells. Two anti-α-DG antibodies were used: IIH6C4 and PA5-193223. For IIH6C4, the results were inconsistent and high inter-experiment variation was observed. PA5-193223 reproducibly detected a single band of ~ 55 kDa. While α-DG core of ~ 50 kDa was previously reported (Yoshida-Moriguchi *et al.*, 2010), functional α-DG typically shows a molecular weight of 120-150 kDa (Barresi and Campbell, 2006). It is possible that this antibody preferentially binds unmodified unfunctional core α-DG as it was raised against a synthetic peptide (HVGKHEYFMHATDK) corresponding to an internal sequence of α-DG. However, since the detected molecular weight was rarely reported and non-specific binding could not be ruled out, the data was disregarded.

7.4.3 Overexpressing LARGE1 in HEK293T

The main enzyme involved in α-DG glycosylation (LARGE1) was overexpressed in HEK293T cells. The aim was to compare the inhibition ability of soluble α-DG produced from WT HEK293T cells versus α-DG produced from HEK293T overexpressing LARGE1. The Ad5/hLARGE1-EGFP construct was used to transduce HEK293T. The overexpression of LARGE1 was verified by qPCR which showed comparable expression of GAPDH between the WT and transduced cells (average Ct values of 16.13 and 16.4, respectively) but significantly higher expression of LARGE1 in the transduced cells (average Ct value of 15.6 versus a value of 21 in the WT cells, p-value

0.0164). Subsequently, α-DG-Fc construct was expressed in the WT and the LARGE1-transduced HEK293T cells in addition to 293F cells. However, after the purity of the samples was assessed following protein G column purification, samples collected from HEK293T were found to contain high levels of impurities. Thus, only α-DG purified from 293F was used in inhibition assays. Overexpressing LARGE1 in 293F was considered but due to time constraints it was not performed and other experiments were prioritized.

7.4.4 Purification of α-DG-Fc recombinant protein using AKTA

After expressing the α-DG-Fc construct as described in the Methods and Materials section, the supernatants were collected for purification using HiTrap protein G high-performance purification column installed in a Fast Protein Liquid Chromatography instrument (AKTA Amersham Biosciences). The purification process, however, was not successful as no peak was visualized during the elution. Western blot analysis revealed that the protein was present in the supernatant but not in the flow-through or elutions which indicated that it was not eluted. Factors that could have contributed to this included: the protein precipitated/adsorbed on the column/filter, the pH of the elution buffer was suboptimal, or the flow was distorted by air bubbles/valve malfunction (Cytiva, 2020). Thus, the samples were instead purified using the Thermo Scientific NAb Protein G Spin Kit as detailed in section **2.19.3**.

7.4.5 Dot blot to measure virus-α-DG binding

Dot blot analysis to assess and compare the virus-α-DG binding of the study clones was applied. The results, however, were not reproducible across the experiments and the replicates within each experiment were inconsistent. This could be due to sample leakage or/and uneven pressure inside the apparatus. Additionally, a high background despite changing the blocking conditions was

observed. Thus, an accurate comparison could not be made and the experiment was terminated.

7.5 Future perspectives

The data presented herein were highly reproducible and consistent. However, further experiments are needed to add to its robustness and clarity. For example, all the data of the study were derived from infectivity assays using MLV-based pseudotypes. While pseudotyping was proven to be a reliable surrogate for some viruses, some inconsistencies were reported in the literature (see introduction section **1.10.6**). However, a comparison of LASV pseudotypes produced using different backbones revealed the superiority of the MLV system with up to a 5-fold increase in infectious titers (Cosset *et al.*, 2009). Furthermore, comparing a replication-competent LASV with the MLV-based LASV pseudotypes showed similar entry requirements and kinetics (Rojek *et al.*, 2008). While these findings are reassuring, confirming our data using a replication-competent virus would further support its credibility.

A reverse genetics approach was previously applied to produce a recombinant LCMV (Rojek *et al.*, 2008, Sanchez and de la Torre, 2006). In these studies, full-length S and L segments were supplied in two separate plasmids containing T7 or Pol I promoter and co-transfected with T7/Pol I-coding plasmid. LCMV NP and L genes were supplied in trans for the replication and expression of the S and L segments. The produced rLCMV grew to comparable titres and induced similar disease in mice as an authentic LCMV virus (Sanchez and de la Torre, 2006). Thus, these systems would allow measuring phenotypes imparted by the study isolates in the context of productive infections.

Another drawback of the assays applied here is that they only enable inferences to be made about the infectivity in general without specifying the step of the entry involved. Although the data from the KI/KO and the inhibition assays indicated the involvement of the viral receptor, a direct measurement of the virus-receptor interactions would be useful. Assays such as ELISA and VOPBA have been used to quantify LCMV-α-DG binding (Kunz *et al.*, 2005,

Kunz *et al.*, 2001). Another widely used technique to measure protein-protein interaction is the Surface Plasmon Resonance (SPR) analysis. The assay involves the immobilization of a ligand (e.g. receptor) on a sensor chip. The binding to a flow-through analyte (e.g. viral particles) results in a change in the angle of the reflected beam which can be then measured in real-time (Drescher *et al.*, 2018, Drescher *et al.*, 2009). SPR has the advantage of being a label-free assay and the sample containing the analyte does not need to be purified. Experiments to identify a potintial alternative receptor whether one of the previously proposed for LASV/LCMV or a yet unidentified novel receptor would be also of high relevance. Members of TIM and TAM families were previously proposed as alternative receptors for LASV/LCMV (see introduction section **1.8.2)**. It is important, however, to carefully plan experiments assessing TIM/TAM requirements especially when inhibitors are used. It was found, for instance, that LCMV entry can be blocked by inhibiting c-Met (a TAM receptor) using EMD at a concentration of 10 µg/ml (Oppliger *et al.*, 2016). However, in another study, EMD specificity to c-Met was found to be reduced at high concentrations and was able to inhibit other kinases at 10 µg/ml including Axl (another TAM receptor proposed for LASV/LCMV entry) (Bladt *et al.*, 2013). Another example is the inhibition of Axl by genistein. This compound does not only inhibit multiple kinases but also has multiple activities that can ultimately have an inhibitory effect on LASV infection (Shimojima *et al.*, 2012).

One important aspect of LCMV entry is the role of LARGE1-dependent modification of α-DG. It has previously been found that high- and low-α-DG affinity clones reacted differently to LARGE-1 overexpression. Both showed higher binding to α-DG derived from cells overexpressing LARGE1 than from WT cells (Kunz *et al.*, 2005). However, the high-affinity clones were not blocked when target cells were preincubated with laminin whether or not LARGE1 was overexpressed. The low-affinity clones, on the other hand, were blocked by laminin in a dose-dependent manner and at lower concentrations when LARGE1 was overexpressed (Kunz *et al.*, 2005). Indicating that low-

affinity clones could not compete against the natural ligand of α-DG and even less so when LARGE1 was overexpressed. It would be intriguing to see if such an effect exists for our clones since they seem to have a different affinity to α-DG.

It is also important to further investigate the role of each of the identified mutations. For example, threonine at position 211, which was the only residue that was strictly species-specific, reproducibly reduced the infectivity on different backgrounds in murine and primate cell lines. It is, therefore, possible that this residue contributed to the fitness of the virus in the new host in a way that negatively affected its receptor binding. Mutations conferring immune escape are often associated with fitness costs including reduced infectivity/receptor affinity (Hoffmann *et al.*, 2022, Chen and Wei, 2022, Lynch *et al.*, 2015). Thus, experiments such as neutralization assays using sera collected from the animals of the outbreak could provide insight into the role of K211T in this regard.

While this study focused on the GPC gene due to its essential role in the early steps of the virus life cycle, the contribution of other viral factors cannot be excluded. Adaptations in other viral genes may have existed and exploring this possibility could provide a more comprehensive understanding of the outbreak. Indeed, it was previously reported that the tropism and persistence of some LCMV strains were associated with adaptations in both GPC and the polymerase gene (Matloubian *et al.*, 1993).

Finally, LCMV and LASV share many features and have similar receptor usage and antigenicity. Hence, LCMV was frequently used as a model for LASV. One of the intended purposes of this study was to generate data that could be extendable to LASV. While this was not achievable in the time frame of the study, it would be interesting in the future to test the effect of the mutations identified here on LASV infectivity.

7.6 Summary

The data obtained here suggest that the NHP clones have an increased infectivity over the mouse clones in most of the tested cell lines and this increase can be mapped to a few GPC residues. Specifically, four mutations (or a subset of them) seemed to account for the majority of this increase: F106S, I260L, V451I, and L468S. The mouse clone carrying these mutations (M10) displayed an NHP-like phenotype despite lacking the other three mutations characterizing the NHP clones (S119H, K211T, and I247M) which further supports the role of the four mutations. The data also suggest that the effect of the mutations is collective rather than individual as no single mutation caused a significant increase in the infectivity except I260L (in some assays). On the other hand, K211T alone reproducibly caused a decrease in the infectivity on different backgrounds and S119H/I247M seemed to rescue this reduction. A hypothetical series of events of this outbreak is that the four mutations emerged in the mouse population resulting in increased infectivity and making the virus more transmissible which in turn facilitated the cross-species transmission. But it is also possible that the four mutations emerged in the NHPs following the spillover from mice followed by reverse zoonosis, hence, the four mutations were spotted in a mouse clone. K211T occurred in NHPs possibly as a resistance or immune escape mutation but also caused a reduction in the receptor binding. This was followed by the emergence of the compensatory mutations S119H and I247M to mitigate the effect of K211T. Although never confirmed, reports from the site of the outbreak mentioned the possible circulation of LCMV at least two years prior to the outbreak which could mean that the NHPs in the enclosure were not immunologically naïve. This makes the emergence of immune escape mutations plausible.

The data also suggest that the superior infectivity of NHP clones was due to increased affinity to α-DG or/and an alternative receptor. There were several lines of evidence supporting the existence of an alternative receptor for the NHP clones: they were able to infect α-DG-KO cell lines and blocking with

soluble α-DG could not achieve 100% inhibition. Additionally, the residual infectivity was comparable in both assays (~ 25%). However, the NHP clones also seem to have a higher affinity to α-DG than the mouse clones as suggested by the inhibition data in L929.

The existence of alternative receptors for some LCMV strains was previously proposed. Nonetheless, these strains were not affected or only mildly affected by the absence of α-DG (Kunz *et al.*, 2004, Smelt *et al.*, 2001a, Bakkers *et al.*, 2022). On the other hand, the clones of this study showed a high dependency on α-DG even when an alternative route might have been used. More than 70% of the infectivity was abolished when α-DG was knocked out which raises the question of the fitness advantage of acquiring an affinity for a receptor that promotes remarkably less efficient entry. There is evidence that OWAs switch receptors as a mechanism to evade entry restriction factors (Stott *et al.*, 2020a). Whether this is the case here or not, however, warrants further investigation.

Chapter. 8: Appendices

8.1 The NHP samples serology and PCR results:

UKHSA ID	Lab ID	Study ID	Species	Date collected	Date received	UKHSA result		Lab result
						Serology	PCR	
H06 336 0621 01	NA14	NHP1	Geoffroy's marmoset	-	23/08/2006	NT	Positive	Positive
H06 336 0625 01	NA18	NHP2	Black & white colobus	06/07/2005	23/08/2006	NT	Positive	Positive
H06 094 0753 01	NA74	NHP3	Geoffroy's marmoset	27/01/2006	-	NT	Positive	Positive
H06 336 0613 01	NA76	NHP4	Concolor gibbon	-	23/08/2006	Negative	Negative	Positive
H06 230 0544 01		-	Linne's two-toed sloth	-	05/06/2006	Positive	NT	NT
H06 230 0545 01		-	Linne's two-toed sloth	-	05/06/2006	Positive	NT	NT
H06 230 0551 01		-	Chimpanzee	-	05/06/2006	Positive	NT	NT
H06 230 0553 01		-	Black & white colobus	-	05/06/2006	Positive	Positive	NT
H06 230 0555 01		-	Chimpanzee	-	05/06/2006	Positive	NT	NT
H06 230 0556 01		-	Chimpanzee	-	05/06/2006	Positive	NT	NT
H06 276 0592 02		-	Geoffroy's marmoset	-	06/07/2006	Positive	NT	NT
H06 276 0593 01		-	Geoffroy's marmoset	-	06/07/2006	Positive	NT	NT
H07 196 0592 01		-	Gorilla	26/02/2007		Positive	NT	NT
H07 196 0608 01		-	Allen's swamp monkey	20/03/2007		Positive	NT	NT
H07 196 0623 01		-	Spider monkey	18/08/2006		Positive	NT	NT
H07 196 0626 01		-	Chimpanzee	18/08/2006		Positive	NT	NT
H07 196 0628 01		-	Chimpanzee	12/10/2006		Positive	NT	NT
H07 196 0629 01		-	Chimpanzee	06/07/2006		Positive	NT	NT
H07 196 0630 01		-	Chimpanzee	12/10/2006		Positive	NT	NT

H07 196 0631 01		-	Chimpanzee	12/10/2006	Positive	NT	NT
H07 196 0632 01		-	Chimpanzee	18/08/2006	Positive	NT	NT
H07 196 0633 01		-	Chimpanzee	12/10/2006	Positive	NT	NT
H06 094 0752 01	NA73	-	Geoffroy's marmoset	08/01/2006	NT	Positive	Negative
H06 336 0622 01	NA15	-	Purple-faced langur	26/01/2006	NT	Positive	Negative

8.2 The mouse samples serology and PCR results:

UKHSA ID	Lab ID	Study ID	Collection Date	UKHSA PCR	Lab PCR Results
H07 196 0643 01	NA28	M1	08/08/2006	NT	Positive
H07 196 0645 01	NA29	M2	08/08/2006	NT	Positive
H07 196 0647 01	NA30	M3	08/08/2006	NT	Positive
H07 196 0650 01	NA31	M4	20/07/2006	NT	Positive
H07 196 0656 01	NA32	M5	19/07/2006	NT	Positive
H07 196 0638 01	NA56	M6	18/08/2006	Positive	Positive
H07 196 0649 01	NA58	M7/M8	20/07/2006	Positive	Positive
H07 196 0658 01	NA61	M9	17/07/2006	Positive	Positive
H07 196 0665 01	NA66	M10	24/07/2006	Positive	Positive
H07 196 0674 01	NA67	M11	01/10/2006	Positive	Positive
H07 196 0677 01	NA70	M12	28/09/2006	Positive	Positive
H06 266 0587 01	NA2	-	Before 29/06/2006*	Positive	Negative
H06 266 0588 02	NA3	-	Before 29/06/2006*	Positive	Negative
H06 266 0589 02	NA4	-	Before 29/06/2006*	Positive	Negative
H06 266 0590 03	NA5	-	Before 29/06/2006*	Positive	Positive
H07 196 0637 01		-	11/08/2006	Positive	NT
H07 196 0641 01		-	17/07/2006	Positive	NT
H07 196 0644 01	NA77	-	08/08/2006	NT	Positive
H07 196 0648 01	NA57	-	19/07/2006	Positive	Negative
H07 196 0651 01	NA59	-	24/07/2006	Positive	Positive

H07 196 0652 01	NA62	-	19/07/2006	Positive	Negative
H07 196 0661 01	NA62	-	08/08/2006	Positive	Negative
H07 196 0662 01	NA63	-	04/08/2006	Positive	Negative
H07 196 0663 01	NA64	-	02/08/2006	Positive	Positive
H07 196 0664 01	NA65	-	27/07/2006	Positive	Positive
H07 196 0675 01	NA68	-	06/10/2006	Positive	Positive
H07 196 0676 01	NA69	-	28/09/2006	Positive	Positive
H07 196 0678 01	NA71	-	22/09/2006	Positive	Positive
H07 196 0679 01	NA72	-	21/09/2006	Positive	Positive

8.3 Pathology records as provided by Twycross zoo for LCMV-confirmed cases:

Species	Twycross ID	UKHSA ID	Clinical signs	Necropsy	Histology
Geoffroy's marmoset	3844	H06 094 0753 01	Day 1, was found on floor in the tropical house a few days before and then again on day 1, was weak and ataxic, was having some neurological problems/seizures. On exam was dehydrated, in lean body condition, cool body temp (36.4 degrees c) abdomen seems fluid-filled. Low albumin, high urea, cholesterol and AST. Indicated renal problems. On day 3, was fitting throughout the day (even on diazepam) and so was euthanised.	Hepatitis, nephritis and vasculitis there were multiple white foci within the liver presumed necrosis or inflammation, mesenteric lymph nodes are enlarged, kidneys feel firm (fibrosis?), and a small amount of abdominal oedema.	Hepatitis with thrombophlebitis in the liver with some iron storage, glomerulotubulointerstitial nephritis (with brown proteinaceous fluid in dilated tubules), pneumonia (oedema and congestion of alveoli) with perivascular cuffing (also in heart UR bladder and brain), some iron storage in the liver, small numbers of lymphocytes and plasma cells around meninges, blood vessels, heart, uterus and urinary bladder.

White-fronted marmoset	1076	UN	On day 1, was thin and dehydrated, +++protein in urine, biochemistry shows renal insufficiency and infection, creatinine and phosphate not raised. On day 2, despite fluids and antibiotics, found dead in the morning.	Was mildly jaundiced, with some sub-cut oedema, and within the liver there were white foci of necrosis/inflammation (later found to be capillaria hepatica eggs, which are carried in the livers of certain animals, esp rodents). Found mild to moderate acute multifocal necrotising hepatitis with diffuse mild icterus, liver. Mild fibrosis of kidneys (felt firm), serous atrophy of fat. Some yellow oedema in the abdomen. Congested with blood in the spleen.	Iron storage disease in the liver (haemosiderin deposits are widely present in Kupffer cells and macrophage clusters, granular iron is present in moderate or plentiful amounts in widely distributed clusters of hepatocytes) and inflammatory cells in the liver like macrophages, neutrophils, plasma cells and lymphocytes, renal tubular and papillary necrosis in the kidney with some inflammatory cells, minimal granulomatous hepatitis
White-fronted marmoset	3737	UN	On day 1, good to fat body condition score, was lethargic and weak, and was dehydrated on	Acute necrotising nephritis in kidneys, multifocal necrotising hepatitis in the liver, severe acute subcutaneous	Acute hepatitis and nephritis, widespread intravascular coagulation and vasculitis, within many organs such as the liver and tunic I around the testis.

			examination under isoflurane. On day 3, the marmoset was found dead. Biochemistry showed severely-affected kidney and liver function, and some anaemia and thrombocytopenia	haemorrhages in the skin and superficial muscles (around lateral and dorsal areas of the flanks, the skin on the top of the head, and the medial skin of the right groin and thigh area.), splenomegaly and spleen is congested with blood, mild interstitial pneumonia, pleural effusion, multifocal atherosis in arteries. Also, white foci (1mm) throughout the liver, tinged serous oedema in the abdomen, mild excess blood-tinged fluid in the pleural cavity, and both kidneys have irregular white mottling with haemorrhages throughout.	Severe tubular necrosis and intravascular thrombosis in kidneys, congestion of spleen, sub-cut and intramuscular haemorrhage, mixed inflammatory cells in lungs.
black-and-white colobus	2098	H06 336 0625 01	-	Acute cell necrosis in various organs	-

Purple-faced leaf monkey	4714	H06 336 0622 01	-	Tubular necrosis of kidneys and acute encephalomalacia of the brainstem.	-

8.4 Pathology records as provided by Twycross zoo for LCMV-suspected cases

Species	Date	Comment
Common marmoset	20/01/2003	Died age 4yrs 7mths. Was found off legs and was having fits. Possibly LCMV infection.
Red-handed tamarin	13/04/2003	A very short illness was not well then found dead the next day. Had an average body condition. Likely to be LCMV
Red-handed tamarin	07/05/2003	Some necrotic hepatocytes, and inflammatory cells, kidneys are very autolysed but there are immune cells present. Possible LCMV infection.
Red-handed tamarin	08/05/2003	Had fitting and was found to have pneumonia on PM. The liver was congested and there was increased haemosiderin in cells but no inflammatory cells. In the kidney and adrenal, there was some lymphoplasmacytic infiltration. Very suggestive of LCMV.
Golden lion tamarin	02/11/2003	Died age 8yrs 7mths. He had bruising to the inguinal region and the scrotum had a hepatopathy with occasional necrotic hepatocyte with increased haemosiderin.

		Also had eosinophilic inclusion. Recorded as possible Herpesvirus. But highly likely to be LCMV.
Golden-headed tamarin	04/11/2003	Had a bad nosebleed and the next day was found dead. Recorded as liver failure. Possible LCMV infection
Silvery marmoset	11/11/2003	Died age 3yrs 9mths. Died 2 days after the first clinical signs. Before death, had CNS signs (bad convulsions) and haemorrhaging of skin around the face and groin and down the legs, with a normal body condition. There was mild congestion of the lungs, the liver was a copper colour, and a haemorrhage was found on the meninges. Strongly suggestive of LCMV
Cotton-top tamarin	22/12/2003	Age 4yrs 2mths. The right lung was congested and recorded as possible pneumonia. This could have been caused by LCMV
Red-mantled tamarin	28/01/2004	Died aged around 15 yrs. Had fluid-filled lungs, a compressed and enlarged heart indicating heart failure, and multifocal small white spots on the liver with a lot of liver necrosis and congestion. This indicates a heart problem complicated by a possible LCMV infection.
Silvery marmoset	05/02/2004	Died age 7yrs 8mths. Was weak for 2 days prior to death and increased kidney parameters were found on blood results (decreased protein and albumin, increased urea and creatinine, electrolyte abnormalities, and clotting deficiency with neutrophilia). Recorded cause was possible renal disease. There was mild

		congestion of both lungs, an enlarged liver and interdermal haemorrhage. Strongly suggestive of LCMV infection.
Red-handed tamarin	31/03/2004	Died age 7yrs 4mths He was in good body condition, Externally haemorrhage was detected around the pelvis/igunal area, and severe hepatopathy in the liver. Histology: Kidney: There is disseminated mild to moderate multifocal interstitial and perivascular infiltration by mixed, predominantly mononuclear inflammatory cells Liver: mainly monocytic inflammatory cells, Coarse brown granular cytoplasmic pigment granules are present in many cells, (iron). There are numerous widely dispersed single-cell hepatocyte necroses. Lung: Diffusely congested lung, in which the alveoli are filled with protein-rich faintly basophilic fluid, and in which there is diffuse hypercellularity. Hepatitis with acidophilic bodies and portal phlebitis, vasculitis in the heart, liver and kidney, hepatic haemosiderosis, Pulmonary congestion and oedema. Very similar to LCMV, the characteristic lesions include hepatitis with phlebitis and acidophilic bodies, in the absence of viral inclusions, together with vasculitis in a range of other organs. The presence of significant levels of iron in the liver is

		not uncommon in callitrichids, but there is some evidence to suggest that high levels of hepatic iron do in fact have a negative impact on their health.
Common marmoset	20/04/2004	Died age 3yrs 4mths. Although very autolysed on PM, had perivascular cuffing in the brain, had a mild number of inflammatory cells in the heart, and had congestion and oedema in the lungs. Overall encephalitis and myocarditis, possibly caused by LCMV.
Silvery marmoset	08/12/2004	Was thin, weak and collapsed 2 days prior to death. Had haemorrhage on thighs and abdomen and meningeal haemorrhage. Clinical signs and external appearance strongly relate to LCMV.
Cotton-top tamarin	19/06/2005	died 4 days old. In the lung, there were some macrophages and amniotic debris. In kidneys, there were increased neutrophils, haemorrhage and necrosis. Could this tubulointerstitial nephritis be caused by LCMV?
Cotton-top tamarin	14/07/2005	Died aged 29 days, on post mortem, meninges has inflammatory infiltrate of lymphocytes, plasma cells, macrophages and granulocytes. Some haemorrhage in the brain. In the lungs, there was a haemorrhage with increased fibrin and inflammatory cells. In the spleen, there was a haemorrhage and fibrin accumulation in the pulp with increased neutrophils. Overall there is moderate subacute encephalitis and meningitis, strongly indicates LCMV
Common marmoset	07/05/2006	Died age 2yrs 9mths. Had fit and then died. On post-mortem, had congested oedema in the lungs, the liver was congested and enlarged and there was

		inflammatory cuffing by lymphocytes and there were increased neutrophils. Highly suggestive of LCMV.
Pygmy marmoset	06/02/2007	Age 1 ¾ mths died, unknown cause, lymphocytes in portal areas of the spleen, some pigment in hepatocytes and haemosiderin-laden macrophages in portal areas.
Common marmoset	08/05/2007	Died age 5 yrs 2mths. Had an enlarged liver, kidneys were very pale with a lack of corticomedullary demarcation with glomerulonephritis. Severe necrotising pneumonia with pleuritis and pericarditis. Recorded as a renal disease but LCMV infection could not be ruled out.

8.5 LCMV strains used to design the outer set of the nested PCR primers for GPC amplification:

Strain	NCBI accession No.	Source
811316	FJ607022, FJ607031	(Albarino *et al.*, 2010a)
810850	FJ607021, FJ607030	(Albarino *et al.*, 2010a)
Makokou	KM523323, KM 882857	(N'Dilimabaka *et al.*, 2015)
Douglas-4707	FJ607024; FJ607035	(Albarino *et al.*, 2010a)
810885	FJ607023, FJ607032	(Albarino *et al.*, 2010a)
810896	FJ607026, FJ607037	(Albarino *et al.*, 2010a)
810366	FJ607019, FJ607028	(Albarino *et al.*, 2010a)
810935	FJ607020, FJ607029	(Albarino *et al.*, 2010a)
EEB-7	JN872494, JN8 72495	(Perez-Ruiz *et al.*, 2012)
810362	FJ607027, FJ607038	(Albarino *et al.*, 2010a)
Armstrong	AY847351, M20869	(Armstrong & Lillie, 1934; Grande-Perez *et al.*, 2005; Salvato *et al.*, 1988)
WE	M22138; AF004519	(Romanowski *et al.*, 1985)
WE-UBC- 57135	FJ607025, FJ607036	(Albarino *et al.*, 2010a)
WE-UBC-A337	FJ607034	(Albarino *et al.*, 2010a)
CHV1, CHV2, CHV3	U10157, U10158, U10159	(Stephensen *et al.*, 1995)
WHI	FJ607033	(Albarino *et al.*, 2010a)
Marseille 12	DQ286932, DQ286931	(Emonet *et al.*, 2007)
CH-5692, CH- 5871	AY363903, AF325214, AF325215	(Asper *et al.*, 2001)
HP65-2009	JN546573, JN546574, JN546575, JN546576	(Yama *et al.*, 2012)
Yale	DQ118959	(Albarino *et al.*, 2010a)
MX	EU195888, EU195889	(Tomaskova *et al.*, 2008)
LE	EF164923	(Albarino *et al.*, 2010a)
Bulgaria	GQ862981, GQ862982	(Albarino *et al.*, 2010a)
OQ28	AB627952, AB6 27955	(Takagi *et al.*, 2012)
BRC	AB627953, AB627956	(Takagi *et al.*, 2012)
M1, M2	AB261990, AB261991	(Ike *et al.*, 2007)
CABN, GR01, SN05	FJ895882, FJ895883, FJ895884	(Ledesma *et al.*, 2009)

8.6 iRis digital cell images of EGFP expression in HAP1 transduced and KO cells

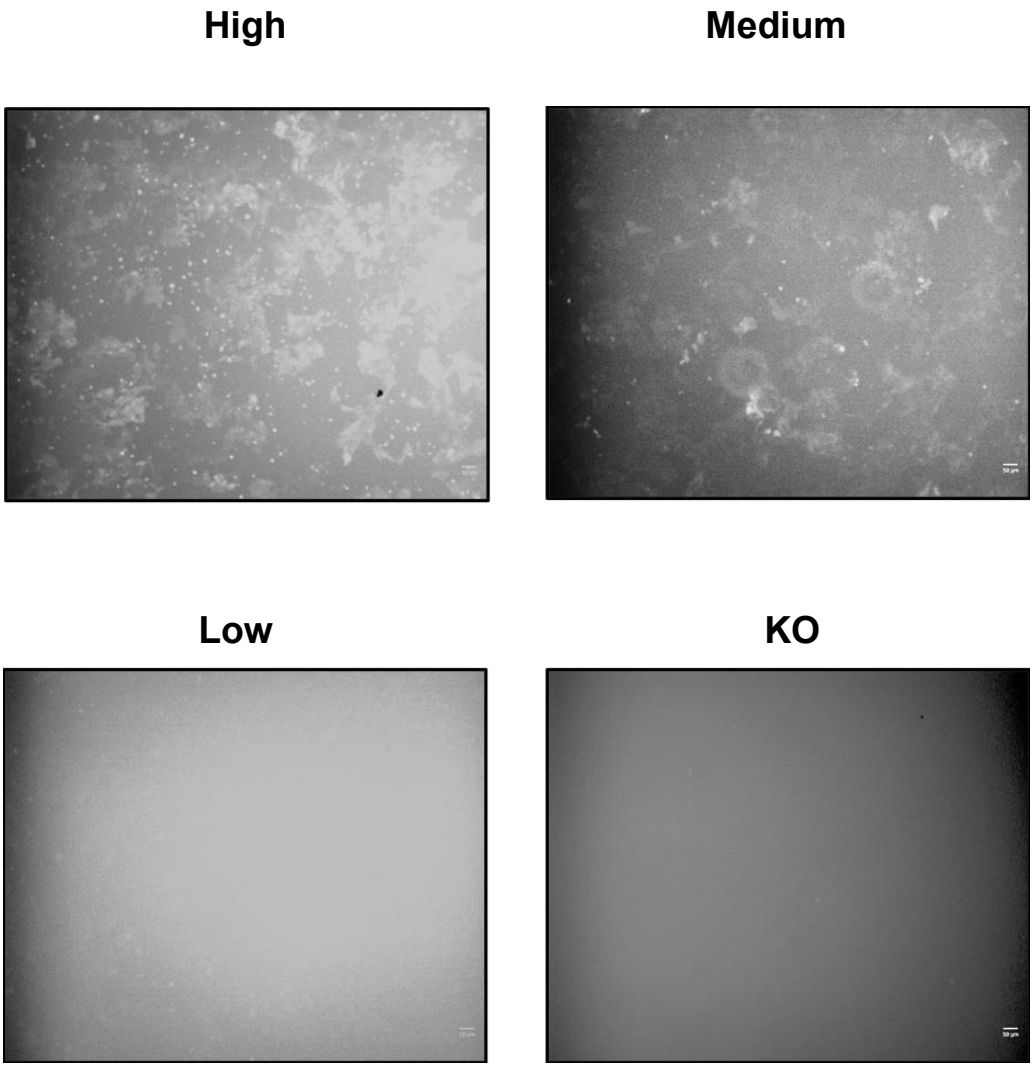


Figure 8-1: EGFP expression in HAP1 KO/KI cells.

High, medium, low, and KO cells were visualized 36-48 hours post sorting in iRis digital cell imaging system for EGFP expression under similar parameters (light 35, gain 18, exposure (ms) 400). Bars at the lower right corners represent a 50 µm scale.

8.7 α-DG-Fc constructs

α-DG (murine)-Fc

ATGGAAACCGACACACTGCTGCTGTGGGTGCTCCTGTTGTGGGTTCCA
GGTTCCACTGGTCACTGGCCCAGTGAACCCTCAGAGGCTGTGAGGGAC
TGGAAGAACCAGCTTGAGGCGTCCATGCACTCAGTTCTCTCCGACTTCC
AGGAGGCTGTTCCCACCGTGGTTGGCATTCCAGACGGTACGGCTGTTG
TCGGGCGCTCATTTCGAGTGAGCATTCCAACGGATTTAATTGCCTCCAG
TGGGGAGATCATCAAGGTGTCTGCAGCAGGGAAGGAGGCCTTACCGTC
TTGGCTACACTGGGACCCACACAGTCATATTTTGGAAGGCCTTCCTCTT
GACACTGATAAAGGTGTGCATTACATCTCAGTGAGTGCTGCACGCCTG
GGAGCCAATGGAAGCCACGTCCCCCAGACTTCCAGTGTGTTCTCTATC
GAGGTCTACCCTGAAGACCACAATGAGCCACAGTCTGTACGGGCAGCC
TCATCAGACCCTGGTGAGGTAGTGCCATCTGCCTGTGCTGCTGATGAG
CCAGTGACTGTCCTTACAGTGATTCTGGATGCTGACCTCACCAAGATGA
CCCCAAAGCAAAGGATCGATCTGTTGAACAGAATGCAGAGCTTCTCAGA
AGTAGAACTTCACAACATGAAGTTGGTGCCTGTAGTGAATAATAGACTA
TTTGACATGTCGGCCTTCATGGCTGGCCCAGGAAATGCAAAGAAAGTG
GTAGAGAATGGGGCTCTCCTGTCCTGGAAACTAGGCTGCTCCTTGAAC
CAGAATAGCGTCCCTGACATCCGTGGTGTAGAAACCCCTGCTAGGGAG
GGTGCTATGTCTGCCCAACTTGGTTATCCTGTGGTGGGTTGGCACATTG
CCAATAAGAAGCCCACTCTCCCCAAACGACTCCGGAGGCAGATCCACG
CCACACCTACACCTGTTACTGCCATTGGACCCCCAACCACGGCCATTCA
GGAGCCACCATCGCGGATAGTGCCTACGCCTACATCTCCAGCCATTGC
ACCTCCAACAGAGACCATGGCTCCTCCTGTCAGGGATCCTGTTCCAGG
GAAGCCCACGGTCACCATTCGGANNCGAGGTGCCATTATTCAGACCCC
AACTCTGGGCCCTATCCAGCCTACTCGGGTGTCAGAAGCTGGTACCAC
GGTTCCTGGCCAGATTCGCCCAACACTGACAATTCCTGGCTATGTAGAG
CCCACAGCCGTTATTACTCCTCCAACAACTACCACAAAGAAGCCACGAG
TGTCCACGCCAAAGCCAGCAACGCCTTCAACTGATTCGTCAACTACCAC
AACTCGGAGGCCAACCAAAAAACCACGGACACCCCGACCAGTGCCCCG
AGTCACCACCAAAGCACCCATCACCAGGTTGGAGACAGCTTCCCCACC
CACTCGAATCCGTACTACCACCAGTGACAAAACTCACACATGCCCTCCA
TGTCCTGCTCCAGAGCTGCTCGGAGGCCCTTCCGTGTTTCTGTTCCCTC
CAAAGCCTAAGGACACCCTGATGATCAGCAGAACCCCTGAAGTGACCT
GCGTGGTGGTGGATGTGTCCCACGAGGATCCCGAAGTGAAGTTCAATT
GGTACGTGGACGGCGTGGAAGTGCACAACGCCAAGACCAAGCCTAGA
GAGGAACAGTACAACAGCACCTACAGAGTGGTGTCCGTGCTGACCGTG
CTGCACCAGGATTGGCTGAACGGCAAAGAGTACAAGTGCAAGGTGTCC
AACAAGGCCCTGCCTGCTCCTATCGAGAAAACCATCAGCAAGGCCAAG
GGCCAGCCTAGGGAACCCCAGGTTTACACACTGCCTCCAAGCCGGGAA
GAGATGACCAAGAACCAGGTGTCCCTGACCTGCCTGGTCAAGGGCTTC
TACCCTTCCGATATCGCCGTGGAATGGGAGAGCAATGGCCAGCCTGAG
AACAACTACAAGACCACACCTCCTGTGCTGGACAGCGACGGCTCATTCT
TCCTGTACAGCAAGCTGACAGTGGACAAGAGCAGATGGCAGCAGGGCA

ACGTGTTCAGCTGCAGCGTGATGCACGAGGCCCTGCACAACCACTACA
CCCAGAAGTCCCTGAGCCTGTCTCCTGGCAAGTGA

α-DG (NHP)-Fc

ATGGAAACCGACACACTGCTGCTGTGGGTGCTCCTGTTGTGGGTTCCA
GGTTCCACTGGTCTAGCCTGGCCCAGTGAACCCTCAGAGGCTGTCAGG
GACTGGGATAACCAGCTTGAGGCATCCATGCACTCAGTGCTCTCAGAC
CTCCACGAGGCTGTTCCCACAGTGGTTGGCATTCCTGATGGCACGGCT
GTCGTCGGGCGCTCATTTCGAGTGACCATTCCAACAGATTTGATTGCCT
CCAGTGGAGACATCATCAAGGTATCAGCAGCAGGGAAGGAGGCTTTGC
CATCTTGGCTGCACTGGGACCCACAGAGCCACACCCTGGAGGGCCTCC
CCCTTGACACTGATAAGGGTGTGCATTACATTTCGGTGAGCGCTGCAC
GGCTGGGGGCCAACGGGAGTCACATCCCCCAGACCTCCAGTGTGTTCT
CCATTGAGGTCTACCCTGAAGACCACAGTGAGCTGCAGTCAGTGAGGA
CAGCCTTCCCAGACCCTGGTGAGGTGGTATCATCTGCCTGTGCTGTGG
ATGAACCTGTGACTGTTTTGACGGTGATTTTGGATGCTGACCTCACCAA
GATGACTCCAAAGCAAAGGATTGACCTCCTTCACAGGATGCGGAGCTT
CTCAGAAGTAGAGCTTCACAACATGAAATTAGTGCCGGTGGTGAATAAC
AGACTATTTGACATGTCGGCCTTCATGGCTGGCCCGGGAAATGCAAAAA
AGGTGGTGGAGAATGGGGCCCTTCTCTCCTGGAAGCTGGGCTGCTCCC
TGAACCAGAACAGTGTGCCTGACATTCGTGGTGTGGAGGCTCCTGCCA
GGGAGGGTGCTATGTCTGCTCAGCTTGGCTACCCTGTGGTGGGTTGGC
ACATCGCCAATAAGAAGCCCCCTCTTCCCAAACGCATCCGGAGGCAGA
TCCATGCCACACCCACACCTGTCACTGCCATTGGGCCCCCAACCACGG
CTATCCAGGAGCCCCCATCCAGGATTGTGCCAACACCCACATCTCCAG
CCATTGCTCCTCCAACAGAGACCATGGCTCCTCCAGTCAGGGATCCTG
TTCCTGGGAAACCCACGGTCACCATCCGGACTCGAGGCGCCATTATTC
AGACCCCAACCCTAGGCCCCATCCAGCCTACTCGGGTGTCAGAAGCAG
GCACCACAGTTCCTGGCCAGATTCGCCCAACGATGACCATTCCTGGCT
ATGTGGAGCCTACTGCAGTTGCTACCCCTCCCACAACCACCACCAAGA
AGCCACGAGTATCCACACCAAAACCAGCAACGCCTTCAACTGACTCCTC
CACCACCACAACTCGCAGGCCAACCAAGAAACCACGGACACCCCGGCC
AGTGCCCCGGGTCACCACCAAAGTTCCTATCACCAGATTGGAAACTGC
CTCACCGCCTACTCGTATTCGCACCACCACCAGTGGAGTGCTAGACAA
AACTCACACATGCCCTCCATGTCCTGCTCCAGAGCTGCTCGGAGGCCC
TTCCGTGTTTCTGTTCCCTCCAAAGCCTAAGGACACCCTGATGATCAGC
AGAACCCCTGAAGTGACCTGCGTGGTGGTGGATGTGTCCCACGAGGAT
CCCGAAGTGAAGTTCAATTGGTACGTGGACGGCGTGGAAGTGCACAAC
GCCAAGACCAAGCCTAGAGAGGAACAGTACAACAGCACCTACAGAGTG
GTGTCCGTGCTGACCGTGCTGCACCAGGATTGGCTGAACGGCAAAGAG
TACAAGTGCAAGGTGTCCAACAAGGCCCTGCCTGCTCCTATCGAGAAA
ACCATCAGCAAGGCCAAGGGCCAGCCTAGGGAACCCCAGGTTTACACA
CTGCCTCCAAGCCGGGAAGAGATGACCAAGAACCAGGTGTCCCTGACC
TGCCTGGTCAAGGGCTTCTACCCTTCCGATATCGCCGTGGAATGGGAG
AGCAATGGCCAGCCTGAGAACAACTACAAGACCACACCTCCTGTGCTG
GACAGCGACGGCTCATTCTTCCTGTACAGCAAGCTGACAGTGGACAAG
AGCAGATGGCAGCAGGGCAACGTGTTCAGCTGCAGCGTGATGCACGA

GGCCCTGCACAACCACTACACCCAGAAGTCCCTGAGCCTGTCTCCTGG
CAAGTGA

Yellow= Kappa signal sequence, Clear= α-DG sequence, gray= human Fc sequence.

Chapter. 9: References

Abraham, J., Corbett, K. D., Farzan, M., Choe, H. & Harrison, S. C. 2010. Structural basis for receptor recognition by New World hemorrhagic fever arenaviruses. *Nature structural & molecular biology,* 17**,** 438-444.

Abudurexiti, A., Adkins, S., Alioto, D., Alkhovsky, S. V., Avsic-Zupanc, T., Ballinger, M. J., Bente, D. A., Beer, M., Bergeron, E., Blair, C. D., Briese, T., Buchmeier, M. J., Burt, F. J., Calisher, C. H., Chang, C., Charrel, R. N., Choi, I. R., Clegg, J. C. S., De La Torre, J. C., De Lamballerie, X., Deng, F., Di Serio, F., Digiaro, M., Drebot, M. A., Duan, X., Ebihara, H., Elbeaino, T., Ergunay, K., Fulhorst, C. F., Garrison, A. R., Gao, G. F., Gonzalez, J. J., Groschup, M. H., Gunther, S., Haenni, A. L., Hall, R. A., Hepojoki, J., Hewson, R., Hu, Z., Hughes, H. R., Jonson, M. G., Junglen, S., Klempa, B., Klingstrom, J., Kou, C., Laenen, L., Lambert, A. J., Langevin, S. A., Liu, D., Lukashevich, I. S., Luo, T., Lu, C., Maes, P., De Souza, W. M., Marklewitz, M., Martelli, G. P., Matsuno, K., Mielke-Ehret, N., Minutolo, M., Mirazimi, A., Moming, A., Muhlbach, H. P., Naidu, R., Navarro, B., Nunes, M. R. T., Palacios, G., Papa, A., Pauvolid-Correa, A., Paweska, J. T., Qiao, J., Radoshitzky, S. R., Resende, R. O., Romanowski, V., Sall, A. A., Salvato, M. S., Sasaya, T., Shen, S., Shi, X., Shirako, Y., Simmonds, P., Sironi, M., Song, J. W., Spengler, J. R., Stenglein, M. D., Su, Z., Sun, S., Tang, S., Turina, M., Wang, B., Wang, C., Wang, H., Wang, J., Wei, T., Whitfield, A. E., Zerbini, F. M., Zhang, J., Zhang, L., Zhang, Y., Zhang, Y. Z., Zhang, Y., et al. 2019. Taxonomy of the order Bunyavirales: update 2019. *Arch Virol,* 164**,** 1949-1965.

Agnihothram, S. S., York, J., Trahey, M. & Nunberg, J. H. 2007. Bitopic Membrane Topology of the Stable Signal Peptide in the Tripartite Junín Virus GP-C Envelope Glycoprotein Complex. *Journal of Virology,* 81**,** 4331-4337.

Aguilar, P. V., Camargo, W., Vargas, J., Guevara, C., Roca, Y., Felices, V., Laguna-Torres, V. A., Tesh, R., Ksiazek, T. G. & Kochel, T. J. 2009. Reemergence of Bolivian hemorrhagic fever, 2007-2008. *Emerg Infect Dis,* 15**,** 1526-1528.

Albariño, C. G., Palacios, G., Khristova, M. L., Erickson, B. R., Carroll, S. A., Comer, J. A., Hui, J., Briese, T., St George, K., Ksiazek, T. G., Lipkin, W. I. & Nichol, S. T. 2010. High diversity and ancient common ancestry of lymphocytic choriomeningitis virus. *Emerg Infect Dis,* 16**,** 1093-1100.

Alberini, I., Del Tordello, E., Fasolo, A., Temperton, N. J., Galli, G., Gentile, C., Montomoli, E., Hilbert, A. K., Banzhoff, A., Del Giudice, G., Donnelly, J. J., Rappuoli, R. & Capecchi, B. 2009. Pseudoparticle neutralization is a reliable assay to measure immunity and cross-reactivity to H5N1 influenza viruses. *Vaccine,* 27**,** 5998-6003.

Alli, A., Ortiz, J. F., Fabara, S. P., Patel, A. & Halan, T. 2021. Management of Lassa Fever: A Current Update. *Cureus,* 13**,** e14797-e14797.

Amanat, F., Duehr, J., Oestereich, L., Hastie, K. M., Ollmann Saphire, E. & Krammer, F. 2018. Antibodies to the Glycoprotein GP2 Subunit Cross-React between Old and New World Arenaviruses. *mSphere,* 3.

Ammerman, N. C., Beier-Sexton, M. & Azad, A. F. 2008. Growth and maintenance of Vero cell lines. *Curr Protoc Microbiol,* Appendix 4**,** Appendix 4E.

Andersen, K. G., Shapiro, B. J., Matranga, C. B., Sealfon, R., Lin, A. E., Moses, L. M., Folarin, O. A., Goba, A., Odia, I., Ehiane, P. E., Momoh, M., England, E. M., Winnicki, S., Branco, L. M., Gire, S. K., Phelan, E., Tariyal, R., Tewhey, R., Omoniwa, O., Fullah, M., Fonnie, R., Fonnie, M., Kanneh, L., Jalloh, S., Gbakie, M., Saffa, S., Karbo, K., Gladden, A. D., Qu, J., Stremlau, M., Nekoui, M., Finucane, H. K., Tabrizi, S., Vitti, J. J., Birren, B., Fitzgerald, M., Mccowan, C., Ireland, A., Berlin, A. M., Bochicchio, J., Tazon-Vega, B., Lennon, N. J., Ryan, E. M., Bjornson, Z., Milner, D. A., Lukens, A. K., Broodie, N., Rowland, M., Heinrich, M., Akdag, M., Schieffelin, J. S., Levy, D., Akpan, H., Bausch, D. G., Rubins, K., Mccormick, J. B., Lander, E. S., Günther, S., Hensley, L., Okogbenin, S., Schaffner, S. F., Okokhere, P. O., Khan, S. H., Grant, D. S., Akpede, G. O., Asogun, D. A., Gnirke, A., Levin, J. Z., Happi, C. T., Garry, R. F., Sabeti, P. C. & Consortium, V. H. F. 2015. Clinical Sequencing Uncovers Origins and Evolution of Lassa Virus. *Cell,* 162**,** 738-750.

Antia, R., Regoes, R. R., Koella, J. C. & Bergstrom, C. T. 2003. The role of evolution in the emergence of infectious diseases. *Nature,* 426**,** 658-661.

Archer, A. M. & Rico-Hesse, R. 2002. High genetic divergence and recombination in Arenaviruses from the Americas. *Virology,* 304**,** 274-281.

Armstrong, C. & Lillie, R. D. 1934. Experimental Lymphocytic Choriomeningitis of Monkeys and Mice Produced by a Virus Encountered in Studies of the 1933 St. Louis Encephalitis Epidemic. *Public Health Reports (1896-1970),* 49**,** 1019-1027.

Armstrong, C., Wallace, J. J. & Louis, R. 1940. Lymphocytic Choriomeningitis: Gray Mice, Mus musculus, a Reservoir for the Infection. *Public Health Reports (1896-1970),* 55**,** 1222-1229.

Asogun, D. A., Adomeh, D. I., Ehimuan, J., Odia, I., Hass, M., Gabriel, M., Ölschläger, S., Becker-Ziaja, B., Folarin, O., Phelan, E., Ehiane, P. E., Ifeh, V. E., Uyigue, E. A., Oladapo, Y. T., Muoebonam, E. B., Osunde, O., Dongo, A., Okokhere, P. O., Okogbenin, S. A., Momoh, M., Alikah, S. O., Akhuemokhan, O. C., Imomeh, P., Odike, M. a. C., Gire, S., Andersen, K., Sabeti, P. C., Happi, C. T., Akpede, G. O. & Günther, S. 2012. Molecular Diagnostics for Lassa Fever at Irrua Specialist Teaching Hospital, Nigeria: Lessons Learnt from Two Years of Laboratory Operation. *PLOS Neglected Tropical Diseases,* 6**,** e1839.

Asper, M., Hofmann, P., Osmann, C., Funk, J., Metzger, C., Bruns, M., Kaup, F.-J., Schmitz, H. & Günther, S. 2001. First Outbreak of Callitrichid Hepatitis in Germany: Genetic Characterization of the Causative Lymphocytic Choriomeningitis Virus Strains. *Virology,* 284**,** 203-213.

Auperin, D. D., Romanowski, V., Galinski, M. & Bishop, D. H. 1984. Sequencing studies of pichinde arenavirus S RNA indicate a novel coding strategy, an ambisense viral S RNA. *J Virol,* 52**,** 897-904.

Bakkers, M. J. G., Moon-Walker, A., Herlo, R., Brusic, V., Stubbs, S. H., Hastie, K. M., Saphire, E. O., Kirchhausen, T. L. & Whelan, S. P. J. 2022. CD164 is a host factor for lymphocytic choriomeningitis virus entry. *Proceedings of the National Academy of Sciences,* 119**,** e2119676119.

Baranowski, E., Ruiz-Jarabo, C. M. & Domingo, E. 2001. Evolution of cell recognition by viruses. *Science,* 292**,** 1102-1105.

Barresi, R. & Campbell, K. P. 2006. Dystroglycan: from biosynthesis to pathogenesis of human disease. *Journal of Cell Science,* 119**,** 199-207.

Barresi, R., Michele, D. E., Kanagawa, M., Harper, H. A., Dovico, S. A., Satz, J. S., Moore, S. A., Zhang, W., Schachter, H., Dumanski, J. P., Cohn, R. D., Nishino, I. & Campbell, K. P. 2004. LARGE can functionally bypass α-dystroglycan glycosylation defects in distinct congenital muscular dystrophies. *Nature Medicine,* 10**,** 696-703.

Barton, L. L. & Hyndman, N. J. 2000. Lymphocytic choriomeningitis virus: reemerging central nervous system pathogen. *Pediatrics,* 105**,** E35.

Barton, L. L., Mets, M. B. & Beauchamp, C. L. 2002. Lymphocytic choriomeningitis virus: Emerging fetal teratogen. *American Journal of Obstetrics and Gynecology,* 187**,** 1715-1716.

Bartosch, B., Dubuisson, J. & Cosset, F.-L. 2003. Infectious hepatitis C virus pseudo-particles containing functional E1-E2 envelope protein complexes. *The Journal of experimental medicine,* 197**,** 633-642.

Basu, A., Li, B., Mills, D. M., Panchal, R. G., Cardinale, S. C., Butler, M. M., Peet, N. P., Majgier-Baranowska, H., Williams, J. D., Patel, I., Moir, D. T., Bavari, S., Ray, R., Farzan, M. R., Rong, L. & Bowlin, T. L. 2011. Identification of a Small-Molecule Entry Inhibitor for Filoviruses. *Journal of Virology,* 85**,** 3106.

Baum, S. G., Lewis, A. M., Rowe, W. P. & Huebner, R. J. 1966. Epidemic Nonmeningitic Lymphocytic-Choriomeningitis-Virus Infection. *New England Journal of Medicine,* 274**,** 934-936.

Benny Borremans, H. L., Sophie Gryseels, Stephan Günther, Rhodes Makundi, Joëlle Goüy De Bellocq 2011. Presence of Mopeia Virus, an African Arenavirus, Related to Biotope and Individual Rodent Host Characteristics: Implications for Virus Transmission. *Vector-Borne and Zoonotic Diseases,* 11**,** 1125-1131.

Bergthaler, A., Flatz, L., Hegazy, A. N., Johnson, S., Horvath, E., Löhning, M. & Pinschewer, D. D. 2010. Viral replicative capacity is the primary determinant of lymphocytic choriomeningitis virus persistence and immunosuppression. *Proceedings of the National Academy of Sciences of the United States of America,* 107**,** 21641-21646.

Beyer, W. R., Miletic, H., Ostertag, W. & Von Laer, D. 2001. Recombinant expression of lymphocytic choriomeningitis virus strain WE glycoproteins: a single amino acid makes the difference. *J Virol,* 75**,** 1061-1064.

Beyer, W. R., Pöpplau, D., Garten, W., Von Laer, D. & Lenz, O. 2003. Endoproteolytic Processing of the Lymphocytic Choriomeningitis Virus Glycoprotein by the Subtilase SKI-1/S1P. *Journal of Virology,* 77**,** 2866-2872.

Bhakta, S. J., Shang, L., Prince, J. L., Claiborne, D. T. & Hunter, E. 2011. Mutagenesis of tyrosine and di-leucine motifs in the HIV-1 envelope cytoplasmic domain results in a loss of Env-mediated fusion and infectivity. *Retrovirology,* 8**,** 37.

Bieniasz, P. D. 2006. Late budding domains and host proteins in enveloped virus release. *Virology,* 344**,** 55-63.

Biggar, R. J., Woodall, J. P., Walter, P. D. & Haughie, G. E. 1975. Lymphocytic Choriomeningitis Outbreak Associated With Pet Hamsters: Fifty-Seven Cases From New York State. *JAMA,* 232**,** 494-500.

Bird, B. H., Githinji, J. W. K., Macharia, J. M., Kasiiti, J. L., Muriithi, R. M., Gacheru, S. G., Musaa, J. O., Towner, J. S., Reeder, S. A., Oliver, J. B., Stevens, T. L., Erickson, B. R., Morgan, L. T., Khristova, M. L., Hartman, A. L., Comer, J. A., Rollin, P. E., Ksiazek, T. G. & Nichol, S. T. 2008. Multiple virus lineages sharing recent common ancestry were associated with a Large Rift Valley fever outbreak among livestock in Kenya during 2006-2007. *Journal of virology,* 82**,** 11152-11166.

Bladt, F., Faden, B., Friese-Hamim, M., Knuehl, C., Wilm, C., Fittschen, C., Grädler, U., Meyring, M., Dorsch, D., Jaehrling, F., Pehl, U., Stieber, F., Schadt, O. & Blaukat, A. 2013. EMD 1214063 and EMD 1204831 Constitute a New Class of Potent and Highly Selective c-Met Inhibitors. *Clinical Cancer Research,* 19**,** 2941-2951.

Blasdell, K. R., Becker, S. D., Hurst, J., Begon, M. & Bennett, M. 2008. Host range and genetic diversity of arenaviruses in rodents, United Kingdom. *Emerging infectious diseases,* 14**,** 1455-1458.

Blesch, A. 2004. Lentiviral and MLV based retroviral vectors for ex vivo and in vivo gene transfer. *Methods,* 33**,** 164-172.

Bonhomme, C. J., Capul, A. A., Lauron, E. J., Bederka, L. H., Knopp, K. A. & Buchmeier, M. J. 2011. Glycosylation modulates arenavirus glycoprotein expression and function. *Virology,* 409**,** 223-233.

Bonhomme, C. J., Knopp, K. A., Bederka, L. H., Angelini, M. M. & Buchmeier, M. J. 2013. LCMV glycosylation modulates viral fitness and cell tropism. *PloS one,* 8**,** e53273-e53273.

Borrow, P., Tishon, A. & Oldstone, M. B. 1991. Infection of lymphocytes by a virus that aborts cytotoxic T lymphocyte activity and establishes persistent infection. *J Exp Med,* 174**,** 203-212.

Bowden, T. A., Crispin, M., Graham, S. C., Harvey, D. J., Grimes, J. M., Jones, E. Y. & Stuart, D. I. 2009. Unusual Molecular Architecture of the Machupo Virus Attachment Glycoprotein. *Journal of Virology,* 83**,** 8259-8265.

Bowen, M. D., Peters, C. J. & Nichol, S. T. 1996a. The phylogeny of New World (Tacaribe complex) arenaviruses. *Virology,* 219**,** 285-90.

Bowen, M. D., Peters, C. J. & Nichol, S. T. 1996b. The phylogeny of New World (Tacaribe complex) arenaviruses. *Virology,* 219**,** 285-290.

Bowen, M. D., Peters, C. J. & Nichol, S. T. 1997. Phylogenetic analysis of the Arenaviridae: patterns of virus evolution and evidence for cospeciation between arenaviruses and their rodent hosts. *Mol Phylogenet Evol,* 8**,** 301-316.

Brancaccio, A. & Adams, J. C. 2017. An evaluation of the evolution of the gene structure of dystroglycan. *BMC Research Notes,* 10**,** 19.

Brouillette, R. B., Phillips, E. K., Patel, R., Mahauad-Fernandez, W., Moller-Tank, S., Rogers, K. J., Dillard, J. A., Cooney, A. L., Martinez-Sobrido, L., Okeoma, C., Maury, W. & Sandri-Goldin, R. M. 2018. TIM-1 Mediates Dystroglycan-Independent Entry of Lassa Virus. *Journal of Virology,* 92**,** e00093-18.

Burri, D. J., Pasqual, G., Rochat, C., Seidah, N. G., Pasquato, A. & Kunz, S. 2012. Molecular characterization of the processing of arenavirus envelope glycoprotein precursors by subtilisin kexin isozyme-1/site-1 protease. *J Virol,* 86**,** 4935-4946.

C.Górecki, D., Derry, J. M. J. & Barnard, E. A. 1994. Dystroglycan: brain localisation and chromosome mapping in the mouse. *Human Molecular Genetics,* 3**,** 1589-1597.

Cao, W., Henry, M. D., Borrow, P., Yamada, H., Elder, J. H., Ravkov, E. V., Nichol, S. T., Compans, R. W., Campbell, K. P. & Oldstone, M. B. 1998a. Identification of alpha-dystroglycan as a receptor for lymphocytic choriomeningitis virus and Lassa fever virus. *Science,* 282**,** 2079-81.

Cao, W., Henry, M. D., Borrow, P., Yamada, H., Elder, J. H., Ravkov, E. V., Nichol, S. T., Compans, R. W., Campbell, K. P. & Oldstone, M. B. 1998b. Identification of alpha-dystroglycan as a receptor for lymphocytic choriomeningitis virus and Lassa fever virus. *Science,* 282**,** 2079-2081.

Cao, Y., Wang, J., Jian, F., Xiao, T., Song, W., Yisimayi, A., Huang, W., Li, Q., Wang, P., An, R., Wang, J., Wang, Y., Niu, X., Yang, S., Liang, H., Sun, H., Li, T., Yu, Y., Cui, Q., Liu, S., Yang, X., Du, S., Zhang, Z., Hao, X., Shao, F., Jin, R., Wang, X., Xiao, J., Wang, Y. & Xie, X. S. 2022. Omicron escapes the majority of existing SARS-CoV-2 neutralizing antibodies. *Nature,* 602**,** 657-663.

Capul, A. A., Perez, M., Burke, E., Kunz, S., Buchmeier, M. J. & De La Torre, J. C. 2007. Arenavirus Z-glycoprotein association requires Z myristoylation but not functional RING or late domains. *Journal of virology,* 81**,** 9451-9460.

Carnell, G. W., Ferrara, F., Grehan, K., Thompson, C. P. & Temperton, N. J. 2015. Pseudotype-based neutralization assays for influenza: a systematic analysis. *Front Immunol,* 6**,** 161.

Cdc. 2022. *Lassa Fever* [Online]. Centers for Disease Control and Prevention, National Center for Emerging and Zoonotic Infectious Diseases (NCEZID), Division of High-Consequence Pathogens and Pathology (DHCPP), Viral Special Pathogens Branch (VSPB). Available: https://www.cdc.gov/vhf/lassa/index.html [Accessed].

Chapman, B. S., Thayer, R. M., Vincent, K. A. & Haigwood, N. L. 1991. Effect of intron A from human cytomegalovirus (Towne) immediate-early gene on heterologous expression in mammalian cells. *Nucleic acids research,* 19**,** 3979-3986.

Charrel, R. N., De Lamballerie, X. & Emonet, S. 2008. Phylogeny of the genus Arenavirus. *Curr Opin Microbiol,* 11**,** 362-368.

Charrel, R. N., De Lamballerie, X. & Fulhorst, C. F. 2001. The Whitewater Arroyo virus: natural evidence for genetic recombination among Tacaribe serocomplex viruses (family Arenaviridae). *Virology,* 283**,** 161-166.

Chen, J. & Wei, G.-W. 2022. Omicron BA.2 (B.1.1.529.2): high potential to becoming the next dominating variant. *ArXiv***,** arXiv:2202.05031v1.

Cifuentes-Munoz, N., Sun, W., Ray, G., Schmitt, P. T., Webb, S., Gibson, K., Dutch, R. E. & Schmitt, A. P. 2017. Mutations in the Transmembrane Domain and Cytoplasmic Tail of Hendra Virus Fusion Protein Disrupt Virus-Like-Particle Assembly. *J Virol,* 91**,** e00152-17.

Cihlar, T. & Ray, A. S. 2010. Nucleoside and nucleotide HIV reverse transcriptase inhibitors: 25 years after zidovudine. *Antiviral Research,* 85**,** 39-58.

Cohen-Dvashi, H., Cohen, N., Israeli, H. & Diskin, R. 2015. Molecular Mechanism for LAMP1 Recognition by Lassa Virus. *J Virol,* 89**,** 7584-7592.

Compans, R. W. 1993. Arenavirus Ultrastructure and Morphogenesis. *In:* SALVATO, M. S. (ed.) *The Arenaviridae.* Boston, MA: Springer US.

Cornberg, M., Kenney, L. L., Chen, A. T., Waggoner, S. N., Kim, S. K., Dienes, H. P., Welsh, R. M. & Selin, L. K. 2013. Clonal exhaustion as a mechanism to protect against severe immunopathology and death from an overwhelming CD8 T cell response. *Front Immunol,* 4**,** 475.

Cornu, T. I. & De La Torre, J. C. 2001. RING finger Z protein of lymphocytic choriomeningitis virus (LCMV) inhibits transcription and RNA replication of an LCMV S-segment minigenome. *Journal of virology,* 75**,** 9415-9426.

Cosset, F.-L., Marianneau, P., Verney, G., Gallais, F., Tordo, N., Pécheur, E.-I., Ter Meulen, J., Deubel, V. & Bartosch, B. 2009. Characterization of Lassa Virus Cell Entry and Neutralization with Lassa Virus Pseudoparticles. *Journal of Virology,* 83**,** 3228.

Cox, R. J., Mykkeltvedt, E., Robertson, J. & Haaheim, L. R. 2002. Non-Lethal Viral Challenge of Influenza Haemagglutinin and Nucleoprotein DNA Vaccinated Mice Results in Reduced Viral Replication. *Scandinavian Journal of Immunology,* 55**,** 14-23.

Criscuolo, E., Giuliani, B., Ferrari, D., Ferrarese, R., Diotti, R. A., Clementi, M., Mancini, N. & Clementi, N. 2022. Proper Selection of In Vitro Cell Model Affects the Characterization of the Neutralizing Antibody Response against SARS-CoV-2. *Viruses,* 14**,** 1232.

Cross, R. W., Woolsey, C., Prasad, A. N., Borisevich, V., Agans, K. N., Deer, D. J., Geisbert, J. B., Dobias, N. S., Fenton, K. A. & Geisbert, T. W. 2022. A recombinant VSV-vectored vaccine rapidly protects nonhuman primates against heterologous lethal Lassa fever. *Cell Reports,* 40**,** 111094.

Cui, X., Meza, B. P., Adler, S. P. & Mcvoy, M. A. 2008. Cytomegalovirus vaccines fail to induce epithelial entry neutralizing antibodies comparable to natural infection. *Vaccine,* 26**,** 5760-5766.

Cummins, D., Mccormick, J. B., Bennett, D., Samba, J. A., Farrar, B., Machin, S. J. & Fisher-Hoch, S. P. 1990. Acute Sensorineural Deafness in Lassa Fever. *JAMA,* 264**,** 2093-2096.

Cytiva. 2020. *Protein purification troubleshooting guide* [Online]. Cytiva. Available: https://cytiva-delivery.sitecorecontenthub.cloud/api/public/content/digi-18407-original [Accessed].

Davis, H. E., Rosinski, M., Morgan, J. R. & Yarmush, M. L. 2004. Charged Polymers Modulate Retrovirus Transduction via Membrane Charge Neutralization and Virus Aggregation. *Biophysical Journal,* 86**,** 1234-1242.

De Wit, E., Munster, V. J., Van Riel, D., Beyer, W. E. P., Rimmelzwaan, G. F., Kuiken, T., Osterhaus, A. D. M. E. & Fouchier, R. a. M. 2010. Molecular Determinants of Adaptation of Highly Pathogenic Avian Influenza H7N7 Viruses to Efficient Replication in the Human Host. *Journal of Virology,* 84**,** 1597-1606.

Doench, J. G., Fusi, N., Sullender, M., Hegde, M., Vaimberg, E. W., Donovan, K. F., Smith, I., Tothova, Z., Wilen, C., Orchard, R., Virgin, H. W., Listgarten, J. & Root, D. E. 2016. Optimized sgRNA design to maximize activity and minimize off-target effects of CRISPR-Cas9. *Nature Biotechnology,* 34**,** 184-191.

Dortmans, J. C. F. M., Dekkers, J., Wickramasinghe, I. N. A., Verheije, M. H., Rottier, P. J. M., Van Kuppeveld, F. J. M., De Vries, E. & De Haan, C. a. M. 2013. Adaptation of novel H7N9 influenza A virus to human receptors. *Scientific Reports,* 3**,** 3058.

Drescher, D. G., Ramakrishnan, N. A. & Drescher, M. J. 2009. Surface plasmon resonance (SPR) analysis of binding interactions of proteins in inner-ear sensory epithelia. *Methods Mol Biol,* 493**,** 323-43.

Drescher, D. G., Selvakumar, D. & Drescher, M. J. 2018. Chapter One - Analysis of Protein Interactions by Surface Plasmon Resonance. *In:* DONEV, R. (ed.) *Advances in Protein Chemistry and Structural Biology.* Academic Press.

Dubay, J. W., Roberts, S. J., Hahn, B. H. & Hunter, E. 1992. Truncation of the human immunodeficiency virus type 1 transmembrane glycoprotein cytoplasmic domain blocks virus infectivity. *J Virol,* 66**,** 6616-6625.

Dubridge, R. B., Tang, P., Hsia, H. C., Leong, P. M., Miller, J. H. & Calos, M. P. 1987. Analysis of mutation in human cells by using an Epstein-Barr virus shuttle system. *Mol Cell Biol,* 7**,** 379-387.

Durbeej, M., Henry, M. D., Ferletta, M., Campbell, K. P. & Ekblom, P. 1998. Distribution of Dystroglycan in Normal Adult Mouse Tissues. *Journal of Histochemistry & Cytochemistry,* 46**,** 449-457.

Dylla, D. E., Michele, D. E., Campbell, K. P. & Mccray, P. B. 2008. Basolateral Entry and Release of New and Old World Arenaviruses from Human Airway Epithelia. *Journal of Virology,* 82**,** 6034-6038.

Eichler, R., Lenz, O., Garten, W. & Strecker, T. 2006. The role of single N-glycans in proteolytic processing and cell surface transport of the Lassa virus glycoprotein GP-C. *Virology journal,* 3**,** 41-41.

Ellwanger, J. H. & Chies, J. a. B. 2017. Keeping track of hidden dangers - The short history of the Sabiá virus. *Revista da Sociedade Brasileira de Medicina Tropical,* 50**,** 3-8.

Enria, D. A., Briggiler, A. M., Fernandez, N. J., Levis, S. C. & Maiztegui, J. I. 1984. Importance of dose of neutralising antibodies in treatment of Argentine haemorrhagic fever with immune plasma. *Lancet,* 2**,** 255-256.

Enria, D. A., Briggiler, A. M., Levis, S., Vallejos, D., Maiztegui, J. I. & Canonico, P. G. 1987. Tolerance and antiviral effect of ribavirin in patients with argentine hemorrhagic fever. *Antiviral Research,* 7**,** 353-359.

Enria, D. A., Briggiler, A. M. & Sánchez, Z. 2008. Treatment of Argentine hemorrhagic fever. *Antiviral research,* 78**,** 132-139.

Enria, D. A. & Maiztegui, J. I. 1994. Antiviral treatment of Argentine hemorrhagic fever. *Antiviral Res,* 23**,** 23-31.

Enria, D. A. & Oro, J. G. B. 2002. Junin Virus Vaccines. *In:* OLDSTONE, M. B. A. (ed.) *Arenaviruses II: The Molecular Pathogenesis of Arenavirus Infections.* Berlin, Heidelberg: Springer Berlin Heidelberg.

Enserink, M. 2000. New Arenavirus Blamed for Recent Deaths in California. *Science,* 289**,** 842.

Escalera-Antezana, J. P., Rodriguez-Villena, O. J., Arancibia-Alba, A. W., Alvarado-Arnez, L. E., Bonilla-Aldana, D. K. & Rodriguez-Morales, A. J. 2020. Clinical features of fatal cases of Chapare virus hemorrhagic fever originating from rural La Paz, Bolivia, 2019: A cluster analysis. *Travel Med Infect Dis***,** 101589.

Eschli, B., Zellweger, R. M., Wepf, A., Lang, K. S., Quirin, K., Weber, J., Zinkernagel, R. M. & Hengartner, H. 2007. Early antibodies specific for the neutralizing epitope on the receptor binding subunit of the lymphocytic choriomeningitis virus glycoprotein fail to neutralize the virus. *J Virol,* 81**,** 11650-11657.

Evans, M. J., Von Hahn, T., Tscherne, D. M., Syder, A. J., Panis, M., Wölk, B., Hatziioannou, T., Mckeating, J. A., Bieniasz, P. D. & Rice, C. M. 2007. Claudin-1 is a hepatitis C virus co-receptor required for a late step in entry. *Nature,* 446**,** 801-805.

Fallet, B., Hao, Y., Florova, M., Cornille, K., De Los Aires, A. V., Girelli Zubani, G., Ertuna, Y. I., Greiff, V., Menzel, U., Hammad, K., Merkler, D., Reddy, S. T., Weill, J. C., Reynaud, C. A. & Pinschewer, D. D. 2020. Chronic Viral Infection Promotes Efficient Germinal Center B Cell Responses. *Cell Rep,* 30**,** 1013-1026.e7.

Fedeli, C., Moreno, H. & Kunz, S. 2018a. Novel Insights into Cell Entry of Emerging Human Pathogenic Arenaviruses. *Journal of Molecular Biology,* 430**,** 1839-1852.

Fedeli, C., Moreno, H. & Kunz, S. 2020. The Role of Receptor Tyrosine Kinases in Lassa Virus Cell Entry. *Viruses,* 12.

Fedeli, C., Torriani, G., Galan-Navarro, C., Moraz, M. L., Moreno, H., Gerold, G. & Kunz, S. 2018b. Axl Can Serve as Entry Factor for Lassa Virus Depending on the Functional Glycosylation of Dystroglycan. *J Virol,* 92.

Ferrara, F., Molesti, E., Böttcher-Friebertshäuser, E., Cattoli, G., Corti, D., Scott, S. & Temperton, N. 2013. The human Transmembrane Protease Serine 2 is necessary for the production of Group 2 influenza A virus pseudotypes. *Journal of Molecular and Genetic Medicine,* 7**,** 309-314.

Fichet-Calvet, E., Becker-Ziaja, B., Koivogui, L. & Günther, S. 2014a. Lassa serology in natural populations of rodents and horizontal transmission. *Vector Borne Zoonotic Dis,* 14**,** 665-674.

Fichet-Calvet, E., Becker-Ziaja, B., Koivogui, L. & Günther, S. 2014b. Lassa serology in natural populations of rodents and horizontal transmission. *Vector borne and zoonotic diseases (Larchmont, N.Y.),* 14**,** 665-674.

Fichet-Calvet, E., Ölschläger, S., Strecker, T., Koivogui, L., Becker-Ziaja, B., Camara, A. B., Soropogui, B., Magassouba, N. F. & Günther, S. 2016. Spatial and temporal evolution of Lassa virus in the natural host population in Upper Guinea. *Scientific reports,* 6**,** 21977-21977.

Fischer, S. A., Graham, M. B., Kuehnert, M. J., Kotton, C. N., Srinivasan, A., Marty, F. M., Comer, J. A., Guarner, J., Paddock, C. D., Demeo, D. L., Shieh, W. J., Erickson, B. R., Bandy, U., Demaria, A., Davis, J. P., Delmonico, F. L., Pavlin, B., Likos, A., Vincent, M. J., Sealy, T. K., Goldsmith, C. S., Jernigan, D. B., Rollin, P. E., Packard, M. M., Patel, M., Rowland, C., Helfand, R. F., Nichol, S. T., Fishman, J. A., Ksiazek, T., Zaki, S. R. & Team, L. I. T. R. I. 2006. Transmission of lymphocytic choriomeningitis virus by organ transplantation. *N Engl J Med,* 354**,** 2235-2249.

Fisher-Hoch, S. P., Mccormick, J. B., Sasso, D. & Craven, R. B. 1988. Hematologic dysfunction in Lassa fever. *Journal of Medical Virology,* 26**,** 127-135.

Flatz, L., Rieger, T., Merkler, D., Bergthaler, A., Regen, T., Schedensack, M., Bestmann, L., Verschoor, A., Kreutzfeldt, M., Brück, W., Hanisch, U.-K., Günther, S. & Pinschewer, D. D. 2010. T Cell-Dependence of Lassa Fever Pathogenesis. *PLOS Pathogens,* 6**,** e1000836.

Forni, D., Pontremoli, C., Pozzoli, U., Clerici, M., Cagliani, R. & Sironi, M. 2018. Ancient Evolution of Mammarenaviruses: Adaptation via Changes in the L Protein and No Evidence for Host-Virus Codivergence. *Genome Biol Evol,* 10**,** 863-874.

Fraser, D. W., Campbell, C. C., Monath, T. P., Goff, P. A. & Gregg, M. B. 1974. Lassa Fever in the Eastern Province of Sierra Leone, 1970–1972. *The American Journal of Tropical Medicine and Hygiene,* 23**,** 1131-1139.

Fuller-Pace, F. V. & Southern, P. J. 1988. Temporal analysis of transcription and replication during acute infection with lymphocytic choriomeningitis virus. *Virology,* 162**,** 260-263.

Garcia, J.-M., Lagarde, N., Ma, E. S. K., De Jong, M. D. & Peiris, J. S. M. 2010. Optimization and evaluation of an influenza A (H5) pseudotyped lentiviral particle-based serological assay. *Journal of Clinical Virology,* 47**,** 29-33.

Gebre, M., Nomburg, J. L. & Gewurz, B. E. 2018. CRISPR–Cas9 Genetic Analysis of Virus–Host Interactions. *Viruses,* 10**,** 55.

Geoghegan, J. L., Senior, A. M., Giallonardo, F. D. & Holmes, E. C. 2016. Virological factors that increase the transmissibility of emerging human viruses. *Proceedings of the National Academy of Sciences,* 113**,** 4170-4175.

Gilden , D. H., Cole , G. A. & Nathanson , N. 1972. Immunopathogenesis of acute central nervous system disease produced by lymphocytic choriomeningitis virus : II. adoptive immunization of virus carriers. *Journal of Experimental Medicine,* 135**,** 874-889.

Giroglou, T., Cinatl, J., Jr., Rabenau, H., Drosten, C., Schwalbe, H., Doerr, H. W. & Von Laer, D. 2004. Retroviral vectors pseudotyped with severe acute

respiratory syndrome coronavirus S protein. *Journal of virology,* 78**,** 9007-9015.

Glaser, L., Stevens, J., Zamarin, D., Wilson, I. A., García-Sastre, A., Tumpey, T. M., Basler, C. F., Taubenberger, J. K. & Palese, P. 2005. A single amino acid substitution in 1918 influenza virus hemagglutinin changes receptor binding specificity. *Journal of virology,* 79**,** 11533-11536.

Goldwater, P. N. 2022. A mouse zoonotic virus (LCMV): A possible candidate in the causation of SIDS. *Medical Hypotheses,* 158**,** 110735.

Goncalves, A.-R., Moraz, M.-L., Pasquato, A., Helenius, A., Lozach, P.-Y. & Kunz, S. 2013. Role of DC-SIGN in Lassa Virus Entry into Human Dendritic Cells. *Journal of Virology,* 87**,** 11504.

Greczmiel, U., Kräutler, N. J., Pedrioli, A., Bartsch, I., Agnellini, P., Bedenikovic, G., Harker, J., Richter, K. & Oxenius, A. 2017. Sustained T follicular helper cell response is essential for control of chronic viral infection. *Science Immunology,* 2**,** eaam8686.

Greenway, D. J., Rugiero, H. R., Parodi, A. S., Frigerio, M., Rivero, E., De La Barrera, J. M., Garzon, F., Boxaca, M., Mettler, N., De Guerrero, L. B. & Nota, N. 1959. Epidemic hemorrhagic fever in Argentina. *Public health reports (Washington, D.C. : 1896),* 74**,** 1011-1014.

Greenwood, A. G. & Sanchez, S. 2002. Serological evidence of murine pathogens in wild grey squirrels (Sciurus carolinensis) in North Wales. *Vet Rec,* 150**,** 543-546.

Grehan, K., Ferrara, F. & Temperton, N. 2015. An optimised method for the production of MERS-CoV spike expressing viral pseudotypes. *MethodsX,* 2**,** 379-384.

Gryseels, S., Baird, S. J., Borremans, B., Makundi, R., Leirs, H. & Goüy De Bellocq, J. 2017. When Viruses Don't Go Viral: The Importance of Host Phylogeographic Structure in the Spatial Spread of Arenaviruses. *PLoS Pathog,* 13**,** e1006073.

Gryseels, S., Rieger, T., Oestereich, L., Cuypers, B., Borremans, B., Makundi, R., Leirs, H., Günther, S. & Goüy De Bellocq, J. 2015. Gairo virus, a novel arenavirus of the widespread Mastomys natalensis: Genetically divergent, but ecologically similar to Lassa and Morogoro viruses. *Virology,* 476**,** 249-256.

Guo, J., Zhang, G., Liu, Y., Cao, J., Zhang, M., Lan, X., Zhang, Y., Liu, C., Xiao, G. & Wang, W. 2020. Functional Characterization of a Lassa Virus Fusion Inhibitors Adaptive Mutant. *bioRxiv***,** 2020.12.23.424274.

Gutierrez-Guerrero, A., Cosset, F.-L. & Verhoeyen, E. 2020. Lentiviral Vector Pseudotypes: Precious Tools to Improve Gene Modification of Hematopoietic Cells for Research and Gene Therapy. *Viruses,* 12**,** 1016.

Han, J., Perez, J. T., Chen, C., Li, Y., Benitez, A., Kandasamy, M., Lee, Y., Andrade, J., Tenoever, B. & Manicassamy, B. 2018. Genome-wide CRISPR/Cas9 Screen Identifies Host Factors Essential for Influenza Virus Replication. *Cell Reports,* 23**,** 596-607.

Hara, Y., Kanagawa, M., Kunz, S., Yoshida-Moriguchi, T., Satz, J. S., Kobayashi, Y. M., Zhu, Z., Burden, S. J., Oldstone, M. B. A. & Campbell, K. P. 2011. Like-acetylglucosaminyltransferase (LARGE)-dependent modification of

dystroglycan at Thr-317/319 is required for laminin binding and arenavirus infection. *Proceedings of the National Academy of Sciences of the United States of America,* 108**,** 17426-17431.

Hastie, K. M., Igonet, S., Sullivan, B. M., Legrand, P., Zandonatti, M. A., Robinson, J. E., Garry, R. F., Rey, F. A., Oldstone, M. B. & Saphire, E. O. 2016. Crystal structure of the prefusion surface glycoprotein of the prototypic arenavirus LCMV. *Nat Struct Mol Biol,* 23**,** 513-521.

Hastie, K. M., Zandonatti, M. A., Kleinfelter, L. M., Heinrich, M. L., Rowland, M. M., Chandran, K., Branco, L. M., Robinson, J. E., Garry, R. F. & Saphire, E. O. 2017. Structural basis for antibody-mediated neutralization of Lassa virus. *Science,* 356**,** 923-928.

Herrador, A., Fedeli, C., Radulovic, E., Campbell, K. P., Moreno, H., Gerold, G. & Kunz, S. 2019. Dynamic Dystroglycan Complexes Mediate Cell Entry of Lassa Virus. *mBio,* 10**,** e02869-18.

Heyndrickx, L., Heath, A., Sheik-Khalil, E., Alcami, J., Bongertz, V., Jansson, M., Malnati, M., Montefiori, D., Moog, C., Morris, L., Osmanov, S., Polonis, V., Ramaswamy, M., Sattentau, Q., Tolazzi, M., Schuitemaker, H., Willems, B., Wrin, T., Fenyö, E. M. & Scarlatti, G. 2012. International network for comparison of HIV neutralization assays: the NeutNet report II. *PLoS One,* 7**,** e36438.

Hoffmann, M., Zhang, L. & Pöhlmann, S. 2022. Omicron: Master of immune evasion maintains robust ACE2 binding. *Signal Transduction and Targeted Therapy,* 7**,** 118.

Holmes, E. C., Ghedin, E., Miller, N., Taylor, J., Bao, Y., St George, K., Grenfell, B. T., Salzberg, S. L., Fraser, C. M., Lipman, D. J. & Taubenberger, J. K. 2005. Whole-Genome Analysis of Human Influenza A Virus Reveals Multiple Persistent Lineages and Reassortment among Recent H3N2 Viruses. *PLOS Biology,* 3**,** e300.

Holmes, K. V. 2005. Adaptation of SARS Coronavirus to Humans. *Science,* 116**,** e210127.

Hotchin, J. & Benson, L. 1963. The Pathogenesis of Lymphocytic Choriomeningitis in Mice: the Effects of Different Inoculation Routes and the Footpad Response. *The Journal of Immunology,* 91**,** 460-468.

Hsu, E. C., Iorio, C., Sarangi, F., Khine, A. A. & Richardson, C. D. 2001. CDw150(SLAM) is a receptor for a lymphotropic strain of measles virus and may account for the immunosuppressive properties of this virus. *Virology,* 279**,** 9-21.

Hsu, H.-L., Millet, J. K., Costello, D. A., Whittaker, G. R. & Daniel, S. 2016. Viral fusion efficacy of specific H3N2 influenza virus reassortant combinations at single-particle level. *Scientific Reports,* 6**,** 35537.

Huang, M. T. & Gorman, C. M. 1990. Intervening sequences increase efficiency of RNA 3' processing and accumulation of cytoplasmic RNA. *Nucleic acids research,* 18**,** 937-947.

Hulseberg, C. E., Fénéant, L., Szymańska, K. M. & White, J. M. 2018. Lamp1 Increases the Efficiency of Lassa Virus Infection by Promoting Fusion in Less Acidic Endosomal Compartments. *MBio,* 9**,** e01818-17.

Ibraghimov-Beskrovnaya, O., Milatovich, A., Ozcelik, T., Yang, B., Koepnick, K., Francke, U. & Campbell, K. P. 1993. Human dystroglycan: skeletal muscle cDNA, genomic structure, origin of tissue specific isoforms and chromosomal localization. *Hum Mol Genet,* 2**,** 1651-1657.

Ibukun, F. I. 2020. Inter-Lineage Variation of Lassa Virus Glycoprotein Epitopes: A Challenge to Lassa Virus Vaccine Development. *Viruses,* 12.

Igonet, S., Vaney, M. C., Vonrhein, C., Vonhrein, C., Bricogne, G., Stura, E. A., Hengartner, H., Eschli, B. & Rey, F. A. 2011. X-ray structure of the arenavirus glycoprotein GP2 in its postfusion hairpin conformation. *Proc Natl Acad Sci U S A,* 108**,** 19967-19972.

Isaac, A. B., Karolina, W., Temitope, A. A., Anuska, R., Joanne, E., Deborah, A., Bianca, O. C., Filip, T., Zofia, P., Oluwasegun, O. I., Oluwaferanmi, O. & Grace, B. T. 2022. PROSPECTS OF LASSA FEVER CANDIDATE VACCINES. *Afr J Infect Dis,* 16**,** 46-58.

Israeli, H., Cohen-Dvashi, H., Shulman, A., Shimon, A. & Diskin, R. 2017. Mapping of the Lassa virus LAMP1 binding site reveals unique determinants not shared by other old world arenaviruses. *PLoS Pathog,* 13**,** e1006337.

Iwasaki, M., Ngo, N., Cubitt, B., Teijaro, J. R. & De La Torre, J. C. 2015. General Molecular Strategy for Development of Arenavirus Live-Attenuated Vaccines. *Journal of Virology,* 89**,** 12166-12177.

Iwasaki, M., Urata, S., Cho, Y., Ngo, N. & De La Torre, J. C. 2014. Cell entry of lymphocytic choriomeningitis virus is restricted in myotubes. *Virology,* 458-459**,** 22-32.

Jae, L. T., Raaben, M., Herbert, A. S., Kuehne, A. I., Wirchnianski, A. S., Soh, T. K., Stubbs, S. H., Janssen, H., Damme, M., Saftig, P., Whelan, S. P., Dye, J. M. & Brummelkamp, T. R. 2014. Virus entry. Lassa virus entry requires a trigger-induced receptor switch. *Science,* 344**,** 1506-10.

Jae, L. T., Raaben, M., Riemersma, M., Van Beusekom, E., Blomen, V. A., Velds, A., Kerkhoven, R. M., Carette, J. E., Topaloglu, H., Meinecke, P., Wessels, M. W., Lefeber, D. J., Whelan, S. P., Van Bokhoven, H. & Brummelkamp, T. R. 2013. Deciphering the glycosylome of dystroglycanopathies using haploid screens for lassa virus entry. *Science,* 340**,** 479-83.

Jahrling, P. B. & Peters, C. J. 1984. Passive antibody therapy of Lassa fever in cynomolgus monkeys: importance of neutralizing antibody and Lassa virus strain. *Infection and immunity,* 44**,** 528-533.

Jemielity, S., Wang, J. J., Chan, Y. K., Ahmed, A. A., Li, W., Monahan, S., Bu, X., Farzan, M., Freeman, G. J., Umetsu, D. T., Dekruyff, R. H. & Choe, H. 2013. TIM-family Proteins Promote Infection of Multiple Enveloped Viruses through Virion-associated Phosphatidylserine. *PLOS Pathogens,* 9**,** e1003232.

Jenkins, G. M., Rambaut, A., Pybus, O. G. & Holmes, E. C. 2002. Rates of molecular evolution in RNA viruses: a quantitative phylogenetic analysis. *J Mol Evol,* 54**,** 156-165.

Kahan, S. M. & Zajac, A. J. 2019. Immune Exhaustion: Past Lessons and New Insights from Lymphocytic Choriomeningitis Virus. *Viruses,* 11**,** 156.

Kaletsky, R. L., Simmons, G. & Bates, P. 2007. Proteolysis of the Ebola Virus Glycoproteins Enhances Virus Binding and Infectivity. *Journal of Virology,* 81**,** 13378.

Kanagawa, M., Saito, F., Kunz, S., Yoshida-Moriguchi, T., Barresi, R., Kobayashi, Y. M., Muschler, J., Dumanski, J. P., Michele, D. E., Oldstone, M. B. & Campbell, K. P. 2004. Molecular recognition by LARGE is essential for expression of functional dystroglycan. *Cell,* 117**,** 953-964.

Kaplan, C., Healing, T. D., Evans, N., Healing, L. & Prior, A. 1980. Evidence of infection by viruses in small British field rodents. *Journal of Hygiene,* 84**,** 285-294.

Kellam, P. & Larder, B. A. 1995. Retroviral recombination can lead to linkage of reverse transcriptase mutations that confer increased zidovudine resistance. *J Virol,* 69**,** 669-674.

King, B., Temperton, N. J., Grehan, K., Scott, S. D., Wright, E., Tarr, A. W. & Daly, J. M. 2016. Technical considerations for the generation of novel pseudotyped viruses. *Future Virology,* 11**,** 47-59.

King, B. R., Kellner, S., Eisenhauer, P. L., Bruce, E. A., Ziegler, C. M., Zenklusen, D. & Botten, J. W. 2017. Visualization of the lymphocytic choriomeningitis mammarenavirus (LCMV) genome reveals the early endosome as a possible site for genome replication and viral particle pre-assembly. *The Journal of general virology,* 98**,** 2454-2460.

Kleinstiver, B. P., Pattanayak, V., Prew, M. S., Tsai, S. Q., Nguyen, N. T., Zheng, Z. & Joung, J. K. 2016. High-fidelity CRISPR–Cas9 nucleases with no detectable genome-wide off-target effects. *Nature,* 529**,** 490-495.

Kotecki, M., Reddy, P. S. & Cochran, B. H. 1999. Isolation and characterization of a near-haploid human cell line. *Exp Cell Res,* 252**,** 273-280.

Kranzusch, P. J. & Whelan, S. P. J. 2011. Arenavirus Z protein controls viral RNA synthesis by locking a polymerase-promoter complex. *Proceedings of the National Academy of Sciences of the United States of America,* 108**,** 19743-19748.

Kräutler, N. J., Yermanos, A., Pedrioli, A., Welten, S. P. M., Lorgé, D., Greczmiel, U., Bartsch, I., Scheuermann, J., Kiefer, J. D., Eyer, K., Menzel, U., Greiff, V., Neri, D., Stadler, T., Reddy, S. T. & Oxenius, A. 2020. Quantitative and Qualitative Analysis of Humoral Immunity Reveals Continued and Personalized Evolution in Chronic Viral Infection. *Cell Reports,* 30**,** 997-1012.e6.

Kunz, S. 2009. Receptor binding and cell entry of Old World arenaviruses reveal novel aspects of virus-host interaction. *Virology,* 387**,** 245-249.

Kunz, S., Edelmann, K. H., De La Torre, J. C., Gorney, R. & Oldstone, M. B. 2003. Mechanisms for lymphocytic choriomeningitis virus glycoprotein cleavage, transport, and incorporation into virions. *Virology,* 314**,** 168-178.

Kunz, S., Rojek, J. M., Kanagawa, M., Spiropoulou, C. F., Barresi, R., Campbell, K. P. & Oldstone, M. B. 2005. Posttranslational modification of alpha-dystroglycan, the cellular receptor for arenaviruses, by the glycosyltransferase LARGE is critical for virus binding. *J Virol,* 79**,** 14282-14296.

Kunz, S., Sevilla, N., Mcgavern, D. B., Campbell, K. P. & Oldstone, M. B. 2001. Molecular analysis of the interaction of LCMV with its cellular receptor [alpha]-dystroglycan. *The Journal of cell biology,* 155**,** 301-310.

Kunz, S., Sevilla, N., Rojek, J. M. & Oldstone, M. B. A. 2004. Use of alternative receptors different than α-dystroglycan by selected isolates of lymphocytic choriomeningitis virus. *Virology,* 325**,** 432-445.

Lavillette, D., Tarr, A. W., Voisset, C., Donot, P., Bartosch, B., Bain, C., Patel, A. H., Dubuisson, J., Ball, J. K. & Cosset, F. L. 2005. Characterization of host-range and cell entry properties of the major genotypes and subtypes of hepatitis C virus. *Hepatology,* 41**,** 265-274.

Le Rhun, A., Escalera-Maurer, A., Bratovič, M. & Charpentier, E. 2019. CRISPR-Cas in Streptococcus pyogenes. *RNA Biol,* 16**,** 380-389.

Lee, K. J., Novella, I. S., Teng, M. N., Oldstone, M. B. & De La Torre, J. C. 2000. NP and L proteins of lymphocytic choriomeningitis virus (LCMV) are sufficient for efficient transcription and replication of LCMV genomic RNA analogs. *Journal of virology,* 74**,** 3470-3477.

Lelke, M., Brunotte, L., Busch, C. & Günther, S. 2010. An N-Terminal Region of Lassa Virus L Protein Plays a Critical Role in Transcription but Not Replication of the Virus Genome. *Journal of Virology,* 84**,** 1934.

Lemke, G. & Rothlin, C. V. 2008. Immunobiology of the TAM receptors. *Nat Rev Immunol,* 8**,** 327-336.

Letko, M., Marzi, A. & Munster, V. 2020. Functional assessment of cell entry and receptor usage for SARS-CoV-2 and other lineage B betacoronaviruses. *Nature Microbiology,* 5**,** 562-569.

Levingston Macleod, J. M., D'antuono, A., Loureiro, M. E., Casabona, J. C., Gomez, G. A. & Lopez, N. 2011. Identification of two functional domains within the arenavirus nucleoprotein. *J Virol,* 85**,** 2012-2023.

Li, H., Buck, T., Zandonatti, M., Yin, J., Moon-Walker, A., Fang, J., Koval, A., Heinrich, M. L., Rowland, M. M., Diaz Avalos, R., Schendel, S. L., Parekh, D., Zyla, D., Enriquez, A., Harkins, S., Sullivan, B., Smith, V., Chukwudozie, O., Watanabe, R., Robinson, J. E., Garry, R. F., Branco, L. M., Hastie, K. M. & Saphire, E. O. 2022. A cocktail of protective antibodies subverts the dense glycan shield of Lassa virus. *Science Translational Medicine,* 14**,** eabq0991.

Li, J. L., Cornman, R. S., Evans, J. D., Pettis, J. S., Zhao, Y., Murphy, C., Peng, W. J., Wu, J., Hamilton, M., Boncristiani, H. F., Zhou, L., Hammond, J. & Chen, Y. P. 2014. Systemic spread and propagation of a plant-pathogenic virus in European honeybees, Apis mellifera. *mBio,* 5**,** e00898-13.

Li, K., Yan, S., Wang, N., He, W., Guan, H., He, C., Wang, Z., Lu, M., He, W., Ye, R., Veit, M. & Su, S. 2020. Emergence and adaptive evolution of Nipah virus. *Transbound Emerg Dis,* 67**,** 121-132.

Li, Q., Liu, Q., Huang, W., Li, X. & Wang, Y. 2018. Current status on the development of pseudoviruses for enveloped viruses. *Reviews in Medical Virology,* 28**,** e1963.

Li, S., Sun, Z., Pryce, R., Parsy, M.-L., Fehling, S. K., Schlie, K., Siebert, C. A., Garten, W., Bowden, T. A., Strecker, T. & Huiskonen, J. T. 2016. Acidic pH-Induced Conformations and LAMP1 Binding of the Lassa Virus Glycoprotein Spike. *PLOS Pathogens,* 12**,** e1005418.

Lin, H., Yutzey, K. E. & Konieczny, S. F. 1991. Muscle-specific expression of the troponin I gene requires interactions between helix-loop-helix muscle regulatory factors and ubiquitous transcription factors. *Mol Cell Biol,* 11**,** 267-80.

Lin, Y.-C., Boone, M., Meuris, L., Lemmens, I., Van Roy, N., Soete, A., Reumers, J., Moisse, M., Plaisance, S., Drmanac, R., Chen, J., Speleman, F., Lambrechts, D., Van De Peer, Y., Tavernier, J. & Callewaert, N. 2014. Genome dynamics of the human embryonic kidney 293 lineage in response to cell biology manipulations. *Nature Communications,* 5**,** 4767.

Liu, H., Wei, P., Kappler, J. W., Marrack, P. & Zhang, G. 2022. SARS-CoV-2 Variants of Concern and Variants of Interest Receptor Binding Domain Mutations and Virus Infectivity. *Frontiers in Immunology,* 13.

Liu, S., Yang, W., Shen, L., Turner, J. R., Coyne, C. B. & Wang, T. 2009. Tight junction proteins claudin-1 and occludin control hepatitis C virus entry and are downregulated during infection to prevent superinfection. *Journal of virology,* 83**,** 2011-2014.

López, N. & Franze-Fernández, M. T. 2007. A single stem-loop structure in Tacaribe arenavirus intergenic region is essential for transcription termination but is not required for a correct initiation of transcription and replication. *Virus Res,* 124**,** 237-244.

Loureiro, M. E., Wilda, M., Levingston Macleod, J. M., D'antuono, A., Foscaldi, S., Marino Buslje, C. & Lopez, N. 2011. Molecular determinants of arenavirus Z protein homo-oligomerization and L polymerase binding. *Journal of virology,* 85**,** 12304-12314.

Loureiro, M. E., Zorzetto-Fernandes, A. L., Radoshitzky, S., Chi, X., Dallari, S., Marooki, N., Leger, P., Foscaldi, S., Harjono, V., Sharma, S., Zid, B. M., Lopez, N., De La Torre, J. C., Bavari, S. & Zuniga, E. 2018. DDX3 suppresses type I interferons and favors viral replication during Arenavirus infection. *PLoS Pathog,* 14**,** e1007125.

Lucke, V. M. & Bennett, A. M. 1982. An outbreak of hepatitis in marmosets in a zoological collection. *Lab Anim,* 16**,** 73-77.

Lukashevich, I. S., Djavani, M., Shapiro, K., Sanchez, A., Ravkov, E., Nichol, S. T. & Salvato, M. S. 1997. The Lassa fever virus L gene: nucleotide sequence, comparison, and precipitation of a predicted 250 kDa protein with monospecific antiserum. *J Gen Virol,* 78 (Pt 3)**,** 547-51.

Lv, Z., Chu, Y. & Wang, Y. 2015. HIV protease inhibitors: a review of molecular selectivity and toxicity. *HIV/AIDS (Auckland, N.Z.),* 7**,** 95-104.

Lynch, R. M., Wong, P., Tran, L., O'dell, S., Nason, M. C., Li, Y., Wu, X. & Mascola, J. R. 2015. HIV-1 fitness cost associated with escape from the VRC01 class of CD4 binding site neutralizing antibodies. *J Virol,* 89**,** 4201-4213.

Macher, A. M. & Wolfe, M. S. 2006. Historical Lassa fever reports and 30-year clinical update. *Emerging infectious diseases,* 12**,** 835-837.

Macneil, A., Ströher, U., Farnon, E., Campbell, S., Cannon, D., Paddock, C. D., Drew, C. P., Kuehnert, M., Knust, B., Gruenenfelder, R., Zaki, S. R., Rollin, P. E., Nichol, S. T. & Team, L. T. I. 2012. Solid organ transplant-associated lymphocytic choriomeningitis, United States, 2011. *Emerging infectious diseases,* 18**,** 1256-1262.

Mahmutovic, S., Clark, L., Levis, Silvana c., Briggiler, Ana m., Enria, Delia a., Harrison, Stephen c. & Abraham, J. 2015. Molecular Basis for Antibody-Mediated Neutralization of New World Hemorrhagic Fever Mammarenaviruses. *Cell Host & Microbe,* 18**,** 705-713.

Maiztegui, J. I., Fernandez, N. J. & De Damilano, A. J. 1979. Efficacy of immune plasma in treatment of Argentine haemorrhagic fever and association between treatment and a late neurological syndrome. *Lancet,* 2**,** 1216-1217.

Maiztegui, J. I., Mckee, K. T., Jr., Barrera Oro, J. G., Harrison, L. H., Gibbs, P. H., Feuillade, M. R., Enria, D. A., Briggiler, A. M., Levis, S. C., Ambrosio, A. M., Halsey, N. A. & Peters, C. J. 1998. Protective efficacy of a live attenuated vaccine against Argentine hemorrhagic fever. AHF Study Group. *J Infect Dis,* 177**,** 277-283.

Mallajosyula, V. V., Citron, M., Ferrara, F., Lu, X., Callahan, C., Heidecker, G. J., Sarma, S. P., Flynn, J. A., Temperton, N. J., Liang, X. & Varadarajan, R. 2014. Influenza hemagglutinin stem-fragment immunogen elicits broadly neutralizing antibodies and confers heterologous protection. *Proc Natl Acad Sci U S A,* 111**,** E2514-E2523.

Malm, M., Saghaleyni, R., Lundqvist, M., Giudici, M., Chotteau, V., Field, R., Varley, P. G., Hatton, D., Grassi, L., Svensson, T., Nielsen, J. & Rockberg, J. 2020. Evolution from adherent to suspension: systems biology of HEK293 cell line development. *Scientific Reports,* 10**,** 18996.

Mamchaoui, K., Trollet, C., Bigot, A., Negroni, E., Chaouch, S., Wolff, A., Kandalla, P. K., Marie, S., Di Santo, J., St Guily, J. L., Muntoni, F., Kim, J., Philippi, S., Spuler, S., Levy, N., Blumen, S. C., Voit, T., Wright, W. E., Aamiri, A., Butler-Browne, G. & Mouly, V. 2011. Immortalized pathological human myoblasts: towards a universal tool for the study of neuromuscular disorders. *Skeletal Muscle,* 1**,** 34.

Manning, J. T., Forrester, N. & Paessler, S. 2015. Lassa virus isolates from Mali and the Ivory Coast represent an emerging fifth lineage. *Front Microbiol,* 6**,** 1037.

Mateo, M., Reynard, S., Journeaux, A., Germain, C., Hortion, J., Carnec, X., Picard, C., Baillet, N., Borges-Cardoso, V., Merabet, O., Vallve, A., Barron, S., Jourjon, O., Lacroix, O., Duthey, A., Dirheimer, M., Jouvion, G., Moreau, P.-H., Fellmann, L., Carbonnelle, C., Raoul, H., Tangy, F. & Baize, S. 2021. A single-shot Lassa vaccine induces long-term immunity and protects

cynomolgus monkeys against heterologous strains. *Science Translational Medicine,* 13**,** eabf6348.
Matloubian, M., Kolhekar, S. R., Somasundaram, T. & Ahmed, R. 1993. Molecular determinants of macrophage tropism and viral persistence: importance of single amino acid changes in the polymerase and glycoprotein of lymphocytic choriomeningitis virus. *J Virol,* 67**,** 7340-7349.
Matullo, C. M., Regan, K. J., Hensley, H., Curtis, M. & Rall, G. F. 2010. Lymphocytic Choriomeningitis Virus-Induced Mortality in Mice Is Triggered by Edema and Brain Herniation. *Journal of Virology,* 84**,** 312-320.
Mccormick, J. B., King, I. J., Webb, P. A., Johnson, K. M., O'sullivan, R., Smith, E. S., Trippel, S. & Tong, T. C. 1987a. A Case-Control Study of the Clinical Diagnosis and Course of Lassa Fever. *The Journal of Infectious Diseases,* 155**,** 445-455.
Mccormick, J. B., King, I. J., Webb, P. A., Scribner, C. L., Craven, R. B., Johnson, K. M., Elliott, L. H. & Belmont-Williams, R. 1986. Lassa fever. Effective therapy with ribavirin. *The New England journal of medicine,* 314**,** 20-26.
Mccormick, J. B., Webb, P. A., Krebs, J. W., Johnson, K. M. & Smith, E. S. 1987b. A Prospective Study of the Epidemiology and Ecology of Lassa Fever. *The Journal of Infectious Diseases,* 155**,** 437-444.
Merten, O.-W., Schweizer, M., Chahal, P. & Kamen, A. 2014. Manufacturing of viral vectors: part II. Downstream processing and safety aspects. *Pharmaceutical Bioprocessing,* 2**,** 237-251.
Meyer, B. J. & Southern, P. J. 1993. Concurrent sequence analysis of 5' and 3' RNA termini by intramolecular circularization reveals 5' nontemplated bases and 3' terminal heterogeneity for lymphocytic choriomeningitis virus mRNAs. *J Virol,* 67**,** 2621-2627.
Monath, T. P. 2019. A short history of Lassa fever: the first 10–15 years after discovery. *Current Opinion in Virology,* 37**,** 77-83.
Monath, T. P., Mertens, P. E., Patton, R., Moser*, C. R., Baum, J. J., Pinneo, L., Gary, G. W. & Kissling, R. E. 1973. A hospital epidemic of Lassa fever in Zorzor, Liberia, March-April 1972. *The American Journal of Tropical Medicine and Hygiene,* 22**,** 773-779.
Monney, L., Sabatos, C. A., Gaglia, J. L., Ryu, A., Waldner, H., Chernova, T., Manning, S., Greenfield, E. A., Coyle, A. J., Sobel, R. A., Freeman, G. J. & Kuchroo, V. K. 2002. Th1-specific cell surface protein Tim-3 regulates macrophage activation and severity of an autoimmune disease. *Nature,* 415**,** 536-541.
Montali, R. J., Connolly, B. M., Armstrong, D. L., Scanga, C. A. & Holmes, K. V. 1995. Pathology and immunohistochemistry of callitrichid hepatitis, an emerging disease of captive New World primates caused by lymphocytic choriomeningitis virus. *The American journal of pathology,* 147**,** 1441-1449.
Montali, R. J., Scanga, C. A., Pernikoff, D., Wessner, D. R., Ward, R. & Holmes, K. V. 1993. A Common-Source Outbreak of Callitrichid Hepatitis in Captive Tamarins and Marmosets. *The Journal of Infectious Diseases,* 167**,** 946-950.
Moolla, N. & Weyer, J. 2020. Chapter 5 - The Arenaviridae. *In:* ENNAJI, M. M. (ed.) *Emerging and Reemerging Viral Pathogens.* Academic Press.

Moraz, M. L., Pythoud, C., Turk, R., Rothenberger, S., Pasquato, A., Campbell, K. P. & Kunz, S. 2013. Cell entry of Lassa virus induces tyrosine phosphorylation of dystroglycan. *Cell Microbiol,* 15**,** 689-700.

Morin, B., Coutard, B., Lelke, M., Ferron, F., Kerber, R., Jamal, S., Frangeul, A., Baronti, C., Charrel, R., De Lamballerie, X., Vonrhein, C., Lescar, J., Bricogne, G., Gunther, S. & Canard, B. 2010a. The N-terminal domain of the arenavirus L protein is an RNA endonuclease essential in mRNA transcription. *PLoS Pathog,* 6**,** e1001038.

Morin, B., Coutard, B., Lelke, M., Ferron, F., Kerber, R., Jamal, S., Frangeul, A., Baronti, C., Charrel, R., De Lamballerie, X., Vonrhein, C., Lescar, J., Bricogne, G., Günther, S. & Canard, B. 2010b. The N-terminal domain of the arenavirus L protein is an RNA endonuclease essential in mRNA transcription. *PLoS Pathog,* 6**,** e1001038.

Mou, H., Smith, J. L., Peng, L., Yin, H., Moore, J., Zhang, X.-O., Song, C.-Q., Sheel, A., Wu, Q., Ozata, D. M., Li, Y., Anderson, D. G., Emerson, C. P., Sontheimer, E. J., Moore, M. J., Weng, Z. & Xue, W. 2017. CRISPR/Cas9-mediated genome editing induces exon skipping by alternative splicing or exon deletion. *Genome Biology,* 18**,** 108.

Moya, A., Holmes, E. C. & González-Candelas, F. 2004. The population genetics and evolutionary epidemiology of RNA viruses. *Nat Rev Microbiol,* 2**,** 279-288.

Muntoni, F., Brockington, M., Godfrey, C., Ackroyd, M., Robb, S., Manzur, A., Kinali, M., Mercuri, E., Kaluarachchi, M., Feng, L., Jimenez-Mallebrera, C., Clement, E., Torelli, S., Sewry, C. A. & Brown, S. C. 2007. Muscular dystrophies due to defective glycosylation of dystroglycan. *Acta myologica : myopathies and cardiomyopathies : official journal of the Mediterranean Society of Myology,* 26**,** 129-135.

Murphy, H. & Ly, H. 2022. Understanding Immune Responses to Lassa Virus Infection and to Its Candidate Vaccines. *Vaccines (Basel),* 10.

Mylne, A. Q., Pigott, D. M., Longbottom, J., Shearer, F., Duda, K. A., Messina, J. P., Weiss, D. J., Moyes, C. L., Golding, N. & Hay, S. I. 2015. Mapping the zoonotic niche of Lassa fever in Africa. *Trans R Soc Trop Med Hyg,* 109**,** 483-492.

Naeini, M. B., Bianconi, V., Pirro, M. & Sahebkar, A. 2020. The role of phosphatidylserine recognition receptors in multiple biological functions. *Cellular & Molecular Biology Letters,* 25**,** 23.

Neuman, B., Adair, B., Burns, J., Milligan, R., Buchmeier, M. & Yeager, M. 2005. Complementarity in the Supramolecular Design of Arenaviruses and Retroviruses Revealed by Electron Cryomicroscopy and Image Analysis. *Journal of virology,* 79**,** 3822-3830.

Nguyen, M. & Haenni, A. L. 2003. Expression strategies of ambisense viruses. *Virus Res,* 93**,** 141-150.

Nie, Y., Wang, P., Shi, X., Wang, G., Chen, J., Zheng, A., Wang, W., Wang, Z., Qu, X., Luo, M., Tan, L., Song, X., Yin, X., Chen, J., Ding, M. & Deng, H. 2004. Highly infectious SARS-CoV pseudotyped virus reveals the cell tropism and its

correlation with receptor expression. *Biochem Biophys Res Commun,* 321**,** 994-1000.

Niemeyer, D., Stenzel, S., Veith, T., Schroeder, S., Friedmann, K., Weege, F., Trimpert, J., Heinze, J., Richter, A., Jansen, J., Emanuel, J., Kazmierski, J., Pott, F., Jeworowski, L. M., Olmer, R., Jaboreck, M.-C., Tenner, B., Papies, J., Walper, F., Schmidt, M. L., Heinemann, N., Möncke-Buchner, E., Baumgardt, M., Hoffmann, K., Widera, M., Thao, T. T. N., Balázs, A., Schulze, J., Mache, C., Jones, T. C., Morkel, M., Ciesek, S., Hanitsch, L. G., Mall, M. A., Hocke, A. C., Thiel, V., Osterrieder, K., Wolff, T., Martin, U., Corman, V. M., Müller, M. A., Goffinet, C. & Drosten, C. 2022. SARS-CoV-2 variant Alpha has a spike-dependent replication advantage over the ancestral B.1 strain in human cells with low ACE2 expression. *PLOS Biology,* 20**,** e3001871.

Okokhere, P., Colubri, A., Azubike, C., Iruolagbe, C., Osazuwa, O., Tabrizi, S., Chin, E., Asad, S., Ediale, E., Rafiu, M., Adomeh, D., Odia, I., Atafo, R., Aire, C., Okogbenin, S., Pahlman, M., Becker-Ziaja, B., Asogun, D., Fradet, T., Fry, B., Schaffner, S. F., Happi, C., Akpede, G., Günther, S. & Sabeti, P. C. 2018. Clinical and laboratory predictors of Lassa fever outcome in a dedicated treatment facility in Nigeria: a retrospective, observational cohort study. *Lancet Infect Dis,* 18**,** 684-695.

Olayemi, A., Cadar, D., Magassouba, N., Obadare, A., Kourouma, F., Oyeyiola, A., Fasogbon, S., Igbokwe, J., Rieger, T., Bockholt, S., Jérôme, H., Schmidt-Chanasit, J., Garigliany, M., Lorenzen, S., Igbahenah, F., Fichet, J. N., Ortsega, D., Omilabu, S., Günther, S. & Fichet-Calvet, E. 2016. New Hosts of The Lassa Virus. *Sci Rep,* 6**,** 25280.

Oldstone, M. B. A. 2002. Biology and Pathogenesis of Lymphocytic Choriomeningitis Virus Infection. *In:* OLDSTONE, M. B. A. (ed.) *Arenaviruses II: The Molecular Pathogenesis of Arenavirus Infections.* Berlin, Heidelberg: Springer Berlin Heidelberg.

Oldstone, M. B. A., Ware, B. C., Horton, L. E., Welch, M. J., Aiolfi, R., Zarpellon, A., Ruggeri, Z. M. & Sullivan, B. M. 2018. Lymphocytic choriomeningitis virus Clone 13 infection causes either persistence or acute death dependent on IFN-1, cytotoxic T lymphocytes (CTLs), and host genetics. *Proc Natl Acad Sci U S A,* 115**,** E7814-e7823.

Onianwa, O. 2017. *Investigation of Arenavirus and Filovirus Infections in Rodents and Non-Human Primates in the United Kingdom.* Doctor of Philosophy, University of Nottingham.

Oppliger, J., Torriani, G., Herrador, A. & Kunz, S. 2016. Lassa Virus Cell Entry via Dystroglycan Involves an Unusual Pathway of Macropinocytosis. *J Virol,* 90**,** 6412-6429.

Owsianka, A. M., Tarr, A. W., Keck, Z. Y., Li, T. K., Witteveldt, J., Adair, R., Foung, S. K., Ball, J. K. & Patel, A. H. 2008. Broadly neutralizing human monoclonal antibodies to the hepatitis C virus E2 glycoprotein. *J Gen Virol,* 89**,** 653-659.

Ozono, S., Zhang, Y., Ode, H., Sano, K., Tan, T. S., Imai, K., Miyoshi, K., Kishigami, S., Ueno, T., Iwatani, Y., Suzuki, T. & Tokunaga, K. 2021. SARS-CoV-2 D614G

spike mutation increases entry efficiency with enhanced ACE2-binding affinity. *Nature Communications,* 12**,** 848.

Paessler, S. & Walker, D. H. 2013. Pathogenesis of the Viral Hemorrhagic Fevers. *Annual Review of Pathology: Mechanisms of Disease,* 8**,** 411-440.

Palacios, G., Druce, J., Du, L., Tran, T., Birch, C., Briese, T., Conlan, S., Quan, P. L., Hui, J., Marshall, J., Simons, J. F., Egholm, M., Paddock, C. D., Shieh, W. J., Goldsmith, C. S., Zaki, S. R., Catton, M. & Lipkin, W. I. 2008. A new arenavirus in a cluster of fatal transplant-associated diseases. *N Engl J Med,* 358**,** 991-8.

Palomares, K., Vigant, F., Van Handel, B., Pernet, O., Chikere, K., Hong, P., Sherman, S. P., Patterson, M., An, D. S., Lowry, W. E., Mikkola, H. K., Morizono, K., Pyle, A. D. & Lee, B. 2013. Nipah virus envelope-pseudotyped lentiviruses efficiently target ephrinB2-positive stem cell populations in vitro and bypass the liver sink when administered in vivo. *J Virol,* 87**,** 2094-2108.

Parekh, B. S. & Buchmeier, M. J. 1986. Proteins of lymphocytic choriomeningitis virus: antigenic topography of the viral glycoproteins. *Virology,* 153**,** 168-178.

Parrish, C. R., Holmes, E. C., Morens, D. M., Park, E.-C., Burke, D. S., Calisher, C. H., Laughlin, C. A., Saif, L. J. & Daszak, P. 2008. Cross-species virus transmission and the emergence of new epidemic diseases. *Microbiology and molecular biology reviews : MMBR,* 72**,** 457-470.

Parrish, C. R., Murcia, P. R. & Holmes, E. C. 2015. Influenza Virus Reservoirs and Intermediate Hosts: Dogs, Horses, and New Possibilities for Influenza Virus Exposure of Humans. *Journal of Virology,* 89**,** 2990-2994.

Pasqual, G., Rojek, J. M., Masin, M., Chatton, J. Y. & Kunz, S. 2011. Old world arenaviruses enter the host cell via the multivesicular body and depend on the endosomal sorting complex required for transport. *PLoS Pathog,* 7**,** e1002232.

Peng, R., Xu, X., Jing, J., Wang, M., Peng, Q., Liu, S., Wu, Y., Bao, X., Wang, P., Qi, J., Gao, G. F. & Shi, Y. 2020. Structural insight into arenavirus replication machinery. *Nature,* 579**,** 615-619.

Peyrard, M., Seroussi, E., Sandberg-Nordqvist, A. C., Xie, Y. G., Han, F. Y., Fransson, I., Collins, J., Dunham, I., Kost-Alimova, M., Imreh, S. & Dumanski, J. P. 1999. The human LARGE gene from 22q12.3-q13.1 is a new, distinct member of the glycosyltransferase gene family. *Proc Natl Acad Sci U S A,* 96**,** 598-603.

Pinneo, L. & Pinneo, R. 1971. Mystery Virus from Lassa. *The Leading Voice of Nursing Since 1900 | AJN,* 71**,** 1352-1355.

Pinschewer, D. D., Perez, M. & De La Torre, J. C. 2003a. Role of the virus nucleoprotein in the regulation of lymphocytic choriomeningitis virus transcription and RNA replication. *J Virol,* 77**,** 3882-7.

Pinschewer, D. D., Perez, M. & De La Torre, J. C. 2003b. Role of the virus nucleoprotein in the regulation of lymphocytic choriomeningitis virus transcription and RNA replication. *J Virol,* 77**,** 3882-3887.

Poch, O., Blumberg, B. M., Bougueleret, L. & Tordo, N. 1990. Sequence Comparison of Five Polymerases (L proteins) of Unsegmented Negative-strand RNA

Viruses: Theoretical Assignment of Functional Domains. *Journal of General Virology,* 71**,** 1153-1162.

Pontremoli, C., Forni, D., Cagliani, R., Pozzoli, U., Riva, S., Bravo, I. G., Clerici, M. & Sironi, M. 2017. Evolutionary analysis of Old World arenaviruses reveals a major adaptive contribution of the viral polymerase. *Mol Ecol,* 26**,** 5173-5188.

Pontremoli, C., Forni, D. & Sironi, M. 2019. Arenavirus genomics: novel insights into viral diversity, origin, and evolution. *Curr Opin Virol,* 34**,** 18-28.

Qi, X., Lan, S., Wang, W., Schelde, L. M., Dong, H., Wallat, G. D., Ly, H., Liang, Y. & Dong, C. 2010. Cap binding and immune evasion revealed by Lassa nucleoprotein structure. *Nature,* 468**,** 779-783.

Qian, Z., Dominguez, S. R. & Holmes, K. V. 2013. Role of the spike glycoprotein of human Middle East respiratory syndrome coronavirus (MERS-CoV) in virus entry and syncytia formation. *PLoS One,* 8**,** e76469.

Qin, J. Y., Zhang, L., Clift, K. L., Hulur, I., Xiang, A. P., Ren, B.-Z. & Lahn, B. T. 2010. Systematic comparison of constitutive promoters and the doxycycline-inducible promoter. *PloS one,* 5**,** e10611-e10611.

Raaben, M., Jae, L. T., Herbert, A. S., Kuehne, A. I., Stubbs, S. H., Chou, Y. Y., Blomen, V. A., Kirchhausen, T., Dye, J. M., Brummelkamp, T. R. & Whelan, S. P. 2017. NRP2 and CD63 Are Host Factors for Lujo Virus Cell Entry. *Cell Host Microbe,* 22**,** 688-696 e5.

Radoshitzky, S. R., Abraham, J., Spiropoulou, C. F., Kuhn, J. H., Nguyen, D., Li, W., Nagel, J., Schmidt, P. J., Nunberg, J. H., Andrews, N. C., Farzan, M. & Choe, H. 2007. Transferrin receptor 1 is a cellular receptor for New World haemorrhagic fever arenaviruses. *Nature,* 446**,** 92-96.

Radoshitzky, S. R., Bào, Y., Buchmeier, M. J., Charrel, R. N., Clawson, A. N., Clegg, C. S., Derisi, J. L., Emonet, S., Gonzalez, J. P., Kuhn, J. H., Lukashevich, I. S., Peters, C. J., Romanowski, V., Salvato, M. S., Stenglein, M. D. & De La Torre, J. C. 2015. Past, present, and future of arenavirus taxonomy. *Arch Virol,* 160**,** 1851-1874.

Radoshitzky, S. R., Buchmeier, M. J., Charrel, R. N., Clegg, J. C. S., Gonzalez, J. J., Gunther, S., Hepojoki, J., Kuhn, J. H., Lukashevich, I. S., Romanowski, V., Salvato, M. S., Sironi, M., Stenglein, M. D., De La Torre, J. C. & Consortium, I. R. 2019. ICTV Virus Taxonomy Profile: Arenaviridae. *J Gen Virol,* 100**,** 1200-1201.

Raju, T. N. K. 2000. The Nobel Chronicles. *The Lancet,* 356**,** 172.

Rivers, T. M. & Mcnair Scott, T. F. 1935. Meningitis in man caused by a filterable virus. *Science,* 81**,** 439-440.

Robinson, J. E., Hastie, K. M., Cross, R. W., Yenni, R. E., Elliott, D. H., Rouelle, J. A., Kannadka, C. B., Smira, A. A., Garry, C. E., Bradley, B. T., Yu, H., Shaffer, J. G., Boisen, M. L., Hartnett, J. N., Zandonatti, M. A., Rowland, M. M., Heinrich, M. L., Martínez-Sobrido, L., Cheng, B., De La Torre, J. C., Andersen, K. G., Goba, A., Momoh, M., Fullah, M., Gbakie, M., Kanneh, L., Koroma, V. J., Fonnie, R., Jalloh, S. C., Kargbo, B., Vandi, M. A., Gbetuwa, M., Ikponmwosa, O., Asogun, D. A., Okokhere, P. O., Follarin, O. A., Schieffelin, J. S., Pitts, K. R.,

Geisbert, J. B., Kulakoski, P. C., Wilson, R. B., Happi, C. T., Sabeti, P. C., Gevao, S. M., Khan, S. H., Grant, D. S., Geisbert, T. W., Saphire, E. O., Branco, L. M. & Garry, R. F. 2016a. Most neutralizing human monoclonal antibodies target novel epitopes requiring both Lassa virus glycoprotein subunits. *Nature Communications,* 7**,** 11544.

Robinson, J. E., Hastie, K. M., Cross, R. W., Yenni, R. E., Elliott, D. H., Rouelle, J. A., Kannadka, C. B., Smira, A. A., Garry, C. E., Bradley, B. T., Yu, H., Shaffer, J. G., Boisen, M. L., Hartnett, J. N., Zandonatti, M. A., Rowland, M. M., Heinrich, M. L., Martínez-Sobrido, L., Cheng, B., De La Torre, J. C., Andersen, K. G., Goba, A., Momoh, M., Fullah, M., Gbakie, M., Kanneh, L., Koroma, V. J., Fonnie, R., Jalloh, S. C., Kargbo, B., Vandi, M. A., Gbetuwa, M., Ikponmwosa, O., Asogun, D. A., Okokhere, P. O., Follarin, O. A., Schieffelin, J. S., Pitts, K. R., Geisbert, J. B., Kulakoski, P. C., Wilson, R. B., Happi, C. T., Sabeti, P. C., Gevao, S. M., Khan, S. H., Grant, D. S., Geisbert, T. W., Saphire, E. O., Branco, L. M. & Garry, R. F. 2016b. Most neutralizing human monoclonal antibodies target novel epitopes requiring both Lassa virus glycoprotein subunits. *Nat Commun,* 7**,** 11544.

Rojek, J. M., Sanchez, A. B., Nguyen, N. T., De La Torre, J. C. & Kunz, S. 2008. Different mechanisms of cell entry by human-pathogenic Old World and New World arenaviruses. *J Virol,* 82**,** 7677-7687.

Rojek, J. M., Spiropoulou, C. F., Campbell, K. P. & Kunz, S. 2007. Old World and Clade C New World Arenaviruses Mimic the Molecular Mechanism of Receptor Recognition Used by α-Dystroglycan's Host-Derived Ligands. *Journal of Virology,* 81**,** 5685-5695.

Rose, J. K. & Bergmann, J. E. 1983. Altered cytoplasmic domains affect intracellular transport of the vesicular stomatitis virus glycoprotein. *Cell,* 34**,** 513-524.

Rowe, W. P., Pugh, W. E., Webb, P. A. & Peters, C. J. 1970. Serological relationship of the Tacaribe complex of viruses to lymphocytic choriomeningitis virus. *J Virol,* 5**,** 289-292.

Salam, A. P., Cheng, V., Edwards, T., Olliaro, P., Sterne, J. & Horby, P. 2021. Time to reconsider the role of ribavirin in Lassa fever. *PLOS Neglected Tropical Diseases,* 15**,** e0009522.

Salami, K., Gouglas, D., Schmaljohn, C., Saville, M. & Tornieporth, N. 2019. A review of Lassa fever vaccine candidates. *Current Opinion in Virology,* 37**,** 105-111.

Salas, R., De Manzione, N., Tesh, R. B., Rico-Hesse, R., Shope, R. E., Betancourt, A., Godoy, O., Bruzual, R., Pacheco, M. E., Ramos, B. & Et Al. 1991. Venezuelan haemorrhagic fever. *Lancet,* 338**,** 1033-1036.

Salvato, M., Borrow, P., Shimomaye, E. & Oldstone, M. B. 1991. Molecular basis of viral persistence: a single amino acid change in the glycoprotein of lymphocytic choriomeningitis virus is associated with suppression of the antiviral cytotoxic T-lymphocyte response and establishment of persistence. *J Virol,* 65**,** 1863-1869.

Salvato, M. S., Schweighofer, K. J., Burns, J. & Shimomaye, E. M. 1992. Biochemical and immunological evidence that the 11 kDa zinc-binding protein of

lymphocytic choriomeningitis virus is a structural component of the virus. *Virus Research,* 22**,** 185-198.
Sanchez, A. B. & De La Torre, J. C. 2006. Rescue of the prototypic Arenavirus LCMV entirely from plasmid. *Virology,* 350**,** 370-380.
Sandrin, V., Boson, B., Salmon, P., Gay, W., NèGre, D., Le Grand, R., Trono, D. & Cosset, F. O.-L. C. 2002. Lentiviral vectors pseudotyped with a modified RD114 envelope glycoprotein show increased stability in sera and augmented transduction of primary lymphocytes and CD34+ cells derived from human and nonhuman primates. *Blood,* 100**,** 823-832.
Sanford, K. K., Earle, W. R. & Likely, G. D. 1948. The growth in vitro of single isolated tissue cells. *J Natl Cancer Inst,* 9**,** 229-246.
Sarute, N. & Ross, S. R. 2017. New World Arenavirus Biology. *Annual Review of Virology,* 4**,** 141-158.
Saunders, A. A., Ting, J. P., Meisner, J., Neuman, B. W., Perez, M., De La Torre, J. C. & Buchmeier, M. J. 2007. Mapping the landscape of the lymphocytic choriomeningitis virus stable signal peptide reveals novel functional domains. *J Virol,* 81**,** 5649-5657.
Scanga, C. A., Holmes, K. V. & Montali, R. J. 1993. Serologic Evidence of Infection with Lymphocytic Choriomeningitis Virus, the Agent of Callitrichid Hepatitis, in Primates in Zoos, Primate Research Centers, and a Natural Reserve. *Journal of Zoo and Wildlife Medicine,* 24**,** 469-474.
Schenborn, E. & Groskreutz, D. 1999. Reporter gene vectors and assays. *Molecular Biotechnology,* 13**,** 29-44.
Schlie, K., Maisa, A., Freiberg, F., Groseth, A., Strecker, T. & Garten, W. 2010. Viral Protein Determinants of Lassa Virus Entry and Release from Polarized Epithelial Cells. *Journal of Virology,* 84**,** 3178.
Scolari, S., Imkeller, K., Jolmes, F., Veit, M., Herrmann, A. & Schwarzer, R. 2016. Modulation of cell surface transport and lipid raft localization by the cytoplasmic tail of the influenza virus hemagglutinin. *Cell Microbiol,* 18**,** 125-136.
Seamer, J. 1965. The growth, reproduction and mortality of mice made immunologically tolerant to lymphocytic choriomeningitis virus by congenital infection. *Archiv für die gesamte Virusforschung,* 15**,** 169-177.
Seiler, P., Senn, B. M., Bründler, M.-A., Zinkernagel, R. M., Hengartner, H. & Kalinke, U. 1999. In Vivo Selection of Neutralization-Resistant Virus Variants But No Evidence of B Cell Tolerance in Lymphocytic Choriomeningitis Virus Carrier Mice Expressing a Transgenic Virus-Neutralizing Antibody. *The Journal of Immunology,* 162**,** 4536-4541.
Sevilla, N., Kunz, S., Holz, A., Lewicki, H., Homann, D., Yamada, H., Campbell, K. P., De La Torre, J. C. & Oldstone, M. B. 2000a. Immunosuppression and resultant viral persistence by specific viral targeting of dendritic cells. *The Journal of experimental medicine,* 192**,** 1249-1260.
Sevilla, N., Kunz, S., Holz, A., Lewicki, H., Homann, D., Yamada, H., Campbell, K. P., De La Torre, J. C. & Oldstone, M. B. 2000b. Immunosuppression and

resultant viral persistence by specific viral targeting of dendritic cells. *J Exp Med,* 192**,** 1249-1260.

Sewlall, N. H., Richards, G., Duse, A., Swanepoel, R., Paweska, J., Blumberg, L., Dinh, T. H. & Bausch, D. 2014. Clinical features and patient management of Lujo hemorrhagic fever. *PLoS Negl Trop Dis,* 8**,** e3233.

Shaffer, J. G., Grant, D. S., Schieffelin, J. S., Boisen, M. L., Goba, A., Hartnett, J. N., Levy, D. C., Yenni, R. E., Moses, L. M., Fullah, M., Momoh, M., Fonnie, M., Fonnie, R., Kanneh, L., Koroma, V. J., Kargbo, K., Ottomassathien, D., Muncy, I. J., Jones, A. B., Illick, M. M., Kulakosky, P. C., Haislip, A. M., Bishop, C. M., Elliot, D. H., Brown, B. L., Zhu, H., Hastie, K. M., Andersen, K. G., Gire, S. K., Tabrizi, S., Tariyal, R., Stremlau, M., Matschiner, A., Sampey, D. B., Spence, J. S., Cross, R. W., Geisbert, J. B., Folarin, O. A., Happi, C. T., Pitts, K. R., Geske, F. J., Geisbert, T. W., Saphire, E. O., Robinson, J. E., Wilson, R. B., Sabeti, P. C., Henderson, L. A., Khan, S. H., Bausch, D. G., Branco, L. M., Garry, R. F. & Consortium, V. H. F. 2014. Lassa fever in post-conflict sierra leone. *PLoS Negl Trop Dis,* 8**,** e2748.

Shao, J., Liang, Y. & Ly, H. 2018. Roles of Arenavirus Z Protein in Mediating Virion Budding, Viral Transcription-Inhibition and Interferon-Beta Suppression. *Methods Mol Biol,* 1604**,** 217-227.

Shaw, G., Morse, S., Ararat, M. & Graham, F. L. 2002. Preferential transformation of human neuronal cells by human adenoviruses and the origin of HEK 293 cells. *The FASEB Journal,* 16**,** 869-871.

Shehu, N. Y., Gomerep, S. S., Isa, S. E., Iraoyah, K. O., Mafuka, J., Bitrus, N., Dachom, M. C., Ogwuche, J. E., Onukak, A. E., Onyedibe, K. I., Ogbaini-Emovon, E., Egah, D. Z., Mateer, E. J. & Paessler, S. 2018. Lassa Fever 2016 Outbreak in Plateau State, Nigeria-The Changing Epidemiology and Clinical Presentation. *Frontiers in public health,* 6**,** 232-232.

Shi, M., Lin, X.-D., Chen, X., Tian, J.-H., Chen, L.-J., Li, K., Wang, W., Eden, J.-S., Shen, J.-J., Liu, L., Holmes, E. C. & Zhang, Y.-Z. 2018. The evolutionary history of vertebrate RNA viruses. *Nature,* 556**,** 197-202.

Shi, R., Shan, C., Duan, X., Chen, Z., Liu, P., Song, J., Song, T., Bi, X., Han, C., Wu, L., Gao, G., Hu, X., Zhang, Y., Tong, Z., Huang, W., Liu, W. J., Wu, G., Zhang, B., Wang, L., Qi, J., Feng, H., Wang, F.-S., Wang, Q., Gao, G. F., Yuan, Z. & Yan, J. 2020. A human neutralizing antibody targets the receptor-binding site of SARS-CoV-2. *Nature,* 584**,** 120-124.

Shimojima, M., Ströher, U., Ebihara, H., Feldmann, H. & Kawaoka, Y. 2012. Identification of cell surface molecules involved in dystroglycan-independent Lassa virus cell entry. *J Virol,* 86**,** 2067-2078.

Shimojima, M., Takada, A., Ebihara, H., Neumann, G., Fujioka, K., Irimura, T., Jones, S., Feldmann, H. & Kawaoka, Y. 2006. Tyro3 Family-Mediated Cell Entry of Ebola and Marburg Viruses. *Journal of Virology,* 80**,** 10109-10116.

Shtanko, O., Watanabe, S., Jasenosky, L. D., Watanabe, T. & Kawaoka, Y. 2011. ALIX/AIP1 is required for NP incorporation into Mopeia virus Z-induced virus-like particles. *Journal of virology,* 85**,** 3631-3641.

Siddle, K. J., Eromon, P., Barnes, K. G., Mehta, S., Oguzie, J. U., Odia, I., Schaffner, S. F., Winnicki, S. M., Shah, R. R., Qu, J., Wohl, S., Brehio, P., Iruolagbe, C., Aiyepada, J., Uyigue, E., Akhilomen, P., Okonofua, G., Ye, S., Kayode, T., Ajogbasile, F., Uwanibe, J., Gaye, A., Momoh, M., Chak, B., Kotliar, D., Carter, A., Gladden-Young, A., Freije, C. A., Omoregie, O., Osiemi, B., Muoebonam, E. B., Airende, M., Enigbe, R., Ebo, B., Nosamiefan, I., Oluniyi, P., Nekoui, M., Ogbaini-Emovon, E., Garry, R. F., Andersen, K. G., Park, D. J., Yozwiak, N. L., Akpede, G., Ihekweazu, C., Tomori, O., Okogbenin, S., Folarin, O. A., Okokhere, P. O., Macinnis, B. L., Sabeti, P. C. & Happi, C. T. 2018. Genomic Analysis of Lassa Virus during an Increase in Cases in Nigeria in 2018. *The New England journal of medicine,* 379**,** 1745-1753.

Singh, M. K., Fuller-Pace, F. V., Buchmeier, M. J. & Southern, P. J. 1987. Analysis of the genomic l rna segment from lymphocytic choriomeningitis virus. *Virology,* 161**,** 448-456.

Smelt, S. C., Borrow, P., Kunz, S., Cao, W., Tishon, A., Lewicki, H., Campbell, K. P. & Oldstone, M. B. 2001a. Differences in affinity of binding of lymphocytic choriomeningitis virus strains to the cellular receptor alpha-dystroglycan correlate with viral tropism and disease kinetics. *Journal of virology,* 75**,** 448-457.

Smelt, S. C., Borrow, P., Kunz, S., Cao, W., Tishon, A., Lewicki, H., Campbell, K. P. & Oldstone, M. B. 2001b. Differences in affinity of binding of lymphocytic choriomeningitis virus strains to the cellular receptor alpha-dystroglycan correlate with viral tropism and disease kinetics. *J Virol,* 75**,** 448-457.

Smith, G. J. D., Vijaykrishna, D., Bahl, J., Lycett, S. J., Worobey, M., Pybus, O. G., Ma, S. K., Cheung, C. L., Raghwani, J., Bhatt, S., Peiris, J. S. M., Guan, Y. & Rambaut, A. 2009. Origins and evolutionary genomics of the 2009 swine-origin H1N1 influenza A epidemic. *Nature,* 459**,** 1122-1125.

Smits, A. H., Ziebell, F., Joberty, G., Zinn, N., Mueller, W. F., Clauder-Münster, S., Eberhard, D., Fälth Savitski, M., Grandi, P., Jakob, P., Michon, A.-M., Sun, H., Tessmer, K., Bürckstümmer, T., Bantscheff, M., Steinmetz, L. M., Drewes, G. & Huber, W. 2019. Biological plasticity rescues target activity in CRISPR knock outs. *Nature Methods,* 16**,** 1087-1093.

Sogoba, N., Rosenke, K., Adjemian, J., Diawara, S. I., Maiga, O., Keita, M., Konaté, D., Keita, A. S., Sissoko, I., Boisen, M., Nelson, D., Oottamasathien, D., Millett, M., Garry, R. F., Branco, L. M., Traoré, S. F., Doumbia, S., Feldmann, H. & Safronetz, D. 2016. Lassa Virus Seroprevalence in Sibirilia Commune, Bougouni District, Southern Mali. *Emerging infectious diseases,* 22**,** 657-663.

Sommerstein, R., Flatz, L., Remy, M. M., Malinge, P., Magistrelli, G., Fischer, N., Sahin, M., Bergthaler, A., Igonet, S., Ter Meulen, J., Rigo, D., Meda, P., Rabah, N., Coutard, B., Bowden, T. A., Lambert, P.-H., Siegrist, C.-A. & Pinschewer, D. D. 2015. Arenavirus Glycan Shield Promotes Neutralizing Antibody Evasion and Protracted Infection. *PLoS pathogens,* 11**,** e1005276-e1005276.

Sommerstein, R., Ramos Da Palma, J., Olschlager, S., Bergthaler, A., Barba, L., Lee, B. P., Pasquato, A. & Flatz, L. 2014. Evolution of recombinant lymphocytic

choriomeningitis virus/Lassa virus in vivo highlights the importance of the GPC cytosolic tail in viral fitness. *J Virol,* 88**,** 8340-8348.

Song, H., Giorgi, E. E., Ganusov, V. V., Cai, F., Athreya, G., Yoon, H., Carja, O., Hora, B., Hraber, P., Romero-Severson, E., Jiang, C., Li, X., Wang, S., Li, H., Salazar-Gonzalez, J. F., Salazar, M. G., Goonetilleke, N., Keele, B. F., Montefiori, D. C., Cohen, M. S., Shaw, G. M., Hahn, B. H., Mcmichael, A. J., Haynes, B. F., Korber, B., Bhattacharya, T. & Gao, F. 2018. Tracking HIV-1 recombination to resolve its contribution to HIV-1 evolution in natural infection. *Nature Communications,* 9**,** 1928.

Stott, R., Strecker, T. & Foster, T. 2020a. Human host cell entry restriction of Lassa and other arenaviruses. *Access Microbiology,* 2.

Stott, R. J., Strecker, T. & Foster, T. L. 2020b. Distinct Molecular Mechanisms of Host Immune Response Modulation by Arenavirus NP and Z Proteins. *Viruses,* 12**,** 784.

Strecker, T., Eichler, R., Meulen, J. T., Weissenhorn, W., Dieter Klenk, H., Garten, W. & Lenz, O. 2003. Lassa Virus Z Protein Is a Matrix Protein Sufficient for the Release of Virus-Like Particles. *Journal of Virology,* 77**,** 10700-10705.

Streicker, D. G., Turmelle, A. S., Vonhof, M. J., Kuzmin, I. V., Mccracken, G. F. & Rupprecht, C. E. 2010. Host phylogeny constrains cross-species emergence and establishment of rabies virus in bats. *Science,* 329**,** 676-679.

Sullivan, B. M., Emonet, S. F., Welch, M. J., Lee, A. M., Campbell, K. P., De La Torre, J. C. & Oldstone, M. B. 2011. Point mutation in the glycoprotein of lymphocytic choriomeningitis virus is necessary for receptor binding, dendritic cell infection, and long-term persistence. *Proc Natl Acad Sci U S A,* 108**,** 2969-2974.

Taft, A. S., Ozawa, M., Fitch, A., Depasse, J. V., Halfmann, P. J., Hill-Batorski, L., Hatta, M., Friedrich, T. C., Lopes, T. J. S., Maher, E. A., Ghedin, E., Macken, C. A., Neumann, G. & Kawaoka, Y. 2015. Identification of mammalian-adapting mutations in the polymerase complex of an avian H5N1 influenza virus. *Nature Communications,* 6**,** 7491.

Tani, H. 2014. Analyses of Entry Mechanisms of Novel Emerging Viruses Using Pseudotype VSV System. *Tropical Medicine and Health,* 42**,** 71 - 82.

Taubenberger, J. K. & Kash, J. C. 2010. Influenza Virus Evolution, Host Adaptation, and Pandemic Formation. *Cell Host & Microbe,* 7**,** 440-451.

Taubenberger, J. K., Reid, A. H., Lourens, R. M., Wang, R., Jin, G. & Fanning, T. G. 2005. Characterization of the 1918 influenza virus polymerase genes. *Nature,* 437**,** 889-893.

Temmam, S., Vongphayloth, K., Baquero, E., Munier, S., Bonomi, M., Regnault, B., Douangboubpha, B., Karami, Y., Chrétien, D., Sanamxay, D., Xayaphet, V., Paphaphanh, P., Lacoste, V., Somlor, S., Lakeomany, K., Phommavanh, N., Pérot, P., Dehan, O., Amara, F., Donati, F., Bigot, T., Nilges, M., Rey, F. A., Van Der Werf, S., Brey, P. T. & Eloit, M. 2022. Bat coronaviruses related to SARS-CoV-2 and infectious for human cells. *Nature,* 604**,** 330-336.

Tobin, E., Asogun, D., Akpede, N., Adomeh, D., Odia, I. & Gunther, S. 2015. Lassa fever in Nigeria: Insights into seroprevalence and risk factors in rural Edo State: A pilot study. *Journal of Medicine in the Tropics,* 17**,** 51-55.

Traub , E. 1936. Persistence of lymphocytic choriomeningitis virus in immun animals and its relation to immunity. *Journal of Experimental Medicine,* 63**,** 847-861.

Traub, E. 1939. Epidemiology of lymphocytic choriomeningitis in a mouse stock observed for four years. *The Journal of experimental medicine,* 69**,** 801-817.

Tuladhar, R., Yeu, Y., Tyler Piazza, J., Tan, Z., Rene Clemenceau, J., Wu, X., Barrett, Q., Herbert, J., Mathews, D. H., Kim, J., Hyun Hwang, T. & Lum, L. 2019. CRISPR-Cas9-based mutagenesis frequently provokes on-target mRNA misregulation. *Nature Communications,* 10**,** 4056.

Urata, S. & Yasuda, J. 2012. Molecular mechanism of arenavirus assembly and budding. *Viruses,* 4**,** 2049-2079.

Urbanowicz, R. A., Mcclure, C. P., King, B., Mason, C. P., Ball, J. K. & Tarr, A. W. 2016a. Novel functional hepatitis C virus glycoprotein isolates identified using an optimized viral pseudotype entry assay. *J Gen Virol,* 97**,** 2265-2279.

Urbanowicz, R. A., Mcclure, C. P., Sakuntabhai, A., Sall, A. A., Kobinger, G., Müller, M. A., Holmes, E. C., Rey, F. A., Simon-Loriere, E. & Ball, J. K. 2016b. Human Adaptation of Ebola Virus during the West African Outbreak. *Cell,* 167**,** 1079-1087.e5.

Vela, E. M., Zhang, L., Colpitts, T. M., Davey, R. A. & Aronson, J. F. 2007. Arenavirus entry occurs through a cholesterol-dependent, non-caveolar, clathrin-mediated endocytic mechanism. *Virology,* 369**,** 1-11.

Vezza, A. C., Clewley, J. P., Gard, G. P., Abraham, N. Z., Compans, R. W. & Bishop, D. H. 1978. Virion RNA species of the arenaviruses Pichinde, Tacaribe, and Tamiami. *J Virol,* 26**,** 485-497.

Vilibic-Cavlek, T., Savic, V., Ferenc, T., Mrzljak, A., Barbic, L., Bogdanic, M., Stevanovic, V., Tabain, I., Ferencak, I. & Zidovec-Lepej, S. 2021. Lymphocytic Choriomeningitis—Emerging Trends of a Neglected Virus: A Narrative Review. *Tropical Medicine and Infectious Disease,* 6**,** 88.

Walker, D. H., Wulff, H., Lange, J. V. & Murphy, F. A. 1975. Comparative pathology of Lassa virus infection in monkeys, guinea-pigs, and Mastomys natalensis. *Bulletin of the World Health Organization,* 52**,** 523-534.

Walther, W. & Stein, U. 2000. Viral Vectors for Gene Transfer. *Drugs,* 60**,** 249-271.

Wang, J., Cheng, H., Ratia, K., Varhegyi, E., Hendrickson, W. G., Li, J. & Rong, L. 2014. A comparative high-throughput screening protocol to identify entry inhibitors of enveloped viruses. *Journal of biomolecular screening,* 19**,** 100-107.

Watanabe, Y., Bowden, T. A., Wilson, I. A. & Crispin, M. 2019. Exploitation of glycosylation in enveloped virus pathobiology. *Biochimica et Biophysica Acta (BBA) - General Subjects,* 1863**,** 1480-1497.

Watanabe, Y., Raghwani, J., Allen, J. D., Seabright, G. E., Li, S., Moser, F., Huiskonen, J. T., Strecker, T., Bowden, T. A. & Crispin, M. 2018. Structure of the Lassa virus glycan shield provides a model for immunological resistance. *Proc Natl Acad Sci U S A,* 115**,** 7320-7325.

Webb, P. A., Justines, G. & Johnson, K. M. 1975. Infection of wild and laboratory animals with Machupo and Latino viruses. *Bull World Health Organ,* 52**,** 493-499.

Weber, E. L. & Buchmeier, M. J. 1988. Fine mapping of a peptide sequence containing an antigenic site conserved among arenaviruses. *Virology,* 164**,** 30-38.

Weiss, R. A. 2003. HIV and AIDS in relation to other pandemics. Among the viruses plaguing humans, HIV is a recent acquisition. Its outstanding success as an infection poses immense scientific challenges to human health and raises the question "What comes nest?". *EMBO reports,* 4 Spec No**,** S10-S14.

Welm, B. E., Dijkgraaf, G. J., Bledau, A. S., Welm, A. L. & Werb, Z. 2008. Lentiviral transduction of mammary stem cells for analysis of gene function during development and cancer. *Cell Stem Cell,* 2**,** 90-102.

Whitmer, S. L. M., Strecker, T., Cadar, D., Dienes, H. P., Faber, K., Patel, K., Brown, S. M., Davis, W. G., Klena, J. D., Rollin, P. E., Schmidt-Chanasit, J., Fichet-Calvet, E., Noack, B., Emmerich, P., Rieger, T., Wolff, S., Fehling, S. K., Eickmann, M., Mengel, J. P., Schultze, T., Hain, T., Ampofo, W., Bonney, K., Aryeequaye, J. N. D., Ribner, B., Varkey, J. B., Mehta, A. K., Lyon, G. M., 3rd, Kann, G., De Leuw, P., Schuettfort, G., Stephan, C., Wieland, U., Fries, J. W. U., Kochanek, M., Kraft, C. S., Wolf, T., Nichol, S. T., Becker, S., Ströher, U. & Günther, S. 2018. New Lineage of Lassa Virus, Togo, 2016. *Emerg Infect Dis,* 24**,** 599-602.

Whitt, M. A. 2010. Generation of VSV pseudotypes using recombinant ΔG-VSV for studies on virus entry, identification of entry inhibitors, and immune responses to vaccines. *Journal of virological methods,* 169**,** 365-374.

Who. 2020. *Disease Outbreak News; Lassa Fever-Nigeria* [Online]. World Health Organization. Available: https://www.who.int/emergencies/disease-outbreak-news/item/2020-DON245 [Accessed].

Who. 2022a. *Disease Outbreak News; Lassa Fever-Nigeria* [Online]. World Health Organization. Available: https://www.who.int/emergencies/disease-outbreak-news/item/lassa-fever---nigeria [Accessed].

Who. 2022b. *Lassa Fever* [Online]. World Health Organization. Available: https://www.who.int/health-topics/lassa-fever/#tab=tab_1 [Accessed].

Willard, K. A., Alston, J. T., Acciani, M. & Brindley, M. A. 2018. Identification of Residues in Lassa Virus Glycoprotein Subunit 2 That Are Critical for Protein Function. *Pathogens (Basel, Switzerland),* 8**,** 1.

Wolfe, N. D., Dunavan, C. P. & Diamond, J. 2007. Origins of major human infectious diseases. *Nature,* 447**,** 279-283.

Woolhouse, M. & Gaunt, E. 2007. Ecological Origins of Novel Human Pathogens. *Critical Reviews in Microbiology,* 33**,** 231-242.

Woolhouse, M., Scott, F., Hudson, Z., Howey, R. & Chase-Topping, M. 2012. Human viruses: discovery and emergence. *Philosophical transactions of the Royal Society of London. Series B, Biological sciences,* 367**,** 2864-2871.

Woolhouse, M. E. J. 2002. Population biology of emerging and re-emerging pathogens. *Trends in Microbiology,* 10**,** s3-s7.

Woolhouse, M. E. J., Haydon, D. T. & Antia, R. 2005. Emerging pathogens: the epidemiology and evolution of species jumps. *Trends in Ecology & Evolution,* 20**,** 238-244.

Wright, E., Temperton, N. J., Marston, D. A., Mcelhinney, L. M., Fooks, A. R. & Weiss, R. A. 2008. Investigating antibody neutralization of lyssaviruses using lentiviral pseudotypes: a cross-species comparison. *J Gen Virol,* 89**,** 2204-2213.

Wright, R., Johnson, D., Neumann, M., Ksiazek, T. G., Rollin, P., Keech, R. V., Bonthius, D. J., Hitchon, P., Grose, C. F., Bell, W. E. & Bale, J. F. 1997. Congenital lymphocytic choriomeningitis virus syndrome: a disease that mimics congenital toxoplasmosis or Cytomegalovirus infection. *Pediatrics,* 100**,** E9.

Xing, J., Ly, H. & Liang, Y. 2015. The Z Proteins of Pathogenic but Not Nonpathogenic Arenaviruses Inhibit RIG-i-Like Receptor-Dependent Interferon Production. *Journal of Virology,* 89**,** 2944-2955.

Yahalom-Ronen, Y., Tamir, H., Melamed, S., Politi, B., Shifman, O., Achdout, H., Vitner, E. B., Israeli, O., Milrot, E., Stein, D., Cohen-Gihon, I., Lazar, S., Gutman, H., Glinert, I., Cherry, L., Vagima, Y., Lazar, S., Weiss, S., Ben-Shmuel, A., Avraham, R., Puni, R., Lupu, E., Bar-David, E., Sittner, A., Erez, N., Zichel, R., Mamroud, E., Mazor, O., Levy, H., Laskar, O., Yitzhaki, S., Shapira, S. C., Zvi, A., Beth-Din, A., Paran, N. & Israely, T. 2020. A single dose of recombinant VSV-ΔG-spike vaccine provides protection against SARS-CoV-2 challenge. *Nature Communications,* 11**,** 6402.

Yoshida-Moriguchi, T., Yu, L., Stalnaker, S. H., Davis, S., Kunz, S., Madson, M., Oldstone, M. B., Schachter, H., Wells, L. & Campbell, K. P. 2010. O-mannosyl phosphorylation of alpha-dystroglycan is required for laminin binding. *Science,* 327**,** 88-92.

Yutzey, K. E., Kline, R. L. & Konieczny, S. F. 1989. An internal regulatory element controls troponin I gene expression. *Mol Cell Biol,* 9**,** 1397-405.

Zapata, J. C., Pauza, C. D., Djavani, M. M., Rodas, J. D., Moshkoff, D., Bryant, J., Ateh, E., Garcia, C., Lukashevich, I. S. & Salvato, M. S. 2011. Lymphocytic choriomeningitis virus (LCMV) infection of macaques: a model for Lassa fever. *Antiviral Res,* 92**,** 125-138.

Zarrin, A. A., Malkin, L., Fong, I., Luk, K. D., Ghose, A. & Berinstein, N. L. 1999. Comparison of CMV, RSV, SV40 viral and Vlambda1 cellular promoters in B and T lymphoid and non-lymphoid cell lines. *Biochim Biophys Acta,* 1446**,** 135-139.

Zeng, C., Evans, J. P., Pearson, R., Qu, P., Zheng, Y.-M., Robinson, R. T., Hall-Stoodley, L., Yount, J., Pannu, S., Mallampalli, R. K., Saif, L., Oltz, E., Lozanski, G. & Liu, S.-L. 2020. Neutralizing antibody against SARS-CoV-2 spike in COVID-19 patients, health care workers, and convalescent plasma donors. *JCI Insight,* 5.

Zhang, G., Gurtu, V. & Kain, S. R. 1996. An enhanced green fluorescent protein allows sensitive detection of gene transfer in mammalian cells. *Biochem Biophys Res Commun,* 227**,** 707-711.

Zhang, Q., Fu, Y., Thakur, C., Bi, Z., Wadgaonkar, P., Qiu, Y., Xu, L., Rice, M. K., Zhang, W., Almutairy, B. & Chen, F. 2020. CRISPR-Cas9 gene editing causes alternative splicing of the targeting mRNA. *Biochemical and Biophysical Research Communications,* 528**,** 54-61.

Zhang, Y., Zhang, Q., Gao, Y., He, X., Kong, H., Jiang, Y., Guan, Y., Xia, X., Shu, Y., Kawaoka, Y., Bu, Z. & Chen, H. 2012. Key Molecular Factors in Hemagglutinin and PB2 Contribute to Efficient Transmission of the 2009 H1N1 Pandemic Influenza Virus. *Journal of Virology,* 86**,** 9666-9674.

Zhou, S., Liu, Q., Wu, X., Chen, P., Wu, X., Guo, Y., Liu, S., Liang, Z., Fan, C. & Wang, Y. 2016. A safe and sensitive enterovirus A71 infection model based on human SCARB2 knock-in mice. *Vaccine,* 34**,** 2729-2736.

Zhu, S., Wan, W., Zhang, Y., Shang, W., Pan, X., Zhang, L.-K. & Xiao, G. 2019. Comprehensive Interactome Analysis Reveals that STT3B Is Required for N-Glycosylation of Lassa Virus Glycoprotein. *Journal of Virology,* 93**,** e01443-19.

Zhuang, C., Pannecouque, C., De Clercq, E. & Chen, F. 2019. Development of non-nucleoside reverse transcriptase inhibitors (NNRTIs): Our past twenty years. *Acta Pharmaceutica Sinica B,* 10**,** 961-978.